11. Status of Higgs Boson Physics

Revised September 2017 by M. Carena (Fermi National Accelerator Laboratory and the University of Chicago), C. Grojean (DESY, Hamburg, and Humboldt University, Berlin), M. Kado (Laboratoire de l'Accélérateur Linéaire, Orsay), and V. Sharma (University of California, San Diego).

I. Introduction

Understanding the mechanism that breaks the electroweak symmetry and generates the masses of the known elementary particles has been one of the fundamental endeavors in particle physics. The discovery in 2012 by the ATLAS [1] and the CMS [2] Collaborations of a new resonance with a mass of approximately 125 GeV and the subsequent studies of its properties with a much larger data set have provided the first portrait of this mechanism. The mass of this boson has been precisely measured and its production and decay rates are found to be consistent, within errors, with the standard model (SM) predictions. Nevertheless, several channels are yet out of reach experimentally and the couplings of the Higgs boson to light fermions are yet to be proven. At the same time, many theoretical questions remain unanswered. New questions about what lies behind

the Higgs boson have come to fore. Nonetheless, five years since its discovery, the Higgs boson has turned into a new tool to explore the manifestations of the SM and to probe the physics landscape beyond it.

In the SM [3] the electroweak interactions are described by a gauge field theory invariant under the $\mathrm{SU}(2)_L \times \mathrm{U}(1)_Y$ symmetry group. The mechanism of electroweak symmetry breaking (EWSB) [4] provides a general framework to keep untouched the structure of these gauge interactions at high energies and still generate the observed masses of the W and Z gauge bosons. The EWSB mechanism posits a self-interacting complex doublet scalar field, whose CP-even neutral component acquires a vacuum expectation value (VEV) $v \approx 246\,\mathrm{GeV}$, which sets the scale of electroweak symmetry breaking. Three massless Goldstone bosons are generated and are absorbed to give masses to the W and Z gauge bosons. The remaining component of the complex doublet becomes the Higgs boson – a new fundamental scalar particle. The masses of all fermions are also a consequence of EWSB since the Higgs doublet is postulated to couple to the fermions through Yukawa interactions.

All measurements of the Higgs boson properties are so far indicating that the observations are compatible with a minimal EWSB sector. Nevertheless, within the current precision a more complex sector with additional states is not ruled out, nor has it been established whether the Higgs boson is an elementary particle or whether it has an internal structure like any other scalar particles observed before it.

Without the Higgs boson, the calculability of the SM would have been spoiled. In particular, perturbative unitarity [5, 6] would be lost at high energies since the longitudinal W/Z boson scattering amplitude would grow with the increase in centre-of-mass energy. In addition, the radiative corrections to the gauge boson self-energies would exhibit dangerous logarithmic divergences that would be difficult to reconcile with EW precision data. With the discovery of the Higgs boson, the SM is a spontaneously broken gauge theory and as such it could a priori be consistently extrapolated well above the masses of the W and Z bosons. Hence, formally there is no need for new physics at the EW scale. However, as the SM Higgs boson is a scalar particle, at the quantum level it has sensitivity to high energy thresholds. Quite generally, the Higgs mass is affected by the presence of heavy particles and receives quantum corrections proportional to highest energy scale which destabilize the weak scale barring a large fine tuning of unrelated parameters. This is known as the hierarchy or naturalness problem [7].

There are two broad classes of models addressing the naturalness problem[1]: one is based on a new fermion-boson symmetry in nature called supersymmetry (SUSY) [9–11]. This is a weakly coupled approach to EWSB, and in this case, the Higgs boson remains elementary and the corrections to its mass are screened at the scale at which SUSY is broken and remain insensitive to the details of the physics at higher scales. These theories predict at least three neutral Higgs particles and a pair of charged Higgs particles [12]. One of the neutral Higgs bosons, most often the lightest CP-even Higgs, has properties

[1] Another solution to the naturalness problem is to lower the fundamental scale of quantum gravity, like for instance in models with large extra-dimensions, see Ref. [8].

that resemble those of the SM Higgs boson. It is referred to as a SM-like Higgs boson, meaning that its couplings are close to the ones predicted in the SM.

The other approach invokes the existence of strong interactions at a scale of the order of a TeV or above and induces strong breaking of the electroweak symmetry [13]. In the original incarnation of this second approach, dubbed technicolor, the strong interactions themselves trigger EWSB without the need of a Higgs boson. Another possibility, more compatible with the ATLAS and CMS discovery, is that the strong interactions produce four light resonances identified with the Higgs doublet and EWSB proceeds through vacuum misalignment [14] (see Refs. [15, 16] for recent reviews). The Higgs boson could also correspond to the Goldstone boson associated with the spontaneous breaking of scale invariance [17, 18]. However, this dilaton/radion scenario now requires jumbled model-building to be consistent with the constraints from the coupling measurements.

Both approaches can have important effects on the phenomenology of the Higgs boson associated with EWSB. Also, in each case the Higgs role in unitarization of scattering amplitudes is shared by other particles that remain targets of experimental searches.

The naturalness problem has been the prime argument for new physics at the TeV scale, and sizable effects on the Higgs boson properties were expected. But the agreement of the Higgs couplings with the SM predictions, together with the strong bounds from precision electroweak and flavor data leaves open the possibility that the Higgs boson may well be elementary, weakly coupled and solitary up to the Planck scale, rendering the EW vacuum potentially metastable. However, absence of evidence is not evidence of absence. It is possible that new states present at the TeV scale to stabilize the Higgs mass might simply be elusive at the LHC because they do not carry a color charge. Twin Higgs [19] models were the first incarnation of this neutral naturalness idea [20]. More recent and extreme proposals [21] rely on the cosmological evolution of the Universe to drive the Higgs boson mass to a value much smaller than the cutoff of the theory and aim at alleviating the hierarchy problem without the need for TeV scale new physics.

Extensions of the SM Higgs sector without low-energy supersymmetry will also be discussed in this review. These type of models do not address the naturalness problem in a specific manner, but provide grounds to explore new Higgs boson signals in a more model-independent way, with different types of coupling structure to fermions and gauge bosons. Extended Higgs sectors are usually quite restricted by experimental constraints from precision electroweak measurements as well as constraints from flavor data.

This review is organized as follow. Section II is a theoretical review of the SM Higgs boson, its properties, production mechanisms and decay rates. In Section III, the experimental measurements are described. In Section IV, the combination of the main Higgs boson production and decay channels is presented. In Section V, measurements of the main quantum numbers and CP properties of the Higgs boson are reported and the bounds on its total width are discussed. In Section VI, a general theoretical framework to describe the deviations of the Higgs couplings from the SM predictions is introduced and the experimental measurements of these Higgs couplings is reviewed. Measurements of differential cross sections are outlined. Section VII presents, in detail, some interesting models proposed for Higgs extensions of the SM and considers their experimental signatures. Section VIII provides a short summary and a brief outlook.

II. The standard model and the mechanism of electroweak symmetry breaking

In the SM [3], electroweak symmetry breaking [4] is responsible for generating mass for the W and Z gauge bosons rendering the weak interactions short ranged. The SM scalar potential reads:

$$V(\Phi) = m^2\Phi^\dagger\Phi + \lambda(\Phi^\dagger\Phi)^2 \tag{11.1}$$

with the Higgs field Φ being a self-interacting $\mathrm{SU}(2)_L$ complex doublet (four real degrees of freedom) with weak hypercharge $Y{=}1$ (the hypercharge is normalized such that $Q = T_{3L} + Y/2$, Q being the electric charge and T_{3L} the diagonal generator of $\mathrm{SU}(2)_L$):

$$\Phi = \frac{1}{\sqrt{2}}\begin{pmatrix} \sqrt{2}\phi^+ \\ \phi^0 + ia^0 \end{pmatrix}, \tag{11.2}$$

where ϕ^0 and a^0 are the CP-even and CP-odd neutral components, and ϕ^+ is the complex charged component of the Higgs doublet, respectively. $V(\Phi)$ is the most general renormalizable scalar potential and if the quadratic term is negative the neutral component of the scalar doublet acquires a non-zero vacuum expectation value (VEV)

$$\langle\Phi\rangle = \frac{1}{\sqrt{2}}\begin{pmatrix} 0 \\ v \end{pmatrix}, \tag{11.3}$$

with $\phi^0 = H + \langle\phi^0\rangle$ and $\langle\phi^0\rangle \equiv v$, inducing the spontaneous breaking of the SM gauge symmetry $\mathrm{SU}(3)_C \times \mathrm{SU}(2)_L \times \mathrm{U}(1)_Y$ into $\mathrm{SU}(3)_C \times \mathrm{U}(1)_{\rm em}$. The global minimum of the theory defines the ground state, and spontaneous symmetry breaking implies that there is a symmetry of the system that is not respected by the ground state. From the four generators of the $\mathrm{SU}(2)_L \times \mathrm{U}(1)_Y$ gauge group, three are spontaneously broken, implying that they lead to non-trivial transformations of the ground state and indicate the existence of three massless Goldstone bosons identified with three of the four Higgs field degrees of freedom. The Higgs field couples to the W_μ and B_μ gauge fields associated with the $\mathrm{SU}(2)_L \times \mathrm{U}(1)_Y$ local symmetry through the covariant derivative appearing in the kinetic term of the Higgs Lagrangian,

$$\mathcal{L}_{\rm Higgs} = (D_\mu\Phi)^\dagger(D^\mu\Phi) - V(\Phi)\,, \tag{11.4}$$

where $D_\mu\Phi = (\partial_\mu + ig\sigma^a W^a_\mu/2 + ig'YB_\mu/2)\Phi$, g and g' are the SU(2) and U(1) gauge couplings, respectively, and $\sigma^a, a = 1,2,3$ are the usual Pauli matrices. As a result, the neutral and the two charged massless Goldstone degrees of freedom mix with the gauge fields corresponding to the broken generators of $\mathrm{SU}(2)_L \times \mathrm{U}(1)_Y$ and become, in the unitarity gauge, the longitudinal components of the Z and W physical gauge bosons, respectively. The Z and W gauge bosons acquire masses,

$$m_W^2 = \frac{g^2v^2}{4}\,, \quad m_Z^2 = \frac{(g'^2 + g^2)v^2}{4}. \tag{11.5}$$

The fourth generator remains unbroken since it is the one associated to the conserved $\mathrm{U}(1)_{\rm em}$ gauge symmetry, and its corresponding gauge field, the photon, remains massless.

Similarly the eight color gauge bosons, the gluons, corresponding to the conserved $SU(3)_C$ gauge symmetry with 8 unbroken generators, also remain massless. Hence, from the initial four degrees of freedom of the Higgs field, two are absorbed by the $W^\pm$ gauge bosons, one by the Z gauge boson, and there is one remaining degree of freedom, H, that is the physical Higgs boson — a new scalar particle. The Higgs boson is neutral under the electromagnetic interactions and transforms as a singlet under $SU(3)_C$ and hence does not couple at tree level to the massless photons and gluons.

The fermions of the SM acquire mass through renormalizable interactions between the Higgs field and the fermions: the Yukawa interactions,

$$\mathcal{L}_{\text{Yukawa}} = -\hat{h}_{d_{ij}} \bar{q}_{L_i} \Phi \; d_{R_j} - \hat{h}_{u_{ij}} \bar{q}_{L_i} \tilde{\Phi} u_{R_j} - \hat{h}_{l_{ij}} \bar{l}_{L_i} \Phi \; e_{R_j} + h.c., \tag{11.6}$$

which respect the symmetries of the SM but generate fermion masses once EWSB occurs. In the above, $\tilde{\Phi} = i\sigma_2 \Phi^*$ and q_L (l_L) and u_R, d_R (e_R) are the quark (lepton) $SU(2)_L$ doublets and singlets, respectively, while each term is parametrized by a 3×3 matrix in family space. The mass term for neutrinos is omitted, but could be added in an analogous manner to the up-type quarks when right-handed neutrinos are supplementing the SM particle content (neutrinos can also acquire Majorana masses via non-renormalizable dimension-5 interactions with the Higgs field). Once the Higgs acquires a VEV, and after rotation to the fermion mass eigenstate basis that also diagonalizes the Higgs-fermion interactions, $\hat{h}_{f_{ij}} \to h_{f_i} \delta_{ij}$, all fermions acquire a mass given by $m_{f_i} = h_{f_i} v/\sqrt{2}$. The indices $i, j = 1, 2, 3$ refer to the three families in the up-quark, down-quark or charged lepton sectors. It should be noted that the EWSB mechanism provides no additional insight on possible underlying reasons for the large variety of masses of the fermions, often referred to as the flavor hierarchy. The fermion masses, accounting for a large number of the free parameters of the SM, are simply translated into Yukawa couplings.

II.1. The SM Higgs boson mass, couplings and quantum numbers

The SM Higgs boson is a CP-even scalar of spin 0. Its mass is given by $m_H = \sqrt{2\lambda}\, v$, where λ is the Higgs self-coupling parameter in $V(\Phi)$. The expectation value of the Higgs field, $v = (\sqrt{2}G_F)^{-1/2} \approx 246\,\text{GeV}$, is fixed by the Fermi coupling G_F, which is determined with a precision of 0.6 ppm from muon decay measurements [22]. The quartic coupling λ is a free parameter in the SM, and hence, there is no a priori prediction for the Higgs mass. Moreover the sign of the mass parameter $m^2 = -\lambda v^2$ is crucial for the EW symmetry breaking to take place, but is not specified in the SM. The experimentally measured Higgs mass, $m_H \simeq 125\,\text{GeV}$, implies that $\lambda \simeq 0.13$ and $|m| \simeq 88.8\,\text{GeV}$.

The Higgs boson couplings to the fundamental particles are set by their masses. This is a new type of interaction; very weak for light particles, such as up and down quarks, and electrons, but strong for heavy particles such as the W and Z bosons and the top quark. More precisely, the SM Higgs couplings to fundamental fermions are linearly proportional to the fermion masses, whereas the couplings to bosons are proportional to the square of the boson masses. The SM Higgs boson couplings to gauge bosons and fermions, as well

as the Higgs boson self coupling, are summarized in the following Lagrangian:

$$\mathcal{L} = - g_{Hff}\bar{f}fH + \frac{g_{HHH}}{6}H^3 + \frac{g_{HHHH}}{24}H^4 + \delta_V V_\mu V^\mu \left(g_{HVV}H + \frac{g_{HHVV}}{2}H^2\right) \tag{11.7}$$

with

$$g_{Hf\bar{f}} = \frac{m_f}{v},\ g_{HVV} = \frac{2m_V^2}{v},\ g_{HHVV} = \frac{2m_V^2}{v^2},\ g_{HHH} = \frac{3m_H^2}{v},\ g_{HHHH} = \frac{3m_H^2}{v^2},$$

where $V = \mathrm{W}^\pm$ or Z and $\delta_W = 1, \delta_Z = 1/2$. As a result, the dominant mechanisms for Higgs boson production and decay involve the coupling of H to W, Z and/or the third generation quarks and leptons. The Higgs boson coupling to gluons [23, 24] is induced at leading order by a one-loop process in which H couples to a virtual $t\bar{t}$ pair. Likewise, the Higgs boson coupling to photons is also generated via loops, although in this case the one-loop graph with a virtual W^+W^- pair provides the dominant contribution [12] and the one involving a virtual $t\bar{t}$ pair is subdominant.

II.2. The SM custodial symmetry

The SM Higgs Lagrangian, $\mathcal{L}_{\text{Higgs}} + \mathcal{L}_{\text{Yukawa}}$ of Eq. (11.4) and Eq. (11.6), is, by construction, $\mathrm{SU}(2)_L \times \mathrm{U}(1)_Y$ gauge invariant, but it also has an approximate global symmetry. In the limit $g' \to 0$ and $h_f \to 0$, the Higgs sector has a global $\mathrm{SU}(2)_R$ symmetry, and hence in such a limit it is invariant under a global $\mathrm{SU}(2)_L \times \mathrm{SU}(2)_R$ symmetry, with $\mathrm{SU}(2)_L$ just being the global variant of the SM chiral gauge symmetry. This symmetry is preserved for non-vanishing Yukawa couplings, provided $h_u = h_d$. Once the Higgs acquires a VEV, both the $\mathrm{SU}(2)_L$ and $\mathrm{SU}(2)_R$ symmetry groups are broken but the diagonal subgroup $\mathrm{SU}(2)_{L+R}$ remains unbroken and is the subgroup that defines the custodial symmetry of the SM [25].

In the limit $g' \to 0$, the W and Z gauge bosons have equal mass and form a triplet of the $\mathrm{SU}(2)_{L+R}$ unbroken global symmetry. Using the expressions for the W and Z gauge boson masses in term of the gauge couplings, one obtains

$$\frac{m_W^2}{m_Z^2} = \frac{g^2}{g'^2 + g^2} = \cos^2\theta_W \quad \text{or} \quad \rho \equiv \frac{m_W^2}{m_Z^2 \cos^2\theta_W} = 1 \tag{11.8}$$

at tree level. The custodial symmetry protects the above relation between the W and Z masses under radiative corrections. All corrections to the ρ parameter are therefore proportional to terms that break the custodial symmetry. For instance, radiative corrections involving the Higgs are proportional to $\sin^2\theta_W$, $\delta\rho = -11 G_F m_Z^2 \sin^2\theta_W \log(m_H^2/m_Z^2)/(24\sqrt{2}\pi^2)$, and vanish in the limit $g \to 0$. Since $m_t \neq m_b$, there are also relevant radiative corrections generated by massive fermions. They are proportional to $m_t^2 + m_b^2 - 2(m_t^2 m_b^2)\log(m_t^2/m_b^2)/(m_t^2 - m_b^2)$ and would indeed vanish for $m_t = m_b$ [26].

II.3. Stability of the Higgs potential

The discovery of a scalar particle with mass $m_H \approx 125\,\text{GeV}$ has far reaching consequences within the SM framework. In particular, the precise value of m_H determines

the value of the quartic coupling λ at the electroweak scale and makes it possible to study its behavior up to high energy scales. A larger value of m_H would have implied that the Higgs self-coupling would become non-perturbative at some scale Λ that could be well below the Planck scale. Specifically, from the measured values of the Higgs, top, W and Z masses and of the strong gauge coupling, all within their experimental uncertainties, it follows that the Higgs quartic coupling remains perturbative all the way up to M_{Planck} [5, 6, 27], like the SM gauge and Yukawa couplings, thereby rendering the SM a consistent, calculable theory.

However, for the value of Higgs mass experimentally measured, the EW vacuum of the Higgs potential is most likely metastable. Indeed, the high energy evolution of λ shows that it becomes negative at energies $\Lambda = \mathcal{O}(10^{10} - 10^{12})$ GeV, with a broader range if the top quark mass exceeds its current measured value by 3σ. When this occurs, the SM Higgs potential develops an instability and the long term existence of the EW vacuum is challenged. This behavior may call for new physics at an intermediate scale before the instability develops, i.e., below M_{Planck} or, otherwise, the electroweak vacuum remains metastable [28]. Reference [29] studied how new physics at M_{Planck} could influence the stability of the EW vacuum and possibly modify this conclusion. The consequences of the instability of the EW vacuum on high-scale inflation have been discussed in Refs. [30].

Within the SM framework, the relevant question is the lifetime of the EW metastable vacuum that is determined by the rate of quantum tunneling from this vacuum into the true vacuum of the theory (for the most recent computation of the EW vacuum lifetime within the SM, see Refs. [31]). The running of the Higgs self coupling slows down at high energies with a cancellation of its β-function at energies just one to two orders of magnitude below the Planck scale [32, 33]. This slow evolution of the quartic coupling is responsible for saving the EW vacuum from premature collapse, allowing it to survive much longer times than those from astrophysical considerations. It might help the Higgs boson to play the role of an inflaton [34] (see, however, Ref. [35] and references therein for potential issues with this Higgs-as-an-inflaton idea).

II.4. Higgs production and decay mechanisms

Reviews of the SM Higgs boson's properties and phenomenology, with an emphasis on the impact of loop corrections to the Higgs boson decay rates and cross sections, can be found in Refs. [36–43]. The state-of-the-art of the theoretical calculations in the main different production channels is summarized in Table 11.1.

II.4.1. Production mechanisms at hadron colliders

The main production mechanisms at the Tevatron collider and the LHC are gluon fusion, weak-boson fusion, associated production with a gauge boson and associated production with a pair of $t\bar{t}$ quarks. Figure 11.1 depicts representative diagrams for these dominant Higgs production processes.

The cross sections for the production of a SM Higgs boson as a function of $\sqrt{s}$, the center of mass energy, for pp collisions, including bands indicating the theoretical uncertainties, are summarized in Fig. 11.2(left) [44]. A detailed discussion, including

Table 11.1: State-of-the-art of the theoretical calculations in the main Higgs production channels in the SM, and the major MC tools used in the simulations

ggF	VBF	VH	$t\bar{t}H$
Fixed order:	Fixed order:	Fixed order:	Fixed order:
NNLO QCD + NLO EW	NNLO QCD	NLO QCD+EW	NLO QCD
(HIGLU, iHixs, FeHiPro, HNNLO)	(VBF@NNLO)	(V2HV and HAWK)	(Powheg)
Resummed:	Fixed order:	Fixed order:	(MG5_aMC@NLO)
NNLO + NNLL QCD	NLO QCD + NLO EW	NNLO QCD	
(HRes)	(HAWK)	(VH@NNLO)	
Higgs p_T:			
NNLO+NNLL			
(HqT, HRes)			
Jet Veto:			
N3LO+NNLL			

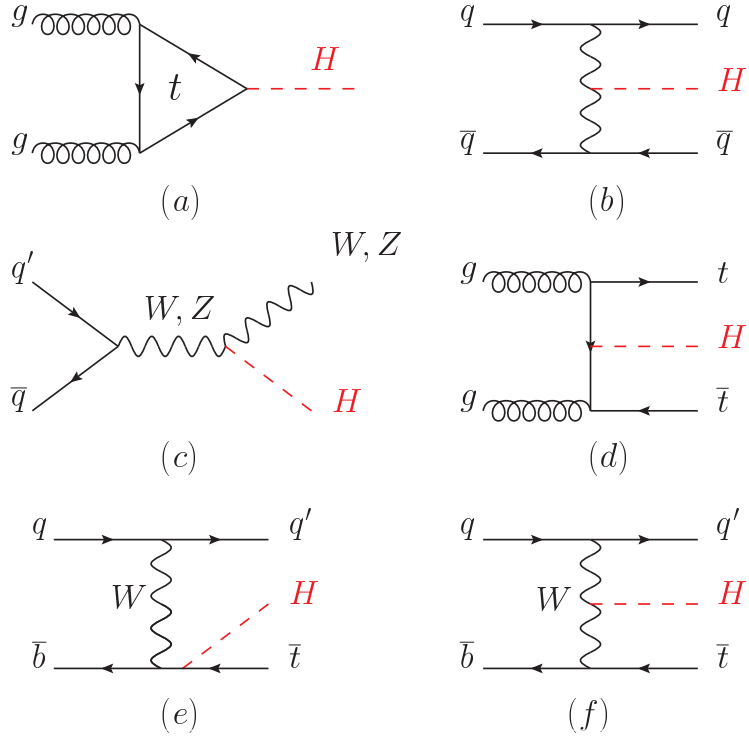

Figure 11.1: Main Leading Order Feynman diagrams contributing to the Higgs production in (a) gluon fusion, (b) Vector-boson fusion, (c) Higgs-strahlung (or associated production with a gauge boson), (d) associated production with a pair of top (or bottom) quarks, (e-f) production in association with a single top quark.

uncertainties in the theoretical calculations due to missing higher-order effects and

Table 11.2: The SM Higgs boson production cross sections for $m_H = 125\,\text{GeV}$ in pp collisions ($p\bar{p}$ collisions at $\sqrt{s} = 1.96\,\text{TeV}$ for the Tevatron), as a function of the center of mass energy, $\sqrt{s}$. The predictions for the LHC energies are taken from Refs. [40–43], the ones for the Tevatron energy are from Ref. [45]. The predictions for the ggF channel at the LHC include the latest N3LO results leading to reduced theoretical uncertainties by a factor around 2 compared to the N2LO results.

$\sqrt{s}$ (TeV)	Production cross section (in pb) for $m_H = 125\,\text{GeV}$					
	ggF	VBF	WH	ZH	$t\bar{t}H$	total
1.96	$0.95^{+17\%}_{-17\%}$	$0.065^{+8\%}_{-7\%}$	$0.13^{+8\%}_{-8\%}$	$0.079^{+8\%}_{-8\%}$	$0.004^{+10\%}_{-10\%}$	1.23
7	$16.9^{+5\%}_{-5\%}$	$1.24^{+2\%}_{-2\%}$	$0.58^{+3\%}_{-3\%}$	$0.34^{+4\%}_{-4\%}$	$0.09^{+8\%}_{-14\%}$	19.1
8	$21.4^{+5\%}_{-5\%}$	$1.60^{+2\%}_{-2\%}$	$0.70^{+3\%}_{-3\%}$	$0.42^{+5\%}_{-5\%}$	$0.13^{+8\%}_{-13\%}$	24.2
13	$48.6^{+5\%}_{-5\%}$	$3.78^{+2\%}_{-2\%}$	$1.37^{+2\%}_{-2\%}$	$0.88^{+5\%}_{-5\%}$	$0.50^{+9\%}_{-13\%}$	55.1
14	$54.7^{+5\%}_{-5\%}$	$4.28^{+2\%}_{-2\%}$	$1.51^{+2\%}_{-2\%}$	$0.99^{+5\%}_{-5\%}$	$0.60^{+9\%}_{-13\%}$	62.1

experimental uncertainties on the determination of SM parameters involved in the calculations can be found in Refs. [40–43]. These references also contain state-of-the-art discussions on the impact of PDF uncertainties, QCD scale uncertainties and uncertainties due to different procedures for including higher-order corrections matched to parton shower simulations as well as uncertainties due to hadronization and parton-shower events.

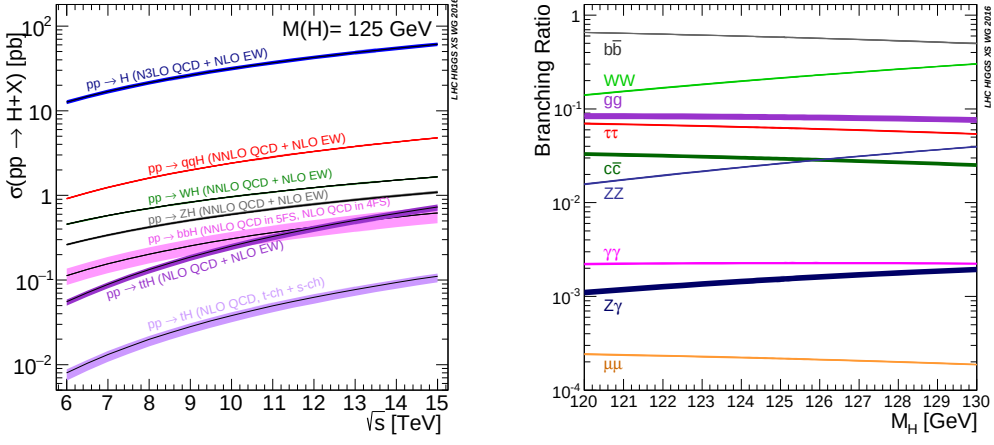

Figure 11.2: (Left) The SM Higgs boson production cross sections as a function of the center of mass energy, $\sqrt{s}$, for pp collisions [44]. The VBF process is indicated here as qqH. The theoretical uncertainties are indicated as bands. (Right) The branching ratios for the main decays of the SM Higgs boson near $m_H = 125\,\text{GeV}$ [42, 43]. The theoretical uncertainties are indicated as bands.

Table 11.2, from Refs. [40–43], summarizes the Higgs boson production cross sections and relative uncertainties for a Higgs mass of 125 GeV, for $\sqrt{s} = 7$, 8, 13 and 14 TeV. The Higgs boson production cross sections in $p\bar{p}$ collisions at $\sqrt{s} = 1.96$ TeV for the Tevatron are obtained from Ref. [45].

(i) Gluon fusion production mechanism

At high-energy hadron colliders, the Higgs boson production mechanism with the largest cross section is the gluon-fusion process, $gg \to H + X$, mediated by the exchange of a virtual, heavy top quark [46]. Contributions from lighter quarks propagating in the loop are suppressed proportional to m_q^2. QCD radiative corrections to the gluon-fusion process are very important and have been studied in detail. Including the full dependence on the (top, bottom, charm) quark and Higgs boson masses, the cross section has been calculated at the next-to-leading order (NLO) in α_s [47, 48]. To a very good approximation, the leading top-quark contribution can be evaluated in the limit $m_t \to \infty$ by matching the SM to an effective theory. The gluon-fusion amplitude is then evaluated from an effective Lagrangian containing a local $HG^a_{\mu\nu}G^{a\,\mu\nu}$ operator [23, 24]. In this approximation the cross section is known at NLO [49], at next-to-next-to-leading order (NNLO) [50], and recently the computation at next-to-next-to-next-to-leading order (N3LO) has been completed [51]. The validity of the effective theory with infinite m_t is greatly enhanced by rescaling the result by the exact LO result: $\sigma = (\sigma^{LO}_{m_t}/\sigma^{LO}_{m_t=\infty}) \times \sigma_{m_t=\infty}$ [43]. The large top-quark mass approximation after this rescaling of the cross section yields NNLO calculations that has been established to be at the percent level accuracy by means of approximate calculations of the m_t dependence based on asymptotic expansions [52].

The LO and NLO QCD corrections amount to about 80% of the total cross section at N3LO given below. The NNLO corrections further enhance the cross section by approximately 30% of the LO plus NLO result (at $\mu_f = \mu_r = m_H/2$). Electroweak radiative corrections have been computed at NLO and increase the LO cross section by about 5% for $m_H \simeq 125$ GeV [53]. Mixed QCD-electroweak corrections of $O(\alpha\alpha_s)$ are presently unknown [43].

The NLO and NNLO fixed-order QCD predictions for the gluon-fusion cross section have been improved by resumming the soft, virtual and collinear gluon contributions to the cross section at next-to-next-to-leading logarithmic (NNLL) and partial NNNLL accuracy [55]. Precise predictions for the gluon-fusion cross section for different Higgs boson masses and LHC energies, and including detailed error estimates, have been obtained by combining the NNLO fixed-order QCD results with soft-gluon resummation at NNLL or NNNLL accuracy and two-loop electroweak corrections, and using the most recent sets of parton distribution functions [54, 56].

The perturbative QCD computation has been recently extended to N3LO. At this order the perturbation series is rather stable with a mere enhancement of 3% of the total cross section, with a central value quite insensitive to threshold resummation effects with the scale choice mentioned above [51, 57, 43]. At the LHC with a center-of-mass energy of 13 TeV, the most up-to-date value for the production cross section of a 125 GeV Higgs boson amounts to [43]

$$\sigma_{ggF}^{N3LO} = 48.6\,\text{pb}^{+2.2\,\text{pb}(+4.6\%)}_{-3.3\,\text{pb}(-6.7\%)}(\text{theory}) \pm 1.6\,\text{pb}(3.2\%)(\text{PDF} + \alpha_s).$$

Besides considering the inclusive Higgs boson production cross section at the LHC, it is important to study differential distributions in order to probe the properties of the Higgs boson in a detailed way. A more exclusive account of Higgs production is also required because experimental analyses often impose cuts on the final states in order to improve the signal-to-background ratio. To this end, it is useful to define benchmark cuts and compare the differential distributions obtained at various levels of theoretical accuracy (i.e., at NLO or NNLO) with Monte Carlo generators. Many search modes for the Higgs boson are carried out by separating the events according to the number of jets or the transverse momentum and rapidity of the Higgs boson. For $p_T < 30\,\text{GeV}$, predictions for the transverse-momentum distribution can only be trusted after large logarithms of the form $\alpha_s^n \ln^{2n-1}(m_H/p_T)$ have been resummed to all orders in perturbation theory [58]. This has been accomplished with NNLL accuracy [59], and the results have been matched onto the fixed-order prediction at NNLO [60]. Electroweak corrections have been studied in Ref. [61]. The effect of the non-zero quark mass on the transverse momentum spectrum has most recently been considered in Ref. [62], while the effect of the finite top mass on other differential observables has been studied in Refs. [63, 64]. There has been much activity in computing Higgs plus jet(s) production processes at NLO (see e.g. Refs. [65, 66] for associated production with one and two jets, respectively), and even at NNLO [67]. In addition, efforts to improve the calculation of the Higgs production cross section with a jet veto (the "0-jet bin") by resumming large logarithms of the form $\alpha_s^n \ln^{2n-1}(m_H/p_T^{\text{veto}})$ at NNLL order and beyond [68] have been made. Recently, reference results for the resummed cross section at NNLL have been combined with the N3LO result for the inclusive cross section to obtain accurate predictions for the jet-veto efficiency and zero-jet cross section [69]. Accurate predictions for the jet-veto cross section are required, e.g., to suppress the $t\bar{t}$ background in the $H \to WW$ channel [70].

(ii) Vector boson fusion production mechanism

The SM Higgs production mode with the second-largest cross section at the LHC is vector boson fusion (VBF). At the Tevatron collider, VBF also occurred, but for $m_H = 125\,\text{GeV}$ had a smaller cross section than Higgs production in association with a W or Z boson. Higgs production via VBF, $qq \to qqH$, proceeds by the scattering of two (anti-)quarks, mediated by t- or u-channel exchange of a W or Z boson, with the Higgs boson radiated off the weak-boson propagator. The scattered quarks give rise to two hard jets in the forward and backward regions of the detector. Because of the color-singlet nature of the weak-gauge boson exchange, gluon radiation from the central-rapidity regions is strongly suppressed. These characteristic features of VBF processes can be exploited to distinguish them from overwhelming QCD backgrounds, including gluon-fusion induced Higgs + 2 jet production, and from s-channel WH or ZH production with a hadronically decaying weak gauge boson. After the application of specific selection cuts, the VBF channel provides a clean environment, not only for Higgs searches but also for the determination of Higgs boson couplings at the LHC [71].

Computations for total cross sections and differential distributions to Higgs production via VBF including NLO QCD and EW corrections have been presented in Refs. [37, 72] and are available in the form of flexible parton-level Monte-Carlo generators. Parton-shower effects have been considered in Ref. [73]. The NNLO QCD corrections to the total rate have been presented in Refs. [74]. They reduce the residual scale uncertainties on the inclusive cross section to approximately 2%. The uncertainties due to parton distributions are estimated to be at the same level. Fully differential predictions at NNLO have been computed recently [75], suggesting that the cross section under VBF cuts receives NNLO corrections that are larger than in the inclusive case and may reach O(5-6%).

(iii) WH and ZH associated production mechanism

The next most relevant Higgs boson production mechanisms after gluon fusion and VBF at the LHC, and the most relevant ones after gluon fusion at the Tevatron collider, are associated production with W and Z gauge bosons. The cross sections for the associated production processes, $pp \to VH + X$, with $V = W^{\pm}, Z$ receive contributions at NLO given by NLO QCD corrections to the Drell–Yan cross section [76–78] and from NLO EW corrections. The latter, unlike the QCD corrections, do not respect the factorization into Drell–Yan production since there are irreducible box contributions already at one loop [79]. At NNLO, the Drell-Yan-like corrections to WH production also give the bulk of the corrections to ZH production [80]. For ZH production there are, however, gluon-gluon induced contributions that do not involve a virtual Z gauge boson but are such that the Z gauge boson and H boson couple to gluons via top-quark loops [81]. In addition, WH and ZH production receive non Drell–Yan-like corrections in the $q\bar{q}'$ and $q\overline{q}$ initiated channels, respectively, at the NNLO level, where the Higgs is radiated off top-quark loops [82]. The full QCD corrections up to NNLO order, the NLO EW corrections and the NLO corrections to the gluon-gluon channel are available in VH@NNLO [83].

As neither the Higgs boson nor the weak gauge bosons are stable particles, their decays also have to be taken into account. Providing full kinematical information for the decay products can furthermore help in the suppression of large QCD backgrounds. Differential distributions for the processes $pp \to WH \to \nu_\ell \ell H$ and $pp \to ZH \to \ell^+\ell^- H/\nu_\ell \bar{\nu}_\ell H$, including NLO QCD and EW corrections, have been presented in Ref. [84]. The NNLO QCD corrections to differential observables for WH production at the LHC, including the leptonic decays of the W boson and the decay of the Higgs boson into a $b\bar{b}$ pair, are presented in Ref. [85]. Calculations at the same level, including also the ZH process have been performed [86, 87]. The WH production mode has also been matched to a parton shower at NNLO accuracy [88]. The WH and ZH production modes, together with Higgs production in association with a top-quark pair, provide a relatively clean environment for studying the decay of the Higgs boson into bottom quarks.

(iv) Higgs production in association with $t\bar{t}$

Higgs radiation off top quarks, $pp \to t\bar{t}H$, provides a direct probe of the top-Higgs Yukawa coupling. The LO cross section for this production process was computed in Ref. [89]. Later, the NLO QCD corrections [90] were evaluated yielding a moderate increase in the total cross section of at most 20%, but significantly reducing the scale

dependence of the inclusive cross section. The total theoretical errors, estimated by combining the uncertainties from factorization and renormalization scales, strong gauge coupling, and parton distributions, amount to 10–15% of the corresponding inclusive cross section. Interfaces between NLO QCD calculations for $t\bar{t}H$ production with parton-shower Monte Carlo programs have been provided in Ref. [91]. These programs provide the most flexible tools to date for the computation of differential distributions, including experimental selection cuts and vetoes on the final-state particles and their decay products.

(v) Other single Higgs production mechanisms at the LHC

The Higgs production in association with a single top quark, though subdominant, can bring valuable information, in particular regarding the sign of the top Yukawa coupling. This is due to an almost totally destructive interference between two large contributions, one where the Higgs couples to a space-like W boson and the other where it couples to the top quark. This process has been computed at NLO in a five-flavor scheme [92] and amounts to about 90 fb at $\sqrt{s} = 14\,\text{TeV}$ (with the opposite sign of the top Yukawa coupling, the cross section increases by one order of magnitude).

The Higgs boson production in association with bottom quarks is known at NNLO in the case of five quark flavors [93–95]. The coupling of the Higgs boson to a b quark is suppressed in the SM by the bottom-quark mass over the Higgs VEV, m_b/v, implying that associated production of a SM Higgs boson with b quarks is small at the LHC. Yet, at high energy, large logarithms are present and need to be resummed, leading to an enhancement of the inclusive cross section. At $\sqrt{s} = 14\,\text{TeV}$ the $b\bar{b}H$ cross section can be as large as 550 fb, still two orders of magnitude below the ggF production cross section. In a two Higgs doublet model or a supersymmetric model, which will be discussed in Section VII, this coupling is proportional to the ratio of neutral Higgs boson vacuum expectation values, $\tan\beta$, and can be significantly enhanced for large values of this ratio. Consequently, the $b\bar{b}H$ mode can even become the dominant production process for the Higgs boson.

The Higgs production in association with charm quarks is also known at NNLO and is about 85 fb at $\sqrt{s} = 13\,\text{TeV}$.

(vi) Double Higgs production at the LHC

The main interest in the double Higgs production is that it can provide invaluable information on the Higgs potential. In particular, it gives access to the Higgs cubic self-interaction. The dominant production is via gluon fusion $gg \to HH$. The NLO [96] and NNLO [97] fixed order corrections to $gg \to HH$ are known in the infinite top mass limit and, recently, the complete NLO corrections with all top quark mass effects also became available [98]. The QCD corrections are large, typically doubling the cross section from LO to NLO and further enhancing it by 20% from NLO to NNLO. At the differential level, the destructive interference between the box and the triangle contributions complicates the predictions made in the infinite top mass limit for both the HH invariant mass and the leading Higgs p_T distributions. With an inclusive cross section of about 40 fb at $\sqrt{s} = 13\,\text{TeV}$ and a difficult signal vs. background discrimination,

the double Higgs production remains a challenging channel to probe and will greatly benefit from the high-luminosity run of the LHC.

II.4.2. Production mechanisms at e^+e^- colliders

The main Higgs boson production cross sections at an e^+e^- collider are the Higgs-strahlung process $e^+e^- \to ZH$ [6, 23, 99], and the WW fusion process [100] $e^+e^- \to \bar{\nu}_e\nu_e W^*W^* \to \bar{\nu}_e\nu_e H$. The cross-section for the Higgs-strahlung process scales as s^{-1} and is dominant at low energies, while the cross-section for the WW fusion process scales as $\ln(s/m_H^2)$ and dominates at high energies [101–103]. The ZZ fusion mechanism, $e^+e^- \to e^+e^-Z^*Z^* \to e^+e^-H$, also contributes to Higgs boson production, with a cross-section suppressed by an order of magnitude with respect to that of WW fusion. The process $e^+e^- \to t\bar{t}H$ [104, 105] becomes important for $\sqrt{s} \geq 500\,\text{GeV}$. For a more detailed discussion of Higgs production properties at lepton colliders see, for example, Refs. [38, 39, 106, 107] and references therein.

II.4.3. SM Higgs branching ratios and total width

For the understanding and interpretation of the experimental results, the computation of all relevant Higgs decay widths is essential, including an estimate of their uncertainties and, when appropriate, the effects of Higgs decays into off-shell particles with successive decays into lighter SM ones. A Higgs mass of about 125 GeV allows to explore the Higgs couplings to many SM particles. In particular the dominant decay modes are $H \to b\bar{b}$ and $H \to WW^*$, followed by $H \to gg$, $H \to \tau^+\tau^-$, $H \to c\bar{c}$ and $H \to ZZ^*$. With much smaller rates follow the Higgs decays into $H \to \gamma\gamma$, $H \to \gamma Z$ and $H \to \mu^+\mu^-$. Since the decays into gluons, diphotons and $Z\gamma$ are loop induced, they provide indirect information on the Higgs couplings to WW, ZZ and $t\bar{t}$ in different combinations. The uncertainties in the branching ratios include the missing higher-order corrections in the theoretical calculations as well as the errors in the SM input parameters, in particular fermion masses and the QCD gauge coupling, involved in the decay. In the following the state-of-the-art of the theoretical calculations will be discussed and the reader is referred to Refs. [40, 41, 108] for detail.

The evaluation of the radiative corrections to the fermionic decays of the SM Higgs are implemented in HDECAY [109] at different levels of accuracy. The computations of the $H \to b\bar{b}$ and $H \to c\bar{c}$ decays include the complete massless QCD corrections up to N4LO, with a corresponding scale dependence of about 0.1% [110]. Both the electroweak corrections to $H \to b\bar{b}$, $c\bar{c}$ as well as $H \to \tau^+\tau^-$ are known at NLO [111] providing predictions with an overall accuracy of about 1-2% for $m_H \simeq 125\,\text{GeV}$.

The loop induced decays of the SM Higgs are known at NLO and partially beyond that approximation. For $H \to gg$, the QCD corrections are known up to N3LO in the limit of heavy top quarks [112, 48] and the uncertainty from the scale dependence is about 3%. For the $H \to \gamma\gamma$, the full NLO QCD corrections are available [48, 113] and the three-loop QCD corrections have also been evaluated [114]. The NLO electroweak corrections to $H \to gg$ and $H \to \gamma\gamma$ have been computed in Ref. [115]. All these corrections are implemented in HDECAY [109]. For $m_H = 125\,\text{GeV}$, the overall impact of known QCD and EW radiative effects turns out to be well below 1%. In addition, the contribution of

the $H \to \gamma e^+ e^-$ decay via virtual photon conversion has been computed in Ref. [116]. The partial decay width $H \to Z\gamma$ is only implemented at LO in HDECAY, including the virtual W, top-, bottom-, and τ-loop contributions. The QCD corrections have been calculated and are at the percent level [117], The theoretical uncertainty due to unknown electroweak corrections is estimated to be less than 5%, an accuracy that will be hard to achieve in measurements of this processes at the LHC.

The decays $H \to WW/ZZ \to 4f$ can be simulated with the Prophecy4f Monte-Carlo generator [118] that includes complete NLO QCD and EW corrections for Higgs decays into any possible four-fermion final state. All calculations are consistently performed with off-shell gauge bosons, without any on-shell approximation. For the SM Higgs boson the missing higher-order corrections are estimated to be roughly 0.5%. Such uncertainties will have to be combined with the parametric uncertainties, in particular those associated to the bottom-quark mass and the strong gauge coupling, to arrive at the full theory uncertainties. A detailed treatment of the differential distributions for a Higgs decay into four charged leptons in the final state is discussed in Refs. [42, 119].

The total width of a 125 GeV SM Higgs boson is $\Gamma_H = 4.07 \times 10^{-3}\,\text{GeV}$, with a relative uncertainty of $^{+4.0\%}_{-3.9\%}$. The branching ratios for the most relevant decay modes of the SM Higgs boson as a function of m_H, including the most recent theoretical uncertainties, are shown in Fig. 11.2(right) and listed for $m_H = 125\,\text{GeV}$ in Table 11.3. Further details of these calculations can be found in Refs. [108, 120] and in the reviews [37–43].

Table 11.3: The branching ratios and the relative uncertainty [42, 43] for a SM Higgs boson with $m_H = 125\,\text{GeV}$.

Decay channel	Branching ratio	Rel. uncertainty
$H \to \gamma\gamma$	2.27×10^{-3}	$^{+5.0\%}_{-4.9\%}$
$H \to ZZ$	2.62×10^{-2}	$^{+4.3\%}_{-4.1\%}$
$H \to W^+W^-$	2.14×10^{-1}	$^{+4.3\%}_{-4.2\%}$
$H \to \tau^+\tau^-$	6.27×10^{-2}	$^{+5.7\%}_{-5.7\%}$
$H \to b\bar{b}$	5.84×10^{-1}	$^{+3.2\%}_{-3.3\%}$
$H \to Z\gamma$	1.53×10^{-3}	$^{+9.0\%}_{-8.9\%}$
$H \to \mu^+\mu^-$	2.18×10^{-4}	$^{+6.0\%}_{-5.9\%}$

III. The experimental profile of the Higgs boson

An indirect experimental bound on the SM Higgs boson can be obtained by comparing precision electroweak data with SM predictions, that have a weak, logarithmic dependence

on M_H. A global fit to electroweak data suggests $m_H = 96^{+22}_{-19}\,\text{GeV}$, or $m_H < 134\,\text{GeV}$ at 90% confidence level [121].

The announcement on July 4, 2012 of the observation [1, 2] at the LHC of a narrow resonance with a mass of about 125 GeV was an important landmark in the decades-long direct search [122, 123] for the SM Higgs boson. This was followed by a detailed exploration of properties of the Higgs boson at the different runs of the LHC at $\sqrt{s} = 7$, 8 and 13 TeV.

The dataset delivered so far by LHC, while the Run 2 is still ongoing, corresponds to an integrated luminsoity exceeding $100\,\text{fb}^{-1}$ see Table 11.4. The datasets effectively useful for analysis need to take into account the data-taking efficiency with fully operational detecors and the data quality efficiency. The typical total inefficiency for both the ATLAS and CMS experiments are approximately 10%.

Table 11.4: The LHC running conditions and delivered data samples.

Year	$\sqrt{s}$ (TeV)	$\int$ L.dt (fb^{-1})	Run Period
2010	7	0.04	Run 1
2011	7	6.1	Run 1
2012	8	23.3	Run 1
2015	13	4.2	Run 2
2016	13	40.8	Run 2
2017	13	in progress (> 40)	Run 2

III.1. The principal decay channels to vector bosons

For a given m_H, the sensitivity of a search channel depends on the production cross section of the Higgs boson, its decay branching fraction, reconstructed mass resolution, selection efficiency and the level of background in the final state. For a low-mass Higgs boson ($110\,\text{GeV} < m_H < 150\,\text{GeV}$) where the natural width is only a few MeV, five decay channels play an important role at the LHC. In the $H \to \gamma\gamma$ and $H \to ZZ \to 4\ell$ channels, all final state particles can be very precisely measured and the reconstructed m_H resolution is excellent (typically 1-2%). While the $H \to W^+W^- \to \ell^+\nu_\ell\ell'^-\bar{\nu}_{\ell'}$ channel has relatively large branching fraction, the m_H resolution is poor (approximately 20%) due to the presence of neutrinos. The $H \to b\bar{b}$ and the $H \to \tau^+\tau^-$ channels suffer from large backgrounds and a intermediate mass resolution of about 10% and 15% respectively. For $m_H > 150\,\text{GeV}$, the sensitive search channels are $H \to WW$ and $H \to ZZ$ where the W or Z boson decays into a variety of leptonic and hadronic final states. These decay channels of the Higgs boson are searched for in the five Higgs boson production processes (ggF, VBF, WH, ZH and $t\bar{t}H$) described in Section II.4.1.

The candidate events in each Higgs boson decay channel are split into several mutually exclusive categories (or event tags) based on the specific topological, kinematic or other

features present in the event. The categorization of events increases the sensitivity of the overall analysis and allows a separation of different Higgs boson production processes. Most categories are dominated by signal from one Higgs decay mode but contain an admixture of various Higgs production processes. For example, a typical VBF selection requires Higgs boson candidates to be accompanied by two energetic jets ($\geq 30\,\text{GeV}$) with a large dijet mass ($\geq 400\,\text{GeV}$) and separated by a large pseudorapidity ($\Delta\eta_{jj} \geq 3.5$). While such a category is enriched in Higgs bosons produced via VBF, the contamination from the gluon fusion production mechanism can be significant. Hence a measurement of the signal rate in the VBF category does not imply a measurement of VBF production cross-section. Simulations are used to determine the relative contributions of the various Higgs production modes in a particular category.

III.1.1. $H \to \gamma\gamma$

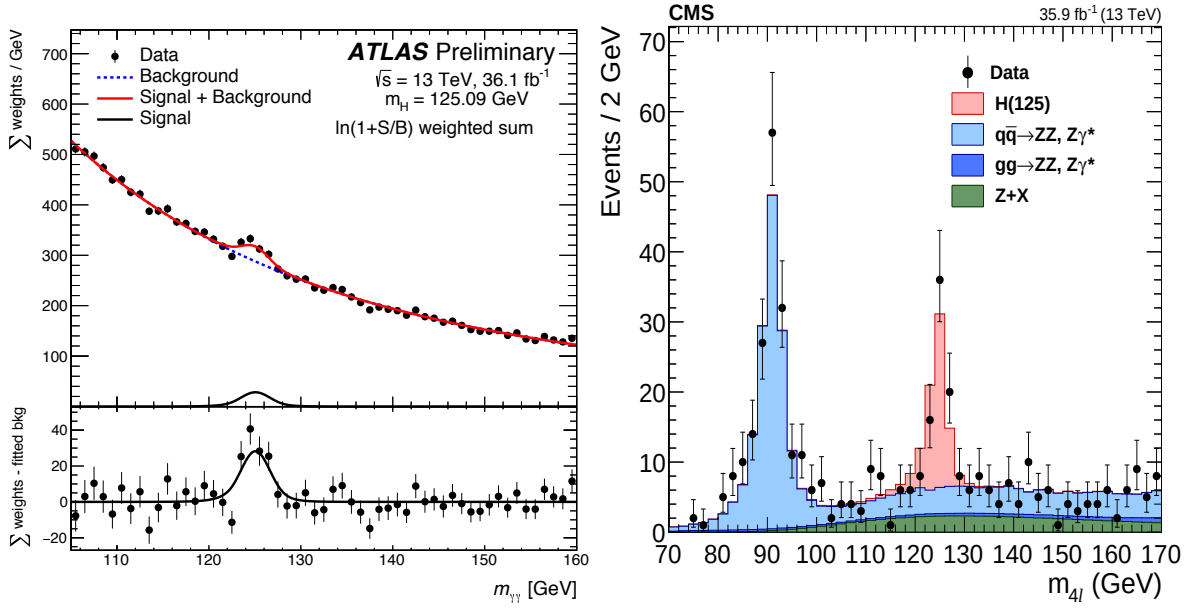

Figure 11.3: (Left) The invariant mass distribution of diphoton candidates, with each event weighted by the ratio of signal-to-background in each event category, observed by ATLAS [124] at Run 2. The residuals of the data with respect to the fitted background are displayed in the lower panel. (Right) The $m_{4\ell}$ distribution from CMS [125] Run 2 data.

In the $H \to \gamma\gamma$ channel a search is performed for a narrow peak over a smoothly falling background in the invariant mass distribution of two high p_T photons. The background in this channel is conspicuous and stems from prompt $\gamma\gamma$ processes for the irreducible backgrounds, and the γ+jet and dijet processes for the reducible backgrounds where one jet fragments typically into a leading π^0. In order to optimize search sensitivity and also to separate the various Higgs production modes, ATLAS and CMS experiments split events into several mutually exclusive categories. Diphoton events containing a high p_T

muon or electron, or missing energy ($E_T^{\rm miss}$) consistent with the decay of a W or Z boson are tagged in the VH production category. Diphoton events containing energetic dijets with a large mass and pseudorapidity difference are assigned to the VBF production category, and the remaining events are considered either in the VH category when the two jets are compatible with the hadronic decay of a W or a Z, or in the gluon fusion production category. While the leptonic VH category is relatively pure, the VBF category has significant contamination from the gluon fusion process. Events which are not picked by any of the above selections are further categorized according to their expected $m_{\gamma\gamma}$ resolution and signal-to-background ratio. Categories with good m_H resolution and larger signal-to-background ratio contribute most to the sensitivity of the search.

Both ATLAS and CMS have studied in detail the calibration of the energy response of photons, in particular using $Z \to e^+e^-$, $Z \to \mu^+\mu^-\gamma$ and the response of muons in the calorimeter (for ATLAS) from $Z \to \mu^+\mu^-$ events. This information is used to correct the simulated signal mass lineshapes. In each category, parametric signal models are adjusted to these lineshape to provide a functional form for the signal. Simple monotonic functional forms of the backgrounds are determined by a fit to the $m_{\gamma\gamma}$ distribution in each category. All categories are fitted simultaneously to determine the signal yield at the measured combined Run 1 mass of 125.09 GeV discussed in Section III.2. The $m_{\gamma\gamma}$ distribution after combining all categories is shown for the ATLAS experiment in Fig. 11.3 using Run 2 data.

The signal strength $\mu = (\sigma \cdot {\rm BR})_{\rm obs}/(\sigma \cdot {\rm BR})_{\rm SM}$, which is the observed product of the Higgs boson production cross section (σ) and its branching ratio (BR) in units of the corresponding SM values, is 1.17 ± 0.27 for ATLAS [126] in Run 1 and 0.99 ± 0.14 in Run 2 [124]. The signal strengths [2] measured in Run 1 and Run 2 by the CMS collaboration are $0.78^{+0.26}_{-0.23}$ [127] and $1.16^{+0.15}_{-0.14}$ [128] respectively.

III.1.2. $H \to ZZ^* \to \ell^+\ell^-\ell'^+\ell'^-$

In the $H \to ZZ^* \to \ell^+\ell^-\ell'^+\ell'^-$ channel a search is performed for a narrow mass peak over a small continuous background dominated by non-resonant ZZ^* production from $q\overline{q}$ annihilation and gg fusion processes. The contribution and the shape of this irreducible background is taken from simulation. The subdominant and reducible backgrounds stem from $Z + b\bar{b}$, $t\bar{t}$ and $Z +$ jets events. Their contribution is suppressed by requirements on lepton isolation and lepton impact parameter and their yield is estimated from control samples in data.

To help distinguish the Higgs signal from the dominant non-resonant ZZ^* background, both ATLAS [129] and CMS [130] use a matrix element likelihood approach to construct a kinematic discriminant built for each 4ℓ event based on the ratio of complete leading-order matrix elements $|{\mathcal{M}_{sig}}^2/{\mathcal{M}_{bkg}}^2|$ for the signal ($gg \to H \to 4\ell$) and background($q\overline{q} \to ZZ \to 4\ell$) hypotheses. The signal matrix element $\mathcal{M}_{sig}$ is computed assuming $m_H = m_{4\ell}$. To further enhance the sensitivity to a signal, various techniques are used by the experiments based on the matrix element or a multivariate analyses.

[2] The Run 1 results for the ATLAS and CMS experiments are at fixed values of $m_H =$ 125.4 GeV and 124.7 GeV.respectively.

To enhance the sensitivity to VBF and VH production processes, the ATLAS and CMS experiments divide 4ℓ events into mutually exclusive categories. Events containing dijets with a large mass and pseudorapidity difference populate the VBF category. ATLAS requires the presence of an additional lepton in the VH category. In events with less than two jets, CMS uses the $p_T^{4\ell}$ to distinguish between production via the gluon fusion and the VH/VBF processes.

Since the $m_{4\ell}$ resolutions and the reducible background levels are different in the 4μ, $4e$ and $2e2\mu$ subchannels, they are analyzed separately and the results are then combined. The distribution of the reconstructed invariant mass of the four leptons for the CMS experiment [125] is given in Fig. 11.3 (right), showing a clear excess at a mass of approximately $m_H = 125\,\text{GeV}$. Both experiments also observe a clear peak at $m_{4\ell} = 91\,\text{GeV}$ from the production of a Z boson on-mass-shell and decaying to four leptons due typically to the emission of an off-shell photon from one of the primary leptons from the Z boson decay.

The signal strengths μ for the inclusive $H \to 4\ell$ production measured by the ATLAS and CMS experiments are $1.44^{+0.40}_{-0.33}$ at $m_H = 125.36\,\text{GeV}$ [129] and $0.93^{+0.29}_{-0.25}$ at $m_H = 125.6\,\text{GeV}$ [131] respectively, in Run 1. The signal strengths measured by the ATLAS and CMS experiments in Run 2 are $1.28^{+0.21}_{-0.19}$ [132] and $1.05^{+0.19}_{-0.25}$ [125] respectively, both measurements are made at the combined Run 1 Higgs mass of $m_H = 125.09\,\text{GeV}$.

III.1.3. Measurement of the Higgs boson mass

To measure the mass of the Higgs boson, ATLAS and CMS collaborations rely on the two high mass resolution and sensitive channels, $\gamma\gamma$ and ZZ. The ATLAS & CMS approaches are very similar in these two analyses with small differences on the usage of categories, additional discriminating variables and per-event errors. In these two channels the mass resolutions range from 1.4 GeV to 2 GeV for ATLAS and from 1.0 GeV to 2.8 GeV for CMS. The best mass resolution is obtained for both experiments in the diphoton channel for central diphoton pairs (typically for events where both photons are not converted). The signal strengths in the $\gamma\gamma$ and ZZ channels are assumed to be independent and not constrained to the expected rate ($\mu = 1$) for the SM Higgs boson.

Figure 11.4 summarizes all measurements of the Higgs boson mass, including the individual and combined Run 1 measurements [133] and preliminary Run 2 measurement by ATLAS [134] for both the diphoton and the 4ℓ channels and CMS [125] for the 4ℓ channel. The CMS collaboration has also reported a preliminary best fit mass in the diphoton channel of $m_H = 125.4\,\text{GeV}$ with a statistical uncertainty of 150 MeV and a systematic uncertainty preliminarily evaluated as between 200 MeV and 300 MeV

In the diphoton channel, as discussed in Section V.3.2 a mass shift is expected to be induced by the deformation of the mass lineshape of the signal in presence of background, from the interference between the Higgs boson production and the continuum irreducible background. It is a small but non negligible effect of approximately 35 MeV [135] for a Higgs boson width close to that of the SM. This effect could be larger if the width of the discovered particle were to be completely different. This effect estimated by ATLAS with

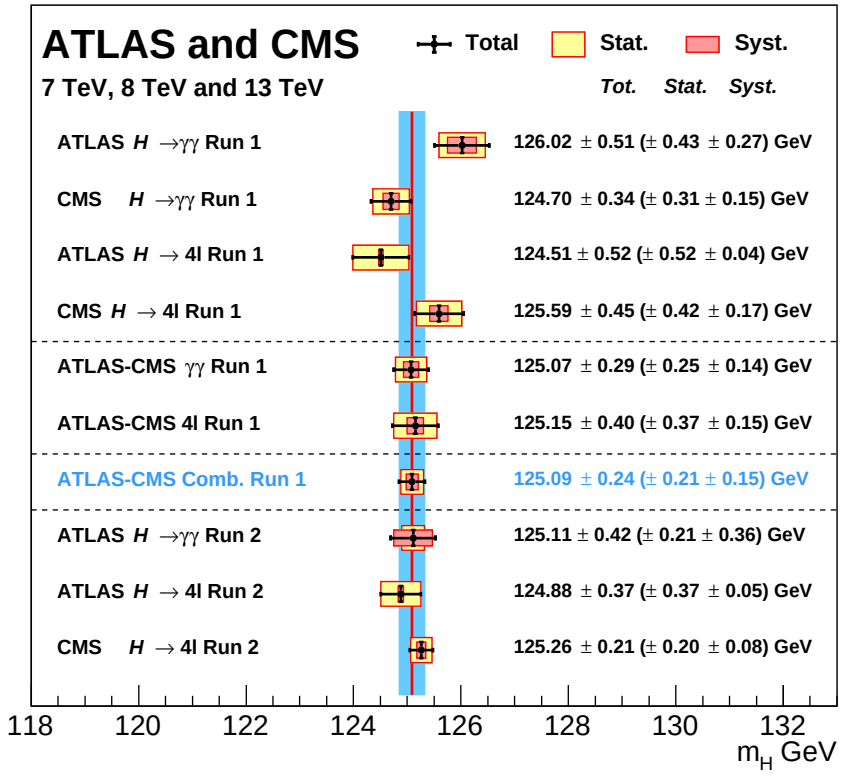

Figure 11.4: Summary of the CMS and ATLAS mass measurements in the $\gamma\gamma$ and ZZ channels in Run 1 and Run 2.

a full simulation is still relatively small with respect to the total uncertainty on the mass and is therefore neglected.

III.1.4. $H \to W^+W^- \to \ell^+\nu\ell^-\overline{\nu}$

In this intricate channel, experiments search for an excess of events with two leptons of opposite charge accompanied by missing energy and up to two jets. Events are divided into several categories depending on the lepton flavor combination (e^+e^-, $\mu^+\mu^-$and $e^\pm\mu^\mp$) and the number of accompanying jets ($N_{\text{jet}} = 0, 1, \geq 2$). The $N_{\text{jet}} \geq 2$ category is optimized for the VBF production process by selecting two leading jets with a large pseudorapidity difference and with a large mass ($m_{jj} > 500\,\text{GeV}$).

Backgrounds contributing to this channel are numerous and depend on the category of selected events. Reducing them and accurately estimating the remainder is a major challenge in this analysis. For events with opposite-flavor lepton and no accompanying high p_T jets, the dominant background stems from non-resonant WW production. Events with same-flavor leptons suffer from large Drell–Yan contamination. The $t\overline{t}$, Wt and W + jets (with the jet misidentified as a lepton) events contaminate all categories. Non-resonant WZ, ZZ and $W\gamma$ processes also contribute to the background at a sub-leading level.

A requirement of large missing transverse energy ($E_T^{\rm miss}$) is used to reduce the Drell–Yan and multijet backgrounds. In the e^+e^- and $\mu^+\mu^-$ categories, events with $m_{\ell\ell}$ consistent with the Z mass are vetoed. The $t\bar{t}$ background is suppressed by a veto against identified b-jets or low p_T muons (assumed to be coming from semileptonic b-hadron decays within jets) and tight isolation requirements diminish the W+jets background. The scalar nature of the Higgs boson and the $V-A$ nature of the W boson decay implies that the two charged leptons in the final state are preferentially emitted at small angles with respect to each other. Therefore the dilepton invariant mass ($m_{\ell\ell}$) and the azimuthal angle difference between the leptons ($\Delta\phi_{\ell\ell}$) are used to discriminate between the signal and non-resonant WW events. The transverse mass, constructed from the dilepton p_T ($p_T^{\ell\ell}$), $E_T^{\rm miss}$ and the azimuthal angle between $E_T^{\rm miss}$ and $p_T^{\ell\ell}$, is defined as $m_T = \sqrt{2p_T^{\ell\ell}E_T^{\rm miss}(1-\cos\Delta\phi_{E_T^{\rm miss}\ell\ell})}$ and serves as an effective discriminant against backgrounds. The transverse mass variable also tracks the Higgs boson mass but with a poor mass resolution. All residual background rates except for the small contributions from non-resonant WZ, ZZ and $W\gamma$ are evaluated from control samples devised from data.

ATLAS fits the m_T distributions and observes [136] an excess at $m_H = 125.36\,\text{GeV}$ with a local significance of 6.1σ similar to that expected from a 125 GeV SM Higgs boson. The measured inclusive signal strength is $\mu = 1.09^{+0.23}_{-0.21}$. In the VBF category an excess with a significance of 3.2σ corresponding to a signal strength of $\mu = 1.27^{+0.53}_{-0.45}$ is observed [136]. The CMS analysis of 0 and 1 jet categories, using all lepton flavor combinations, shows [137] an excess with an observed significance of 4.3σ, lower than the expected sensitivity of 5.8σ for a 125.6 GeV SM Higgs boson. CMS observes [137] no significant excess in the VBF production mode and sets a 95% CL limit on the signal strength of $\mu_{\rm VBF} < 1.7$ for $m_H = 125.6\,\text{GeV}$.

The ATLAS and CMS experiments have also searched for the associated Higgs boson production (VH) in this channel. The signal consists of up to three (WH) or four (ZH) high p_T isolated leptons with missing transverse energy and low hadronic activity. The major backgrounds stem from triboson and diboson production where each boson decays leptonically. ATLAS observes [138] an excess at $m_H = 125.36\,\text{GeV}$ with a local significance of 2.5σ corresponding to a $\mu_{VH} = 3.0^{+1.6}_{-1.0}$. CMS instead sets [137] a 95% CL limit of $\mu_{VH} < 4.7$.

In this channel the full Run 2 dataset has not yet been analysed by ATLAS or CMS. The main results are still from Run 1 [136, 137]. There have been partial analyses made with Run 2 data at 13 TeV by both the ATLAS and CMS experiments. The former has analyzed the WW decay mode in the VBF and VH production mode with 2015 dataset corresponding to an integrated luminosity of $5.8\,\text{fb}^{-1}$ [139]. The latter has performed a more complete analysis with the full 2015 dataset and $15.2\,\text{fb}^{-1}$ of 2016 data, with most production channels covered in the cleaner opposite flavor electron-muon decay mode of the WW pair [140].

III.2. Decays to fermions

At hadron colliders, the most promising channel for probing the coupling of the Higgs

field to the quarks and leptons are $H \to b\bar{b}$ and $H \to \tau^+\tau^-$, respectively. For a Higgs boson with $m_H \approx 125\,\text{GeV}$, the branching fraction to $b\bar{b}$ is about 57% and to $\tau^+\tau^-$ is about 6%. Nevertheless, the presence of very large backgrounds makes the isolation of a Higgs boson signal in these channels quite challenging.

III.2.1. $H \to \tau^+\tau^-$

In the $H \to \tau\tau$ search, τ leptons decaying to electrons (τ_e), muons (τ_μ) and hadrons (τ_{had}) are considered. The $\tau^+\tau^-$ invariant mass ($m_{\tau\tau}$) is reconstructed from a kinematic fit of the visible products from the two τ leptons and the missing energy observed in the event. Due to the presence of missing neutrinos, the $m_{\tau^+\tau^-}$ resolution is poor ($\approx 15\%$). As a result, a broad excess over the expected background in the $m_{\tau\tau}$ distribution is searched for. The major sources of background stem from Drell–Yan $Z \to \tau^+\tau^-$ and $Z \to e^+e^-$, W+jets, $t\bar{t}$ and multijet production. Events in all subchannels are divided into categories based on the number and kinematic properties of additional energetic jets in the event. The sensitivity of the search is generally higher for categories with one or more additional jets. The VBF category, consisting of a τ pair with two energetic jets separated by a large pseudorapidity, has the best signal-to-background ratio and search sensitivity, followed by the $\tau^+\tau^-$+1 jet category. The signal to background discrimination relies in part on the $m_{\tau\tau}$ resolution, which improves with the boost of the Higgs boson. The non-VBF categories are further subdivided according to the observed boost of the $\tau^+\tau^-$ system. CMS primarily uses the reconstructed $m_{\tau\tau}$ as the final discriminating variable [141] while the ATLAS experiment combines various kinematic properties of each event categories with multivariate techniques to build the final discriminant [142].

Searches for $H \to \tau^+\tau^-$ decays in the VH production mode are also performed in final states where the W or Z boson decays into leptons or jets. The irreducible background in this search arises from non-resonant WZ and ZZ diboson production. The reducible backgrounds originate from W, Z, and $t\bar{t}$ events that contain at least one fake lepton in the final state due to a misidentified jet. The shape and yield of the major backgrounds in each category is estimated from control samples in data. Contributions from non-resonant WZ and ZZ diboson production are estimated from simulations but corrected for reconstruction efficiency using control samples formed from observed data.

For the CMS experiment, the significance of the observed excess at $m_H = 125\,\text{GeV}$ in Run 1 is 3.2 standard deviations, close to the expected 3.7 standard deviations sensitivity, and corresponds to a signal strength of $\mu = 0.86 \pm 0.29$. The observed (expected) deviation from the background-only hypothesis in ATLAS corresponds to a local significance of 4.5 (3.4) standard deviations and the best fit value of the signal strength is $\mu = 1.43^{+0.43}_{-0.37}$ [142].

When the ATLAS and CMS $H \to \tau\tau$ Run 1 measurements are combined [143], the significance of the observed excess corresponding to $m_H = 125.09\,\text{GeV}$ is 5.5 standard deviations and the combined signal strength is $\mu = 1.11^{+0.24}_{-0.22}$, consistent with the Standard Model expectation.

In the CMS analysis of 2016 data [144], the strategy was improved using additional categories aiming at the inclusive production of the Higgs boson and binned in transverse momentum of the $\tau^+\tau^-$ system, and for the VBF production, the analysis is binned as a

function of the dijet mass. This analysis reached a sensitivity of 4.7 standard deviations with a dataset corresponding to an integrated luminosity of $35.9\,\text{fb}^{-1}$. CMS observes an excess with a significance of 4.9 standard deviations. In conjunction with the Run 1 results, this provides an unambiguous observation of the direct coupling of the Higgs boson to taus, in the vector boson fusion production mode.

III.2.2. $H \to b\bar{b}$

In the search for the decay of the Higgs boson to a pair of b-quarks the most sensitive production modes are the associated WH and ZH processes allowing use of the leptonic W and Z decays for triggering, and to purify the signal and reject QCD backgrounds. The W bosons are reconstructed via their leptonic decay $W \to \ell\bar{\nu}_\ell$ where $\ell = e, \mu$ or τ. The Z bosons are reconstructed via their decay into $e^+e^-, \mu^+\mu^-$or $\nu\bar{\nu}$. The Higgs boson candidate mass is reconstructed from two b-tagged jets in the event. Backgrounds arise from production of W and Z bosons in association with gluon, light and heavy-flavored jets (V+jets), $t\bar{t}$, diboson (ZZ and WZ with $Z \to b\bar{b}$) and QCD multijet processes. Due to the limited $m_{b\bar{b}}$ mass resolution, a SM Higgs boson signal is expected to appear as a broad enhancement in the reconstructed dijet mass distribution. The crucial elements in this search are b-jet tagging with high efficiency and low fake rate, accurate estimate of b-jet momentum and estimate of backgrounds from various signal depleted control samples constructed from data.

At the Tevatron, the $H \to b\bar{b}$ channel contributes the majority of the Higgs boson search sensitivity below $m_H = 130\,\text{GeV}$. The CDF and D0 experiments use multivariate analysis (MVA) techniques that combine several discriminating variables into a single final discriminant used to separate signal from background. Each channel is divided into exclusive subchannels according to various lepton, jet multiplicity, and b-tagging characteristics in order to group events with similar signal-to-background ratio and thus optimize the overall search sensitivity. The combined CDF and D0 data show [145, 123] an excess of events with respect to the predicted background in the 115–140 GeV mass range in the most sensitive bins of the discriminant distributions suggesting the potential presence of a signal. At $m_H = 125\,\text{GeV}$ the observed signal strength $\mu = 1.59^{+0.69}_{-0.72}$.

In order to reduce the dominant V+jets background at the LHC, following Ref. [146], experiments select a region in the VH production phase space where the vector boson is significantly boosted and recoils from the $H \to b\bar{b}$ candidate with a large azimuthal angle $\Delta\phi_{VH}$. For each channel, events are categorized into different $p_T(V)$ regions with varying signal/background ratios. Events with higher $p_T(V)$ have smaller backgrounds and better $m_{b\bar{b}}$ resolution. CMS uses [147] MVA classifiers based on kinematic, topological and quality of b-jet tagging and trained on different values of m_H to separate Higgs boson signal in each category from backgrounds. The MVA outputs for all categories are then fit simultaneously.

The nominal results from ATLAS are also based on a combination [148] of (i) a multivariate analysis of their 8 TeV data, incorporating various kinematic variables in addition to $m_{b\bar{b}}$ and b-tagging information and (ii) a statistical analysis of their 7 TeV data centered on $m_{b\bar{b}}$ as the main discriminant. In both cases customized control samples devised from data are used to constrain the contributions of the dominant

$H \to b\bar{b}$	Tevatron	ATLAS Run 1	CMS Run 1	ATLAS Run 2	CMS Run 2
VH	1.6 ± 0.7	$0.52 \pm 0.32 \pm 0.24$	1.0 ± 0.5	$1.20 \pm 0.24 \pm 0.28$	1.2 ± 0.4
VBF	—	-0.8 ± 2.3	$2.8 \pm 1.4 \pm 0.8$	-3.9 ± 2.8	-3.7 ± 2.7
ttH	—	$1.4 \pm 0.6 \pm 0.8$	0.7 ± 1.9	$2.1 \pm 0.5 \pm 0.9$	$1.19 \pm 0.5 \pm 0.7$
Inclusive	—	—	—	—	2.3 ± 1.7
PDG Comb.	1.6 ± 0.7	0.6 ± 0.4	1.1 ± 0.5	1.2 ± 0.3	1.2 ± 0.4

Table 11.5: Summary of the results of searches for a Higgs boson decaying to a pair of b-quarks by the ATLAS and CMS collaborations. The results are given in terms of measured signal strength. Where available the uncertainty the total uncertainty is reported as the statistical and systematic contributions separately and in this order.

background processes. The net observed(expected) deviation from background-only hypothesis corresponds to a significance of 1.4(2.6) standard deviations and a signal strength of $\mu = 0.5 \pm 0.4$.

In Run 2, both ATLAS and CMS have updated their results with similar analyses as those performed at Run 1. The larger dataset of approximately $36\,\text{fb}^{-1}$ of data collected in 2015 and 2016, and the increase in signal cross sections of nearly a factor of 3 at the centre-of-mass energy of 13 TeV with respect to 7 TeV, have brought the two experiment to achieve a sensitivity very close to that required to claim an evidence for this decay mode in the VH production. The expected significance for a SM Higgs boson is 3.0 standard deviations for ATLAS [149] and 2.8 standard deviations for CMS [150]. Both ATLAS and CMS observe significant excesses corresponding to 3.5 and 3.3 standard deviations respectively. When combined with results obtained in Run 1, the observed (expected) significance of the excesses are 3.6 (4.0) and 3.8 (3.8) standard deviations respectively. These results provide direct evidence for the Higgs boson decay to a $b\bar{b}$ through the VH production mode. All these results are summarized in Table 11.5.

The LHCb collaboration has also performed a search for the VH production with subsequent decay of the Higgs boson to a pair of b-quarks [151] with $1.98\,\text{fb}^{-1}$ of data taken at a centre-of-mass energy of 8 TeV. The final state is required to have two reconstructed b quarks and one lepton in the LHCb acceptance of $2 < \eta < 5$. The sensitivity of this search is an expected 95% CL exclusion of 84 times the SM production rate. This analysis is also used to set a limit on the VH production with the subsequent decay of the Higgs boson in a pair of c quarks with a 95% CL limit at $6.4{\times}10^3$ times the SM production rate, while the expected sensitivity corresponds to an exclusion of $7.9{\times}10^3$ times the SM production rate.

ATLAS and CMS have also searched for $H \to b\bar{b}$ in the VBF production mode. The event topology consists of two "VBF-tagging" energetic light-quark jets in the forward and backward direction relative to the beam direction and two b-tagged jets in the central region of the detector. Due to the electroweak nature of the process, for the signal events,

no energetic jet activity is expected in the rapidity gap between the two "VBF-tagging" jets. The dominant background in this search stems from QCD production of multijet events and the hadronic decays of vector bosons accompanied by additional jets. A contribution of Higgs boson events produced in the ggF process but with two or more associated jets is expected in the signal sample. The signal is expected as a broad enhancement in the $m_{b\bar{b}}$ distribution over the smoothly falling contribution from the SM background processes. Both ATLAS [152] and CMS [153] have produced results in this channel with Run 1 data, but with limited sensitivity. CMS has performed a similar analysis with Run 2 data [154]. The results are summarized in Table 11.5.

Two of the main difficulties for the VBF production mode are the large QCD background and the difficulty in triggering events fully hadronic events. Both difficulties are addressed, by the proposal made in Ref. [155], where the requirement of an additional photon in the final state reduces the background through an interference effect and enhances the possibilities for triggering. This analysis has been carried out by the ATLAS experiment at Run 2 [156] (see Table 11.5).

The sensitivity in the inclusive search for the Higgs boson in the ggF production mode with $H \to b\bar{b}$ is limited by the overwhelming background from the inclusive production of $p\bar{p} \to b\bar{b} + X$ via the strong interaction. For this reason, no meaningful results exist with the Run 1 dataset for this production mode. With the increase in centre-of-mass energy to 13 TeV, and by taking advantage of the harder transverse momentum spectrum of the $gg \to H$ production mode with respect to the QCD background, a search for high p_T Higgs boson decaying to a pair of b-quarks in association with a energetic (and thus triggerable) Initial State Radiation (ISR) jet, has been performed by CMS [157]. For this novel analysis with the Run 2 data, CMS requires jets clustered with the anti-k_T algorithm [158] with a distance parameter of 0.8, with a transverse momentum in excess of 450 GeV. As in the case of VH production mode, this analysis is sensitive also to the $VZ, Z \to b\bar{b}$ production, which is an important step in the validation of the analysis chain. The $Z \to b\bar{b}$ decay is observed with a significance of 5.8 standard deviations, in good agreement with the expected sensitivity of 5.1 standard deviations. The expected sensitivity to the observation of a Higgs boson is 0.7 standard deviations while CMS observes an excess at $m_H = 125$ GeV of 1.5 standard deviations.

III.3. Higgs production in association with top quarks or in top decays

III.3.1. The associated production with top quark pairs

As discussed in Section II, the coupling of the Higgs particle to top quarks plays a special role in the electroweak symmetry breaking mechanism and in its possible extensions. Substantial indirect evidence of this coupling is provided by the compatibility of observed rates of the Higgs boson in the principal discovery channels, given that the main production process – the gluon fusion – is dominated by a top quark loop. Direct evidence of this coupling at the LHC and the future e^+e^- colliders will be mainly available through the $t\bar{t}H$ final state and will permit a clean measurement of the top quark-Higgs boson Yukawa coupling. The $t\bar{t}H$ production cross section at the LHC is small in comparison with the ggF or even VH production modes. The production cross

section for a 125 GeV Higgs boson in pp collisions at $\sqrt{s} = 8$ TeV of about 130 fb makes it challenging to measure the $t\bar{t}H$ process with the LHC Run 1 dataset. However in Run 2 the increase in cross section at $\sqrt{s} = 13$ TeV is substantial, reaching approximately 510 fb. For a sensitive search, It is currently important to target as many accessible experimental signatures as possible. The analysis channels for such complex final states can be separated in four classes according to the decays of the Higgs boson. In each of these classes, most of the decay final states of the top quarks are considered. The topologies related to the decays of the top quarks are denoted 0L, 1L and 2L, for the fully hadronic, semi-leptonic and dilepton decay final states respectively of the $t\bar{t}$.

The first (i) analysis in this set is the search for $t\bar{t}H$ production in the $H \to \gamma\gamma$ channel. This analysis relies on the search for a narrow mass peak in the $m_{\gamma\gamma}$ distribution. The background is estimated from the $m_{\gamma\gamma}$ sidebands. The sensitivity in this channel is mostly limited by the available statistics. The second (ii) is the search for the Higgs boson decaying to ZZ^* and subsequently to four leptons (electrons or muons). This channel is currently limited by the low statistics due to the small branching fraction of the Z decays to leptons. The third (iii) is the search in the $H \to b\bar{b}$ channel. This search is intricate due to the large backgrounds, both physical and combinatorial in resolving the $b\bar{b}$ system from the Higgs decay, in events with six jets and four b-tagged jets. Already with the Run 1 dataset, the sensitivity of this analysis is strongly impacted by the systematic uncertainties on the background predictions. The fourth (iv) channel is a specific search for $\tau^+\tau^-$ where the two tau leptons decay to hadrons. Finally, the W^+W^- , $\tau^+\tau^-$ and ZZ^* final states can be searched for inclusively in multilepton event topologies. The corresponding $t\bar{t}H$ modes can be decomposed in terms of the decays of the Higgs boson and those of the top quarks as having two b-quarks and four W bosons (or two W and two taus, or two W and two Z) in the final state.

ATLAS and CMS have provided a complete set of results in these channels and their combination with the Run 1 data [166, 167, 168]. Results for most of these channels have been updated with Run 2 data.

With the large increase in production cross section for the ttH associated production process of a factor of 3.9 from 7 TeV to 13 TeV, an outstanding goal of the Run 2 physics program is the study of these channels.

ATLAS and CMS have analyzed the Run 2 data with the full 2016 dataset and for some channels the 2015 dataset as well, to search for this production mode in most channels: the diphoton [124], $H \to 4\ell$ [132], the $H \to b\bar{b}$ [169] and multilepton [170] for ATLAS and the diphoton [128], $H \to 4\ell$ [125], and the multilepton [171, 172] for CMS. The $H \to b\bar{b}$ channel has been updated with a partial dataset corresponding to an integrated luminosity of 12.9 fb^{-1} [173] by CMS. All results are summarized in Table 11.6.

With the increase in centre-of-mass energy and recorded luminosity clean channels such as the $t\bar{t}(H \to \gamma\gamma)$ with sensitivity limited largely by the statistical uncertainty will play an increasingly important role. With the results obtained so far with the current dataset, there is substantial evidence for the production of the Higgs boson in association with a pair of top quarks.

Table 11.6: Summary of the results of searches for a Higgs boson in association with a top quark pair by the ATLAS and CMS collaborations. The results are given in terms of measured signal strength. Where availale the uncertainty the total uncertainty is reported as the statistical and systematic contributions separately and in this order.

$t\bar{t}H$	ATLAS Run 1	CMS Run 1	ATLAS Run 2	CMS Run 2
$H \to \gamma\gamma$	$1.3\ ^{+2.6}_{-1.7}\ ^{+2.5}_{-1.7}$	$1.2\ ^{+2.5}_{-1.7}\ ^{+2.6}_{-1.8}$	$0.6\ ^{+0.7}_{-0.6} \pm 0.2$	$1.9^{+1.5}_{-1.2}$
$H \to 4\ell$	—	—	< 1.9 (68% CL)	0.0 ± 1.2
$b\bar{b}$	$1.4 \pm 1.0 \pm 0.6$	$1.6\ ^{+1.6}_{-1.5}$	$0.8 \pm 0.3 \pm 0.6$	-0.2 ± 0.8
$WW/\tau\tau/ZZ$	$1.4 \pm 0.6 \pm 1.0$	3.3 ± 1.4	$1.6 \pm 0.3 \pm 0.4$	1.5 ± 0.5 (0-τ) $0.72\ ^{+0.62}_{-0.53}$ (τ)
Comb.	$1.7 \pm 0.5 \pm 0.8$	$2.8\ ^{+1.0}_{-0.9}$	$1.2 \pm 0.2\ ^{+0.3}_{-0.2}$	—

III.3.2. The associated production with a single top quark

An additional production mode of the Higgs boson in association with a top quark is the single top associated production mode. There is an interesting similarity between this production mode and the $H \to \gamma\gamma$ decay mode. Both processes proceed through either the top Yukawa coupling or the interaction of the Higgs boson with the W-boson, with a negative interference between the two. Representative Feynman diagrams for this production process are shown in Fig. 11.1. Contrary to the diphoton decay channel, in this production mode the interference occurs at the tree level and is dominant. This process can therefore be used to further discriminate a negative relative sign between the couplings of the Higgs boson to fermions and its couplings to gauge bosons (the detailed dependence of the cross section as a function of coupling modifiers, taking into account the interference, is given in Section VI.2.1.2-ii).

The ATLAS and CMS experiments have produced specific searches for the tH production mode with the Run 1 and Run 2 data exploiting a variety of Higgs boson decay modes resulting in final states with photons, bottom quarks, and multiple charged leptons, including tau leptons. In particular the latest result with the Run 2 data obtained by CMS searches for multi-leptonic decay signatures from the $H \to WW^*$, $H \to \tau^+\tau^-$ and $H \to ZZ^*$ modes [174], this analysis restricts values of the top-Higgs coupling modifier κ_t to $[-1.25, 1.60]$ at 95% CL. CMS has also performed an analysis of the 2015 dataset to search for the $H \to b\bar{b}$ mode [175] yielding much less stringent constraints.

The diphoton channel has also been used to search specifically for this production mode by the ATLAS experiment using Run 1 data [167], yielding the restricted range of allowed values at the 95% CL to $[-1.3, 8]$.

III.3.3. Flavor changing neutral current decays of the top quark

The discovery of the Higgs boson at a mass smaller than the top quark mass opened a

new decay channel for the top quark. The decays of the top quark to a Higgs boson and a charm or an up quark proceed through a Flavor Changing Neutral Current (FCNC) which are forbidden at the tree level and suppressed at higher orders through the Glashow–Iliopoulos–Maiani (GIM) mechanism [3]. The SM prediction for these branching fractions is $\mathrm{BR}(t \to Hc) = 10^{-15}$ and two orders of magnitude less for the Hu final state. These decay channels of the top quark are, therefore, very interesting to probe possible FCNC interactions in the Higgs Yukawa couplings to the quark sector, see Section VII.

ATLAS has searched for FCNC top decays specifically in channels involving a Higgs boson with subsequent decays to two photons [176] and a pair of b-quarks [178]. It has also reinterpreted a search for the ttH production in the multilepton final state (discussed in Section III.6.1) [168]. The latter channel covers Higgs boson decays to a pair of W-bosons and a pair of taus. No significant excess was observed in any of the specific channels (as discussed in Section III.6.1, a slight excess is observed in the ttH multilepton channel) and 95% CL upper limits are set on $\mathrm{BR}(t \to Hc) < 0.46\%$ with an expected sensitivity of 0.25% and $\mathrm{BR}(t \to Hu) < 0.45\%$ with an expected sensitivity of 0.29%. CMS has performed a search for these FCNC top decays in the diphoton and multilepton channels [179], placing a 95% CL upper limit on $\mathrm{BR}(t \to Hc) < 0.40\%$ with an expected sensitivity of 0.43%.

From these limits on branching fractions, constraints on non flavor-diagonal Yukawa couplings of a FCNC sector Lagrangian of the form:

$$\mathcal{L}_{FCNC} = \lambda_{tcH}\bar{t}Hc + \lambda_{tuH}\bar{t}Hu + h.c.$$

can be derived. The 95% CL observed (expected) upper limits from ATLAS on the $|\lambda_{tcH}|$ and $|\lambda_{tuH}|$ couplings are 0.13 (0.10) and 0.13 (0.10), respectively.

The results above are derived from the combination of several channels for searches performed with Run 1 data. Both ATLAS and CMS have produced updates of individual channels with Run 2 data. The ATLAS collaboration has searched for FCNC top decays with subsequent decays of the Higgs boson to a pair of photons [177], yiedling a 95% CL upper limit on $\mathrm{BR}(t \to Hc) < 0.22\%$ with an expected sensitivity of 0.16%. The CMS collaboration has searched for FCNC top decays with subsequent decays of the Higgs boson to a pair of b quarks [180], yiedling a 95% CL upper limit on $\mathrm{BR}(t \to Hc) < 0.47\%$ with an expected sensitivity of 0.44%.

III.4. Higgs boson pair production

Higgs boson pair production in the SM is rare. It is however a very interesting final state to search in two specific modes: (i) the search for non-resonant production of the Higgs boson pair and (ii) the search for resonant production of two Higgs bosons in the decay of a heavier particle.

The measurement of non-resonant Higgs pair production is important for constraining Higgs self-couplings. In the SM the main non-resonant production mode of two Higgs bosons in the final state proceeds through a loop (mainly of top quarks) (Fig. 11.5a). Another production mode is via the trilinear coupling of the Higgs boson (Fig. 11.5b),

Table 11.7: Summary of the final states investigated in the search for Higgs boson pair production by ATLAS and CMS. (**) denotes results obtained with the 2015 dataset corresponding to an integrated luminosity of approximately $3\,\text{fb}^{-1}$, (*) denotes results obtained with a partial 2016 dataset corresponding to an integrated luminosity of approximately $12\,\text{fb}^{-1}$ and the other results reported correspond to the full 2016 dataset. Results are 95% CL upper limits on the observed (expected) SM signal strengths.

Channel	ATLAS	CMS
$b\bar{b}\gamma\gamma$	117 (161)** [187]	19 (17) [188]
$b\bar{b}b\bar{b}$	29 (38)* [189]	342 (308)** [190]
$b\bar{b}\tau^+\tau^-$	—	30 (25) [191]
$b\bar{b}W^+W^-$	—	79 (89) [192]
$W^+W^-\gamma\gamma$	747 (386)* [193]	—

whose amplitude is not negligible compared to the former. These diagrams interfere negatively making the overall production rate smaller than what would be expected in the absence of a trilinear coupling.

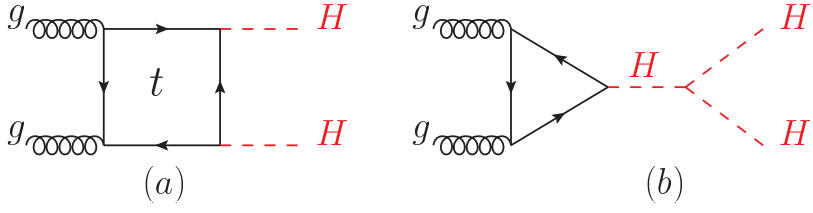

Figure 11.5: Feynman diagrams contributing to Higgs boson pair production through (a) a top- and b-quark loop and (b) through the self couplings of the Higgs boson.

III.4.1. Searches for Higgs boson pair production

The searches for Higgs boson pair production both resonant and non-resonant are very interesting probes for a variety of theories beyond the SM, and can be done in a large number of Higgs boson decay channels. At Run 1 the ATLAS and CMS collaborations have searched for both resonant and non resonant Higgs boson pair production in the following channels: (i) $HH \to b\bar{b}\gamma\gamma$ [181]; (ii) $HH \to b\bar{b}\tau^+\tau^-$ [182]; (iii) $HH \to b\bar{b}b\bar{b}$ [183]; and (iv) $HH \to WW^*\gamma\gamma$ [182]. (iv) in final states containing multiple leptons (electrons or muons) covering the WW^*WW^*, WW^*ZZ^*, ZZ^*ZZ^*, $ZZ^*\tau^+\tau^-$, $WW^*\tau^+\tau^-$, $ZZ^*b\bar{b}$, $\tau^+\tau^-\tau^+\tau^-$ channels [184]; (v) $\gamma\gamma\tau^+\tau^-$ channels [184].

At Run 2 most of these channels have been updated both by the ATLAS and CMS collaborations and the results are summarized in Table 11.7.

III.4.2. The Higgs self coupling

The Higgs boson self coupling is an extremely important direct probe of the Higgs potential with implications on our understanding of the electroweak phase transition. Constraints on the self coupling in HHH final states is an outstanding long term goal of the LHC, however with the current projected sensitivities a measurement will be extremely difficult even with the full HL-LHC dataset of 3 ab^{-1}.

In the SM the Higgs boson pair production through the trilinear Higgs has an on-shell component and a large off-shell component. The on-shell $H \rightarrow H^*H^*$ is strongly disfavored, requiring two off-shell Higgs bosons in the final state. The sensitivity region to the trilinear coupling production as in Fig. 11.5-b, is mainly in the kinematic region where the two Higgs boson in the final state are on-shell and the Higgs boson acts as a propagator (off-shell). As discussed in the introduction to this section, this process interferes negatively with the background Higgs boson pair production (Fig. 11.5a). In the SM hypothesis sensitivity to the trilinear coupling requires the measurement of a deficit in the Higgs boson pair production, in a similar way as the off-shell couplings measurement as explained in Section V.2.

The measurements of the trilinear coupling requires separating the contributions to the overall Higgs boson pair production and in particular measure the deficit expected in the case of SM couplings. However in the regime of relatively high trilinear coupling, the observation will be an excess of events with respect to the expected background. In this case a simple limit can be set. The direct searches described in Section VII.8.i.c can be reinterpreted in terms of the ratio of the trilinear coupling to the top Yukawa coupling which controls the production rate and a limit on the trilinear coupling, assuming a top Yukawa coupling modifier of 1 can be set. Using the $b\bar{b}\gamma\gamma$ channel alone the Run 2 dataset allows to exclude trilinear couplings in excess of 15 times the SM value at 95% CL.

Preliminary studies for the sensitivity on the trilinear coupling with 3 ab^{-1} have been carried out in several channels by ATLAS and CMS. Three channels have been investigated: (i) the $HH \rightarrow b\bar{b}\gamma\gamma$; (ii) the $HH \rightarrow b\bar{b}\tau^+\tau^-$; and (iii) the $HH \rightarrow b\bar{b}W^+W^-$. The prospects in channel (i) have been studied by both the ATLAS [194] and the CMS [195] collaborations, yielding a sensitivity of 1.05σ and 1.6σ respectively to overall Higgs boson pair production. Both collaborations have studied the channel (ii) yielding a sensitivity of 0.6σ [196] and 0.9σ [195] to Higgs boson pair production respectively. CMS collaboration has studied the channel (iii) showing its low sensitivity [195]. As an example, the ATLAS prospects in the $b\bar{b}\gamma\gamma$ channel yield for the full HL-LHC luminosity, an expected significance of an excess of 1.05 standard deviations for a SM trilinear coupling [194] which will translate on an upper limit on the total HH cross section of approximately twice the SM value. This corresponds to an exclusion limit of -0.8$< \lambda/\lambda_{SM} <$7.7 at 95% CL. The asymmetry in the limits is due to the different acceptance of the selection when the signal is dominated by the trilinear coupling mode at high λ and by the gluon-fusion di-Higgs production dominant at low λ. It should be noted that there is a large uncertainty on these projections related both to the modeling of signal and the backgrounds, the very difficult high pile-up environment (both for reconstruction and trigger) and the design of the upgraded detectors.

Preliminary studies suggest that a direct measurement of the quartic coupling will be out of reach even at a very high energy 100 TeV hadron collider.

III.5. Searches for rare decays of the Higgs boson

III.5.1. $H \to Z\gamma$

The search for $H \to Z\gamma$ is performed in the final states where the Z boson decays into opposite sign and same flavor leptons ($\ell^+\ell^-$), ℓ here refers to e or μ. While the branching fraction for $H \to Z\gamma$ is comparable to $H \to \gamma\gamma$ (about 10^{-3}) at $m_H = 125\,\text{GeV}$, the observable signal yield is brought down by the small branching ratio of $Z \to (e^+e^- + \mu^+\mu^-) = 6.7 \times 10^{-2}$. In these channels, the $m_{\ell\ell\gamma}$ mass resolution is excellent (1-3%) so the analyses search for a narrow mass peak over a continuous background. The major backgrounds arise from the $Z + \gamma$ final state radiation in Drell–Yan decays and $Z +$ jets processes where a jet is misidentified as a photon. The ratio of signal over background in this channel is typically of the order of 0.5%. In a narrow window of a few GeV around 125 GeV, several hundreds of events are expected.

Events are divided into mutually exclusive categories on the basis of the expected $m_{Z\gamma}$ resolution and the signal-to-background ratio. A VBF category is formed for $H \to Z\gamma$ candidates which are accompanied by two energetic jets separated by a large pseudorapidity. While this category contains only about 2% of the total event count, the signal-to-noise is about an order of magnitude higher. The search for a Higgs boson is conducted independently in each category and the results from all categories are then combined.

No excess of events is observed in either ATLAS or CMS experiments in the Run 1 data. The CMS expected and observed 95% CL upper limits for $m_H = 125\,\text{GeV}$ [197] on the signal strength μ are 10 and 9.5 respectively. The ATLAS expected and observed upper limits [198] on the signal strength μ are 9 and 11 respectively for a SM $m_H = 125.5\,\text{GeV}$.

The ATLAS collaboration has performed an analysis of the full 2015 and 2016 Run 2 data to search for the $Z\gamma$ decay mode [199], no significant excess is observed and 95% CL observed (expected) upper limits on the signal strength are 6.6 (5.2).

III.5.2. $H \to \mu^+\mu^-$

The branching fraction in the $H \to \mu^+\mu^-$ channel for a 125 GeV SM Higgs boson is 2.2×10^{-4}, about ten times smaller than that for $H \to \gamma\gamma$. The dominant and irreducible background arises from the $\text{Z}/\gamma^* \to \mu^+\mu^-$ process which has a rate several orders of magnitude larger than that from the SM Higgs boson signal. Due to the precise muon momentum measurement achieved by ATLAS and CMS, the $m_{\mu^+\mu^-}$ mass resolution is excellent ($\approx 2 - 3\%$). A search is performed for a narrow peak over a large but smoothly falling background. For optimal search sensitivity, events are divided into several categories. Either taking advantage of the superior muon momentum measurement in the central region, events can be subdivided by the pseudorapidity of the muons, or designing selections aiming at specific production processes such in particular as the vector boson fusion.

Table 11.8: Summary of the results of searches for lepton flavor violating decays of the Higgs boson in the $\tau\mu$ channel from ATLAS and CMS. For the result with a *, the expected sensitivity was not reported but appears consistent with the observed.

	ATLAS (Run 1)	CMS (Run 1)	CMS (Run 2)
BR($H \to \tau\mu$)	$(0.53 \pm 0.51)\%$	$(0.84^{+0.39}_{-0.37})\%$	$(0.00 \pm 0.12)\%$
95% CL Obs. (Exp.)	1.43% (1.01%)	1.51% (0.75%)	0.25% (0.25%)
$H \to \tau e$ 95% CL Obs. (Exp.)	1.02% (1.21%)	0.69%*	0.61% (0.37%)

No excess in the $m_{\mu^+\mu^-}$ spectrum is observed near 125 GeV. From an analysis of their Run 1 data, ATLAS sets [200] an observed (expected) 95% CL upper limit on the signal strength $\mu < 7.0$ (7.2). The CMS analysis [201] of their 7 and 8 TeV data sets an observed (expected) limit of $\mu < 7.4$ (6.5).

A search carried out by the ATLAS experiment using the 2015 and 2016 data [202] showed no excess at 125 GeV. A signal strength of $\mu = -0.1 \pm 1.4$ was measured, yielding an observed (expected) 95% CL upper limit on the signal strength of $\mu < 2.8$ (2.9).

III.5.3. $H \to e^+e^-$

A search similar to the $H \to \mu^+\mu^-$, is performed by CMS in the di-electron channel [201]. In this search channel there the contribution from the peaking background from Higgs boson decays to diphoton mis-identified as di-electrons (when mostly converted photons are faking electrons) needs to be assessed. The sensitivity to the SM Higgs decays is negligible given the extremely small branching fraction to e^+e^-, approximately 40,000 times smaller than the branching fraction to dimuons. It is nevertheless interesting to probe this decay channel to search for potential large anomalous couplings. Assuming a SM Higgs boson production cross section, the observed limit on the branching fraction at the 95% CL is 0.0019 [201], five orders of magnitude larger than the expected SM prediction.

III.5.4. Lepton flavor violating (LFV) Higgs boson decays

Given the Yukawa suppression of the couplings of the Higgs boson to quarks and leptons of the first two generations and the small total width of the Higgs boson, new physics contributions could easily have sizable branching fractions. One very interesting possibility is the Lepton Flavor Violating (LFV) decays of the Higgs boson, in particular in the $\tau\mu$ and τe modes. These decays are suppressed in the SM but could be enhanced in theories such as two-Higgs-doublet models (discussed in Section VII).

There are already constraints on LFV Yukawa couplings $|Y_{\tau\mu}|$ from channels such as the $\tau \to 3\mu$ or $\tau \to \mu\gamma$, or a re-interpretation of the search for Higgs decays to $\tau^+\tau^-$. A direct search at the LHC however complements these indirect limits. The search for LFV decays in the $\tau\mu$ channel have been done with the Run 1 dataset in several channels according to the subsequent decay of the τ. The results from CMS [203] and for ATLAS for the hadronic [204], the leptonic [205] decays of the tau, and their combination [205] are reported in Table 11.8. It is interesting to note that the analysis strategies for the di-lepton $\tau_{lep}\mu$ channel are very different between the ATLAS [205] and CMS [203].

As shown in Table 11.8 an excess was observed in this channel by CMS with a significance of 2.5σ, while in ATLAS the excess is smaller, about $1\ \sigma$ in Run 1. CMS has performed the search again with the full 2016 Run 2 [206] dataset and a multivariate analysis. The observed best fit branching fraction is $(0.00 \pm 0.12)\%$. These limits are reported in Table 11.8.

ATLAS and CMS have also performed a search for the LFV Higgs boson decays in the τe and μe channels [205, 207, 206], no significant excess was observed and 95% CL limits are reported in Table 11.8 for the τe channel only. For the μe channel, the constraints from the $\mu \to e\gamma$ experiments [208] are much stronger than those from the direct LFV Higgs decay search. However these indirect constraints can be relaxed by the cancellation of LFV effects from new physics.

III.5.5. Probing charm- and light-quark Yukawa couplings

Probing the Yukawa couplings to quarks of the second or even the first generation is extremely challenging given the overwhelming background and the much smaller signal rates. The possibility of probing the Yukawa coupling to the charm has been discussed in Ref. [209] where indirect bounds on the charm Yukawa coupling are estimated from a combined fit to the Higgs data. The direct impact of Higgs decays to a pair of charm quarks on the direct search for $H \to b\overline{b}$ is also investigated.

Another possibility to access the Higgs Yukawa coupling has been discussed in Ref. [210], through the decays of the Higgs boson to a final state with charmonium: $H \to J/\Psi\gamma$. Higgs decays in this final state have been searched for by the ATLAS collaboration [211]. The sensitivity of this analysis is however several orders of magnitude above the branching fraction estimated for the SM coupling $\mathrm{BR}(H \to J/\Psi\gamma) = (2.8 \pm 0.2) \times 10^{-6}$ [210]. The ATLAS collaboration [211] has also searched for Higgs decays to $\Upsilon(nS)\gamma$ where $(n = 1, 2, 3)$, a channel with much lower sensitivity than the $H \to b\overline{b}$ to the Yukawa coupling to b-quarks.

More recently the ATLAS collaboration has searched for another quarkonia final state where the Higgs boson decays to $\phi\gamma$ [212] at the LHC Run 2 and a center-of-mass energy of 13 TeV, with a specific trigger. This channel could probe deviations from the strange-quark Yukawa coupling of the Higgs boson. Its sensitivity is several orders of magnitude above the expectation from the SM Higgs boson. Other quarkonia final states, such as the $\rho\gamma$, which could potentially probe the Yukawa coupling to light quarks, can also be searched for.

III.5.6. Rare decays outlook

Rare decays such as those described in the above sections have a clearly limited sensitivity. They however already deliver interesting messages. For example, if the coupling of the Higgs boson to muons was as strong as it is to top quarks, this mode should have been observed. The observed Higgs boson couplings are manifestly non-universal. Further developing these rare decay modes is an important component of the high luminosity program of the LHC to directly probe the couplings of the Higgs boson, and to potentially measure the Yukawa coupling of the Higgs boson to fermions of

the second generation, in particular to muons. It is also an integral part of the physics program of the discussed potential future Higgs factories.

III.6. Searches for non-standard model decay channels

The main decay and production properties of the observed Higgs boson are consistent with predictions of the SM. It may however have other decay channels beyond those anticipated in the SM. Among these and of great interest are the invisible decays into stable particles that interact very weakly with the detector, and that are undetected, such as Dark Matter particle candidates. Other non standard decay channels that have been investigated are the decays of the Higgs particle to hidden valley or dark particles.

III.6.1. Invisible decays of the Higgs boson

The discovery of the Higgs boson immediately raised the question of its couplings to dark matter and how it could be used to reveal its existence at colliders, using the Higgs boson as a portal to dark matter (see Ref. [213] and references therein). If kinematically accessible and with a sufficiently large coupling to the Higgs boson, dark matter particles, such as, e.g., neutralinos in SUSY models, graviscalars in models with extra dimensions or heavy neutrinos in the context of four-generation fermion models, would manifest themselves as invisible decays of the Higgs boson, thus strongly motivating searches for the invisible decays of the Higgs boson.

To identify an invisibly decaying Higgs boson at the LHC, it must be produced in association with other particles. Searches for invisible decays of the Higgs particle at the LHC have been carried out in three associated production modes of the Higgs boson with the highest SM cross sections and target events with large missing energy.

The ggF production mode has the largest SM cross section but it usually results in the Higgs boson being created alone and hence leaving no characteristic signature in the detector of its invisible decay. One way to search for invisible decays in ggF production mode is to look for events with the "monojet" topology arising from initial state gluon radiation and containing missing energy. The major irreducible background in such searches stems from Z + jets events where the Z boson decays into a pair of neutrinos. The analysis with the best sensitivity targets the VBF production topology but suffers from large backgrounds arising from events with two jets and large missing energy. The VH mode has much smaller cross section but the presence of a W or Z boson allows a variety of final states that can be tagged with relatively low background.

ATLAS [214–217], and CMS [218–221] have searched for such final states but have observed no significant excess over predicted backgrounds. Table 11.9 summarizes the 95% CL limits on the invisible decays of the Higgs boson assuming SM Higgs boson production cross section and corresponding detector acceptances.

The CMS experiment has updated the search for invisible decays of the Higgs boson in the gluon fusion, the vector boson fusion and the associated production with a vector boson channels (both with subsequent leptonic and hadronic decays) using Run 2 data collected in 2015 [222] and has produced a combination with Run 1 channels, yielding a limit on the invisible branching fraction of 24% with an expected sensitivity of 23%.

Table 11.9: Summary of the channels searched for and the corresponding 95% CL limits from ATLAS and CMS on the branching fraction for the Higgs boson decay to invisible particles assuming a SM Higgs boson production cross section. The results in parentheses are the expected exclusions. [*] indicates analyses based only on 8 TeV data. When combining Run 1 results and the results from the $\approx 2\,\text{fb}^{-1}$ of 13 TeV data acquired in 2015, the CMS observed (expected) limit improves to < 32 (26) % at 95% CL.

	ATLAS (Run 1)	CMS (Run 1)	CMS (13 TeV, 2015)
ggF (monojet); $H \to$ inv.	–	67 (71) % [*]	-
VBF; $H \to$ inv.	28 (31) %	57 (40) % [*]	69 (62) %
$Z \to \ell^+\ell^-$; $H \to$ inv.	75 (62)%	75 (91) %	125 (125)%
$Z \to b\bar{b}$; $H \to$ inv.	–	182 (189) % [*]	-
$Z \to jj$; $H \to$ inv.	78 (86)%	–	-
Combination of all direct searches	25 (27)%	36 (30) %	-

This constraint can then be further used to probe Higgs portal models to Dark Matter [223], where an additional weakly interacting particle χ with mass lower than $m_H/2$ is introduced as Dark Matter candidate and where the Higgs boson is considered as the only mediator between the SM particles and Dark Matter. In this model it is interesting to express the limit on the invisible branching fraction in terms of strength of interaction of Dark Matter with standard matter, *i.e.* in terms of it interaction cross section with nucleons $\sigma_{\chi-N}$. In this model the couplings of the Higgs boson to SM particles are assumed to be those of the SM and the interaction of the Higgs boson with the nucleon is parametrized in Higgs-Nucleon form factor estimated using lattice QCD calculations [223]. The exclusion limits from the constraints on invisible Higgs decays, both direct and indirect from the measurement of the coupling properties of the Higgs boson can be compared to direct detection experiments. For comparison the limit at 90% CL on the invisible branching fraction of $\text{BR}_{inv} < 24\%$ [222] is used and converted into limits on $\sigma_{\chi-N}$ under several hypotheses on the nature of Dark Matter particles depending mainly on their spin (scalar- or fermion-like). These results are shown in Fig. 11.6.

The ATLAS collaboration has performed a search for invisible decays of the Higgs boson in the associated production mode ZH with the Z boson subsequently decaying to a pair charged leptons (e^+e^- or $\mu^+\mu^-$) with the full 2015 and 2016 dataset [222].

III.6.2. Exotic Higgs boson decays

The 125 GeV Higgs boson not only serves as a probe for potential dark matter candidates, but also to search for other exotic particles arising from fields associated with a low-mass hidden sector. Such hidden sectors are composed of fields that are singlets under the SM gauge group $\text{SU}(3) \times \text{SU}(2) \times U(1)$. These models are referred to as hidden valley models [224, 225]. Since a light Higgs boson is a particle with a narrow width, even modest couplings to new states can give rise to a significant modification of Higgs phenomenology through exotic decays. Simple hidden valley models exist in which the

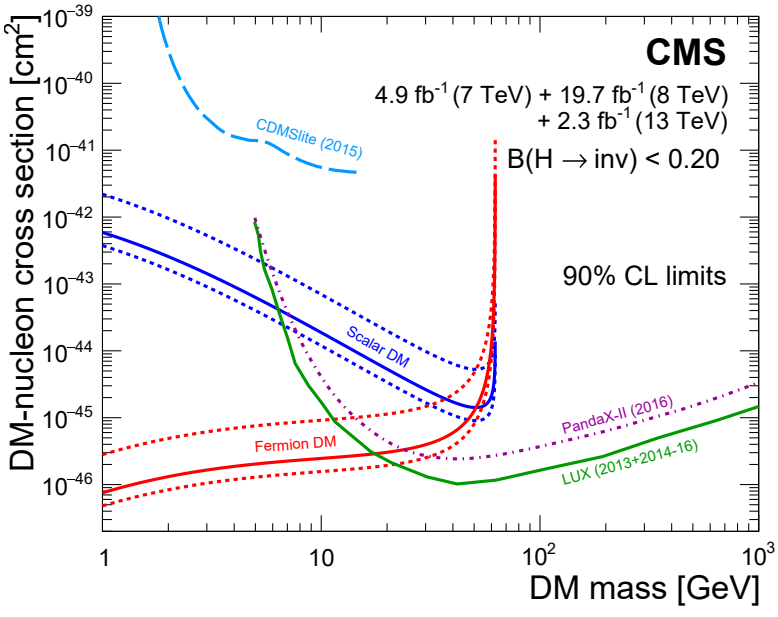

Figure 11.6: 90% CL upper limits on the WIMP-nucleon scattering cross section as a function of the Dark Matter particle mass. Spin-independent results excluded and favored regions from direct detection experiments are also shown.

Higgs boson decays to an invisible fundamental particle, which has a long lifetime to decay back to SM particles through a small mixing with the SM Higgs boson; Reference [225] describes an example. The Higgs boson may also decay to a pair of hidden valley "v-quarks," which subsequently hadronize in the hidden sector, forming "v-mesons." These mesons often prefer to decay to the heaviest state kinematically available, so that a possible signature is $H \to 4b$. Some of the v-mesons may be stable, implying a mixed missing energy plus heavy flavor final state. In other cases, the v-mesons may decay to leptons, implying the presence of low mass lepton resonances in high- H_T events [226]. Other scenarios have been studied [227] in which Higgs bosons decay predominantly into light hidden sector particles, either directly, or through light SUSY states, and with subsequent cascades that increase the multiplicity of hidden sector particles. In such scenarios, the high multiplicity hidden sector particles, after decaying back into the SM, appear in the detector as clusters of collimated leptons known as lepton jets.

A variety of models have been investigated searching for final states involving dark photons and hidden valley scalars. The resulting topologies searched for are prompt electron jets in the WH production process [228], displaced muonic jets [229], four muons final state, and long lived weakly interacting particles [230]. The latter occur not only in hidden valley scenarios, but also in gauge-mediated extensions of the minimal supersymmetric standard model (MSSM), the MSSM with R-parity violation, and inelastic dark matter [231]. Finally the CMS collaboration has performed a search for pair production of light bosons [232]. Such a scenario can occur in supersymmetric models with additional hidden (or dark) valleys.

IV. Combining the main channels

The analysis strategy used by the LHC and Tevatron experiments to perform the searches for the Higgs boson has been based on the Higgs decay modes. It is a natural choice given that it focusses on the decay products of the object searched for. However, for each channel, exclusive subchannels have been defined according to the Higgs production processes and in the results presented these subchannels have been combined. The natural extension of this approach in order to probe further the production and decay modes of the Higgs boson is to combine the analysis channels together. Such a combination is also used in Section VI to further measure the coupling properties of the Higgs boson.

At the LHC or the Tevatron, the total cross section cannot be measured in any of the production modes. As a consequence, neither the absolute branching fractions nor the total natural width of the Higgs boson can be directly measured. However, a combined measurement of the large variety of categories described in Section III, with different sensitivities to various production and decay modes permits a wide variety of measurements of the production, decay or in general coupling properties. These measurements require, in general, a limited but nevertheless restrictive number of assumptions.

In this section, results will be given combining not only different channels, but also the ATLAS and CMS results together [143]. These results are obtained with the Run 1 data only and are the current state-of-the-art in terms of combined measurements of the coupling properties of the Higgs boson, as no combination including the Run 2 data analyses has been performed by the experiments to date. These results were derived by the two collaborations, taking rigorously into account all correlations in the systematic uncertainties and in the large number of channels and their categories. This combination has led the two collaborations to a more precise experimental portrait of the Higgs boson. This concludes and synthesizes the analyses of the main production and decay channels of the Higgs boson at the Run 1 of the LHC.

In this section, only the results on the main Higgs boson production and decay modes will be discussed. The combination framework is briefly described herein and in more detail in the previous issue of this review [233]. This framework will also be used in Section VI, to discuss the measurements of the coupling properties of the Higgs boson.

IV.1. Principles of the combination

The combination of the Higgs boson analysis channels in each experiment and for the two experiments together is done using a fit of a signal and background model to the data. As described above the data is made of a large number of categories, aiming at reconstructing exclusive production and decay modes. In the combination of ATLAS and CMS [143] there are approximately 600 categories. The combination is a simultaneous fit to all these categories, using a reduced number of parameters of interest and a Higgs boson mass fixed at its measured value (see Section III.2). The much larger number of categories present in the ATLAS and CMS combination [143], is due to additional

separation in terms of finer exclusive production regions, decay channels of the Z and the W bosons, and taus, control regions where little-to-no signal is present, and different center-of-mass energies. It should be noted that the individual combination performed by ATLAS [234] included two additional decay channels: the $\mu^+\mu^-$ and $Z\gamma$, for the sake of simplicity these channels were omitted in the ATLAS-CMS combination. In addition, a $H \to b\bar{b}$ analysis performed by CMS [235] and included in its own combination, has been omitted from the ATLAS-CMS combination.

The key to understanding how the combination of channels works relies on the combination master formula, which expresses for each category, indexed by c, of a given channel (typically a category covers mostly one decay mode, but possibly various production modes), the measured number of signal events n_s^c as a function of a limited number of parameters as follows:

$$n_s^c = (\sum_{i,f} \mu_i \, \sigma_i^{SM} \times A_{if}^c \times \varepsilon_{if}^c \times \mu_f \, \mathrm{BR}_f^{SM}) \times \mathcal{L}^c \tag{11.9}$$

The production index is defined as $i \in \{ggH, VBF, VH, ttH\}$ and the decay index is defined as $f \in \{\gamma\gamma, WW, ZZ, bb, \tau\tau\}$ while σ_i^{SM} and BR_f^{SM} are the corresponding production cross sections and decay branching fractions, estimated as described in Section II, assuming that the Higgs boson is that of the SM. A_{if}^c and ε_{if}^c are the signal acceptance and the reconstruction efficiency for given production and decay modes in the category c. $\mathcal{L}^c$ is the integrated luminosity used for that specific category. For the purpose of this review, these parameters can be considered as fixed[3].

The parameters of interest in the master formula are the signal strength parameters μ_i and μ_f. It is important to note that the formula relies on the factorization of the production cross section and decay branching fraction, which assumes the narrow width approximation. The width of the Higgs boson will be discussed in Section V, however for the precision needed here, the fact that the Higgs boson has been observed in decay channels with high mass resolution as a resonance is sufficient to validate this hypothesis. It is also manifest in the above equation that the ten parameters for the production modes (μ_i) and decay modes (μ_f) cannot be determined simultaneously. This illustrates that total cross sections or branching fractions cannot be measured without further assumptions in this fit.

The master formula also illustrates an important caveat to the measurement of signal strength parameters. In case these are interpreted as scale factors of the production cross sections or branching fractions, then all the other quantities such as the acceptances and efficiencies, A_{if}^c and ε_{if}^c, need to be assumed as independent and fixed to their estimated values for the SM Higgs boson. An additional important caveat to note concerning these combined results is that only the normalizations are varied, while the discriminating variables for the signal are not modified and are still used in the fit. These caveats are of

[3] In the combination performed by the ATLAS and CMS experiments the systematic uncertainties on these parameters are taken into account by allowing these parameters to vary in the fit.

particular importance in the use of the combination to measure the coupling properties of the Higgs boson as discussed in Section VI. For relatively small perturbations of the couplings of the Higgs boson from the SM values, this hypothesis is valid.

However the 25 products, $\mu_i \times \mu_f$, can be considered as free parameters and in principle measurable (if there is sufficient sensitivity from specific categories). Measuring the products of signal strengths can be viewed as the measurements of the cross sections times the branching fraction, $\sigma \cdot \mathrm{BR}$. The results are reported in Fig. 11.7 for the combination of ATLAS and CMS.

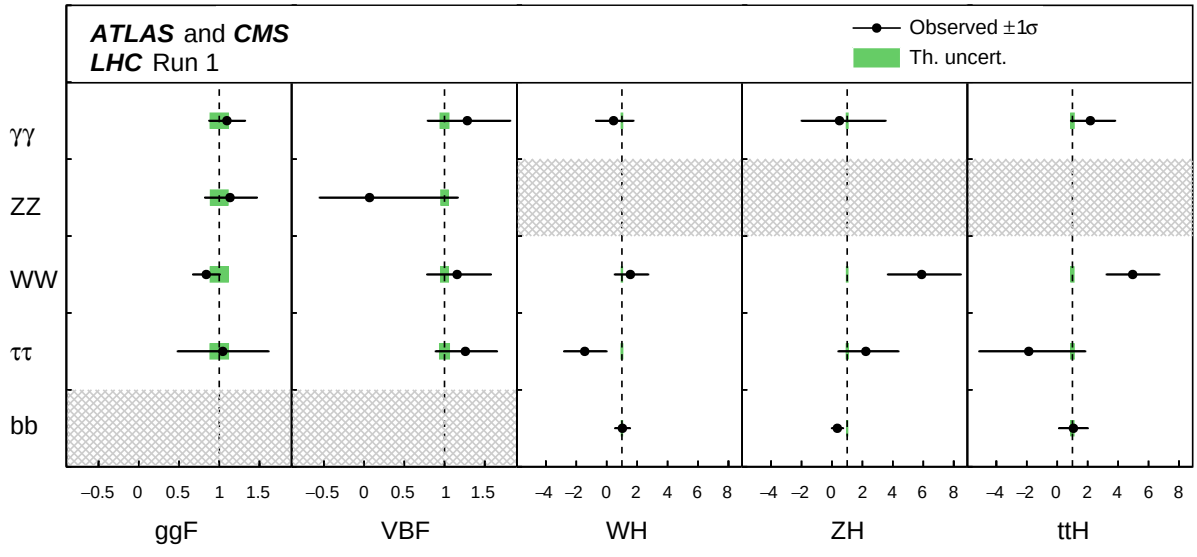

Figure 11.7: Combined measurements of the products $\sigma \cdot \mathrm{BR}$ for the five main production and five main decay modes. The hatched combinations require more data for a meaningful confidence interval to be provided.

It is remarkable that of the 25 possible combinations of production and decay modes in the main channels, the fit to ATLAS and CMS data allows the measurement of 20. A coherent picture emerges with an excellent consistency between the observation in each channel and the expectation for a SM Higgs boson.

This 20 parameter fit quantifies, with very little theoretical input, the current experimental knowledge of the main production and decays modes. Other fits involving ratios of cross sections, which also are little sensitive to theory uncertainties are performed and reported in Ref. [233].

The most constrained fit in this combination, and historically the first made, allows for only one single parameter to vary *i.e.* $\forall(i,f), \mu_i = \mu_f = \mu$. This global signal strength model provides the most precise and simple probe of the compatibility of the signal with the SM Higgs boson. This model is sensitive to any deviation from the SM Higgs boson couplings provided that these deviations do not cancel overall. The combined global signal strength is

$$\mu = 1.09 \pm 0.07\ (\mathrm{stat}) \ \pm 0.04\ (\mathrm{expt}) \ \pm 0.03\ (\mathrm{th.\,bkg}) \ \pm 0.07\ (\mathrm{th.\,sig})$$

This overall signal strength is fully compatible with the SM expectation of 1, with a precision of 10%. It is interesting to note that the major uncertainties in this first measurement arises from the limited precision in the theoretical predictions for the signal production processes.

IV.2. Main decay modes and observation of Higgs decays to taus

Despite the large number of decay channels, since the cross sections cannot be independently measured, from the measurements described in this section it is impossible to measure decay branching fractions without a loss of generality. The simplest assumption that can be made is that the production cross sections are those of the SM Higgs boson, which is equivalent to assuming that for all i indices $\mu_i = 1$. All branching fractions μ_f can then be measured in a simple 5 parameter fit. The result of this fit is reported in terms of significances in Table 11.10.

Table 11.10 also reports the results of a similar combination by each experiment from their data. For the main discovery modes $\gamma\gamma$, ZZ and WW, the combined significance is not computed as these decay modes have been firmly established by each experiment independently. However for the $\tau^+\tau^-$ and $b\bar{b}$ decay modes these results shed new combined light on the observation significance in these channels.

For the $\tau^+\tau^-$ channel, ATLAS and CMS are both sensitive and have observed excesses in their data. The individual results are not sufficiently significant to claim an observation, but combined they are. This conclusion can be made also in a more generic manner using the ratio of branching fractions model described above. It should be noted that in the search for $H \to \tau\tau$ decay, the most sensitive production mode is the VBF process, the experimental evidence for which is discussed in Section IV.3.

As illustrated in Table 11.10, ATLAS and CMS are both much less sensitive to the $H \to b\bar{b}$ decay mode. The available sensitivity comes mostly from the VH process, as discussed earlier in this section. The combined significance of 3.7σ at Run 1 was sufficient to suggest evidence, however ATLAS and CMS observations were both low with respect to the rate expected for the SM Higgs boson. At Run 2, this channel benefited largely from the increased production cross sections at 13 TeV and the much larger dataset expected.

IV.3. Main production modes and evidence for VBF production

As discussed earlier, most analysis channels are divided into several exclusive categories allowing for an increased overall sensitivity and to measure the various Higgs production modes. The cross sections of the main production modes can be measured assuming that the branching fractions are those of the SM Higgs boson, *i.e.* for all f indices $\mu_f = 1$. These assumptions lead to a 5 parameter combination. The results are reported in terms of significances of observation of the production modes are reported in Table 11.11.

The gluon fusion production process is the dominant production mode. Although no numerical estimate of combined significance of observation for this process has been given by the experiments, it is considered as established due to the overwhelming evidence from the three main discovery channels. None of the other production modes have been

Table 11.10: Summary of the significances of the excesses observed for the main decay processes. The $\gamma\gamma$, ZZ, and W^+W^- decay modes have been established at more than 5σ by both the ATLAS and CMS experiments individually, the combined observation significance therefore exceeds 5σ and is not reported here.

	Expected	Observed
$\gamma\gamma$	4.6σ (ATLAS) 5.3σ (CMS)	5.2σ (ATLAS) 4.6σ (CMS)
ZZ	6.2σ (ATLAS) 6.3σ (CMS)	8.1σ (ATLAS) 6.5σ (CMS)
WW	5.9σ (ATLAS) 5.4σ (CMS)	6.5σ (ATLAS) 4.7σ (CMS)
$\tau^+\tau^-$	3.4σ (ATLAS) 3.9σ (CMS)	4.5σ (ATLAS) 3.8σ (CMS)
$b\bar{b}$	2.6σ (ATLAS) 2.5σ (CMS)	1.4σ (ATLAS) 2.1σ (CMS)
$\tau^+\tau^-$ (Combined)	5.0σ	5.5σ
$b\bar{b}$ (Combined)	3.7σ	2.6σ

Table 11.11: Summary of the combined significance of observation for the main production processes. The ggF process has been established at more than 5σ by both the ATLAS and CMS experiments individually, the combined observation significance far exceeds 5σ and is not reported here.

	Expected		Observed	
ggF	Ind.	Obs.	Ind.	Obs.
VBF		4.6σ		5.4σ
WH		2.7σ		2.4σ
ZH		2.9σ		2.3σ
VH		4.2σ		3.5σ
ttH		2.0σ		4.4σ

firmly established by the experiments individually. These show that for the VBF mode, the combination has a large sensitivity and produced a combined observation of 5.4σ, establishing this process with a rate compatible with that expected from the SM Higgs boson. A similar conclusion can be reached but with assumptions from the fit to the ratio $\sigma_{VBF}/\sigma_{ggF}$ discussed earlier in this section.

It is interesting to note that despite the low sensitivity to the ttH production mode, the excesses observed in several ttH channels (discussed in Section III.6.1), lead to a significance of direct observation for ttH production in excess of 4σ. The compatibility of this observation with the SM production rate was at the 2.3σ level at Run 1. It improved significantly at Run 2 thanks to the higher center-of-mass energy of 13 TeV.

V. Main quantum numbers and width of the Higgs boson

V.1. Main quantum numbers J^{PC}

Probing the Higgs boson quantum numbers is essential to further unveiling its coupling properties. The measurements of the signal event yields of the observed new state in all the channels discussed in Sections III and IV and their compatibility with the SM Higgs boson predictions, give a qualitative, but nonetheless compelling indication of its nature. This qualitative picture is further complemented by the implications of the observation of the particle in the diphoton channel. According to the Landau–Yang theorem [236], the observation made in the diphoton channel excludes the spin-1 hypothesis and restricts possibilities for the spin of the observed particle to 0 or 2.

The Landau–Yang theorem does not apply if the observed state is not decaying to a pair of photons but to a pair of scalars subsequently decaying to two very collimated pairs of photons (as for example in the case of $H \to a_1 a_1 \to 4\gamma$). This possibility has not been rigorously excluded but is not experimentally favored since tight selection criteria are applied on the electromagnetic shower shapes of the reconstructed photons. A more systematic analysis of shower shapes and the fraction of conversions could be performed to further discriminate between the single prompt photon and the two overlapping photons hypotheses. There are also potential theoretical loopholes concerning the applicability of the Landau–Yang theorem, such as off-shell vector boson decays. However, for the observed particle not to be of spin 0 and +1 parity would require an improbable conspiracy of effects. It is nevertheless important to test this hypothesis independently, in particular since the measurements of coupling properties of the Higgs boson assume that the observed state is CP-even.

V.1.1. Charge conjugation

The charge conjugation quantum number is multiplicative, therefore given that the Higgs-like particle is observed in the $H \to \gamma\gamma$ channel, and given that photons are C-odd eigenstates, assuming C conservation, the observed neutral particle should be C-even.

V.1.2. Spin and parity

To probe the spin and parity quantum numbers of the discovered particle, a systematic analysis of its production and decay processes is performed in several analyses, designed to be independent of the event yields measured and relying instead on the production and the decay angles, and on the threshold distributions as long as a significant signal is observed (*i.e.* an excess over the expected background that can be used to further discriminate between signal hypotheses). These analyses are based on probing various alternative models of spin and parity. These models can be expressed in terms of an effective Lagrangian [237] or in terms of helicity amplitudes [238, 239]. The two approaches are equivalent. In the following, the effective Lagrangian formalism is chosen to describe the models considered and a restricted number of models are discussed [237]. In the analysis performed by CMS [238] a larger number of models have been investigated,

however the main channels studied by both experiments are essentially the same and the main conclusions are similar and fully consistent.

(i) Spin-0 model

The interaction Lagrangian relevant for the analysis of spin-0 particle interaction with a pair of W- or Z-boson with either fixed or mixed SM and BSM CP-even couplings or CP-odd couplings, is the following:

$$\begin{aligned}\mathcal{L}_0^{W,Z} \supset \Big\{ & \cos(\alpha)\kappa_{SM}[\frac{1}{2}g_{HZZ}Z_\mu Z^\mu + g_{HWW}W_\mu^+ W^{-\mu}] \\ & - \frac{1}{4\Lambda}[\cos(\alpha)\kappa_{HZZ}Z_{\mu\nu}Z^{\mu\nu} + \sin(\alpha)\kappa_{AZZ}Z_{\mu\nu}\tilde{Z}^{\mu\nu}] \\ & - \frac{1}{2\Lambda}[\cos(\alpha)\kappa_{HWW}W_{\mu\nu}^+ W^{-\mu\nu} + \sin(\alpha)\kappa_{AWW}W_{\mu\nu}^+ \tilde{W}^{-\mu\nu}]\Big\} H_0,\end{aligned} \tag{11.10}$$

where $V^\mu = Z^\mu, W^{+\mu}$ are the vector boson fields, $V^{\pm\mu\nu}$ are the reduced field tensors and $\tilde{V}^{\pm\mu\nu} = 1/2\,\varepsilon^{\mu\nu\rho\sigma}V_{\rho\sigma}$ are the dual tensor fields. Ans Λ defines an effective theory energy scale. The factors $\kappa_{SM}, \kappa_{HZZ}, \kappa_{HWW}, \kappa_{AZZ}, \kappa_{AWW}$ denote the coupling constants corresponding of the coupling of the SM, BSM CP-even and CP-odd components of the Higgs field H_0 to the W and Z fields. The mixing angle α allows for the production of CP-mixed state and the CP-symmetry is broken when $\alpha \neq 0, \pi$.

This formalism can be used to probe both CP-mixing for a spin-0 state or specific alternative hypotheses such as a pure CP-odd state ($J^P = 0^-$) corresponding to $\alpha = \pi/2$, $\kappa_{SM} = \kappa_{HVV} = 0$ and $\kappa_{AVV} = 1$. A BSM CP-even state $J^P = 0^+$ corresponds to $\alpha = 0$, $\kappa_{SM} = \kappa_{AVV} = 0$ and $\kappa_{HVV} = 1$. These hypotheses are compared to the SM Higgs boson hypothesis corresponding to $\alpha = 0$ and $\kappa_{HVV} = \kappa_{AVV} = 0$ and $\kappa_{SM} = 1$.

(ii) Spin-2 model

The graviton inspired interaction Lagrangian for a spin-2 boson $X^{\mu\nu}$ for a color, weak and electromagnetic singlet spin-2 resonance uniquely interacting with the energy momentum tensor $\mathcal{T}^{V,f}$ of vector bosons V or fermions f, can be written as follows [240]:

$$\mathcal{L}_2 \supset \frac{1}{\Lambda}\left[\sum_V \xi_V \mathcal{T}_{\mu\nu}^V X^{\mu\nu} + \sum_f \xi_f \mathcal{T}_{\mu\nu}^f X^{\mu\nu}\right]$$

Where the strength of the interaction is determined by the couplings ξ_V and ξ_f. The simplest scenario, referred to as the universal couplings (UC), corresponds to $\xi_V = \xi_f$. These models predict a large branching ratio to photons (of approximately 5%) and negligible couplings to massive gauge bosons (W and Z). Such scenarios are therefore disfavored and other models are investigated where the couplings of the W, Z and γ are assumed to be independent. Universality of the couplings refers to $\xi_g = \xi_q$. Two other scenarios are considered with low light-quark fraction where $\xi_q = 0$ and the low gluon-fraction where $\xi_q = 2\xi_g$. In these scenarios a large enhancement of the tail of the transverse momentum of the spin-2 state is expected and requires a further selection

requirement in order to probe the models within the range of validity of the effective field theory. Two requirements are considered, $p_T^X < 300\,\text{GeV}$ and $p_T^X < 125\,\text{GeV}$ [237].

V.1.3. Probing fixed J^P scenarios

At the LHC, the determination of the spin and CP properties of the Higgs boson is done independently from the total rates measurement, it uses a global angular helicity analysis and, when applicable, the study of threshold effects. The channels used for this analysis, $H \to \gamma\gamma$, $H \to W^{(*)}W^{(*)} \to \ell\nu\ell\nu$ and $H \to Z^{(*)}Z^{(*)} \to 4\ell$, are those where the observation of a signal is unambiguous.

At the Tevatron, an analysis using the threshold distribution of the production of the discovered state [241] in the associated production mode VH with subsequent decay to a pair of b-quarks was performed by the D0 collaboration.

(i) The VH production at D0

The mass of the VH system is a powerful discriminant to distinguish a $J^P = 0^+$, with a threshold behavior in $d\sigma/dM^2 \sim \beta$ from 0^- or 2^+ with threshold behaviors respectively in $\sim \beta^3$ and $\sim \beta^5$ (for a graviton like spin 2) [241]. The VH mass observable, not only discriminates signal hypotheses, but also has an increased separation between the 0^- and 2^+ hypotheses with respect to the backgrounds, thus allowing, with a small and not yet significant signal yield, to exclude that the observed state is 0^- at 98% CL [242] and 2^+ at the 99.9% CL [243].

(ii) The $\gamma\gamma$ channel at the LHC

In the $H \to \gamma\gamma$ channel, the analysis is performed inclusively using the production angle $\cos\theta^*_{CS}$ and the transverse momentum of the diphoton pair [237]. The definition chosen for the polar angle in the rest frame is the Collins–Soper frame, which is defined as the bisector axis of the momenta of the incoming protons in the diphoton rest frame. The SM Higgs signal distribution is expected to be uniform with a cutoff due to the selection requirements on the photons transverse momentum. The $H \to \gamma\gamma$ channel is mostly sensitive to the gluon-initiated spin-2 production scenarios, which yield a $\cos\theta^*_{CS}$ distribution peaking at values close to 1. The limits are derived from a fit of the signal in bins of $\cos\theta^*_{CS}$ and diphoton transverse momentum and are summarized in Fig. 11.8 (right) for ATLAS, only combined results are shown. The data shows a good compatibility with the SM 0^+ hypothesis and contributes strongly to the exclusion of several Spin-2 scenarios. The conclusions are the same from CMS results [238].

(iii) The $H \to W^{(*)}W^{(*)} \to \ell\nu\ell\nu$ channel at the LHC

In the $H \to W^{(*)}W^{(*)} \to \ell\nu\ell\nu$ channel, the production and decay angles cannot be easily reconstructed due to the presence of neutrinos in the final state, however sensitivity arises from the V-A structure of the decay of the W bosons. A scalar state thus yields a clear spin correlation pattern that implies that the charged leptons e or μ from the decays of the W bosons are produced close to one another in the transverse plane. This feature, which impacts observables such as the azimuthal angle between the two leptons $\Delta\Phi_{\ell\ell}$ or their invariant mass $M_{\ell\ell}$ in addition of the threshold behavior of the decay which

is used in kinematic variables such as the transverse mass defined in Section III, can be used to discriminate between various spin and parity hypotheses. The approach adopted by ATLAS uses a multivariate discriminant, whereas CMS uses a 2D-fit of the dilepton mass and the transverse mass. The results of the $H \to W^{(*)}W^{(*)} \to \ell\nu\ell\nu$ analyses alone are summarized in Fig. 11.8 for ATLAS and in combination with other channels. Spin-1 hypotheses (1^+ and 1^-) have also been tested with this channel by ATLAS and CMS. ATLAS and CMS exclude the 1^+ and 1^- hypotheses at more than 95% CL.

(iv) The $H \to Z^{(*)}Z^{(*)} \to 4\ell$ channel at the LHC

The $H \to Z^{(*)}Z^{(*)} \to 4\ell$ coupling analysis, as described in Section III, also uses a discriminant based on the 0^+ nature of the Higgs boson to further discriminate the signal from the background. In this analysis this feature is used to discriminate between signal hypotheses. The observables sensitive to the spin and parity are [244] the masses of the two Z bosons (due to the threshold dependence of the mass of the off-shell Z boson), two production angle θ^* and Φ_1, and three decay angles, Φ, θ_1 and θ_2. The production and decay angles defined as:

– θ_1 and θ_2, the angles between the negative final state lepton and the direction of flight of Z_1 and Z_2 in the rest frame.

– Φ, the angle between the decay planes of the four final state leptons expressed in the four lepton rest frame.

– Φ_1, the angle defined between the decay plane of the leading lepton pair and a plane defined by the vector of the Z_1 in the four lepton rest frame and the positive direction of the proton axis.

– θ^*, the production angle of the Z_1 defined in the four lepton rest frame with respect to the proton axis.

These angles are illustrated in Fig. 11.8. There are two approaches to this analysis. The first, used by CMS, is a matrix element likelihood approach where a kinematic discriminant is defined based on the ratio of the signal and background probabilities. These probabilities are defined using the leading-order matrix elements. A similar approach is also performed by ATLAS as a cross check of their main result. The main approach adopted by ATLAS is the combination of sensitive observables with a Boosted Decision Tree. These analyses are sensitive to various J^P hypotheses and in particular discriminate the 0^+ hypothesis from the 0^-. In all scenarios investigated and for both the ATLAS and CMS experiments, the data are compatible with the 0^+ hypothesis. ATLAS [239] and CMS [238] exclude a pseudoscalar nature of the observed boson at CL_S levels of 98% and 99.8%.

V.1.4. Probing CP-mixing and anomalous HVV couplings

The careful study of the kinematic properties of the events observed in the $H \to Z^{(*)}Z^{(*)} \to 4\ell$ and $H \to W^{(*)}W^{(*)} \to \ell\nu\ell\nu$ channel, and in particular the angular distributions described above, allows one to further probe the HVV coupling beyond testing fixed hypotheses. Assuming that the observed particle is a spin-0 state, and using several discriminating observables in the $H \to Z^{(*)}Z^{(*)} \to 4\ell$ and $H \to W^{(*)}W^{(*)} \to \ell\nu\ell\nu$

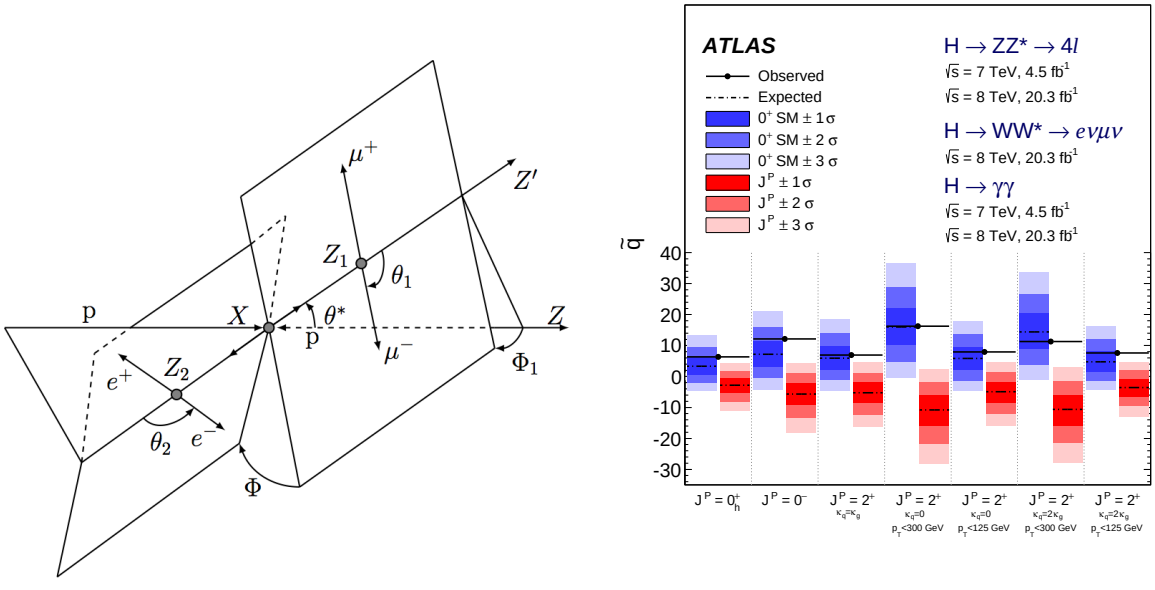

Figure 11.8: (Left) Definition of the production and decay angles defined for the $H \to Z^{(*)}Z^{(*)} \to 4\ell$ final state [238]. (Right) Expected distributions of the test statistic for the SM hypothesis (in blue) and several alternative spin and parity hypotheses (in red).

channels, the anomalous terms in the formalism of Eq. (11.10) can be probed. In the approach of helicity amplitudes used by CMS [238], all terms are essentially equivalent, except for one additional phase which is neglected in Eq. (11.10).

Results are derived in terms of the parameters $\tilde{\kappa}_{HVV} = v/\Lambda\,\kappa_{HVV}$ and $\tilde{\kappa}_{AVV} = v/\Lambda\,\kappa_{AVV}$, and more precisely as measurements of $\tilde{\kappa}_{HVV}/\kappa_{SM}$ and $\tan\alpha\,.\,\tilde{\kappa}_{AVV}/\kappa_{SM}$ as shown in Fig. 11.9. These parameters can be interpreted as mixing parameters of a tensor anomalous CP-even coupling and a CP-odd component. The measurements are made in the $H \to Z^{(*)}Z^{(*)} \to 4\ell$ and $H \to W^{(*)}W^{(*)} \to \ell\nu\ell\nu$ channels independently and then combined assuming that the $\tilde{\kappa}_{HVV}/\kappa_{SM}$ and $\tan\alpha\,.\,\tilde{\kappa}_{AVV}/\kappa_{SM}$ are the same for the W and Z vector bosons. Only the combination of the WW and ZZ channels is shown in Fig. 11.9. The asymmetric shape of the likelihood as a function of $\tilde{\kappa}_{HWW,HZZ}/\kappa_{SM}$ is mainly due to the interference between the BSM and the SM contributions that give a maximal deviation from the SM predictions for negative relative values of the BSM couplings. In Fig. 11.9 the expected likelihood profiles for a SM Higgs boson are also displayed. While no significant deviation from the SM Higgs boson expectation is observed, the precision of the measurements of the mixing parameters is fairly low. The results and conclusions from the CMS measurements [238] are very similar.

Individual ZZ^* channel measurements have been carried out at Run 2 by both ATLAS [132] and CMS [245].

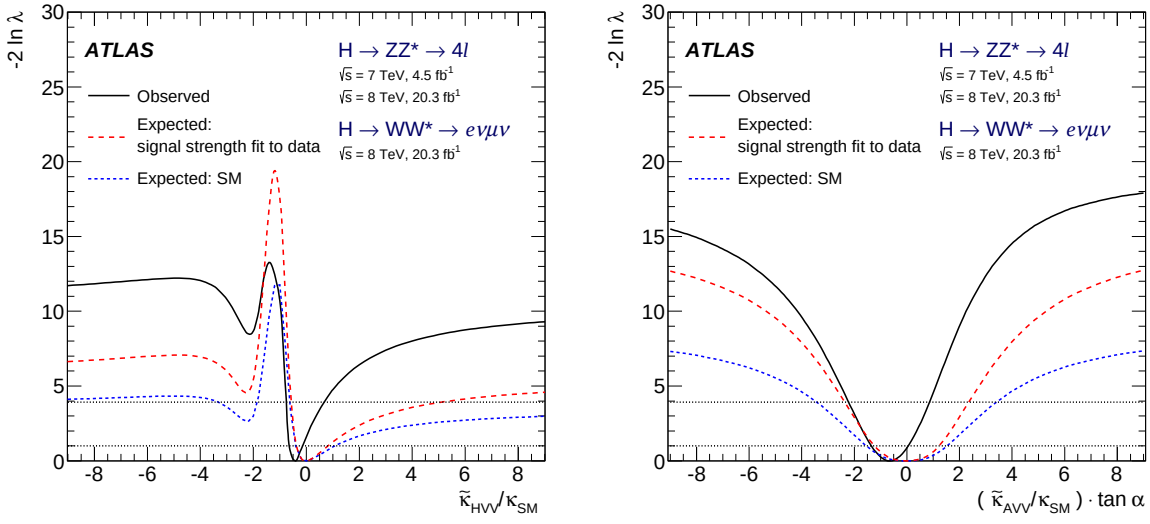

Figure 11.9: Likelihood profiles for the $\tilde{\kappa}_{HVV}$ and $\tilde{\kappa}_{AVV} \cdot \tan\alpha$ parameters, representing respectively CP-even and CP-odd anomalous couplings of the Higgs boson.

V.2. Off-shell couplings of the Higgs boson

In the dominant gluon fusion production mode with a subsequent decay of the Higgs boson into a pair of Z bosons, the production cross section of a off-shell Higgs boson is known to be sizable. This follows as a consequence of the enhanced couplings of the Higgs boson to the longitudinal polarizations of the massive vector bosons at high energy.

The off-shell to on-shell cross section ratio is approximately 8% in the SM. Still the Higgs contribution to VV production at large invariant mass remains small compared to the background. It is nevertheless interesting to probe Higgs production in this regime as it is sensitive to new physics beyond the SM.

The difficulty in the off-shell VV analysis, beyond the small signal-to-background ratio, is due to a large negative interference between the signal and the $gg \to VV$ background. The resulting presence of a SM Higgs boson signal in the far off-shell domain results in a deficit of events with respect to the expectation from background only events. It is only when the off-shell couplings of the Higgs boson are larger than expected in the SM that the presence of a signal appears as an excess over the background expectation. One additional intricacy arises from the precision in the prediction of the rate for $gg \to VV$, a loop process at lowest order, and its interference with the signal. At the time of the publications of the results from the ATLAS [246] and CMS [247] a full NLO prediction had not been computed.

It is interesting to note that in this regime the Higgs boson is studied as a propagator and not as a particle. The measurement of its off-shell couplings is therefore absolute and does not rely on the knowledge of the total Higgs boson width. The off-shell couplings constraints can then be used to indirectly constrain the natural width of the Higgs boson, under specific assumptions detailed in Section V.3.3.

This measurement has been carried out in the $H \to ZZ \to 4\ell$, $H \to ZZ \to \ell\ell\nu\nu$ and

$H \to WW \to \ell\nu\ell\nu$ channels. To enhance the sensitivity of the analysis the knowledge of the full kinematics of the events is important. In particular the signal and the background can be further distinguished by the invariant mass of the VV system, which is more accurately accessible in the $H \to ZZ \to 4\ell$ channel. Angular distributions also play an important role in this analysis. For these reasons the $H \to Z^{(*)}Z^{(*)} \to 4\ell$ channel is significantly more sensitive than $H \to W^{(*)}W^{(*)} \to \ell\nu\ell\nu$. The CMS results in Refs. [247] and [248] include the VBF and VH processes through the selection of two additional jets in the final state. The ATLAS results do not have a specific selection for the VBF or VH production processes, but their contributions are taken into account.

Limits on the off-shell rates have been reported for the two channels by ATLAS [246] and CMS [248]. The combined results assuming that the off-shell rates in the ZZ and WW channels scale equally, are given for two different hypotheses on the VBF production rate: fixing it to its SM value or scaling it as the gluon fusion rate. The observed (expected) limits on the off-shell rate fraction with respect to its SM expectation is 6.7 (9.1) for ATLAS [246] with the VBF rate fixed to its SM value and 2.4 (6.2) for CMS [248] where no assumption is made on the relative production rates of gluon-fusion and VBF. In both cases the custodial symmetry is assumed and the ratio of the rates in the ZZ and WW decays are fixed to those of the Standard Model. Results without this assumption have also been reported in Ref. [248].

V.3. The Higgs boson width

In the SM, the Higgs boson width is very precisely predicted once the Higgs boson mass is known. For a mass of 125.1 GeV, the Higgs boson has a very narrow width of 4.2 MeV. It is dominated by the fermionic decays partial width at approximately 75%, while the vector boson modes are suppressed and contribute 25% only.

At the LHC or the Tevatron, in all production modes, only the cross sections times branching fractions can be measured. As a consequence, the total natural width of the Higgs boson cannot be inferred from measurements of Higgs boson rates. Direct constraints on the Higgs boson width are much larger than the expected natural width of the SM Higgs boson.

V.3.1. Direct constraints

Analysis of the reconstructed mass lineshape in the two channels with a good mass resolution, the $H \to \gamma\gamma$ and $H \to Z^{(*)}Z^{(*)} \to 4\ell$, allow for a direct measurement of the width of the SM Higgs boson. The intrinsic mass resolution in these channels is about 1–2 GeV, much larger than the expected width of the SM Higgs boson. As a result only upper limits on the Higgs boson width have been measured by ATLAS [249] and CMS [125]. The two main challenges of direct constraints on the width through the measurement of the lineshape are: (i) the modeling of resolution uncertainties and (ii) the modeling of the interference between the signal and the continuum background which can be sizable for large widths, in particular in the range where direct constraints are set. Given that these interference effects are small with respect to the individual channels sensitivity, they are neglected in deriving constraints on the total width. The

Table 11.12: Run 1 observed (expected) direct 95% CL constraints on the natural width of the 125 GeV resonance from fits to the $\gamma\gamma$ and ZZ mass spectra and to the 4ℓ vertex lifetime. *The CMS measurement from the 4ℓ mass lineshape was performed using Run 2 data.

Experiment	$M_{\gamma\gamma}$ mass spectrum	$M_{4\ell}$ spectrum	4ℓ vertex lifetime
ATLAS	$< 5.0(6.2)$ GeV	$< 2.6(6.2)$ GeV	—
CMS	$< 2.4(3.1)$ GeV	$< 1.1(1.6)$ GeV*	$> 3.5 \times 10^{-12}$ GeV

combined constraints however, being more precise could be affected by the interference. ATLAS [249] has therefore not combined the constraints on the width from the two channels. The results are reported in Table 11.12. These constraints are still three orders of magnitude larger than the expected SM width and are fully compatible with the SM hypothesis.

Another direct constraint on the Higgs boson width can be obtained in the $H \to Z^{(*)}Z^{(*)} \to 4\ell$ channel, from the measurement of the average lifetime of the Higgs boson calculated from the displacement of the four-lepton vertex from the beam spot. This analysis has been carried out by CMS [247], using the measured decay length. The measured $c\tau_H$ is 2^{+25}_{-2} μm, yielding an observed (and expected) limit at the 95% CL of $c\tau_H < 57(56)\,\mu$m. From this upper limit on the lifetime of the Higgs boson. The 95% CL lower limit on its natural width is $\Gamma_H > 3.5 \times 10^{-12}$ GeV.

V.3.2. Indirect constraints from mass shift in the diphoton channel

In the diphoton channel, it was noticed in [250], that the effect of the interference between the main signal $gg \to H \to \gamma\gamma$ and the continuum irreducible background $gg \to \gamma\gamma$, taking into account detector resolution effects, is responsible for a non negligible mass shift. The size of the mass shift depends on the total width of the Higgs boson and it was suggested that measuring this mass shift could provide a constraint on the width [250]. It was further noticed that the mass shift has a dependence also on the diphoton transverse momentum. The total width of the Higgs boson could therefore be constrained using the diphoton channel alone.

Further studies were performed by the ATLAS collaboration to estimate the size of the expected mass shift [135]. The expected shift in mass in the diphoton channel is 35 ± 9 MeV for the SM Higgs boson. Very preliminary studies of the sensitivity of this method to estimate the width of the Higgs boson in the high-luminosity regime have been made by ATLAS [251] and yield an expected 95% CL upper limit on the total width of approximately 200 MeV from 3 ab^{-1} of 14 TeV data.

V.3.3. Indirect constraints from on-shell rate in the diphoton channel

In the diphoton channel, it was noticed in Ref. [252], that the interference between the main signal $gg \to H \to \gamma\gamma$ amplitude and the continuum irreducible background $gg \to \gamma\gamma$ amplitude generates non-negligible change in the on-shell cross sections, as a result of the existence of a relative phase between these amplitudes. The size of this on-shell interference effect depends on the total width of the Higgs boson and it was

suggested that measuring this on-shell cross section precisely could provide a constraint on the Higgs total width. This interference effect yields around 2% reduction for the $gg \to H \to \gamma\gamma$ cross section measurement. The current evaluation of this interference effect is performed at NLO and has $-30\% + 50\%$ uncertainty, due to the fact that the large relative phase is driven by the two-loop $gg \to \gamma\gamma$ background amplitude [250, 252]. This on-shell interference effect has dependence on the p_T of the diphoton system and the photon polar angle in the diphoton rest frame, which can be further exploited to improve the measurement to constrain the Higgs total width.

Taking the ratios of the on-shell cross section of Higgs to diphoton channel and the cross section of Higgs to four-leptons channel where the interference effect is negligible could put bound on the Higgs total width. This ratio is free from many dominant sources of systematic uncertainties for cross section measurements, *i.e.*, PDF uncertainty and luminosity uncertainty, and can be further improved by the accumulation of the LHC data. From this cross section ratio measurement alone, a preliminary estimation of the current limit from this interference effect with current 30% precision puts an upper bound of 800 MeV on the Higgs boson total width and the limit improves to 60 MeV with $3\,\text{ab}^{-1}$ of 14 TeV data [252, 253].

V.3.4. Indirect constraints from off-shell couplings

Using simultaneously on-shell and off-shell measurements in the VV channels, it was noticed [254] that the total width of the Higgs could be constrained. This can be illustrated from the parametrization of the signal strength measurements both on-shell ($\mu_{\text{on-shell}}$) and off-shell ($\mu_{\text{off-shell}}$) as a function of the couplings modifiers κ_g and κ_V parameterizing the main process $gg \to H \to VV$. The on-shell signal strength can be written as:

$$\mu_{\text{on-shell}} = \frac{\kappa^2_{g,\,\text{on-shell}}\,\kappa^2_{V,\,\text{on-shell}}}{\Gamma_H/\Gamma_{SM}}$$

while in the case of the off-shell signal strength where the Higgs boson is a propagator:

$$\mu_{\text{off-shell}} = \kappa^2_{g,\,\text{off-shell}}\,\kappa^2_{V,\,\text{off-shell}}$$

A bound on the Higgs width can then be obtained from the measurements of the on-shell and off-shell signal strengths. This assumes that no new physics alters the Higgs boson couplings in the off-shell regime, *i.e.*, that the running of its couplings is negligible in the off-shell regime. Both ATLAS [246] and CMS [247, 248] have used their off-shell production limits to constrain the width of the Higgs boson.

Both ATLAS and CMS analyses use the kinematic event characteristics to further gain in sensitivity to discriminate between the signal and background. The ATLAS analysis assumes that there are no anomalous couplings of the Higgs boson to vector bosons, and obtains 95% CL observed (expected) upper limit on the total width of $5.7\times\Gamma_{SM}$ ($9.0\times\Gamma_{SM}$) [246]. In the CMS analysis, the observed (expected) limit on the total width is $6.2\times\Gamma_{SM}$ ($9.8\times\Gamma_{SM}$) for the ZZ channel only [247]. In addition in the CMS analysis, results are also derived allowing for anomalous couplings of the Higgs boson, therefore reducing the discriminating power of the kinematic variables used in the analysis but

reducing the model dependence. The observed (expected) limit on the total width is $10.9\times\Gamma_{SM}$ ($17.4\times\Gamma_{SM}$) [247].

The CMS experiment has also combined the ZZ and W^+W^- channels while keeping the gluon-fusion and VBF production processes separate. For the gluon fusion mode the observed (expected) combined upper limit at the 95% CL on the total width of the Higgs boson is $2.4\times\Gamma_{SM}$ ($6.2\times\Gamma_{SM}$) [248], while for the VBF production mode the exclusion limits are $19.3\times\Gamma_{SM}$ ($34.4\times\Gamma_{SM}$) [248].

ATLAS has also performed a study of the prospects for measuring the Higgs width in the four lepton channel alone. Projecting to a luminosity of $3\,\mathrm{ab}^{-1}$, it was concluded that, within assumptions similar to the ones mentioned above, the width of the Higgs boson could be constrained with the following precision [255]:

$$\Gamma_H = 4.2^{+1.5}_{-2.1}\,\mathrm{MeV}.$$

VI. Probing the coupling properties of the Higgs boson

As discussed in Section II, within the SM, all the Higgs couplings are fixed unambiguously once all the particle masses are known. Any deviation in the measurement of the couplings of the Higgs boson could therefore signal physics beyond the SM.

Measuring the Higgs couplings without relying on the SM assumption requires a general framework treating deviations from the SM coherently at the quantum level in order to provide theoretical predictions for relevant observables to be confronted with experimental data. The first attempt in that direction was the development of the so-called κ-formalism [256] where the SM Higgs couplings are rescaled by factors κ, keeping the same Lorentz structure of the interactions. This formalism allows for simple interpretation of the signal strengths μ measured in the various Higgs channels and it has been used to test various physics scenarios, like the existence of additional new particles contributing to the radiative Higgs production and decays, or to probe various symmetries of the SM itself, as for example the custodial symmetry. But the κ-formalism has obvious limitations and certainly does not capture the most general deformations of the SM, even under the assumptions of heavy and decoupling new physics. A particularly acute shortcoming at the time Higgs physics is entering a precision era is the lack of proficiency of the κ's to assert the richness of kinematical distributions beyond simple signal strength measurements. Several extensions and alternative approaches are being developed as part of the activities of the Higgs cross-section working group.

The Higgs Pseudo-Observable (HPO) approach [257] is providing a particularly elegant formalism to report the data in terms of a finite set of on-shell form factors parametrizing amplitudes of physical processes subject to constraints from Lorentz invariance and other general requirements like analyticity, unitarity, and crossing symmetry. These form factors are expanded in powers of kinematical invariants of the process around the known poles of SM particles, assuming that poles from BSM particles are absent in the relevant energy regime. A set of HPOs have been proposed to characterize both the Higgs decays

and the EW Higgs production channels, thus exploring different kinematical regimes. Prospective studies concluded that these HPOs can be measured/bounded at the percent level at the HL-LHC and could therefore be used to constrain some explicit models of New Physics.

Another interesting approach to characterize the possible Higgs coupling deviations induced by physics beyond the SM is the use of Effective Field Theories (EFT). This approach assumes again that the new physics degrees of freedom are sufficiently heavy to be integrated out and they simply give rise to effective interactions among the light SM particles. By construction the effective Lagrangians cannot account for deviations in Higgs physics induced by light degrees of freedom, unless they are added themselves as extra fields in the effective Lagrangians. In Section VII, several examples of models with light degrees of freedom affecting Higgs production and decay rates will be presented. The main advantage of EFTs is their prowess to relate different observables in different sectors and at different energies to constrain a finite set of effective interactions among the SM degrees of freedom. In an EFT, the SM Lagrangian is extended by a set of higher-dimensional operators, and it reproduces the low-energy limit of a more fundamental UV description. It will be assumed that the Higgs boson is part of a CP-even EW doublet. This is motivated by the apparent relation between the Higgs couplings and the masses of the various particles which naturally follows under this assumption of a linear realization of the $\mathrm{SU}(2)_L \times \mathrm{U}(1)_Y$ symmetry of the SM. There have been some recent attempts to write the most general EFT bypassing this assumption, see for instance [258].

VI.1. Effective Lagrangian framework

The EFT has the same field content and the same linearly-realized $\mathrm{SU}(3)_C \times \mathrm{SU}(2)_L \times \mathrm{U}(1)_Y$ local symmetry as the SM. The difference is the presence of operators with canonical dimension D larger than 4. These are organized in a systematic expansion in D, where each consecutive term is suppressed by a larger power of a high mass scale. Assuming baryon and lepton number conservation, the most general Lagrangian takes the form

$$\mathcal{L}_{\text{eff}} = \mathcal{L}_{\text{SM}} + \sum_i c_i^{(6)} \mathcal{O}_i^{(6)} + \sum_j c_j^{(8)} \mathcal{O}_j^{(8)} + \cdots . \tag{11.11}$$

The list of dimension-6 operators was first classified in a systematic way in Ref. [259] after the works of Ref. [260]. Subsequent analyses pointed out the presence of redundant operators, and a minimal and complete list of operators was finally provided in Ref. [261][4]. For a single family of fermions, there are 76 real ways to deform the SM generated by 59 independent operators (with the 3 families of fermions of the SM, flavor indices can be added to these 59 operators, and furthermore, new operator structures, that have been dismissed by means of Fierz transformations in the single family case, have to be

[4] Complete classifications of D=8 operators have recently appeared in the literature, see Ref. [262]. Still, in this review, the EFT Lagrangians will be truncated at the level of dimension-6 operators.

Table 11.13: List of 17 CP-even operators affecting, at tree-level, only Higgs production and decay rates (left) as well as EW observables (right). See text for notations.

Ops. affecting Higgs physics only	Ops. affecting Higgs and EW physics
$\mathcal{O}_r = \lvert\Phi\rvert^2 \lvert D_\mu\Phi\rvert^2$	$\mathcal{O}_W = \frac{ig}{2}\big(\Phi^\dagger\sigma^i \overleftrightarrow{D}^\mu\Phi\big)(D^\nu W_{\mu\nu})^i$
$\mathcal{O}_6 = \lambda\lvert\Phi\rvert^6$	$\mathcal{O}_B = \frac{ig'}{2}\big(\Phi^\dagger \overleftrightarrow{D}^\mu\Phi\big)(\partial^\nu B_{\mu\nu})$
$\mathcal{O}_{BB} = \frac{g'^2}{4}\lvert\Phi\rvert^2 B_{\mu\nu}B^{\mu\nu}$	$\mathcal{O}_T = \frac{1}{2}\big(\Phi^\dagger \overleftrightarrow{D}^\mu\Phi\big)^2$
$\mathcal{O}_{WW} = \frac{g^2}{4}\lvert\Phi\rvert^2 W^i_{\mu\nu}W^{i\,\mu\nu}$	$\mathcal{O}_{HB} = ig'\,(D^\mu\Phi)^\dagger(D^\nu\Phi)B_{\mu\nu}$
$\mathcal{O}_{GG} = \frac{g_S^2}{4}\lvert\Phi\rvert^2 G^A_{\mu\nu}G^{A\mu\nu}$	$\mathcal{O}_{Hu} = i\,(\bar{u}_R\gamma^\mu u_R)\,\big(\Phi^\dagger\overleftrightarrow{D}_\mu\Phi\big)$
$\mathcal{O}_{yu} = y_u\,\lvert\Phi\rvert^2\,\bar{q}_L\tilde{\Phi}u_R$	$\mathcal{O}_{Hd} = i\,\big(\bar{d}_R\gamma^\mu d_R\big)\,\big(\Phi^\dagger\overleftrightarrow{D}_\mu\Phi\big)$
$\mathcal{O}_{yd} = y_d\,\lvert\Phi\rvert^2\,\bar{q}_L\Phi d_R$	$\mathcal{O}_{He} = i\,\big(\bar{l}_R\gamma^\mu l_R\big)\,\big(\Phi^\dagger\overleftrightarrow{D}_\mu\Phi\big)$
$\mathcal{O}_{ye} = y_e\,\lvert\Phi\rvert^2\,\bar{L}_L\Phi e_R$	$\mathcal{O}_{Hq} = i\,(\bar{q}_L\gamma^\mu q_L)\,\big(\Phi^\dagger\overleftrightarrow{D}_\mu\Phi\big)$
	$\mathcal{O}^{(3)}_{Hq} = i\,\big(\bar{q}_L\gamma^\mu\sigma^i q_L\big)\,\big(\Phi^\dagger\sigma^i\overleftrightarrow{D}_\mu\Phi\big)$

Table 11.14: List of 8 dipoles operators. See text for notations.

Dipoles ops.
$\mathcal{O}_{uB} = g'\,(\bar{q}_L\tilde{\Phi}\sigma^{\mu\nu}u_R)\,B_{\mu\nu}$
$\mathcal{O}_{uW} = g\,(\bar{q}_L\sigma^i\tilde{\Phi}\sigma^{\mu\nu}u_R)\,W^i_{\mu\nu}$
$\mathcal{O}_{uG} = g_S\,(\bar{q}_L\tilde{\Phi}\sigma^{\mu\nu}t^A u_R)\,G^A_{\mu\nu}R$
$\mathcal{O}_{dB} = g'\,(\bar{q}_L\Phi\sigma^{\mu\nu}d_R)\,B_{\mu\nu}$
$\mathcal{O}_{dW} = g\,(\bar{q}_L\sigma^i\Phi\sigma^{\mu\nu}d_R)\,W^i_{\mu\nu}$
$\mathcal{O}_{dG} = g_S\,(\bar{q}_L\Phi\sigma^{\mu\nu}t^A d_R)\,G^A_{\mu\nu}$
$\mathcal{O}_{lB} = g'\,(\bar{L}_L\Phi\sigma^{\mu\nu}l_R)\,B_{\mu\nu}$
$\mathcal{O}_{lW} = g\,(\bar{L}_L\sigma^i\Phi\sigma^{\mu\nu}l_R)\,W^i_{\mu\nu}$

considered, for a total of 2499 real deformations [263]). Of particular interest are the 17 CP-invariant operators, in addition to 8 dipole operators, that affect, at tree-level, the Higgs production and decay rates [264–266]. A convenient list of these operators can be found in Table 11.13, and Table 11.14. The other operators completing the basis of dimension-6 operators can be found in Ref. [266].

The SM gauge couplings are denoted by g', g, g_S while $y_{u,d,e}$ are the SM Yukawa couplings (in the mass eigenstate basis that diagonalizes the general Yukawa coupling matrices $Y_{u,d,l}$) and λ is the SM Higgs quartic coupling. We denote by $i\Phi^\dagger\overleftrightarrow{D}^\mu\Phi$ the Hermitian derivative $i\Phi^\dagger(D^\mu\Phi) - i(D^\mu\Phi)^\dagger\Phi$, $\sigma^{\mu\nu} \equiv i[\gamma^\mu,\gamma^\nu]/2$ and $\tilde{\Phi}$ is the Higgs charge-conjugate doublet: $\tilde{\Phi} = i\sigma^2\Phi^*$. Each operator $\mathcal{O}_{yu,yd,ye}$ is further assumed to be

flavor-aligned with the corresponding fermion mass term, as required in order to avoid large Flavor-Changing Neutral Currents (FCNC) mediated by the tree-level exchange of the Higgs boson. This implies one coefficient for the up-type quarks (c_{yu}), one for down-type quarks (c_{yd}), and one for the charged leptons (c_{ye}), i.e. the $c_{yu,ud,ye}$ matrices should be proportional to the identity matrix in flavor space.

The choice of the basis of operators is not unique and using the equations of motion, i.e., performing field redefinitions, different dimension-6 operators can be obtained as linear combinations of the operators in the previous tables and of four-fermion operators. Some relations between common bases of operators can be found for instance in Refs. [265, 263]. Different bases have different advantages. For instance the so-called SILH basis [264] better captures the low-energy effects of universal theories in which new physics couples to SM bosons only. The Warsaw basis [261] on the other hand mostly includes vertex corrections and easily connects operators to observables [266]. The basis defined in Table 11.13, and Table 11.14 is particularly well suited for an analysis of the Higgs data. The reason is that the eight operators of the left-hand side of Table 11.13, in the vacuum with $|\Phi|^2 = v^2/2$, merely redefine the SM input parameters and therefore were left unconstrained at tree-level before Higgs data are considered. These eight operators modify the physical Higgs vertices and can be probed via the decay processes $H \to \gamma\gamma, Z\gamma, \bar{b}b, \bar{\tau}\tau$ and the production channels $gg \to H, VV \to H, pp \to \bar{t}tH$ and $gg \to HH$. Section VI.2 illustrates how the Higgs data accumulated at the LHC can (partially) constrain these eight operators, following the initial phenomenological study of Ref. [266]. The other nine operators of Table 11.13 are tightly constrained by the LEP EW precision measurements (the measurements of the Z-boson couplings to quarks and leptons on the Z-pole) and by diboson production.[5]

The minimal flavor violation assumption imposes Yukawa dependences in the eight dipole operators. For the light generations of fermions, this dependence lowers the induced deviations in the Higgs rates below the experimental sensitivity reachable in any foreseeable future. The corresponding operators in the top sector are not suppressed but they are already constrained by the limit of the top dipole operators imposed by the bounds on the neutron electric dipole moment, on the $b \to s\gamma$ and $b \to s\ell^+\ell^-$ rates and on the $t\bar{t}$ cross section [269, 265].

Automatic tools [265, 240] are being developed to analyze the experimental data within an EFT framework.

VI.2. Probing coupling properties

As described in Section III a framework was developed by the ATLAS and CMS collaboration [143], individually and together, to combine the very large number of exclusive categories aimed at reconstructing the five main decay modes and the five main production modes of the Higgs boson. The general conclusions of this combination

[5] There remains an accidental flat direction [267] in the fit of anomalous gauge boson couplings using LEP2 data on diboson production alone. This flat direction can be lifted when LHC Higgs data are considered [268].

in terms of production cross sections and decay modes, illustrating the compatibility of the observation with the expectation from the SM Higgs boson is given in Section III. The same framework with its master formula Eq. (11.9) can be used to further measure coupling properties of the Higgs boson under specific additional assumptions.

VI.2.1. Combined measurements of the coupling properties of H

(i) From effective Lagrangians to Higgs observables

All 8 operators of the effective Lagrangian that were unconstrained before the Higgs data induce, at tree-level, deviations in the Higgs couplings that either respect the Lorentz structure of the SM interactions, or generate simple new interactions of the Higgs boson to the W and Z field strengths, or induce some contact interactions of the Higgs boson to photons (and to a photon and a Z boson) and gluons that take the form of the ones that are generated by integrating out the top quark. In other words, the Higgs couplings are described, in the unitary gauge, by the following effective Lagrangian [256, 42]

$$\begin{aligned}\mathcal{L} &= \kappa_3 \frac{m_H^2}{2v} H^3 + \kappa_Z \frac{m_Z^2}{v} Z_\mu Z^\mu H + \kappa_W \frac{2m_W^2}{v} W_\mu^+ W^{-\mu} H \\ &+ \kappa_g \frac{\alpha_s}{12\pi v} G^a_{\mu\nu} G^{a\mu\nu} H + \kappa_\gamma \frac{\alpha}{2\pi v} A_{\mu\nu} A^{\mu\nu} H + \kappa_{Z\gamma} \frac{\alpha}{\pi v} A_{\mu\nu} Z^{\mu\nu} H \\ &+ \kappa_{VV} \frac{\alpha}{2\pi v} \left(\cos^2\theta_W Z_{\mu\nu} Z^{\mu\nu} + 2\, W^+_{\mu\nu} W^{-\mu\nu} \right) H \\ &- \left(\kappa_t \sum_{f=u,c,t} \frac{m_f}{v} f\overline{f} + \kappa_b \sum_{f=d,s,b} \frac{m_f}{v} f\overline{f} + \kappa_\tau \sum_{f=e,\mu,\tau} \frac{m_f}{v} f\overline{f} \right) H.\end{aligned} \tag{11.12}$$

The correspondence between the effective coefficients of the dimension-6 operators and the κ's can be found for instance in Ref. [43]. In the SM, the Higgs boson does not couple to massless gauge bosons at tree level, hence $\kappa_g = \kappa_\gamma = \kappa_{Z\gamma} = 0$. Nonetheless, the contact operators are generated radiatively by SM particles loops. In particular, the top quark gives a contribution to the 3 coefficients $\kappa_g, \kappa_\gamma, \kappa_{Z\gamma}$ that does not decouple in the infinite top mass limit. For instance, in that limit $\kappa_\gamma = \kappa_g = 1$ [23, 24, 270].

The coefficient for the contact interactions of the Higgs boson to the W and Z field strengths is not independent but obeys the relation

$$(1 - \cos^4\theta_W)\kappa_{VV} = \sin 2\theta_W \kappa_{Z\gamma} + \sin^2\theta_W \kappa_{\gamma\gamma}. \tag{11.13}$$

This relation is a general consequence of the custodial symmetry [265], which also imposes $\kappa_Z = \kappa_W$ at leading order ($\kappa_Z/\kappa_W - 1$ is a measure of custodial symmetry breaking and as such is already constrained by electroweak precision data and the bounds on anomalous gauge couplings). When the Higgs boson is part of an $\mathrm{SU}(2)_L$ doublet, the custodial symmetry could only be broken by the $\mathcal{O}_T = \frac{1}{2}\left(\Phi^\dagger \overleftrightarrow{D}^\mu \Phi\right)^2$ operator at the level of dimension-6 operators and it is accidentally realized among the interactions with four derivatives, like the contact interactions considered.

The coefficient κ_3 can be accessed directly only through double Higgs production processes, hence it will remain largely unconstrained at the LHC. The LHC will also have a limited sensitivity on the coefficient κ_τ since the lepton contribution to the Higgs production cross section remains subdominant and the only way to access the Higgs coupling is via the $H \to \tau^+\tau^-$ and possibly $H \to \mu^+\mu^-$ channels. Until the associated production of a Higgs with a pair of top quarks is observed, the Higgs coupling to the top quark is only probed indirectly via the one-loop gluon fusion production or the radiative decay into two photons. However, these two processes are only sensitive to the combinations of couplings $(\kappa_t + \kappa_g)$ and $(\kappa_t + \kappa_\gamma)$ and not to the individual couplings. Therefore a deviation in the Higgs coupling to the top quark can in principle always be masked by new contact interactions to photons and gluons (and this is precisely what is happening in minimal incarnations of composite Higgs models). The current limited sensitivity in the $t\bar{t}H$ channel leaves elongated ellipses in the direction $\kappa_g = \kappa_\gamma = 1 - \kappa_t$.

The operators already bounded by EW precision data and the limits on anomalous gauge couplings modify in general the Lorentz structure of the Higgs couplings and hence induce some modifications of the kinematical differential distributions [271, [272]. A promising way to have a direct access to the effective coefficients of these operators in Higgs physics is to study the VH associated production with a W or a Z at large invariant mass of the VH system [271, 273]. It has not been estimated yet whether the sensitivity on the determination of the effective coefficients in these measurements can compete with the one derived for the study of anomalous gauge couplings. In any case, these differential distributions could also be a way to directly test the hypothesis that the Higgs boson belongs to an $\mathrm{SU}(2)_L$ doublet together with the longitudinal components of the massive electroweak gauge bosons.

(ii) Interpretations of the experimental data

The measurements of the coupling properties of the Higgs boson are entirely based on the formalism of the effective Lagrangian described in Section VI.2.1.i. Measurements of coupling properties in this framework implies assessing the parameters of the model Eq. (11.12) or combinations of these parameters with different sets of assumptions.

These measurements are carried out with the combination framework described in Section IV where the μ_i and μ_f signal strength parameters are further interpreted in terms of modifiers of the SM couplings κ_k where $k \in \{Z, W, f, g, \gamma, Z\gamma\}$ as in Eq. (11.12). These coupling modifiers κ are fully motivated as leading order coupling scale factors defined such that the cross sections σ_j and the partial decay widths Γ_j associated with the SM particle j scale with the factor κ_j^2 when compared to the corresponding SM prediction. The number of signal events per category for the various production modes are typically estimated at higher orders in the analyses but are scaled by these single LO-inspired factors, thus not taking into account possible intricacies and correlations of these parameters through the higher order corrections. This approximation is valid within the level of precision of current results and their compatibility with the SM expectation.

In this formalism further assumptions are explicitly made: (i) the signals observed in the different search channels originate from a single narrow resonance with a mass of 125 GeV; (ii) similarly to the combination described in Section IV the narrow width

approximation is assumed (to allow the decomposition of signal yields); (iii) the tensor structure of the couplings is assumed to be the same as that of a SM Higgs boson. This means in particular that the observed state is assumed to be a CP-even scalar as in the SM.

Loop-level couplings such as the $gg \to H$, $H \to \gamma\gamma$ and $H \to Z\gamma$ can either be treated effectively, with The κ_g, κ_γ and $\kappa_{Z\gamma}$ as free parameters in the fit or these parameters can be expressed in terms of the know SM field content and as a function of the SM coupling modifiers, in the following way:

$$\begin{aligned} \kappa_g^2(\kappa_t, \kappa_b) &= 1.06\,\kappa_t^2 - 0.07\,\kappa_t\kappa_b + 0.01\,\kappa_b^2, \\ \kappa_\gamma^2(\kappa_F, \kappa_V) &= 1.59\,\kappa_V^2 - 0.66\,\kappa_V\kappa_F + 0.07\,\kappa_F^2, \\ \kappa_{Z\gamma}^2(\kappa_F, \kappa_V) &= 1.12\,\kappa_V^2 - 0.15\,\kappa_V\kappa_F + 0.03\,\kappa_F^2. \end{aligned} \tag{11.14}$$

The $\kappa_{Z\gamma}$ parametrization is used only in the ATLAS combined measurements of the coupling properties of the Higgs boson [234]. Neither the $Z\gamma$ nor the $\mu^+\mu^-$ channels are included in the CMS [235] and the ATLAS-CMS combinations [143], which therefore do not use the $\kappa_{Z\gamma}$ or κ_μ parameters explicitly. The parametrizations are given for a Higgs boson mass hypothesis of 125.09 GeV (and in the last two expressions, all the Higgs-fermion couplings are assumed to be rescaled by an universal multiplicative factor κ_F). It can be noted from the expression of κ_γ that the coupling of the Higgs boson to photons is dominated by the loop of W bosons, and it is affected by the top quark loop mostly through its interference with the W loop. The sensitivity of the current measurements to the relative sign of the fermion and vector boson couplings to the Higgs boson is due to this large negative interference term. The κ_g parameter is expressed in terms of the scaling of production cross sections and therefore also depends on the pp collisions centre-of-mass energy. The parametrizations of κ_γ and $\kappa_{Z\gamma}$ are obtained from the scaling of partial widths and are only dependent on the Higgs boson mass hypothesis. Experiments use a more complete parametrization with the contributions from the b-quarks, τ-leptons in the loop [256, 42].

The global fit is then performed expressing the μ_i and μ_f parameters in terms of a limited number of κ_k parameters or their ratios, under various assumptions. The parametrization for the main production modes are: (i) $\mu_{ggF} = \kappa_g^2$ for the gluon fusion and an effective coupling of the Higgs boson to the gluons; (ii) $\mu_{VBF,VH} = \kappa_V^2$ for the VBF and VH processes when the W and Z couplings are assumed to scale equally, and $\mu_{VBF}^2(\kappa_W, \kappa_Z) = (\kappa_W^2\sigma_{WWH} + \kappa_Z^2\sigma_{ZZH})/(\sigma_{WWH} + \sigma_{ZZH})$, when the couplings to the W and Z bosons are varied independently (σ_{WWH} and σ_{ZZH} denote the VBF cross sections via the fusion of a W and a Z boson respectively, the small interference term is neglected); (iii) $\mu_{ttH} = \kappa_t^2$ for the $t\bar{t}$H production mode. Numerically the production modes signal strengths as a function of the coupling modifiers to the SM fields are:

$$\mu_{ggF} = 1.06\kappa_t^2 + 0.01\kappa_b^2 - 0.07\kappa_t\kappa_b, \quad \text{and} \quad \mu_{VBFF} = 0.74\kappa_W^2 + 0.26\kappa_Z^2.$$

The decay mode signal strengths are parametrized as $\mu_k = \kappa_k^2/\kappa_H^2$ where $k \in \{Z, W, f, g, \gamma, Z\gamma\}$ denotes the decay mode and κ_H the overall modifier of the total width

that affects all the signal yields. κ_H is a priori an independent parameter. However, when it is assumed that the Higgs boson cannot decay to new particles beyond those of the SM, κ_H can also be treated as an effective parameter and expressed in terms of the coupling modifiers to the SM field content. Its general expression is:

$$\kappa_H^2 = 0.57\kappa_b^2 + 0.06\kappa_\tau^2 + 0.03\kappa_c^2 + 0.22\kappa_W^2 + 0.03\kappa_Z^2 + 0.09\kappa_g^2 + 0.0023\kappa_\gamma^2. \qquad (11.15)$$

The general expression of the total width of the Higgs boson can be written as follows:

$$\Gamma_H = \frac{\kappa_H^2 \Gamma_H^{SM}}{1 - \mathrm{BR}_{\mathrm{BSM}}}$$

where Γ_H^{SM} is the total width of the SM Higgs boson and $\mathrm{BR}_{\mathrm{BSM}}$ is the branching fraction of the Higgs boson to new particles beyond the SM.

Specific parametrizations will be made in order to address the following aspects of the coupling properties of the Higgs boson under different assumptions: (i) the relative couplings of the Higgs boson to fermions and bosons; (ii) the potential impact of the presence of new particles beyond the SM either in the loops or both in the loops and the decay of the H; and (iii) also, more general models either of coupling modifiers or their ratios, under different assumptions.

(iii) Relative couplings to bosons and fermions

As will be discussed in Section VII.6.3, it is interesting to probe a model where no additional field content is considered in the decay width of the Higgs boson and where the relative couplings of the Higgs boson to W- and Z-bosons is fixed to its SM value and where all Yukawa couplings scale with one coupling modifier. In this model only SM particles are assumed to contribute to the gluon fusion and the diphoton loops, all fermion couplings modifiers are required to scale simultaneously with a unique factor κ_F and all vector boson couplings modifiers must scale simultaneously with a unique factor κ_V. This parametrization assumes that no new particles affect the direct decays or the loops. It is a two parameters fit with κ_V and κ_F as parameters of interest. The ATLAS-CMS combined results for each channel independently, the combinations of all channels for the two experiments separately and the results and the overall combination are shown in Fig. 11.10.

The global fit is only sensitive to the relative sign of κ_V and κ_F. By convention negative values of κ_F can be considered. Such values are not excluded a priori, but would imply the existence of new physics at a light scale and would also raise questions about the stability of such a vacuum [274]. Among the five main Higgs decay channels, only the $\gamma\gamma$ is sensitive to the sign of κ_F through the interference of the W and t loops as shown in Eq. (11.14). The current global fit disfavors a negative value of κ_F at more than five standard deviations. A specific analysis for the Higgs boson production in association with a single top quark has been proposed [275, 276] in order to more directly probe the sign of κ_F. All available experimental data show a fair agreement of the SM prediction of the couplings of the Higgs boson to fermions and gauge bosons. The results shown

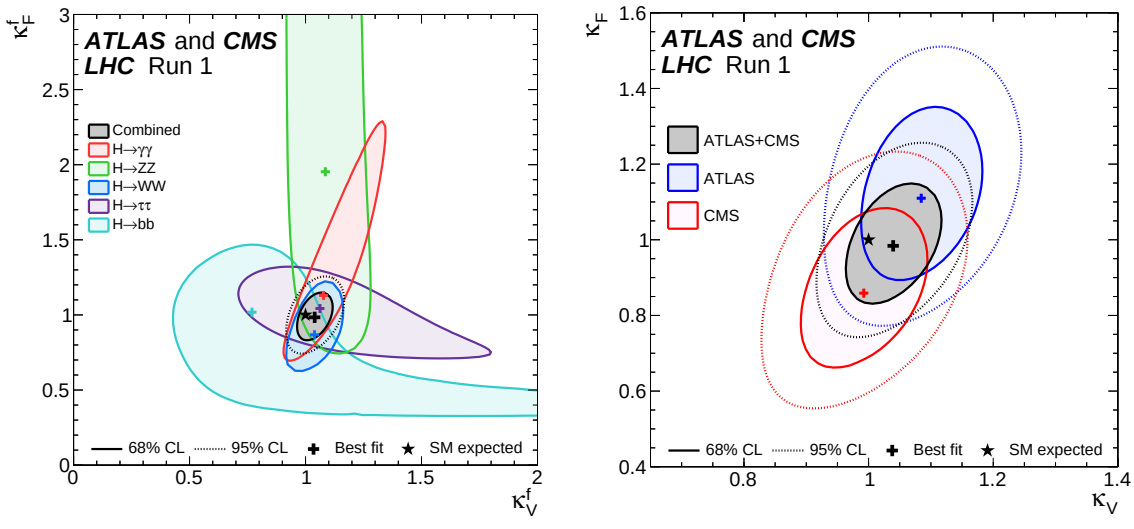

Figure 11.10: Likelihood contours in the (κ_F, κ_V) plane for the ATLAS-CMS combination for the main decay channels separately (left) and for the individual combination of all channels for ATLAS and CMS separately and the complete combined contour (right) [143].

in Fig. 11.10 assume that $\kappa_F \geq 0$, however in Ref. [143], a similar combination is done without this assumption. The combined sensitivity to the exclusion of a negative relative sign, is approximately 5σ in this model. It is interesting to note that although none of the channels have a significant sensitivity to resolve the sign ambiguity, the combination can, mainly through the $W-t$ interference in the $H \to \gamma\gamma$ channel and the $H \to W^+W^-$ channel. The observed exclusion is fully compatible with the expectation [143]. The combined measurements with the Run 1 dataset lead to

$$\kappa_V = 1.04 \pm 0.05 \quad \text{and} \quad \kappa_F = 0.98^{+0.11}_{-0.10},$$

already at the impressive 5% level of accuracy for the κ_V parameter.

(iv) Coupling measurements and probing new physics beyond the SM in loops and in the decay

In the model described above in Section VI.2.1.iii the assumption is that no new fields distort in a perceptible way the loop contributions in the couplings of the H to gluons and photons and the total width, its couplings to known SM particles are then probed. In a first approach to simultaneously probe new physics beyond the SM in the loops and not in the decay and the couplings of the Higgs boson to SM particles, only one assumption is needed *i.e.* that $\text{BR}_{\text{BSM}} = 0$. In this model the coupling of the H to photons and gluons is effective and κ_Z, κ_W, κ_t, $|\kappa_\tau|$, and $|\kappa_b|$ are measured simultaneously. The absolute value of certain coupling modifiers only indicates the complete degeneracy of combined likelihood for the two signs. It can be noted that when the coupling to gluons is not considered effective, there is some sensitivity to the sign of κ_b through the interference

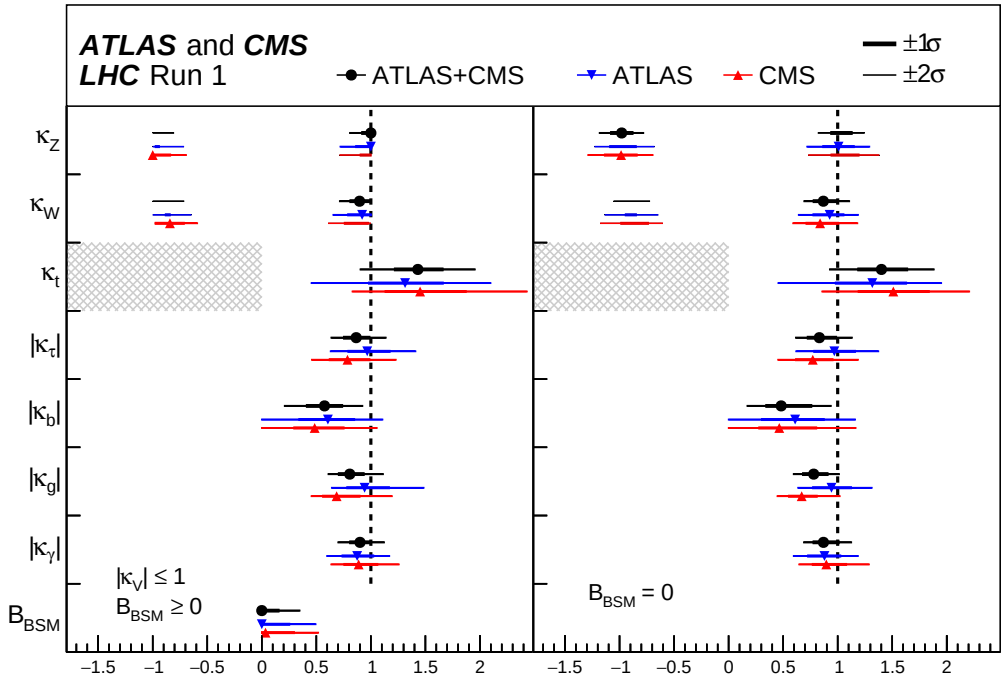

Figure 11.11: ATLAS-CMS combined measurements of coupling modifiers.

between the top and bottom quarks loops in the gluon fusion process. In this model it is interesting to note that the constraints on the top quark Yukawa coupling comes from the ttH direct search channels. The expected precision on κ_t is approximately 40%. As discussed in Section III the excesses observed in the ttH channel yield a large value of $\kappa_t = 1.40^{+0.24}_{-0.21}$. The complete set of results from this model is given in Fig. 11.11 (right).

This model, which assumes that no new particles enter the decay of the Higgs boson, also yields very interesting constraints on new physics in the loops through the effective coupling modifiers κ_g and κ_γ. The measured values of these parameters:

$$\kappa_g = 0.78^{+0.13}_{-0.10} \quad \text{and} \quad \kappa_\gamma = 0.87^{+0.14}_{-0.09}$$

are fully compatible with the expectation for the SM Higgs boson.

A more constrained model fully focussing on BSM scenarios with new heavy particles contributing to the loops (and not directly in the decays *i.e.* $\text{BR}_{\text{BSM}} = 0$) and where all couplings to the SM particles are assumed to be the same as in the Standard Model ($\kappa_W = \kappa_Z = \kappa_t = \kappa_b = \kappa_\tau = 1$) is also used to constrain the κ_g and κ_γ parameters only. The contours of the combined likelihood in the $(\kappa_\gamma, \kappa_g)$ plane for the ATLAS and CMS experiments and their combination are shown in Fig. 11.12.

This general model requires the strong assumption that the the Higgs boson decays only to SM particles. This assumption is necessary due to the degeneracy of solutions given that κ_H is a common factor to all measured signals. The degeneracy can however be resolved using a constraint on the width of the Higgs boson as the one from the off-Shell couplings measurements. This approach was used by the ATLAS experiment [234], thus

yielding a absolute measurement of the couplings of the Higgs boson.

Another well motivated constraint to resolve the aforementioned degeneracy is unitarity. Simply requiring that $\kappa_V \leq 1$ allows to free the $\mathrm{BR}_{\mathrm{BSM}}$ parameter and further probe new physics in the decay of the Higgs boson. An intuitive understanding of how this constraint works can be given by a simple example *e.g.* VBF $H \to W^+W^-$ production where the number of signal events will be parametrized by $(1 - \mathrm{BR}_{\mathrm{BSM}})\kappa_W^4/\kappa_H^2$, where for a number of signal events observed close to the SM expectation, large values of $\mathrm{BR}_{\mathrm{BSM}}$ cannot be compensated by a large value of κ_W and is thus limited. Or in other terms, if $\kappa_W \sim 1$ is preferred from other channels, a low signal in the VBF $H \to W^+W^-$ channel would be a sign of the presence of new physics beyond the SM in the Higgs decays. From this general model all the above parameters can be measured in addition to $\mathrm{BR}_{\mathrm{BSM}}$. The results of this combination are shown in Fig. 11.11 (left). The results for all parameters do not change significantly with respect to the previous model. A limit can however be set on the beyond the SM branching fraction of the Higgs boson at the 95% CL:

$$\mathrm{BR}_{\mathrm{BSM}} < 34\%.$$

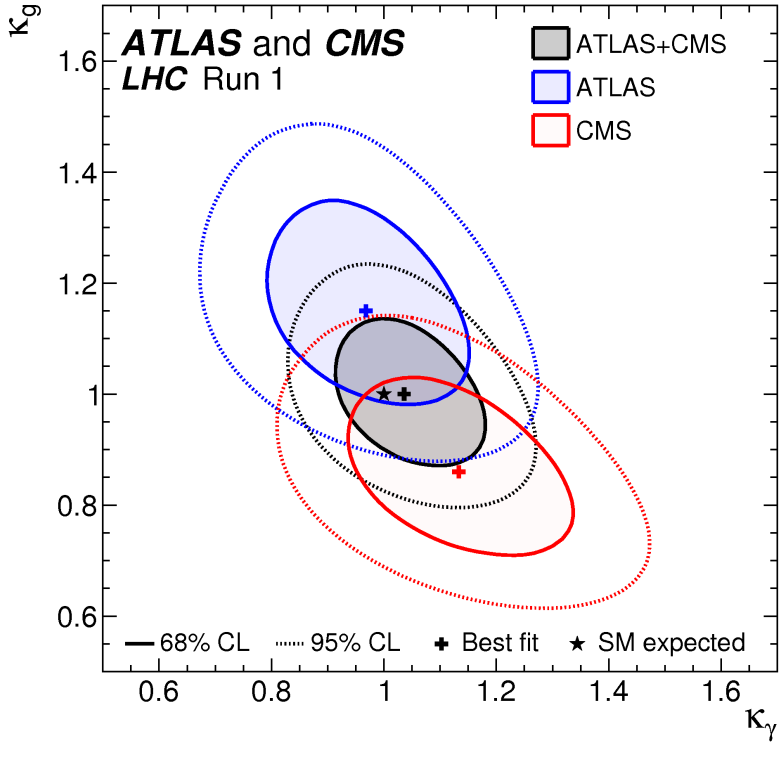

Figure 11.12: Likelihood contours of the global in the $(\kappa_g, \kappa_\gamma)$ plane for the ATLAS-CMS combination for the individual combination of all channels for ATLAS and CMS separately and the complete combined contour [143].

In the second approach, new physics is considered also in the decay thus affecting the total width of the H through decays to particles which are either "invisible" and escape detection in the experiments, or "undetected" which are not distinctive enough to be seen in the current analyses. This approach is complementary to the direct search for invisible decays of the Higgs boson described in Section III. The two approaches can be combined assuming that the undetected branching fraction is negligible. this combination was performed by the ATLAS experiment [277] and yields a limit on the invisible decays of the Higgs boson of $\mathrm{BR}_{inv} < 25\%$ at the 95% CL.

VI.2.2. Differential cross sections

To further characterize the production and decay properties of H, first measurements of fiducial and differential cross sections have been carried out by the ATLAS collaboration [278] and CMS [278] collaborations, both at Run 1 and Run 2 and in several channels: (i) the diphoton, (ii) The four leptons, and (iii) the WW channels. The selection criteria to define the fiducial volume are the following: the two highest transverse momentum (E_T), isolated final state photons, within $|\eta| < 2.37$ and with $105\,\mathrm{GeV} < M_{\gamma\gamma} < 160\,\mathrm{GeV}$ are selected (the transition region between the barrel and endcap calorimeters is not removed); after the pair is selected, the same cut on $E_T/M_{\gamma\gamma}$ as in the event selection *i.e.* in excess of 0.35 (0.25) for the two photons is applied. Several observables have been studied: the transverse momentum rapidity of the diphoton system, the production angle in the Collins–Soper frame, the jet multiplicity, the jet veto fractions for a given jet multiplicity, and the transverse momentum distribution of the leading jet. The following additional observables: the difference in azimuthal angle between the leading and the subleading jets, and the transverse component of the vector sum of the momenta of the Higgs boson and dijet system, have also been measured in two jet events. To minimize the model dependence the differential cross sections are given within a specific fiducial region of the two photons. The observables were chosen to probe the production properties and the spin and parity of the H. The differential cross section in H transverse momentum is given in Fig. 11.13.

VI.2.3. Constraints on non-SM Higgs boson interactions in an effective Lagrangian

An example of the possible use of differential cross sections in constraining non-SM Higgs boson couplings in an EFT is given by the ATLAS collaboration [279]. In this analysis, differential cross section measured in the diphoton channel are used to constrain an effective Lagrangian where the SM is supplemented by dimension six CP-even operators of the Strongly Interacting Light Higgs (SILH) formulation and corresponding CP-odd operators. The diphoton differential cross sections are mainly sensitive to the operators that affect the Higgs boson interactions with gauge bosons and the relevant terms in the effective Lagrangian can be parameterized as:

$$\begin{aligned}\mathcal{L}_{\mathit{eff}} =& \bar{c}_\gamma \mathcal{O}_\gamma + \bar{c}_g \mathcal{O}_g + \bar{c}_{HW} \mathcal{O}_{HW} + \bar{c}_{HB} \mathcal{O}_{HB} + \\ & \tilde{c}_\gamma \tilde{\mathcal{O}}_\gamma + \tilde{c}_g \tilde{\mathcal{O}}_g + \tilde{c}_{HW} \tilde{\mathcal{O}}_{HW} + \tilde{c}_{HB} \tilde{\mathcal{O}}_{HB}\,,\end{aligned} \tag{11.16}$$

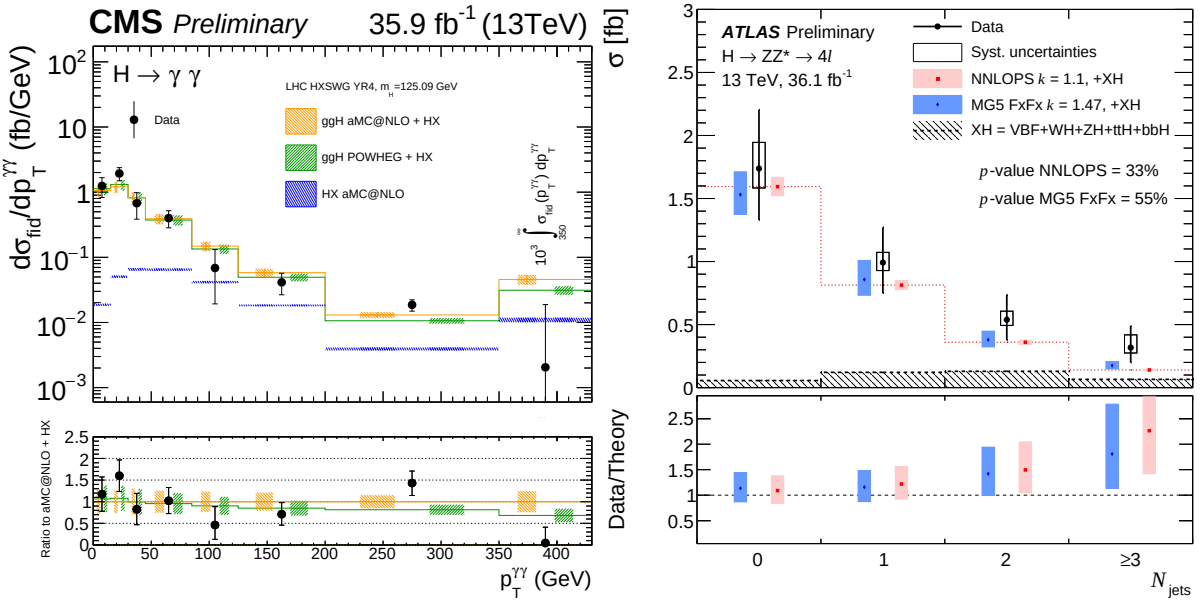

Figure 11.13: Observed differential cross sections in transverse momentum of the H in the diphoton channel, compared to the prediction of the ggF process [278].

where $\overline{c}_i$ and $\tilde{c}_i$ are the effective coefficients corresponding to the CP-even and CP-odd interactions, respectively, see Ref. [264].

The differential distributions used in this combination are: (i) the transverse momentum of the Higgs boson, (ii) the number of reconstructed jets produced in association with the diphoton pair, (iii) the invariant mass of the diphoton system and (iv) the difference in azimuthal angle of the leading and sub-leading jets in events with two or more jets.

This analysis shows how differential information significantly improves the sensitivity to operators that modify the Higgs boson interaction to photons, gluons and vector bosons both from the main gluon fusion and the vector boson fusion production modes.

VI.2.4. Simplified Template Cross Sections

An overarching subject of discussion between the Theory and Experimental communities in the field of Higgs physics has been how experimentalists could best communicate their results for them to be most efficiently used by other communities for further interpretation.

In the field of precision Standard Model measurements, the commonly used practise is that results are given at particle level within a well defined fiducial volume of phase space. The fiducial volume is usualy defined close enough to the experimental reconstruction to minimize the possible variations of the reconstruction efficiency within the particle level fiducial volume. In this way results minimize their dependence on theoretical uncertainties.

Experiments have produced fiducial and unfolded cross sections based on all objects

reconstruced in the event. These measurements could be used for further interpretation. However, in order to perform a proper combination of channels taking into account all experimental systematic uncertainties is non trivial. A proposal [43] was made by the LHC Higgs Cross Section working group to produce results in each decay channel with a well defined fiducial phase space of the Higgs boson (and not its decay products) and for other associated objects pertaining to all channels, such as jets and missing transverse momentum (MET). The definition of the fiducial regions is motivated by maximizing the experimental sensitivity, the isolation of possible BSM effect, and minimizing the dependence on theoretical uncertainties. The number of regions is also minimized avoiding loss of experimental sensitivity. The observable that are measured in this approach are still the standard production cross sections (the gluon fusion, the vector boson fusion, the VH and ttH associated production modes) within the defined fiducial volumes.

In summary, this approach is hybrid. It is fiducial on specific objects to reduce the theory dependence and inclusive in the Higgs kinematics in order to allow for a more straightforward combination. This approach also allows the use of multivariate techcniques to enhance the sensitivity within given fiducial regions, at the expense of a greater extrapolation and therefore increased model dependence.

First results in this framework have been produced by experiments in several channels, including the diphoton and the 4ℓ [124, 128, 125, 132].

VII. New physics models of EWSB in the light of the Higgs boson discovery

The discovery of a light scalar with couplings to gauge bosons and fermions that are apparently consistent with SM predictions and the slow running of the Higgs self-coupling at high energies allows one to consider the SM as a valid perturbative description of nature all the way to the Planck scale. This picture is admittedly very attractive, but it posits that the Higgs boson is an elementary scalar field, which comes with an intrinsic instability of its mass under radiative corrections. This Higgs naturalness problem calls for new physics around the TeV scale. Supersymmetric models are the most elegant solution to maintain the perturbativity of the SM while alleviating the instability issue. Another possibility is that the Higgs boson itself has a finite size and is composite and thus never feels the UV degrees of freedom that would drag its mass to much higher scales. Both classes of models predict specific modifications from the SM Higgs properties.

The realization of supersymmetry at low energies has many good qualities that render it attractive as a model of new physics. First of all since for every SM degree of freedom there is superpartner of different spin but of equal mass and effective coupling to the SM-like Higgs, in the case of exact supersymmetry, an automatic cancellation of quantum corrections to the Higgs mass parameter holds. In practice, it is known that SUSY must be broken in nature since no superpartners of the SM particles have been observed so far. The mass difference between the precise value of any of the particle masses and that of its corresponding superpartner is proportional to the correlated soft supersymmetry breaking parameter, generically called M_{SUSY}. The quantum corrections to the Higgs mass parameter are proportional to M^2_{SUSY}, and provided M_{SUSY} is of order of a few TeV, the fine-tuning problem is solved, in the sense that the low energy mass parameters

of the Higgs sector become insensitive to physics at the GUT or Planck scale. Another interesting feature of SUSY theories is related to the dynamical generation of EWSB [280]. In the SM a negative Higgs mass parameter, m^2, needs to be inserted by hand to induce EWSB, see Eq. (11.1). In SUSY, instead, even if the relevant Higgs mass parameter is positive in the ultraviolet, it may become negative and induce electroweak symmetry breaking radiatively through the strong effect of the top quark-Higgs boson coupling in its renormalization group evolution.

In the following, the Higgs sector will be explored in specific SUSY models. In all of them there is one neutral Higgs boson with properties that resemble those of the SM Higgs boson, whereas additional neutral and charged Higgs bosons are also predicted and are intensively being sought for at the LHC (see Section VII.8). In the simplest SUSY model the lightest Higgs boson mass, that usually plays the role of the SM-like Higgs, is predicted to be less than 135 GeV for stops in the TeV to few TeV mass range [281] whereas, larger values of the SM-like Higgs boson mass – up to about 250 GeV – can be obtained in non-minimal SUSY extensions of the SM [281]. In general, accommodating a SM-like Higgs boson with mass of 125 GeV results in constraints on the supersymmetric parameter space of specific SUSY models. While naturalness dictates relatively light stops and gluinos, the first and second generation of squarks and sleptons couple weakly to the Higgs sector and may be heavy. Moreover, small values of the μ parameter and therefore light Higgsinos, the fermionic superpartners of the Higgs bosons, would be a signature of a natural realization of electroweak symmetry breaking. Such SUSY spectra, consisting of relatively light stops and light Higgsinos, continue to be under intense scrutiny by the experimental collaborations [282] in order to understand if such natural SUSY scenarios endure [283] and can explain why the Higgs boson remains light.

In the context of weakly coupled models of EWSB one can also consider multiple Higgs $\mathrm{SU}(2)_L$ doublets as well as additional Higgs singlets, triplets or even more complicated multiplet structures, with or without low energy supersymmetry. In general for such models one needs to take into account experimental constraints from precision measurements and flavor changing neutral currents. The LHC signatures of such extended Higgs sectors are largely shaped by the role of the exotic scalar fields in EWSB.

The idea that the Higgs boson itself could be a composite bound state emerging from a new strongly-coupled sector has regained some interest. The composite Higgs idea is an interesting incarnation of EWSB via strong dynamics that smoothly interpolates between the standard Technicolor approach and the true SM limit. To avoid the usual conflict with EW data, it is sufficient if not necessary that a mass gap separates the Higgs resonance from the other resonances of the strong sector. Such a mass gap can naturally follow from dynamics if the strongly-interacting sector exhibits a global symmetry, G, broken dynamically to a subgroup H at the scale f, such that, in addition to the three Nambu–Goldstone bosons of SO(4)/SO(3) that describe the longitudinal components of the massive W and Z, the coset G/H contains a fourth Nambu–Goldstone boson that can be identified with the physical Higgs boson. Simple examples of such a coset are SU(3)/SU(2) or SO(5)/SO(4), the latter being favored since it is invariant under the custodial symmetry. It is also possible to have non-minimal custodial cosets with extra Goldstone bosons leading to additional Higgs bosons in the spectrum, see for

instance Ref. [284]. Modern incarnations of composite Higgs models have been recently investigated in the framework of 5D warped models where, according to the principles of the AdS/CFT correspondence, the holographic composite Higgs boson then originates from a component of a gauge field along the 5th dimension with appropriate boundary conditions.

A last crucial ingredient in the construction of viable composite Higgs models is the concept of partial compositeness [285], i.e., the idea that there are only linear mass mixings between elementary fields and composite states. After diagonalization of the mass matrices, the SM particles, fermions and gauge bosons, are admixtures of elementary and composite states and thus they interact with the strong sector, and in particular with the Higgs boson, through their composite component. This setup has important consequences on the flavor properties, chiefly the suppression of large flavor changing neutral currents involving light fermions. It also plays an important role in dynamically generating a potential for the would-be Goldstone bosons. Partial compositeness also links the properties of the Higgs boson to the spectrum of the fermionic resonances, i.e. the partners of the top quark. As in the MSSM, these top partners are really the agents that trigger the EWSB and also generate the mass of the Higgs boson that otherwise would remain an exact Goldstone boson and hence massless. The bounds from the direct searches for the top partners in addition to the usual constraints from EW precision data force the minimal composite Higgs models into some unnatural corners of their parameter spaces [15, 286].

VII.1. Higgs bosons in the minimal supersymmetric standard model (MSSM)

The particle masses and interactions in a supersymmetric theory are uniquely defined as a function of the superpotential and the Kähler potential [287]. A fundamental theory of supersymmetry breaking, however, is unknown at this time. Nevertheless, one can parameterize the low-energy theory in terms of the most general set of soft supersymmetry-breaking operators [281]. The simplest realistic model of low-energy supersymmetry is the minimal supersymmetric extension of the SM (MSSM) [11, 287], that associates a supersymmetric partner to each gauge boson and chiral fermion of the SM, and provides a realistic model of physics at the weak scale. However, even in this minimal model with the most general set of soft supersymmetry-breaking terms more than 100 new parameters are introduced [281]. Fortunately, only a subset of these parameters impact the Higgs phenomenology either directly at tree-level or through quantum effects.

The MSSM contains the particle spectrum of a two-Higgs-doublet model (2HDM) extension of the SM and the corresponding supersymmetric partners. Two Higgs doublets, Φ_1 and Φ_2, with hypercharge $Y = -1$ and $Y = 1$, respectively, are required to ensure an anomaly-free SUSY extension of the SM and to generate mass for down-type quarks/charged leptons (Φ_1)and up-type quarks (Φ_2) [12]. The Higgs potential reads

$$\begin{aligned} V = {} & m_1^2\Phi_1^\dagger\Phi_1 + m_2^2\Phi_2^\dagger\Phi_2 - m_3^2(\Phi_1^T i\sigma_2\Phi_2 + \text{h.c.}) + \frac{1}{2}\lambda_1(\Phi_1^\dagger\Phi_1)^2 + \frac{1}{2}\lambda_2(\Phi_2^\dagger\Phi_2)^2 \\ & + \lambda_3(\Phi_1^\dagger\Phi_1)(\Phi_2^\dagger\Phi_2) + \lambda_4|\Phi_1^T i\sigma_2\Phi_2|^2 + \frac{1}{2}\lambda_5[(\Phi_1^T i\sigma_2\Phi_2)^2 + \text{h.c.}] \\ & + [[\lambda_6(\Phi_1^\dagger\Phi_1) + \lambda_7(\Phi_2^\dagger\Phi_2)]\Phi_1^T i\sigma_2\Phi_2 + \text{h.c.}] \end{aligned} \tag{11.17}$$

where $m_i^2 = \mu^2 + m_{H_i}^2$ $(i = 1, 2)$, with μ being the supersymmetric Higgsino mass parameter and m_{H_i} the soft supersymmetric breaking mass parameters of the two Higgs doublets; $m_3^2 \equiv B\mu$ is associated to the B-term soft SUSY breaking parameter; and λ_i, for $i = 1$ to 7, are all the Higgs quartic couplings.

After the spontaneous breaking of the electroweak symmetry (see Ref. [283] for detail), five physical Higgs particles are left in the MSSM spectrum: one charged Higgs pair, $H^\pm$, one CP-odd neutral scalar, A, and two CP-even neutral states, H and h, with h being the lightest.[6] The Higgs sector at tree level depends on the electroweak gauge coupling constants and the vacuum expectation value v – or equivalently the Z gauge boson mass – and is determined by only two free parameters: $\tan\beta$ - the ratio of the two Higgs doublets' vacuum expectation values v_2/v_1 - and one Higgs boson mass, conventionally chosen to be the CP-odd Higgs boson mass, m_A. The other tree-level Higgs boson masses are then given in terms of these parameters. The tree level value of m_h is maximized not only for $m_A \gg M_Z$ but also for $\tan\beta \gg 1$. For $m_A \gg M_Z$ it acquires a maximum value $m_h = M_Z \cos 2\beta$.

Radiative corrections have a significant impact on the values of Higgs boson masses and couplings in the MSSM. The dominant radiative effects to the SM-like Higgs mass arise from the incomplete cancellation between top and scalar-top (stop) loops and at large $\tan\beta$ also from sbottom and stau loops. The stop, sbottom and stau masses and mixing angles depend on the supersymmetric Higgsino mass parameter μ and on the soft-supersymmetry-breaking parameters [11, 287]: M_Q, M_U, M_D, M_L, M_E, and A_t, A_b A_τ. The first three of these are the left-chiral and the right-chiral top and bottom scalar quark mass parameters. The next two are the left-chiral stau/sneutrino and the right-chiral stau mass parameters, and the last three are the trilinear parameters that enter in the off-diagonal squark/slepton mixing elements: $X_t \equiv A_t - \mu\cot\beta$ and $X_{b,\tau} \equiv A_{b,\tau} - \mu\tan\beta$. At the two-loop level, the masses of the gluino and the electroweak gaugino also enter in the calculations. Radiative corrections to the Higgs boson masses have been computed using a number of techniques, with a variety of approximations; for a discussion see for example Refs. [38, 288, 289] and the corresponding section of the previous edition of this review.

The newly discovered SM-like Higgs boson, if interpreted as the lightest MSSM Higgs with a mass of about 125 GeV, provides information on the possible MSSM parameter space. See Fig. 11.14. and discussion in Ref. [283]

The phenomenology of the Higgs sector depends on the couplings of the Higgs bosons to gauge bosons and fermions. At tree-level, the couplings of the two CP-even Higgs bosons to W and Z bosons are given in terms of the angles α, that diagonalizes the CP-even Higgs squared-mass matrix, and β

$$g_{hVV} = g_V m_V \sin(\beta - \alpha), \quad g_{HVV} = g_V m_V \cos(\beta - \alpha), \tag{11.18}$$

[6] Observe that in the SM sections of this review, H denotes the SM Higgs, whereas in the sections about SUSY, or extensions of the SM with two Higgs doublets, H is used for the heaviest CP-even Higgs boson, since this is the standard notation in the literature, and the 125 GeV SM-like light Higgs boson will be denoted by h.

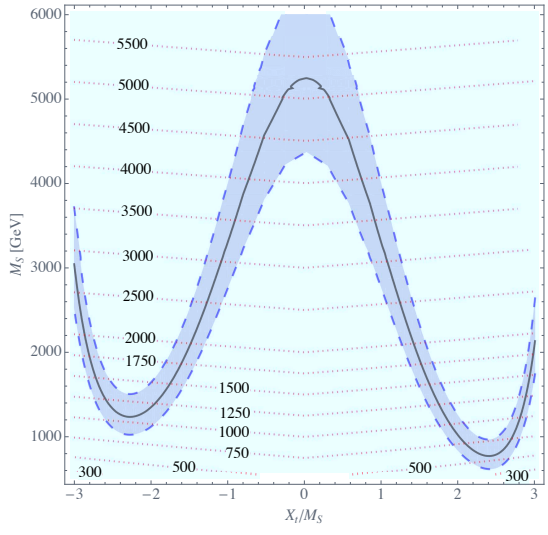

Figure 11.14: Values of the SUSY mass scale $M_{\rm SUSY} = M_S$ versus the stop mixing parameter normalized by the SUSY mass scale $X_t/M_{\rm SUSY}$, for fixed $\tan\beta = 20$, $\mu = 200\,\text{GeV}$ and $M_A = A_t = A_b = A_\tau = M_{\rm SUSY}$. The solid black line corresponds to $M_h = 125\,\text{GeV}$ while in the grey band M_h varies by $\pm 1\,\text{GeV}$. The red dotted lines are iso-values of the stop mass. This figure is based on Ref. [290].

where $g_V \equiv 2m_V/v$, for $V = \text{W}^\pm$ or Z ($g_V m_V$ is the SM hVV coupling). Observe that in the limit $\cos(\beta-\alpha) \to 0$, the lightest CP-even Higgs h behaves as the SM Higgs boson. This situation is called alignment and is achieved in specific regions of parameter space for $m_A \geq M_Z$ [291] or in the large $m_A \gg M_Z$ limit, in which alignment is achieved through decoupling [291, 292]. There are no tree-level couplings of A or $H^\pm$ to VV. The couplings of the Z boson to two neutral Higgs bosons are given by $g_{\phi AZ}(p_\phi - p_A)$, where $\phi = H$ or h, the momenta p_ϕ and p_A point into the vertex, and

$$g_{hAZ} = g_Z \cos(\beta-\alpha)/2, \quad g_{HAZ} = -g_Z \sin(\beta-\alpha)/2\,. \tag{11.19}$$

Charged Higgs-W boson couplings to neutral Higgs bosons and four-point couplings of vector bosons and Higgs bosons can be found in Ref. [12].

The tree-level Higgs couplings to fermions obey the following property: the neutral components of one Higgs doublet, Φ_1, couple exclusively to down-type fermion pairs while the neutral components of the other doublet, Φ_2, couple exclusively to up-type fermion pairs [12]. This Higgs-fermion coupling structure defines the Type-II 2HDM [293]. In the MSSM, fermion masses are generated when both neutral Higgs components acquire vacuum expectation values, and the relations between Yukawa couplings and fermion masses are (in third-generation notation)

$$h_{b,\tau} = \sqrt{2}\, m_{b,\tau}/(v\cos\beta), \qquad h_t = \sqrt{2}\, m_t/(v\sin\beta)\,. \tag{11.20}$$

The couplings of the neutral Higgs bosons to $f\bar{f}$ relative to the SM value, $g m_f/2M_W$,

are given by

$$\begin{aligned} hb\bar{b}: & -\sin\alpha/\cos\beta & ht\bar{t}: & \cos\alpha/\sin\beta\,, \\ Hb\bar{b}: & \cos\alpha/\cos\beta & Ht\bar{t}: & \sin\alpha/\sin\beta\,, \\ Ab\bar{b}: & \gamma_5\tan\beta & At\bar{t}: & \gamma_5\cot\beta\,. \end{aligned} \tag{11.21}$$

In each relation above, the factor listed for $b\overline{b}$ also pertains to $\tau^+\tau^-$. The charged Higgs boson couplings to fermion pairs, normalized to $g/\sqrt{2}M_W$, are given by

$$g_{H^-t\bar{b}}: m_t\cot\beta\frac{1+\gamma_5}{2}+m_b\tan\beta\frac{1-\gamma_5}{2} \qquad g_{H^-\tau^+\nu}: m_\tau\tan\beta\frac{1-\gamma_5}{2}\,. \tag{11.22}$$

The non-standard neutral Higgs bosons have significantly enhanced couplings to down-type fermions at sizeable $\tan\beta$. Radiative corrections can modify significantly the values of the Higgs boson couplings to fermion pairs and to vector boson pairs, through a "radiatively-corrected" value for $\cos(\beta-\alpha)$ [294, 295], as well as from the one-loop vertex corrections to tree-level Higgs-fermion Yukawa couplings [296–303].

VII.1.1. MSSM Higgs boson phenomenology

In the MSSM, the mass, CP properties, decay and production properties of one of the neutral Higgs bosons should agree with the LHC Higgs data. Given that present data allows only for moderate departures from the SM predictions, it implies that some degree of alignment is necessary. The SM-like branching ratios of h can be modified if decays into supersymmetric particles are kinematically allowed, and, in particular, decays into a pair of the lightest supersymmetric particles – i.e. the lightest neutralinos, $\tilde{\chi}^0_1$ – can become dominant and would be invisible if R-parity is conserved [304–306]. Moreover, if light superpartners exist that couple to photons and/or gluons, the h loop-induced coupling to gg and $\gamma\gamma$ could deviate sizably from the corresponding SM predictions [294, 307–310, 311, 312], although such deviations are also significantly constrained by present data

For the heavier Higgs states there are two possibilities to be considered: i) Alignment triggered by decoupling, hence $m_A \geq$ several hundred GeV: The HWW and HZZ couplings are very small. The dominant H, A decay branching ratios strongly depend on $\tan\beta$. The decay modes $H, A \to b\overline{b}$, $\tau^+\tau^-$ dominate when $\tan\beta$ is large (this holds even away from decoupling). For small $\tan\beta$, the $t\bar{t}$ decay mode dominates above its kinematic threshold. For the charged Higgs boson, $H^+ \to t\bar{b}$ dominates. ii) Some degree of alignment without decoupling, hence $m_A \leq$ a few hundred GeV. The main difference with the previous case is that in the low $\tan\beta$ regime ($\tan\beta \leq 5$) additional decay channels may be allowed which involve decays into the lightest SM-like Higgs boson; $A \to Zh$, $H \to hh$ as well as $H \to WW/ZZ$ decay modes are available (they are suppressed in the strict alignment limit). When kinematically open the decays $A/H \to t\bar{t}$ become relevant or even dominant for sufficiently small $\tan\beta$. For the charged Higgs boson, $H^+ \to \tau^+\nu_\tau$ dominates below the $t\bar{b}$ threshold, and also $H^\pm \to W^\pm h$ may be searched for. Both in i) and ii), the heavier Higgs states, H, A and $H^\pm$, are roughly mass degenerate (with masses $\pm$ 20 GeV or less apart). If kinematically allowed, the heavy

Higgs boson decays into charginos, neutralinos and third-generation squarks and sleptons can be important [304].

At hadron colliders, the dominant neutral Higgs production mechanism at moderate values of $\tan\beta$ is gluon fusion, mediated by loops containing heavy top and bottom quarks and the corresponding supersymmetric partners [281]. The effect of light stops that may contribute to the gluon fusion production can be partially cancelled by mixing effects. Higgs boson radiation off bottom quarks becomes important for large $\tan\beta$, where at least two of the three neutral Higgs bosons have enhanced couplings to bottom-type fermions [315–314]. Detailed discussions of the impact of radiative corrections in these search modes are presented in Refs. [316, 317]. The vector boson fusion and Higgs-strahlung production of the CP-even Higgs bosons as well as the associated production of neutral Higgs bosons with top quark pairs have lower production cross sections by at least an order of magnitude with respect to the dominant ones, depending on the precise region of MSSM parameter space [40–43]. Higgs pair production of non-standard MSSM Higgs bosons has been studied in Ref. [318]. For a discussion of charged Higgs boson production at LHC see Refs. [11, 40, 319, 281].

Summarizing, the additional Higgs bosons are sought for mainly via the channels [7]

$$\begin{aligned}
&pp \to A/H \to \tau^+\tau^- \ \text{(inclusive)},\\
&b\bar{b}A/H, A/H \to \tau^+\tau^- \ \text{(with } b\text{-tag)},\\
&b\bar{b}A/H, A/H \to b\bar{b} \ \text{(with } b\text{-tag)},\\
&pp \to t\bar{t} \to H^\pm W^\mp b\bar{b}, \ \ H^\pm \to \tau\nu_\tau \ \ ,\\
&gb \to H^- t \quad \text{or} \quad g\bar{b} \to H^+\bar{t}, \ \ H^\pm \to \tau\nu_\tau \ \ .
\end{aligned} \tag{11.23}$$

After the Higgs boson discovery, updated MSSM benchmarks scenarios have been defined, that highlight interesting conditions for MSSM Higgs searches [42, 321]. They include: i) a moderate mixing scenario in which the light CP-even Higgs boson can be interpreted as the newly discovered state in most of the $m_A - \tan\beta$ plane; ii) a light stop scenario with stop masses in the few to several hundred GeV range that can affect gluon fusion Higgs production; and iii) a tau-phobic scenario that exhibits variations of $\mathrm{BR}(h \to b\bar{b})$ and $\mathrm{BR}(h \to \tau^+\tau^-)$ with respect to their SM values. In the above benchmarks it is also possible to have decays of $H \to hh$ in regions of moderate m_A and moderate $\tan\beta$ as far as one is away from precise alignment. Also for the previous benchmarks, the LHC reach in the traditional $A/H \to \tau^+\tau^-$ search channel varies depending on the values of μ and M_2, that may enable the A/H decays into electroweakinos.

An alternative approach to reduce the large number of parameters relevant to the Higgs sector is to consider that, in the Higgs basis, the only important radiative corrections are

[7] Strong production of a heavy neutral Higgs boson followed by its decay into top pairs is a challenging channel, only most recently being searched for by ATLAS and CMS. Interference effects between the signal and the SM $t\bar{t}$ background need to be carefully taken into account [320].

those affecting the Higgs mass [322]. This approximation is called hMSSM and works well in large regions of parameter space but it breaks down for sizable values of μ and A_t, and moderate values of $\tan\beta$, for which the radiative corrections to the mixing between the two CP even eigenstates become relevant. The effect of such radiative corrections is to allow for alignment for small to intermediate values of $\tan\beta$, independent of the specific value of m_A [323]. In addition, the hMSSM assumption that the right value of the Higgs mass may be obtained for all values of m_A and $\tan\beta$ is in conflict with the MSSM predictions for the Higgs mass for small values of m_A and $\tan\beta \simeq \mathcal{O}(1)$.

Reviews of the properties and phenomenology of the Higgs bosons of the MSSM can be found for example in Refs. [38, 283, 287, 288]. Future precision measurements of the Higgs boson couplings to fermions and gauge bosons together with information on heavy Higgs searches will provide powerful information on the SUSY parameter space [323–326]. For representative references on production mechanisms for the MSSM Higgs bosons at e^+e^- see Ref. [281].

Improvements in our understanding of B-physics observables put indirect constraints on additional Higgs bosons in mass ranges that would be accessible in direct LHC searches. In particular, BR($B_s \to \mu^+\mu^-$), BR($b \to s\gamma$), and BR($B_u \to \tau\nu$) play an important role within minimal flavor-violating (MFV) models [327], in which flavor effects proportional to the CKM matrix elements are induced as in the SM, see e. g. references in Ref. [281].

VII.2. Supersymmetry with singlet extensions

The Higgs mass parameter μ is a supersymmetric parameter, and as such, it should naturally be of order M_{GUT} or M_{Planck}. The fact that phenomenologically it is required that μ be at the electroweak/TeV scale is known as the μ problem [328]. Supersymmetric models with additional singlets can provide a solution to the μ problem, by promoting the μ parameter to a dynamical singlet superfield S that only interacts with the MSSM Higgs doublets through a coupling λ_S at the level of the superpotential. An effective μ is generated when the real scalar component of S acquires a vacuum expectation value v_S, yielding $\mu_{eff} = \lambda_S\, v_S$. After the minimization of the Higgs potential the vacuum state relates the vacuum expectation values of the three CP-even neutral scalars, v_1, v_2 and v_S, to the scalar doublet and singlet soft supersymmetry breaking masses, hence, one expects that these VEVs should all be of order M_{SUSY} and therefore the μ problem is solved.

The addition of a singlet superfield to the MSSM may come along with additional symmetries imposed to the theory. Depending on such symmetries, different models with singlet extensions of the MSSM (xMSSM) have been proposed. Among the most studied examples are the NMSSM with an additional discrete Z_3 symmetry (first introduced in Ref. [329]), the Nearly-Minimal Supersymmetric SM (nMSSM), with additional discrete Z_5^R, and Z_7^R symmetries [330], and the U(1)′-extended MSSM (UMSSM) [331]. A Secluded U(1)′-extended MSSM (sMSSM) [332] contains three singlets in addition to the standard UMSSM Higgs singlet; this model is equivalent to the nMSSM in the limit that the additional singlet VEV's are large, and the trilinear singlet coupling, λ_S, is small [333].

Based on the extended models defined above, we write the most generic supersymmetric and soft supersymmetry breaking scalar potentials for the two MSSM scalar doublets: Φ_1, Φ_2 and the scalar singlet S:

$$\begin{aligned} V_{xMSSM} = & \left|\lambda_S \Phi_2 \cdot \Phi_1 + t_F + \kappa S^2\right|^2 + |\lambda_S S|^2 \left(|\Phi_1|^2 + |\Phi_2|^2\right) \\ & + \frac{g'^2 + g^2}{8}\left(|\Phi_1|^2 - |\Phi_2|^2\right)^2 + \frac{g^2}{2}\left(|\Phi_1|^2 |\Phi_2|^2 - |\Phi_2 \cdot \Phi_1|^2\right) \\ & + \frac{g_1'^2}{2}\left(Q_{\Phi_1}|\Phi_1|^2 + Q_{\Phi_2}|\Phi_2|^2 + Q_S |S|^2\right)^2 \end{aligned} \tag{11.24}$$

$$V_{\rm soft} = m_{H_1}^2 |\Phi_1|^2 + m_{H_2}^2 |\Phi_2|^2 + m_s^2 |S|^2 + \left(A_s \lambda_S S H_u \cdot H_d + \frac{\kappa}{3} A_\kappa S^3 + t_S S + h.c.\right). \tag{11.25}$$

In the above, $\Phi_2 \cdot \Phi_1 = \epsilon_{ij}\Phi_2^i \Phi_1^j$ and the couplings g', g, and g_1' are associated to the $\mathrm{U}(1)_Y$, $\mathrm{SU}(2)_L$, and $\mathrm{U}(1)'$ gauge symmetries, respectively. t_F and t_S are supersymmetric and SUSY breaking tadpole terms, respectively, m_s is a SUSY breaking mass term for the scalar component of the field S, and A_s and A_κ are the trilinear soft SUSY breaking mass parameters associated with the new terms $\lambda_S S \Phi_2 \cdot \Phi_1$ and $\kappa S^3/3$ in the superpotential, with the B-term of the MSSM expressed as $B\mu \equiv A_s \mu_{\mathit{eff}}$. The UMSSM depends on the $\mathrm{U}(1)'$ charges of the Higgs fields, Q_{Φ_1}, Q_{Φ_2} and Q_S, that are free parameters with the restriction that they have to add to zero for the superpotential $\lambda_S S \Phi_2 \Phi_1$ to be gauge invariant. The addition of the singlet scalar field(s) imply that additional CP-even and CP-odd Higgs bosons will appear in the spectra, whereas the charged Higgs sector remains the same as in the MSSM given that the number of Higgs doublets remains unchanged. The mixing with the extra scalar S alters the masses and properties of the physical Higgs bosons. A detailed discussion of typical mass spectra and decay properties in these models can be found for example in Refs. [334, 333]. Moreover, these models have extra neutralinos and in some cases extra neutral gauge bosons, Z'. The extra gauge boson sector is constrained by experimental data through direct Z' searches as well as the $Z - Z'$ mixing angle $\alpha_{ZZ'}$ constrained to be less that $\mathcal{O}(10^{-3})$ by precision electroweak data.

In singlet extensions of the MSSM the lightest CP-even Higgs mass at tree level, $m_{H_1}^{tree}$ receives a contribution from the singlet scalar that renders it larger than the MSSM value, in particular for small values of $\tan\beta$. The tree level upper bound reads[8]

$$m_{H_1}^{tree} \leq M_Z^2 \cos^2 2\beta + \frac{1}{2}\lambda_S^2 v^2 \sin^2 2\beta\,. \tag{11.26}$$

At the one-loop level, the top and stop loops (as well as sbottom and stau loops for large $\tan\beta$) are the dominant contributions, that are common to the MSSM and to all the singlet extensions. Gauge couplings in the UMSSM are small compared to the top quark

[8] Additional gauge interactions in the UMSSM contribute to this increase with a term of $\mathcal{O}(g_1'^2 v^2 (Q_{\phi_2}^2 \cos^2\beta + Q_{\phi_1}^2 \sin^2\beta))$.

Yukawa coupling, hence the one-loop gauge contributions are negligible. Corrections exclusive to the NMSSM and the nMSSM enter only at the two loop level. In the decoupling limit, a value of the lightest SM Higgs mass of about 125 GeV is achievable in all these MSSM extensions, and this remains the case even after higher order corrections are implemented.

A singlet extended supersymmetric Higgs sector opens new avenues for discovery. Since the singlet pseudoscalar particle may be identified as the pseudo-Goldstone boson of a spontaneously broken Peccei–Quinn symmetry, it may become naturally light [335, 336]. Generally, there is mixing of the singlet sector with the MSSM Higgs sector, and for a sufficiently light, singlet dominated scalar or pseudoscalar, h_S or A_S, respectively, the SM-like Higgs boson h may decay to pairs of h_S or A_S. The light scalar and/or pseudoscalar may subsequently decay to $\tau\tau$ or $b\bar{b}$ pairs. Such cascade decays are more difficult to detect than standard searches due to the potentially soft decay products. There is also a rich phenomenology for the decays of the heavy CP-even and CP-odd doublets, A and H into two lighter Higgs bosons such as $H \to hh_S$, hh, h_Sh_S or $A \to A_Sh_S$, A_Sh as well as into a light Higgs boson and a gauge boson: $H \to A_SZ$; $A \to h_SZ$, hZ. If kinematically allowed the heavy Higgs bosons decay into $t\bar{t}$. If the singlet dominated scalar or pseudoscalar are somewhat heavier, the decays $h_S \to WW$ or $A_S \to h_SZ$ will be allowed.

In addition, the light singlet scenario in the NMSSM or nMSSM is typically associated with a light singlino-dominated neutralino. The recently discovered SM-like Higgs boson can then decay to pairs of this neutralino [337, 333], opening an invisible decay mode that is not excluded by present data. All of the Higgs bosons can decay into electroweakinos depending on kinematics and the singlino or higgsino composition of the electroweakinos.

In models with extended singlets, at low $\tan\beta$ it is possible to trade the requirement of a large stop mixing by a sizeable trilinear Higgs-singlet Higgs coupling λ_S, rendering more freedom on the requirements for gluon fusion production. As in the MSSM, mixing in the Higgs sector -additionally triggered by the extra new parameter λ_S - can produce variations in the Higgs–$b\bar{b}$ and Higgs–$\tau^-\tau^+$ couplings that can alter the Higgs to ZZ/WW and diphoton rates. Light charginos at low $\tan\beta$ can independently contribute to enhance the di-photon rate, without altering any other of the Higgs decay rates [310, 338].

There is much activity in exploring the NMSSM phenomenology in the light of the 125 GeV Higgs boson [339], as well as in defining benchmark scenarios with new topologies including Higgs decay chains [340]. An analytic understanding of the alignment condition in the NMSSM is presented in Ref. [341]. The NMSSM with a Higgs boson of mass 125 GeV can be compatible with stop masses of order of the electroweak/TeV scale, thereby reducing the degree of fine tuning necessary to achieve electroweak symmetry breaking (see Fig. 11.15). Interestingly, the alignment conditions point toward a more natural region of parameter space for electroweak symmetry breaking, while allowing for perturbativity of the theory up to the Planck scale and yielding a rich and interesting Higgs boson phenomenology at the LHC.

VII.3. Supersymmetry with extended gauge sectors

In the MSSM, the tree-level value of the lightest CP-even Higgs mass originates from

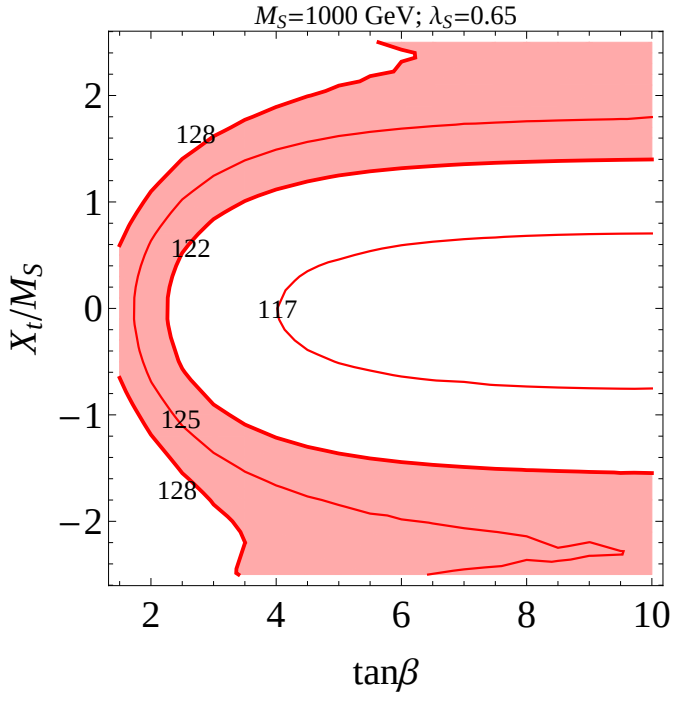

Figure 11.15: Values of the stop mixing parameter normalized to the SUSY mass scale $X_t/M_{\rm SUSY}$, as a function of $\tan\beta$, for $M_{\rm SUSY} \equiv M_S = 1000\,\text{GeV}$, $\lambda_S = 0.65$, and contours of constant values of the Higgs mass $m_h = 125 \pm 3\,\text{GeV}$ shaded in red [342].

the D-term dependence of the scalar potential that comes from the supersymmetric kinetic terms in the Kähler potential. The D-terms lead to tree-level quartic couplings which are governed by the squares of the gauge couplings of the weak interactions, under which the Higgs has non-trivial charges and hence the lightest Higgs mass is bounded to be smaller than M_Z. In the presence of new gauge interactions at the TeV scale, and if the Higgs fields had non-trivial charges under them, new D-term contributions would lead to an enhancement of the tree-level Higgs mass value. Since the low energy gauge interactions reduce to the known $\text{SU}(3)_c \times \text{SU}(2)_L \times \text{U}(1)_Y$ ones, in order for this mechanism to work, the extended gauge and Higgs sectors should be integrated out in a non-supersymmetric way. This means that there must be supersymmetry breaking terms that are of the order of, or larger than, the new gauge boson masses. The tree-level quartic couplings would then be enhanced through their dependence on the square of the gauge couplings of the extended Higgs sector. This effect will be suppressed when the heavy gauge boson masses are larger than the supersymmetry breaking scale and will acquire its full potential only for large values of this scale.

One of the simplest possibilities is to extend the weak interactions to a $\text{SU}(2)_1 \times \text{SU}(2)_2$ sector, such that the known weak interactions are obtained after the spontaneous breaking of these groups to $\text{SU}(2)_L$ [343]. This example is briefly summarized in Ref. [283]. Assuming supersymmetry breaking terms of the order of the new gauge boson masses,

enhancements of order 50 percent of the MSSM D-term contribution to the Higgs mass may be obtained. Such enhancements are sufficient to obtain the measured Higgs mass value without the need for very heavy stops or large stop mixing parameters. This gauge extension leads to new, heavy gauge and Higgs bosons, as well as new neutralinos and charginos, that depending on the region of parameter space can induce novel phenomenology at the LHC. Gauge extensions including new abelian gauge groups have been considered, for instance, in Ref. [344].

Gauge extensions of the MSSM can also lead to an enhancement of the Higgs mass value by modifying the renormalization group evolution of the Higgs quartic coupling to low energies. In the MSSM, the evolution of the quartic coupling is governed by the top-quark Yukawa interactions and depends on the fourth power of the top-quark Yukawa coupling. The neutralino and chargino contributions, which depend on the fourth power of the weak gauge couplings, are small due to the smallness of these couplings. Depending on the values of the soft supersymmetry breaking parameters in the gaugino and Higgsino sectors, the $\mathrm{SU}(2)_1$ gauginos may become light, with masses of the order of the weak scale. Since the $\mathrm{SU}(2)_1$ coupling may be significantly larger than the $\mathrm{SU}(2)_L$ one, for small values of the Higgsino mass parameter μ, the associated charginos and neutralinos may modify the evolution of the quartic coupling in a significant way [345]. This may lead to a significant increase of the lightest CP-even Higgs mass, even for small values of $\tan\beta \simeq 1$ for which the D-term contributions become small.

VII.4. Effects of CP violation

SUSY scenarios with CP-violation (CPV) phases are theoretically appealing, since additional CPV beyond that observed in the K, D, and B meson systems is required to explain the observed cosmic matter-antimatter asymmetry. In the MSSM, CP-violation effects in the Higgs sector appear at the quantum level, while in singlet extensions of the MSSM CP-violation effects can already be effective at tree level. In general, CP-violation effects in the Higgs sector have significant constraints from electric dipole moments data [281].

In the MSSM, the gaugino mass parameters ($M_{1,2,3}$), the Higgsino mass parameter, μ, the bilinear Higgs squared-mass parameter, m_{12}^2, and the trilinear couplings of the squark and slepton fields to the Higgs fields, A_f, may carry non-trivial phases. The two parameter combinations $\arg[\mu A_f (m_{12}^2)^*]$ and $\arg[\mu M_i (m_{12}^2)^*]$ are invariant under phase redefinitions of the MSSM fields [346, 347]. Therefore, if one of these quantities is non-zero, there would be new sources of CP-violation affecting the Higgs sector through radiative corrections [348, 347, 349–353]. The mixing of the neutral CP-odd and CP-even Higgs boson states is no longer forbidden. Hence, m_A is no longer a physical parameter. However, the charged Higgs boson mass $m_{H^\pm}$ is still physical and can be used as an input for the computation of the neutral Higgs spectrum of the theory. For large values of $m_{H^\pm}$, corresponding to the decoupling limit, the properties of the lightest neutral Higgs boson state approach those of the SM Higgs boson. In particular, the upper bound on the lightest neutral Higgs boson mass, takes the same value as in the CP-conserving case [347]. Nevertheless, there still can be significant mixing between the two heavier

neutral mass eigenstates. For a detailed study of the Higgs boson mass spectrum and parametric dependence of the associated radiative corrections, see Refs. [349, 352].

Major variations to the Higgs phenomenology occur in the presence of explicit CPV phases. In the CPV case, vector boson pairs couple to all three neutral Higgs boson mass eigenstates, H_i $(i = 1, 2, 3)$, with couplings

$$g_{H_iVV} = \cos\beta\mathcal{O}_{1i} + \sin\beta\mathcal{O}_{2i}\,, \tag{11.27}$$

$$g_{H_iH_jZ} = \mathcal{O}_{3i}\left(\cos\beta\mathcal{O}_{2j} - \sin\beta\mathcal{O}_{1j}\right) - \mathcal{O}_{3j}\left(\cos\beta\mathcal{O}_{2i} - \sin\beta\mathcal{O}_{1i}\right)\,, \tag{11.28}$$

where the g_{H_iVV} couplings are normalized to the analogous SM coupling and the $g_{H_iH_jZ}$ have been normalized to $g_Z^{\rm SM}/2$. The orthogonal matrix $\mathcal{O}_{ij}$ is relating the weak eigenstates to the mass eigenstates. It has non-zero off-diagonal entries mixing the CP-even and CP-odd components of the weak eigenstates. Moreover, CPV phases imply that all neutral Higgs bosons can couple to both scalar and pseudoscalar fermion bilinear densities. The couplings of the mass eigenstates H_i to fermions depend on the loop-corrected fermion Yukawa couplings (similarly to the CPC case), on $\tan\beta$ and on the $\mathcal{O}_{ji}$ [349, 354].

The production processes of neutral MSSM Higgs bosons in the CPV scenario are similar to those in the CPC scenario. Regarding the decay properties, the lightest mass eigenstate, H_1, predominantly decays to $b\overline{b}$ if kinematically allowed, with a smaller fraction decaying to $\tau^+\tau^-$, similar to the CPC case. If kinematically allowed, a SM-like neutral Higgs boson, H_2 or H_3 can decay predominantly to H_1H_1 leading to many new interesting signals both at lepton and hadron colliders; otherwise it will decay preferentially to $b\overline{b}$.

The discovery of a 125 GeV Higgs boson has put strong constraints on the realization of the CPV scenario within the MSSM. This is partly due to the fact that the observed Higgs rates are close to the SM values, and a large CP-violating component would necessarily induce a large variation in the rate of the SM-like Higgs decay into the weak gauge bosons $W^\pm$ and Z. The measured Higgs mass imposes additional constraints on the realization of this scenario. Once all effects are considered, the CP-odd Higgs A component of the lightest Higgs tends to be smaller than about 10%. This restriction can be alleviated in the NMSSM or more general two Higgs doublet models. CP-violating effects can still be significant in the heavy Higgs sector. For instance, the Higgs bosons H_2 and H_3 may be admixtures of CP-even and CP-odd scalars, and therefore both may be able to decay into pairs of weak gauge bosons. The observation of such decays would be a clear signal of CP-violation. In the MSSM the proximity of the masses of H_2 and H_3 makes the measurement of such effect quite challenging, but in generic two Higgs doublet models, the mass splitting between the two heavy mass eigenstates may become larger, facilitating the detection of CP-violating effects at collider experiments [355].

VII.5. Non-supersymmetric extensions of the Higgs sector

There are many ways to extend the minimal Higgs sector of the SM. In the preceding sections the phenomenology of SUSY Higgs sectors is considered, which at tree level

implies a constrained type-II 2HDM (with restrictions on the Higgs boson masses and couplings). In the following discussion, more generic 2HDM's [12, 293, 356, 357] are presented. These models are theoretically less compelling since they do not provide an explanation for the SM Higgs naturalness problem, but can lead to different patterns of Higgs-fermion couplings, hence, to different phenomenology. It is also possible to consider models with a SM Higgs boson and one or more additional scalar SU(2) doublets that acquire no VEV and hence play no role in the EWSB mechanism. Such models are dubbed Inert Higgs Doublet Models (IHD) [358]. Without a VEV associated to it, a Higgs boson from an inert doublet has no tree-level coupling to gauge bosons and hence cannot decay into a pair of them. Moreover, imposing a Z_2 symmetry that prevents them from coupling to the fermions, it follows that, if the lightest inert Higgs boson is neutral, it becomes a good dark matter candidate with interesting associated collider signals. Recent studies of IHD models in the light of a 125 GeV Higgs have been performed in Ref. [359], showing an interesting interplay between collider and direct dark matter detection signals.

An interesting type of 2HDMs, are those in which an abelian flavor symmetry broken at the electroweak scales creates the fermion mass hierarchies and mixing angles [360]. This idea is based on the Froggatt-Nielsen model [361], where a flavon field couples differently to the SM fermions of different flavor charges. Such flavon acquires a vacuum expectation value, breaking the flavor symmetry but leaving both the flavor breaking and the new physics scales undetermined. In Refs. [362], it was proposed to relate the flavor breaking scale to the electroweak scale by identifying the flavon with the modulus square of the Higgs field. A 2HDM, however, provides a more compelling realization of the electroweak scale flavor breaking idea. In the most ambitious constructions of two Higgs doublet flavor models (2HDFM), the textures of the Yukawa couplings are a result of an abelian flavor symmetry that only allows renormalizable Yukawa couplings of the top quark to the Higgs bosons. All other Yukawa couplings are generated by higher dimensional operators that produce hierarchical entries of the Yukawa matrices, explaining the observed quark masses and mixing angles. Flavor observables, LHC Higgs signal strength measurements, electroweak precision measurements, unitarity and perturbativity bounds, as well as collider searches for new scalar resonances result in precise predictions for the parameters of these 2HDFMs. In particular, correlated departures from SM Higgs couplings, as well as additional Higgs bosons with masses < 700 GeV must be observed at the LHC. Other incarnations of 2HDFMs can aim at only partially explaining the fermion mass hierarchies and be less restrictive.

Other extensions of the Higgs sector can include multiple copies of $\mathrm{SU}(2)_L$ doublets [334, 363], additional Higgs singlets [364], triplets or more complicated combinations of Higgs multiplets. It is also possible to enlarge the gauge symmetry beyond $\mathrm{SU}(2)_L \times \mathrm{U}(1)_Y$ along with the necessary Higgs structure to generate gauge boson and fermion masses. There are two main experimental constraints on these extensions: *(i)* precision measurements which constrain $\rho = m_W^2/(m_Z^2 \cos^2\theta_W)$ to be very close to 1 and *(ii)* flavor changing neutral current (FCNC) effects. In electroweak models based on the SM gauge group, the tree-level value of ρ is determined by the Higgs multiplet structure. By suitable choices for the hypercharges, and in some cases the mass splitting

between the charged and neutral Higgs sector or the vacuum expectation values of the Higgs fields, it is possible to obtain a richer combination of singlets, doublets, triplets and higher multiplets compatible with precision measurements [365]. Concerning the constraints coming from FCNC effects, the Glashow–Weinberg (GW) criterion [366] states that, in the presence of multiple Higgs doublets the tree-level FCNC's mediated by neutral Higgs bosons will be absent if all fermions of a given electric charge couple to no more than one Higgs doublet. An alternative way of suppressing FCNC in a two Higgs doublet model has been considered in Ref. [367], where it is shown that it is possible to have tree level FCNC completely fixed by the CKM matrix, as a result of an abelian symmetry.

VII.5.1. Two-Higgs-doublet models

General two Higgs doublet models [356] can have a more diverse Higgs-fermion coupling structure than in Supersymmetry, and can be viewed as a simple extension of the SM to realize the spontaneous breakdown of $\mathrm{SU}(2)_L \times \mathrm{U}(1)_Y$ to $\mathrm{U}(1)_{\mathrm{em}}$. Quite generally, if the two Higgs doublets contain opposite hypercharges, the scalar potential will contain mixing mass parameters of the kind $m_{12}^2 \Phi_1^T i\sigma_2 \Phi_2 + h.c.$. In the presence of such terms, both Higgs doublets will acquire vacuum expectation values, $v_1/\sqrt{2}$ and $v_2/\sqrt{2}$, respectively, and the gauge boson masses will keep their SM expressions with the Higgs vacuum expectation value v replaced by $v = \sqrt{v_1^2 + v_2^2}$. Apart from the mass terms, the most generic renormalizable and gauge invariant scalar potential for two Higgs doublets with opposite hypercharges contains seven quartic couplings, as presented in Eq. (11.17).

Just as in the MSSM case, after electroweak symmetry breaking and in the absence of CP-violation, the physical spectrum contains a pair of charged Higgs bosons $H^\pm$, a CP-odd Higgs boson A and two neutral CP-even Higgs bosons, h and H. The angles α and β diagonalize the CP-even, and the CP-odd and charged Higgs sectors, respectively. The complete 2HDM is defined only after considering the interactions of the Higgs fields to fermions. Yukawa couplings of the generic form

$$-h_{ij}^a \bar{\Psi}_L^i H_a \Psi_R^j + h.c. \tag{11.29}$$

may be added to the renormalizable Lagrangian of the theory. Contrary to the SM, the two Higgs doublet structure does not ensure the alignment of the fermion mass terms $m_{ij} = h_{ij}^a v_a/\sqrt{2}$ with the Yukawa couplings h_{ij}^a. This implies that quite generally, the neutral Higgs boson will mediate flavor changing interactions between the different mass eigenstates of the fermion fields. Such flavor changing interactions should be suppressed in order to describe properly the Kaon, D and B meson phenomenology. Based on the Glashow–Weinberg criterion, it is clear that the simplest way of avoiding such transitions is to assume the existence of a symmetry that ensures the couplings of the fermions of each given quantum number (up-type and down-type quarks, charged and neutral leptons) to only one of the two Higgs doublets. Different models may be defined depending on which of these fermion fields couple to a given Higgs boson, see Table 11.15. Models of type-I [357] are those in which all SM fermions couple to a single Higgs field. In type-II models [293] down-type quarks and charged leptons couple to a common Higgs field,

Table 11.15: Higgs boson couplings to up, down and charged lepton-type $SU(2)_L$ singlet fermions in the four discrete types of 2HDM models that satisfy the Glashow–Weinberg criterion, from Ref. [368].

Model	2HDM I	2HDM II	2HDM III	2HDM IV
u	Φ_2	Φ_2	Φ_2	Φ_2
d	Φ_2	Φ_1	Φ_2	Φ_1
e	Φ_2	Φ_1	Φ_1	Φ_2

while the up-type quarks and neutral leptons couple to the other. In models of type-III (lepton-specific) quarks couple to one of the Higgs bosons, while leptons couple to the other. Finally, in models of type-IV (flipped), up-type quarks and charged leptons couple to one of the Higgs fields while down-quarks and neutral leptons couple to the other.

The two Higgs doublet model phenomenology depends strongly on the size of the mixing angle α and therefore on the quartic couplings. For large values of m_A, $\sin\alpha \to -\cos\beta$, $\cos\alpha \to \sin\beta$, $\cos(\beta-\alpha) \to 0$, and the lightest CP-even Higgs h behaves as the SM Higgs. The same behavior is obtained if the quartic couplings are such that $\mathcal{M}^2_{12}\sin\beta = -(\mathcal{M}^2_{11} - m^2_h)\cos\beta$. The latter condition represents a situation in which the coupling of h to fermions and weak gauge bosons become the same as in the SM, without decoupling the rest of the non-standard scalars and it is of particular interest due to the fact that the recently discovered Higgs boson has SM-like properties. This situation will be referred to as alignment, as in the MSSM case.

In analogy to the effects of CP violation in the supersymmetric 2HDM, choosing m^2_3, λ_5, λ_6 and λ_7 as complex while all other parameters are real, one has a model that is explicitly CP violating. The three neutral mass eigenstates mixed with each other and the Higgs phenomenology is analogous to the one described for the SUSY case above, with the caveat that when considering the neutral Higgs couplings to the scalar and pseudoscalar fermion bilinear densities the proper weight should be considered for the respective 2HDM's.

In type-II Higgs doublet models, at large values of $\tan\beta$ and moderate values of m_A, the non-standard Higgs bosons H, A and $H^\pm$ couple strongly to bottom quarks and τ leptons. Hence the decay modes of the non-standard Higgs bosons tend to be dominated by b-quark and tau-lepton modes, including top quarks or neutrinos in the case of the charged Higgs. However, for large and negative values of λ_4, the charged Higgs boson mass may be sufficiently heavy to allow on-shell decays $H^\pm \to W^\pm + (H, A)$, via a trilinear coupling

$$g_{H^\pm W^\mp H,A} \simeq \frac{M_W}{v}\sin(\beta-\alpha)(p_{H^+} - p_{H,A})\,, \tag{11.30}$$

where p_{H^+} and $p_{H,A}$ are the charged and neutral scalar Higgs momenta pointing into the vertex. On the other hand, for large and positive values of λ_5, the above charged Higgs decay into a $W^\pm$ and the CP-odd Higgs boson may be allowed, but the heavy Higgs H may be sufficiently heavy to decay into a CP-odd Higgs boson and an on-shell

Z, $H \to Z + A$, via

$$g_{HZA} \simeq \frac{M_Z}{v} \sin(\beta - \alpha)(p_H - p_A). \tag{11.31}$$

The decay $H^\pm \to W^\pm + H$, on the other hand may be allowed only if $\lambda_4 < -\lambda_5$. The couplings controlling all the above decay modes are proportional to $\sin(\beta - \alpha)$ and therefore they are unsuppressed in the alignment limit. Moreover, these could still be the dominant decay modes at moderate values of $\tan\beta$, offering a way to evade the current bounds obtained assuming a dominant decay into bottom quarks or τ leptons.

The quartic couplings are restricted by the condition of stability of the effective potential as well as by the restriction of obtaining the proper value of the lightest CP-even Higgs mass. Close to the alignment limit, the lightest CP-even Higgs mass becomes approximately independent of m_A and is given by

$$\begin{aligned} m_h^2 \simeq & v^2(\lambda_1 \cos^4\beta + \lambda_2 \sin^4\beta + 2\tilde{\lambda}_3 v^2 \cos^2\beta \sin^2\beta) \\ & + v^2(4\lambda_6 \cos^3\beta \sin\beta + 4\lambda_7 \sin^3\beta \cos\beta)\,, \end{aligned} \tag{11.32}$$

where $\tilde{\lambda}_3 = \lambda_3 + \lambda_4 + \lambda_5$.

The stability conditions imply the positiveness of all masses, as well as the avoidance of run-away solutions to large negative values of the fields in the scalar potential. These conditions imply

$$\begin{aligned} & \lambda_1 \geq 0, \quad \lambda_2 \geq 0, \quad \lambda_3 + \lambda_4 - |\lambda_5| \geq -\sqrt{\lambda_1 \lambda_2}, \\ & \lambda_3 \geq -\sqrt{\lambda_1 \lambda_2}, \quad 2|\lambda_6 + \lambda_7| < \frac{\lambda_1 + \lambda_2}{2} + \tilde{\lambda}_3, \end{aligned} \tag{11.33}$$

where the first four are necessary and sufficient conditions in the case of $\lambda_6 = \lambda_7 = 0$, while the last one is a necessary condition in the case all couplings are non-zero. Therefore, to obtain the conditions that allow the decays $H^\pm \to W^\pm H, A$ and $H \to ZA$, λ_3 should take large positive values in order to compensate for the effects of λ_4 and λ_5. For more detailed discussions about 2HDM phenomenology see for example Refs [43, 324, 363, 369–372, 373, 320].

VII.5.2. Higgs triplets

Electroweak triplet scalars are the simplest non-doublet extension of the SM that can participate in the spontaneous breakdown of $\mathrm{SU}(2)_L \times \mathrm{U}(1)_Y$ to $\mathrm{U}(1)_{\mathrm{em}}$. Two types of model have been developed in enough detail to make a meaningful comparison to LHC data: the Higgs triplet model (HTM) [374, 375] and the Georgi–Machacek model [376–379].

The Higgs triplet model extends the SM by the addition of a complex $\mathrm{SU}(2)_L$ triplet scalar field Δ with hypercharge $Y = 2$, and a general gauge-invariant renormalizable potential $V(\Phi, \Delta)$ for Δ and the SM Higgs doublet Φ. The components of the triplet field can be parameterized as

$$\Delta = \frac{1}{\sqrt{2}} \begin{pmatrix} \Delta^+ & \sqrt{2}\Delta^{++} \\ v_\Delta + \delta + i\xi & -\Delta^+ \end{pmatrix}. \tag{11.34}$$

where Δ^+ is a singly-charged field, Δ^{++} is a doubly-charged field, δ is a neutral CP-even scalar, ξ is a neutral CP-odd scalar, and v_Δ is the triplet VEV. The general scalar potential mixes the doublet and triplet components. After electroweak symmetry breaking there are seven physical mass eigenstates, denoted $H^{\pm\pm}$, $H^\pm$, A, H, and h.

A distinguishing feature of the HTM is that it violates the custodial symmetry of the SM; thus the ρ parameter deviates from 1 even at tree level. Letting x denote the ratio of triplet and doublet VEVs, the tree level expression [380] is:

$$\rho = \frac{1+2x^2}{1+4x^2} \,. \tag{11.35}$$

The measured value of the ρ parameter then limits [381] the triplet VEV to be quite small, $x \lesssim 0.03$, or $v_\Delta < 8\,\text{GeV}$. This constraint severely limits the role of the triplet scalar in the EWSB mechanism.

The small VEV of the Higgs triplet in the HTM is a virtue from the point of view of generating neutrino masses without the necessity for introducing right-handed neutrino fields. The gauge invariant dimension four interaction

$$h_{\nu_{ij}}\, \ell_i^T C^{-1} i\sigma_2\, \Delta\, \ell_j \,, \tag{11.36}$$

where ℓ_i are the lepton doublets, C is the charge conjugation matrix, and $h_{\nu_{ij}}$ is a complex symmetric coupling matrix, generates a Majorana mass matrix for the neutrinos:

$$m_{\nu_{ij}} = \sqrt{2} h_{\nu_{ij}} v_\Delta \,. \tag{11.37}$$

This can be combined with the usual neutrino seesaw to produce what is known as the type-II seesaw [382].

The HTM suggests the exciting possibility of measuring parameters of the neutrino mass matrix at the LHC. If the doubly-charged Higgs is light enough and/or its couplings to W^+W^+ are sufficiently suppressed, then its primary decay is into same-sign lepton pairs: $H^{++} \to \ell_i^+ \ell_j^+$; from Eq. (11.36) and Eq. (11.37) it is apparent that these decays are in general lepton-flavor violating with branchings proportional to elements of the neutrino mass matrix [383].

Precision electroweak data constrain the mass spectrum as well as the triplet VEV of the HTM [380, 384, 385]. As described in Ref. [385], these constraints favor a spectrum where H^{++} is the lightest of the exotic bosons, and where the mass difference between H^+ and H^{++} is a few hundred GeV. The favored triplet VEV is a few GeV, which also favors H^{++} decays into W^+W^+ over same-sign dileptons.

The Georgi–Machacek model addresses the ρ parameter constraint directly by building in custodial symmetry. Writing the complex scalar doublet of the SM as a $(2,2)$ under $\text{SU}(2)_L \times \text{SU}(2)_R$, it is obvious that the next simplest construction respecting custodial symmetry is a scalar transforming like a $(3,3)$ [386]. These nine real degrees of freedom correspond to a complex electroweak triplet combined with a real triplet, with the scalar potential required to be invariant under $\text{SU}(2)_R$. Under the custodial $\text{SU}(2)_{L+R}$, they

transform as $1 \oplus 3 \oplus 5$, with a CP-even neutral scalar as the custodial singlet (thus matching the SM Higgs boson), a CP-odd neutral scalar in the custodial triplet, and another CP-even neutral scalar in the custodial 5-plet.

The scalar components can be decomposed as [387]

$$\Xi = \begin{pmatrix} \chi_3^* & \xi_1 & \chi_1 \\ -\chi_2^* & \xi_2 & \chi_2 \\ \chi_1^* & -\xi_1^* & \chi_3 \end{pmatrix}, \tag{11.38}$$

where ξ_2 is a real scalar and the others are complex scalars. Linear combinations of these account for the neutral custodial singlet, a neutral and singly-charged field making up the custodial triplet, and neutral, singly-charged, and doubly-charged fields making up the custodial 5-plet.

When combined with the usual SM doublet field Φ, the electroweak scale v is now related to the doublet and triplet VEVs by

$$v^2 = v_\Phi^2 + 8v_\Xi^2 \, . \tag{11.39}$$

Note that the GM triplets by themselves are sufficient to explain electroweak symmetry breaking and the existence of a 125 GeV neutral boson along with a custodial triplet of Goldstone bosons; the complex doublet field in the GM model is required to generate fermion masses via the usual dimension four Yukawa couplings. This raises the question of whether one can rule out the possibility that the 125 GeV boson is the neutral member of a custodial 5-plet rather than a custodial singlet, without invoking decays to fermions. A conclusive answer is given by observing that the ratio of the branching fractions to W versus Z bosons is completely determined by the custodial symmetry properties of the boson. For a custodial 5-plet, the ratio of the signal strength to WW over that to ZZ is predicted to be 1/4 that of a SM Higgs boson [386, 388], and thus already ruled out by the experimental results presented in Section VI.

Another interesting general feature of Higgs triplet models is that, after mixing, the SM-like neutral boson can have stronger couplings to WW and ZZ than predicted by the SM [379, 389]; this is in contrast to mixing with additional doublets and singlet, which can only reduce the WW and ZZ couplings versus the SM. This emphasizes that LHC Higgs data cannot extract model independent coupling strengths for the Higgs boson [256, 390].

Because of the built-in custodial symmetry, the triplet VEV in the GM model can be large compared to the doublet VEV. The custodial singlet neutral boson from the triplets mixes with the neutral boson from the doublet. Two interesting special cases are (i) the triplet VEV is small and the 125 GeV boson is SM-like except for small deviations, and (ii) the 125 GeV boson is mostly the custodial singlet neutral boson from the electroweak triplets. The phenomenology of the doubly-charged and singly-charged bosons is similar to that of the HTM. The constraints on the GM model from precision electroweak data, LEP data, and current LHC data are described in Refs. [387, 391–394].

VII.6. Composite Higgs models

Within the SM, EWSB is posited but has no dynamical origin. Furthermore, the Higgs boson appears to be unnaturally light. A scenario that remedies these two catches

is to consider the Higgs boson as a bound state of new dynamics becoming strong around the weak scale. The Higgs boson can be made significantly lighter than the other resonances of the strong sector if it appears as a pseudo-Nambu–Goldstone boson, see Refs. [15, 16, 395] for reviews.

VII.6.1. Little Higgs models

The idea behind the Little Higgs models [396, 397] is to identify the Higgs doublet as a (pseudo) Nambu–Goldstone boson while keeping some sizable non-derivative interactions, in particular a largish Higgs quartic interaction. By analogy with QCD where the pions $\pi^{\pm,0}$ appear as Nambu–Goldstone bosons associated to the breaking of the chiral symmetry $\mathrm{SU}(2)_\mathrm{L} \times \mathrm{SU}(2)_\mathrm{R}/\mathrm{SU}(2)$, switching on some interactions that break explicitly the global symmetry will generate masses for the would-be massless Nambu–Goldstone bosons of the order of $g\Lambda_{G/H}/(4\pi)$, where g is the coupling of the symmetry breaking interaction and $\Lambda_{G/H} = 4\pi f_{G/H}$ is the dynamical scale of the global symmetry breaking G/H. In the case of the Higgs boson, the top Yukawa interaction or the gauge interactions themselves will certainly break explicitly (part of) the global symmetry since they act non-linearly on the Higgs boson. Therefore, obtaining a Higgs mass around 100 GeV would demand a dynamical scale $\Lambda_{G/H}$ of the order of 1 TeV, which is known to lead to too large oblique corrections. Raising the strong dynamical scale by at least one order of magnitude requires an additional selection rule to ensure that a Higgs mass is generated at the 2-loop level only

$$m_H^2 = \frac{g^2}{16\pi^2}\Lambda_{G/H}^2 \to m_H^2 = \frac{g_1^2 g_2^2}{(16\pi^2)^2}\Lambda_{G/H}^2 \tag{11.40}$$

The way to enforce this selection rule is through a "collective breaking" of the global symmetry:

$$\mathcal{L} = \mathcal{L}_{G/H} + g_1\mathcal{L}_1 + g_2\mathcal{L}_2. \tag{11.41}$$

Each interaction $\mathcal{L}_1$ or $\mathcal{L}_2$ individually preserves a subset of the global symmetry such that the Higgs remains an exact Nambu–Goldstone boson whenever either g_1 or g_2 is vanishing. A mass term for the Higgs boson can be generated only by diagrams involving simultaneously both interactions. At one-loop, such diagrams are not quadratically divergent, so the Higgs mass is not UV sensitive. Explicitly, the cancellation of the SM quadratic divergences is achieved by a set of new particles around the Fermi scale: gauge bosons, vector-like quarks, and extra massive scalars, which are related, by the original global symmetry, to the SM particles with the same spin. Contrary to supersymmetry, the cancellation of the quadratic divergences is achieved by same-spin particles. These new particles, with definite couplings to SM particles as dictated by the global symmetries of the theory, are perfect goals for the LHC.

The simplest incarnation of the collective breaking idea, the so-called littlest Higgs model, is based on a non-linear σ-model describing the spontaneous breaking SU(5) down to SO(5). A subgroup $\mathrm{SU}(2)_1 \times \mathrm{U}(1)_1 \times \mathrm{SU}(2)_2 \times \mathrm{U}(1)_2$ is weakly gauged. This model contains a weak doublet, that is identified with the Higgs doublet, and a complex weak triplet whose mass is not protected by collective breaking. Other popular little Higgs

models are based on different coset spaces: minimal moose $(\mathrm{SU}(3)^2/\mathrm{SU}(3))$ [398], the simplest little Higgs $(\mathrm{SU}(3)^2/\mathrm{SU}(2)^2)$ [399], the bestest little Higgs $(\mathrm{SO}(6)^2/\mathrm{SO}(6))$ [400] *etc.*For comprehensive reviews, see Refs. [401, 402].

Generically, oblique corrections in Little Higgs models are reduced either by increasing the coupling of one of the gauge groups (in the case of product group models) or by increasing the masses of the W and Z partners, leading ultimately to a fine-tuning of the order of a few percents (see for instance Ref. [403] and references therein). The compatibility of Little Higgs models with experimental data is significantly improved when the global symmetry involves a custodial symmetry as well as a T-parity [404] under which, in analogy with R-parity in SUSY models, the SM particles are even and their partners are odd. Such Little Higgs models would therefore appear in colliders as jet(s) with missing transverse energy [405] and the ATLAS and CMS searches for squarks and gluinos [406] can be recast to obtain limits on the masses of the heavy vector-like quarks. The T-even top partner, with an expected mass below 1 TeV to cancel the top loop quadratic divergence without too much fine-tuning, would decay dominantly into a $t + Z$ pair or into a $b + W$ pair or even into $t + H$. The latest CMS and ATLAS direct searches [407] for vector-like top partners put a lower bound above one TeV on their mass, excluding the most natural region of the parameter space of these models, i.e., there is still fine-tuning at the per cent level.

The motivation for Little Higgs models is to solve the little hierarchy problem, i.e., to push the need for new physics (responsible for the stability of the weak scale) up to around 10 TeV. Per se, Little Higgs models are effective theories valid up to their cutoff scale $\Lambda_{G/H}$. Their UV completions could either be weakly or strongly coupled.

VII.6.2. Models of partial compositeness

Even in composite models, the Higgs boson cannot appear as a regular resonance of the strong sector without endangering the viability of the setup when confronted to data. The way out is that the Higgs appears as a pseudo Nambu–Goldstone boson: the new strongly coupled sector is supposed to be invariant under a global symmetry G spontaneously broken to a subgroup H at the scale f. To avoid conflict with EW precision measurements, the strong interactions themselves should better not break the EW symmetry. Hence the SM gauge symmetry itself should be contained in H. See Table 11.16 for a few examples of coset spaces.

The SM (light) fermions and gauge bosons cannot be part of the strong sector itself since LEP data have already put stringent bounds on the compositeness scale of these particles far above the TeV scale. The gauge bosons couple to the strong sector by a weak gauging of an $\mathrm{SU}(2)\times\mathrm{U}(1)$ subgroup of the global symmetry G. Inspiration for the construction of such models comes from the AdS/CFT correspondence: the components of a gauge field along an extra warped space dimension can be interpreted as the Goldstone boson resulting from the breaking of global symmetry of the strong sector. The couplings of the SM fermions to the strong sector could a priori take two different forms: (i) a bilinear coupling of two SM fermions to a composite scalar operator, $\mathcal{O}$, of the form $\mathcal{L} = y\,\bar{q}_L u_R \mathcal{O} + \mathrm{hc}$ in simple analogy with the SM Yukawa interactions. This is the way fermion masses were introduced in Technicolor theories and it generically

Table 11.16: Global symmetry breaking patterns and the corresponding Goldstone boson contents of the SM, the minimal composite Higgs model, the next to minimal composite Higgs model, and the minimal composite two Higgs doublet model. Note that the SU(3) model does not have a custodial invariance. a denotes a CP-odd scalar while h and H are CP-even scalars.

Model	Symmetry Pattern	Goldstones
SM	SO(4)/SO(3)	W_L, Z_L
–	SU(3)/SU(2)×U(1)	W_L, Z_L, H
MCHM	SO(5)/SO(4)	W_L, Z_L, H
NMCHM	SO(6)/SO(5)	W_L, Z_L, H, a
MC2HM	SO(6)/SO(4)×SO(2)	$W_L, Z_L, h, H, H^\pm, a$

comes with severe flavor problems and calls for extended model building gymnastics [408] to circumvent them; (ii) a linear mass mixing with fermionic vector-like operators: $\mathcal{L} = \lambda_L\, \bar{q}_L \mathcal{Q}_R + \lambda_R \bar{\mathcal{U}}_L u_R$. $\mathcal{Q}$ and $\mathcal{U}$ are two fermionic composite operators of mass M_Q and M_U. Being part of the composite sector, they can have a direct coupling of generic order Y_* to the Higgs boson. In analogy with the photon-ρ mixing in QCD, once the linear mixings are diagonalized, the physical states are a linear combination of elementary and composite fields. Effective Yukawa couplings are generated and read for instance for the up-type quark

$$y = Y_* \sin\theta_L \sin\theta_R \tag{11.42}$$

where $\sin\theta_i = \lambda_i / \sqrt{M_{Q,U}^2 + \lambda_i^2}$, $i = L, R$, measure the amount of compositeness of the SM left- and right-handed up-type quark. If the strong sector is flavor-anarchic, i.e., if the couplings of the Higgs to the composite fermions does not exhibit any particular flavor structure, the relation Eq. (11.42) implies that the light fermions are mostly elementary states ($\sin\theta_i \ll 1$), while the third generation quarks need to have a sizable degree of compositeness. The partial compositeness paradigm offers an appealing dynamical explanation of the hierarchies in the fermion masses. In fact, assuming the strong sector to be almost conformal above the confinement scale, the low-energy values of the mass-mixing parameters $\lambda_{L,R}$ are determined by the (constant) anomalous dimension of the composite operator they mix with. If the UV scale at which the linear mixings are generated is large, then $\mathcal{O}(1)$ differences in the anomalous dimensions can generate naturally large hierarchies in the fermion masses via renormalization group running [409]. While the introduction of partial compositeness greatly ameliorated the flavor problem of the original composite Higgs models, nevertheless it did not solve the issue completely, at least in the case where the strong sector is assumed to be flavor-anarchic [410]. While the partial compositeness set-up naturally emerges in models built in space-times with extra dimensions, no fully realistic microscopic realization of partial compositeness has been proposed in the literature.

Another nice aspect of the partial compositeness structure is the dynamical generation of the Higgs potential that is not arbitrary like in the SM. The Higgs being a pseudo-Nambu–Goldstone boson, its mass does not receive any contribution from the

strong sector itself but it is generated at the one-loop level via the couplings of the SM particles to the strong sector since these interactions are breaking the global symmetries under which the Higgs doublet transforms non-linearly. The leading contribution to the potential arises from top loops and it takes the form

$$V(H) = m_\rho^4 \frac{\sin\theta_{tL}\sin\theta_{tR}}{16\pi^2}\left(\alpha\cos(H/f) + \beta\sin^2(H/f) + \gamma\sin^4(H/f)\right), \tag{11.43}$$

where α, β, γ are numbers of order 1 subject to selection rules following the transformation properties of the top quark under the global symmetries of the strong sector[9], and $m_\rho \approx g_\rho f$ is the typical mass scale of the strong sector resonances. The gauge contribution to the potential takes the form (g denotes the SU(2) gauge coupling)

$$m_\rho^4 \frac{g^2/g_\rho^2}{16\pi^2}\sin^2(H/f), \tag{11.44}$$

which is parametrically suppressed with respect to the top contribution by $g^2/(g_\rho y_t)$. The gauge term is always positive, and cannot trigger EWSB by itself. When $\alpha = 0$, the minimization condition of the potential simply reads

$$\sin^2\frac{\langle H\rangle}{f} = -\frac{\beta}{2\gamma}, \tag{11.45}$$

which implies that the natural expectation is that the scale f is generically of the order of the weak scale. Obtaining $v \ll f$, as required phenomenologically, requires some degree of tuning, which scales like $\xi \equiv v^2/f^2$. A mild tuning of the order of 10% ($\xi \approx 0.1$) is typically enough to comply with electroweak precision constraints. This is an important point: in partial compositeness models, the entire Higgs potential is generated at one loop, therefore the separation between v and f can only be obtained at a price of a tuning. This marks a difference with respect to the Little Higgs models, which realize a parametric hierarchy between the quartic and mass terms through the collective symmetry breaking mechanism. In fact in Little Higgs models, the quartic coupling is a tree-level effect, leading to a potential

$$V(H) \approx \frac{g_{\rm SM}^2}{16\pi^2} m_\rho^2 H^2 + g_{\rm SM}^2 H^4, \tag{11.46}$$

where $g_{\rm SM}$ generically denotes the SM couplings. The minimization condition now reads $v^2/f^2 \sim g_\rho^2/(16\pi^2)$, therefore v is formally loop suppressed with respect to f. This is the

[9] For instance in the SO(5)/SO(4) composite models, when the top quark is embedded into a spinorial representation of SO(5), then $\gamma = 0$ and when it is part of a **5**, **10** or **14** representation, $\alpha = 0$ as it can be inferred by looking at the structure of the H-dependent invariants built out of these representations [411]. The coefficient γ also generically comes with an extra power of the top compositeness fractions.

major achievement of the Little Higgs constructions, which however comes at the price of the presence of sub-TeV vectors carrying EW quantum numbers and therefore giving rise generically to large oblique corrections to the propagators of the W and the Z gauge bosons.

After minimization, the potential Eq. (11.43) leads to an estimate of the Higgs mass as

$$m_H^2 \approx g_\rho^3\, y_t 2\pi^2 v^2. \tag{11.47}$$

It follows that the limit $f \to \infty$, i.e. $\xi \to 0$, is a true decoupling limit: all the resonances of the strong sector become heavy but the Higgs whose mass is protected by the symmetries of the coset G/H. When compared to the experimentally measured Higgs mass, this estimate puts an upper bound on the strength of the strong interactions: $g_\rho \lesssim 2$. In this limit of not so large coupling, the Higgs potential receives additional contributions. In particular, the fermionic resonances in the top sector which follow from the global symmetry structure of the new physics sector can help raising the Higgs mass. For instance in the minimal SO(5)/SO(4) model, using some dispersion relation techniques, one obtains [412]

$$m_H^2 \approx \frac{6}{\pi^2}\frac{m_t^2}{f^2}\frac{m_{Q_4}^2 m_{Q_1}^2}{m_{Q_1}^2 - m_{Q_4}^2}\log\left(\frac{m_{Q_1}}{m_{Q_4}}\right) \tag{11.48}$$

where Q_4 and Q_1 are fermionic color resonances transforming as a weak bi-doublet of hypercharge $Y = 1/6$ and $Y = 7/6$ and a weak singlet with hypercharge $Y = -1/3$. Therefore a 125 GeV mass can be obtained if at least one of the fermionic resonances is lighter than $\sim 1.4\, f$. As in supersymmetric scenarios, the top sector is playing a crucial role in the dynamics of EWSB and can provide the first direct signs of new physics. The direct searches for these top partners, in particular the ones with exotic electric charges 5/3, are already exploring the natural parameter spaces of these models [407], 413, 414].

The main physics properties of a pseudo Nambu–Goldstone Higgs boson can be captured in a model-independent way by a few number of higher-dimensional operators. Indeed, the strong dynamics at the origin of the composite Higgs singles out a few operators among the complete list presented earlier in Section VI: these are the operators that involve extra powers of the Higgs doublets and they are therefore generically suppressed by a factor $1/f^2$ as opposed to the operators that involve extra derivatives or gauge bosons and are suppressed by a factor $1/(g_\rho^2 f^2)$. The relevant effective Lagrangian describing a strongly interacting light Higgs is:

$$\begin{aligned}\mathcal{L}_{\rm SILH} =& \frac{c_H}{2f^2}\left(\partial_\mu\left(\Phi^\dagger\Phi\right)\right)^2 + \frac{c_T}{2f^2}\left(\Phi^\dagger \overleftrightarrow{D}^\mu \Phi\right)^2 - \frac{c_6\lambda}{f^2}\left(\Phi^\dagger\Phi\right)^3 \\ &+ \left(\sum_f \frac{c_f\, y_f}{f^2}\Phi^\dagger\Phi\bar{f}_L\Phi f_R + \text{h.c.}\right).\end{aligned} \tag{11.49}$$

Typically, these new interactions induce deviations in the Higgs couplings that scale like $\mathcal{O}(v^2/f^2)$, hence the measurements of the Higgs couplings can be translated into some

constraints on the compositeness scale, $4\pi f$, of the Higgs boson. The peculiarity of these composite models is that, due to the Goldstone nature of the Higgs boson, the direct couplings to photons and gluons are further suppressed and generically the coupling modifiers defined in Section VI scale like

$$\begin{aligned} \kappa_{W,Z,f} &\sim 1 + \mathcal{O}\left(\frac{v^2}{f^2}\right) , \\ \kappa_{Z\gamma} &\sim \mathcal{O}\left(\frac{v^2}{f^2}\right) , \\ \kappa_{\gamma,g} &\sim \mathcal{O}\left(\frac{v^2}{f^2} \times \frac{y_t^2}{g_\rho^2}\right) , \end{aligned} \tag{11.50}$$

where g_ρ denotes the typical coupling strength among the states of the strongly coupled sector and y_t is the top Yukawa coupling, the largest interaction that breaks the Goldstone symmetry. The $\kappa_{Z\gamma,\gamma,g}$ coupling modifiers are not generated by the strong coupling operators of Eq. (11.49) but some subleading form-factor operator generated by loops of heavy resonances of the strong sector. The coupling modifiers also receive additional contributions from the other resonances of the strong sector, in particular the fermionic resonances of the top sector that are required to be light to generate a 125 GeV Higgs mass. Some indirect information on the resonance spectrum could thus be inferred by a precise measurement of the Higgs coupling deviations. However, it was realized [415] that the task is actually complicated by the fact that, in the minimal models, these top partners give a contribution to both κ_t (resulting from a modification of the top Yukawa coupling) and κ_γ and κ_g (resulting from new heavy particles running into the loops) and the structure of interactions are such that the net effect vanishes for inclusive quantities like $\sigma(gg \to H)$ or $\Gamma(H \to \gamma\gamma)$ as a consequence of the Higgs low energy theorem [23, 24, 270]. So one would need to rely on differential distribution, like the Higgs p_T distribution [416], to *see* the top partner effects in Higgs data [417]. The off-shell channel $gg \to H^* \to 4\ell$ [418] and the double Higgs production $gg \to HH$ [419] can also help to resolve the gluon loop and separate the top and top-partner contributions.

VII.6.3. Minimal composite Higgs models

The minimal composite Higgs models (MCHM) are concrete examples of the partial compositeness paradigm. The Higgs doublet is described by the coset space SO(5)/SO(4) where a subgroup $\mathrm{SU}(2)_L \times \mathrm{U}(1)_Y$ is weakly gauged under which the four Goldstone bosons transform as a doublet of hypercharge 1. There is some freedom on how the global symmetry is acting on the SM fermions: in MCHM4 [411] the quarks and leptons are embedded into spinorial representations of SO(5), while in MHCM5 [420] they are part of fundamental representations (it might also be interesting phenomenologically to consider larger representations like MCHM14 [421] with the SM fermions inside a representation of dimension 14). It is also possible to consider that fermions of different chirality and flavor are in different representations of SO(5), leading to a more varied phenomenology [422]. The non-linearly realized symmetry acting on the Goldstone bosons leads to general

predictions of the coupling of the Higgs boson to the EW gauge bosons. For instance, it can be shown that the quadratic terms in the W and Z bosons read

$$m_W^2(H)\left(W_\mu W^\mu + \frac{1}{2\cos^2\theta_W} Z_\mu Z^\mu\right)$$

with $m_W(H) = \dfrac{gf}{2}\sin\dfrac{H}{f}$. Expanding around the EW vacuum, the expression of the weak scale is:

$$v = f\sin(\langle H\rangle/f), \tag{11.51}$$

and the values of the modified Higgs couplings to the W and Z:

$$g_{HVV} = \frac{2m_V^2}{v}\sqrt{1-v^2/f^2}\,, \quad g_{HHVV} = \frac{2m_V^2}{v^2}(1-2v^2/f^2)\,. \tag{11.52}$$

Note that the Higgs couplings to gauge bosons is always suppressed compared to the SM prediction. This is a general result [423] that holds as long as the coset space is compact.

The Higgs couplings to the fermions depend on the representation which the SM fermions are embedded into. For the most commonly used embedding, considering all fermion doublets and singlets embedded in the same representations, they take the following forms

$$\begin{aligned}
\text{MCHM4}: g_{Hff} &= \frac{m_f}{v}\sqrt{1-v^2/f^2}\,,\\
\text{MCHM5}: g_{Hff} &= \frac{m_f}{v}\frac{1-2v^2/f^2}{\sqrt{1-v^2/f^2}}\,,\\
\text{MCHM14}: g_{Hff} &= \frac{m_f}{v}\left(1 + A(M_{1,4,9})\frac{v^2}{f^2} + O(v^4/f^4)\right)\,,\\
&\text{with } A(M_{1,4,9}) = \frac{3M_1M_4 - 11M_1M_9 + 8M_4M_9}{2M_9(M_1-M_4)}\,.
\end{aligned} \tag{11.53}$$

While, in MHCM4 and MCHM5, the modifications of the couplings depend only on the Higgs compositeness scale, in MCHM14 the leading corrections depend also on the mass spectrum of the resonances parametrized by M_1, M_4 and M_9 [421]. This is due to the fact that more than one SO(5) invariant gives rise to SM fermion masses. The (κ_V, κ_f) experimental fit of the Higgs couplings can be used to derive a lower bound on the Higgs compositeness scale $4\pi f \gtrsim 9\,\text{TeV}$, which is less stringent than the indirect bound obtained from EW precision data, $4\pi f \gtrsim 15\,\text{TeV}$ [424] but more robust and less subject on assumptions [425].

VII.6.4. Twin Higgs models

In all composite models presented above, the particles responsible for canceling the quadratic divergences in the Higgs mass are charged under the SM gauge symmetries. In particular, the top partner carries color charge, implying a reasonably large minimal

production cross section at the LHC. An alternative scenario, which is experimentally quite challenging and might explain the null result in various new physics searches, is the case nowadays referred to as "neutral naturalness" [19, 20], where the particles canceling the 1-loop quadratic divergences are neutral under the SM. The canonical example for such theories is the Twin Higgs model of Ref. [19]. This is an example of a pseudo-Goldstone boson Higgs theory, with an approximate global $SU(4)$ symmetry broken to $SU(3)$. The Twin Higgs model is obtained by gauging the $SU(2)_A \times SU(2)_B$ subgroup of $SU(4)$, where $SU(2)_A$ is identified with the SM $SU(2)_L$, while $SU(2)_B$ is the twin $SU(2)$ group. Gauging this subgroup breaks the $SU(4)$ symmetry explicitly, but quadratically divergent corrections do not involve the Higgs boson when the gauge couplings of the two SU(2) subgroups are equal, $g_A = g_B$. The $SU(4) \to SU(3)$ breaking will also result in the breaking of the twin $SU(2)_B$ group and as a result three of the seven Goldstone bosons will be eaten, leaving 4 Goldstone bosons corresponding to the SM Higgs doublet h. In fact imposing the Z_2 symmetry on the full model will ensure the cancellation of all 1-loop quadratic divergences to the Higgs mass. Logarithmically divergent terms can however arise for example from gauge loops, leading to a Higgs mass of order $g^2 f/4\pi$, which is of the order of the physical Higgs mass for $f \sim 1\,\text{TeV}$. The quadratic divergences from the top sector can be eliminated if the Z_2 protecting the Higgs mass remains unbroken by the couplings that result in the top Yukawa coupling. This can be achieved by introducing top partners charged under a twin $SU(3)_c$. In this case the quadratic divergences are cancelled by top partners that are neutral under the SM gauge symmetries.

Twin Higgs models are low-energy effective theories valid up to a cutoff scale of order $\Lambda \sim 4\pi f \sim 5$–$10\,\text{TeV}$, beyond which a UV completion has to be specified. The simplest such possibility is to also make the Higgs composite, and UV complete the twin-Higgs model via gauge and top partners at masses of the order of a few TeV. A concrete implementation is the holographic twin Higgs model [426], which also incorporates a custodial symmetry to protect the T-parameter from large corrections. It is based on a warped extra dimensional theory with a bulk SO(8) gauge group, which incorporates the $SU(4)$ global symmetry discussed above enlarged to contain the $\text{SU}(2)_L \times \text{SU}(2)_R$ custodial symmetry. In addition the bulk contains either a full $SU(7)$ group or an $SU(3) \times SU(3) \times U(1) \times U(1) \times Z_2$ subgroup of it to incorporate QCD, its twin, and hypercharge. The breaking on the UV brane is to the SM and the twin SM symmetries, while on the IR brane $SO(8) \to SO(7)$, giving rise to the 7 Goldstone bosons, three of which will be again eaten by the twin W, Z. The main difference compared to ordinary composite Higgs models is that in composite twin Higgs models the cancellation of the one-loop quadratic divergences is achieved by the twin partners of order $700\,\text{GeV}$– $1\,\text{TeV}$, which are uncharged under the SM gauge group. This allows the IR scale of the warped extra dimension to be raised to the multi-TeV range without reintroducing the hierarchy problem. The role of the composite partners is to UV complete the theory, rather than the cancellation of the one-loop quadratic divergences. For more details about the composite twin Higgs models, see Refs. [427].

VII.7. Searches for signatures of extended Higgs sectors

The measurements described in Section III have established the existence of one state of the electroweak symmetry breaking sector, compatible with a SM Higgs boson, but not that it is the only one.

Various classes of models beyond the SM discussed above require extended Higgs sectors. These models, and in particular the MSSM and the NMSSM serve as guiding principle of the experimental searches for additional scalar states beyond the SM. However these searches are made as model-independent as possible and can be summarized in the following classes: (i) the search for an additional CP-even state mostly in the high mass domain decaying to vector bosons, which would correspond to the heavy CP-even state in a generic 2HDM where the light state would be the discovered H or a generic additional singlet; (ii) the search for a state in the high mass domain decaying to pairs of fermions, which would correspond a CP-odd A and the heavy CP-even state H in a generic 2HDM; (iii) the search for charged Higgs bosons, which also appear in generic 2HDMs; (iv) the search for a CP-odd state a in the low mass region which appears in the NMSSM; and (v) doubly charged Higgs which are motivated in extensions of the Higgs sector with triplets.

This gives a concise description of the most recent searches performed at the LHC and elsewhere. The complete of final states searched is A summary of these searches in terms of final states is given in Table 11.17 where the corresponding references are given for more details.

(i) Searches for an additional CP-even state

(a) Exclusion limits from LEP

The LEP searches for the SM Higgs boson put a lower limit of 114 GeV on its mass, but also have relevance for non-SM Higgs bosons. These searches were also interpreted as 95% CL upper bounds on the ratio of the coupling g_{HZZ} to its SM prediction as a function of the Higgs boson mass [122]. Among the MSSM new benchmarks, the low-m_H is one example which is disfavored by these searches at low mass, and nearly ruled out by current direct constraints and charged Higgs limits from LHC. Another example is the light CP-even Higgs boson of the NMSSM which is constrained to project predominantly onto the EW singlet component. An additional motivation for these scenarios is given by the slight excess observed at LEP [122] at a Higgs boson mass hypothesis of approximately 98 GeV.

(b) Searches at the LHC

The searches for the SM Higgs boson before the discovery covered a wide range of mass hypotheses. After the discovery, the SM Higgs boson searches have been reappraised to search for a heavy CP-even state. This state could be the heavy CP-even Higgs boson of a 2HDM, or a generic additional singlet. In both cases the natural width of the additional H state can be very different from that of the SM Higgs boson. To preserve unitarity of the longitudinal vector boson scattering and the longitudinal vector boson scattering into fermion pairs, the couplings of the additional CP-even Higgs boson to gauge bosons and

Table 11.17: Summary of references to searches for additional states from extended Higgs sectors, where (BBr) denotes the BaBar experiment, (TeV) the Tevatron experiments. Results using Run 2 data are marked by (*). V denotes either the W or the Z boson.

	ATLAS	CMS	Other experiments
CP-even H			
$H \to \gamma\gamma$	*[428]	*[429, 430]	—
$H \to Z\gamma$	*[431]	*[432]	—
$H \to ZZ \to 4\ell$	*[433]	*[434]	—
$H \to ZZ \to \ell\ell\nu\nu$	*[433]	*[435]	—
$H \to ZZ \to \ell\ell q\overline{q}$	*[436]	*[437]	—
$H \to ZZ \to \nu\nu q\overline{q}$	*[436]	—	—
$H \to WW \to \ell\nu\ell\nu$	[438]	*[435]	—
$H \to WW \to \ell\nu\ell\nu$ (2HDM)	[439]	[440]	—
$H \to WW \to \ell\nu q\overline{q'}$	*[441]	[442, 443]	—
$H \to VV \to q\overline{q'}q\overline{q'}(JJ)$	*[444]	—	—
$H \to hh \to b\overline{b}\tau\tau, b\overline{b}\gamma\gamma, 4b, \gamma\gamma WW^*$	*[187, 189, 445]	*[188, 446]	—
CP-odd A (and/or CP-even H)			
$H, A \to \tau^+\tau^-$	*[447]	*[448]	[449, 450]-TeV [451]-LHCb
$H, A \to \mu^+\mu^-$	[452]	—	—
$H, A \to t\overline{t}$	*[453]	—	
$H, A \to b\overline{b}$	—	*[455, 456]	[457, 458]-TeV
$A \to hV \to b\overline{b}q\overline{q'}, b\overline{b}\ell\nu, b\overline{b}\ell\ell, \ell\ell\tau\tau, \nu\overline{\nu}b\overline{b}$	*[459, 460]	[446]	
Charged $H^\pm$			
$H^\pm \to \tau^\pm\nu$	*[461]	*[462]	—
$H^\pm \to cs$	[463]	[464]	—
$H^\pm \to tb$	*[465]	[466]	—
$H^\pm \to W^\pm Z$	[467]	*[468]	—
$H^\pm \to cb$	—	*[469]	—
CP-odd NMSSM a			
$a \to \mu^+\mu^-$	[470]	*[471]	—
$h \to aa \to 4\mu, 4\tau, 2\mu 2\tau, 4\gamma$	[472, 473]	*[474, 475]	[476]-TeV, [477]-LEP
$\Upsilon_{1s,3s} \to a\gamma$	—	—	[478, 479]-BBr
Doubly charged $H^{\pm\pm}$	*[480, 481]	*[482]	—

fermions should not be too large and should constrain the natural width to be smaller than that of a unique Higgs boson at high mass with couplings to fermions and gauge bosons as predicted by the SM (and provided that trilinear and quartic couplings are not too large and that no new state affects the heavy state total width). It is therefore reasonable to consider total widths for the high mass CP-even state smaller than the equivalent SM width. For the sake of generality these searches should be done as a function of Higgs boson mass and total width. Until recently only two cases have been investigated: (i) the SM width using the complex pole scheme (CPS), and (ii) the narrow width approximation.

Searches for the Higgs boson in the $H \to \gamma\gamma$, $H \to Z\gamma$, $H \to W^{(*)}W^{(*)}$ in the $\ell\nu\ell\nu$ and $\ell\nu q\overline{q}$ channels, and the $H \to Z^{(*)}Z^{(*)}$ searches in the 4ℓ, $\ell\ell q\overline{q}$ and $\ell\ell\nu\nu$ channels have also been done, but in most cases are simple reinterpretations of the SM Higgs search in the CPS scheme. References for these searches are summarized in Table 11.17.

(c) Searches for an additional resonance decaying to a pair of h

In addition to the rare and expected Higgs pair production mode, high mass CP-even Higgs bosons can be searched for in the resonant double Higgs mode. Searches for such processes, where the Higgs boson is used as a tool for searches for new phenomena beyond the SM, have been carried out in four distinct modes depending on the subsequent decays of each Higgs boson. The ATLAS and CMS Collaborations have searched for the $H \to hh \to b\overline{b}\tau\tau$, $b\overline{b}\gamma\gamma$ and the $H \to hh \to 4b$ final states. These channels are the most sensitive in the search for heavy Higgs bosons decaying to a hh pair. The CMS collaboration has performed a search for the $\gamma\gamma WW^*$ final states [483]. For masses hypotheses of an additional Higgs boson below 500 GeV, the two dominant search channels are the $b\overline{b}\gamma\gamma$ and the $b\overline{b}\tau\tau$. For masses above 500 GeV, the most powerful search channel is the $4b$ final state.

(d) Searches for an additional state with the presence of h

In the post-discovery era, analyses searching for additional Higgs bosons need to take into account the presence of the discovered state. For searches with sufficiently high mass resolution to disentangle the additional states which are not degenerate in mass, the strength of the observed state and limits on the signal strength of a potential additional state can be set independently, as discussed in the next section. However in some cases, such as when a channel does not have a sufficiently fine mass resolution or when the states are nearly degenerate in mass, specific analyses need to be designed. There are two examples of such analyses: (i) the search for an additional state in the $H \to W^{(*)}W^{(*)} \to \ell\nu\ell\nu$ channel in ATLAS and (ii) the search for nearly degenerate states in the $H \to \gamma\gamma$ channel with the CMS detector.

The search in the $H \to W^{(*)}W^{(*)} \to \ell\nu\ell\nu$ channel, for an additional state is done using a boosted decision tree combining several discriminating kinematic characteristics to separate the signal from the background and a high mass signal H from the lower mass state h [439]. A simultaneous fit of the two states h and H is then made to test the presence of an additional state. In this case, the usual null hypothesis of background

includes including the SM signal.

The CMS search for nearly degenerate mass states decaying to a pair of photons [484] is more generic and could for instance apply to CP-odd Higgs bosons as well. It consists of a fit to the diphoton mass spectrum using two nearly degenerate mass templates.

(e) Type I 2HDM and fermiophobia

The measurements of coupling properties of H indirectly exclude that the discovered state is fermiophobic. However, the presence of an additional fermiophobic state, as predicted by Type I 2HDMs, is not excluded. Prior to the discovery, ATLAS and CMS have performed searches for a fermiophobic Higgs boson, *i.e.* produced through couplings with vector bosons only (VBF and VH) and decaying in $h_f \to \gamma\gamma$, optimized for fermiophobic signatures in the diphoton channel [485, 486]. CMS has further combined these results with searches for $h_f \to W^+W^-$ and $h_f \to ZZ$ assuming fermiophobic production and decay [487]. CMS excludes a fermiophobic Higgs boson in the range $110\,\text{GeV} < m_H < 188\,\text{GeV}$ at the 95% C.L.

(f) Interpretation benchmarks in the light of the discovered Higgs boson

Two specific benchmark scenarios driven by unitarity relations are proposed in Ref. [42], assuming the existence of an additional state h' with coupling scale factors, i.e., deviations from the couplings predicted for the SM Higgs at the same mass, denoted κ'_V and κ'_F for the couplings of h' to vector bosons and fermions respectively. The gauge boson scattering unitarity then yields the following sum rule

$$\kappa_V^2 + \kappa_V'^2 = 1 \tag{11.54}$$

and the unitarization of the gauge boson scattering to fermions yields

$$\kappa_V \cdot \kappa_F + \kappa'_V \cdot \kappa'_F = 1 \tag{11.55}$$

The two benchmark scenarios are then defined as follows: (i) a single coupling scale factor is assumed for the gauge bosons and the fermions, with an additional parameter to take into account decays to new states; (ii) two parameters are used to describe independently the couplings to fermions and the couplings to vector bosons. A direct application of the latter can be done in the CP-even sector of the type-I 2HDM.

(ii) Searches for additional neutral states ($\phi \equiv h$, H, A) decaying to fermions

(a) Exclusion limits from LEP

In e^+e^- collisions at LEP centre-of-mass energies, the main production mechanisms of the neutral MSSM Higgs bosons were the Higgs-strahlung processes $e^+e^- \to hZ$, HZ and the pair production processes $e^+e^- \to hA$, HA, while the vector boson fusion processes played a marginal role. Higgs boson decays to $b\bar{b}$ and $\tau^+\tau^-$ were used in these searches.

The searches and limits from the four LEP experiments are described in Refs. [488, 489]. The combined LEP data did not contain any excess of events which would imply the

production of a Higgs boson, and combined limits were derived [490]. For $m_A \gg M_Z$ the limit on m_h is nearly that of the SM searches, as $\sin^2(\beta-\alpha) \approx 1$. For high values of $\tan\beta$ and low m_A ($m_A \leq m_h^{max}$), the $e^+e^- \to hA$ searches become the most important, and the lightest Higgs h is non SM-like. In this region, the 95% CL mass bounds are $m_h > 92.8\,\text{GeV}$ and $m_A > 93.4\,\text{GeV}$. In the m_h^{max} scenario, values of $\tan\beta$ from 0.7 to 2.0 are excluded taking $m_t = 174.3\,\text{GeV}$, while a much larger $\tan\beta$ region is excluded for other benchmark scenarios such as the no-mixing one.

A flavor-independent limit for Higgs bosons in the Higgs-strahlung process at LEP has also been set at 112 GeV [491].

Neutral Higgs bosons may also be produced by Yukawa processes $e^+e^- \to f\overline{f}\phi$, where the Higgs particle $\phi \equiv h$, H, A, is radiated off a massive fermion ($f \equiv b$ or $\tau^{\pm}$). These processes can be dominant at low masses, and whenever the $e^+e^- \to h\text{Z}$ and hA processes are suppressed. The corresponding ratios of the $f\overline{f}h$ and $f\overline{f}A$ couplings to the SM coupling are $\sin\alpha/\cos\beta$ and $\tan\beta$, respectively. The LEP data have been used to search for $b\overline{b}\,b\overline{b}$, $b\overline{b}\tau^+\tau^-$, and $\tau^+\tau^-\,\tau^+\tau^-$ final states [492, 493]. Regions of low mass and high enhancement factors are excluded by these searches.

The searches for the Higgs boson at LEP also included the case where it does not predominantly decay to a pair of b quarks. All four collaborations conducted dedicated searches b for the Higgs boson with reduced model dependence, assuming it is produced via the Higgs-strahlung process, and not addressing its flavor of decay, a lower limit on the Higgs mass of 112.9 GeV is set by combining the data of all four experiments [491].

Using an effective Lagrangian approach and combining results sensitive to the $h\gamma\gamma$, $hZ\gamma$ and hZZ couplings, an interpretation of several searches for the Higgs boson was made and set a lower limit of 106.7 GeV on the mass of a Higgs boson that can couple anomalously to photons [491].

(b) Searches at the Tevatron and LHC

The best sensitivity is in the regime with low to moderate m_A and with large $\tan\beta$ which enhances the couplings of the Higgs bosons to down-type fermions. The corresponding limits on the Higgs boson production cross section times the branching ratio of the Higgs boson into down-type fermions can be interpreted in MSSM benchmark scenarios [316]. If $\phi = A, H$ for $m_A > m_h^{\max}$, and $\phi = A, h$ for $m_A < m_h^{\max}$, the most promising channels at the Tevatron are the inclusive $p\overline{p} \to \phi \to \tau^+\tau^-$ process, with contributions from both $gg \to \phi$ and $b\overline{b}\phi$ production, and $b\overline{b}\phi, \phi \to \tau^+\tau^-$ or $\phi \to b\overline{b}$, with $b\tau\tau$ or three tagged b-jets in the final state, respectively. Although Higgs boson production via gluon fusion has a higher cross section in general than via associated production, it cannot be used to study the $\phi \to b\overline{b}$ decay mode since the signal is overwhelmed by the QCD background.

The CDF and D0 collaborations have searched for neutral Higgs bosons produced in association with bottom quarks and which decay into $b\overline{b}$ [457, 458], or into $\tau^+\tau^-$ [449,450]. The most recent searches in the $b\overline{b}\phi$ channel with $\phi \to b\overline{b}$ analyze approximately $2.6\,\text{fb}^{-1}$ of data (CDF) and $5.2\,\text{fb}^{-1}$ (D0), seeking events with at least three b-tagged jets. The cross section is defined such that at least one b quark not from ϕ decay is required to have

$p_T > 20\,\text{GeV}$ and $|\eta| < 5$. The invariant mass of the two leading jets as well as b-tagging variables are used to discriminate the signal from the backgrounds. The QCD background rates and shapes are inferred from data control samples, in particular, the sample with two b-tagged jets and a third, untagged jet. Separate-signal hypotheses are tested and limits are placed on $\sigma(p\overline{p} \to b\overline{b}\phi) \times \text{BR}(\phi \to b\bar{b})$. A local excess of approximately 2.5σ significance has been observed in the mass range of 130–160 GeV, but D0's search is more sensitive and sets stronger limits. The D0 result had an $\mathcal{O}(2\sigma)$ local upward fluctuation in the 110 to 125 GeV mass range. These results have been superseded by the LHC searches and the excess seen in the D0 experiment has not been confirmed elsewhere.

A substantially larger sensitivity in the search for the $\phi \to \tau^+\tau^-$ is obtained with the ATLAS and CMS analyses. The higher centre-of-mass energy reached at the Run 2 brings a substantial though not excessively large increase in sensitivity due to the intermediate masses probed. Both the ATLAS and CMS collaborations have reported the result of their searches in this important channel with the full 2016 dataset. The searches are performed in categories of the decays of the two tau leptons: $e\tau_{\text{had}}$, $\mu\tau_{\text{had}}$, $e\mu$, and $\mu\mu$, where τ_{had} denotes a tau lepton which decays to one or more hadrons plus a tau neutrino, e denotes $\tau \to e\nu\nu$, and μ denotes $\tau \to \mu\nu\nu$. The dominant background comes from $Z \to \tau^+\tau^-$ decays, although $t\bar{t}$, W+jets and Z+jets events contribute as well. Separating events into categories based on the number of b-tagged jets improves the sensitivity in the MSSM. The $b\bar{b}$ annihilation process and radiation of a Higgs boson from a b quark gives rise to events in which the Higgs boson is accompanied by a $b\bar{b}$ pair in the final state. Requiring the presence of one or more b jets reduces the background from Z+jets. Data control samples are used to constrain background rates. The rates for jets to be identified as a hadronically decaying tau lepton are measured in dijet samples, and W+jets samples provide a measurement of the rate of events that, with a fake hadronic tau, can pass the signal selection requirements. Lepton fake rates are measured using samples of isolated lepton candidates and same-sign lepton candidates. Constraints from the CMS searches for $h \to \tau^+\tau^-$ and $h \to b\overline{b}$ are shown in Fig. 11.16 in the m_h-mod+ scenario defined in Ref. [321] and in the hMSSM approximation defined in Ref. [322]. The neutral Higgs boson searches consider the contributions of both the CP-odd and CP-even neutral Higgs bosons with enhanced couplings to bottom quarks, similarly as it was done for the Tevatron results. In Fig. 11.16, decays of the charged Higgs into $\tau\nu$ and of the heavy Higgs H decaying into a pair of SM-like Higgs bosons or gauge bosons, or of A decaying into hZ are also being constrained. In addition, decays of the neutral Higgs bosons into muon pairs are also being explored. Observe that in the $m_h$mod+ scenario the region of $\tan\beta$ lower than 5 does not allow for a Higgs mass m_h close to 125 GeV, as shown in the figure. For the hMSSM scenario, instead, the SM-like Higgs mass is fixed as an input and hence the requirement that it is close to 125 GeV is always fulfilled, although this may imply other limitations as discussed in section VII.1.1.

A search for $\phi \to \mu^+\mu^-$ has also been performed by the ATLAS collaboration [452].

Finally searches for a resonance decaying to a top quark pair were done by ATLAS [495, 453] and CMS [496]. These searches were interpreted as searches for scalar resonances by ATLAS [495], however an important component of these searches is an accurate treatment of the interference effects between the signal and the continuum

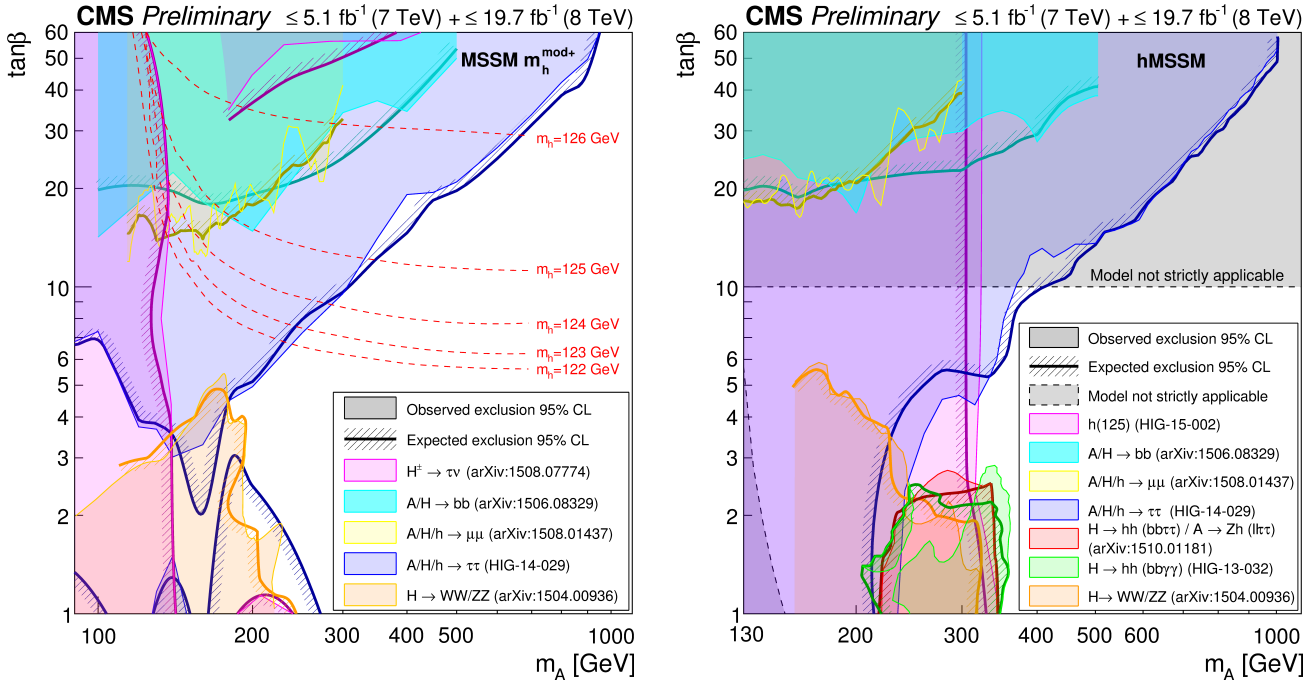

Figure 11.16: The 95% CL exclusion contours in the $(M_A, \tan\beta)$ parameter space for the hMSSM scenario (right panel) and for the m_h-mod+ scenario (left panel), for several search channels [494].

background. These can yield a dip and peak structure instead of a simple peak [373, 320]. The ATLAS Collaboration has performed a search for a high mass state decaying to a pair of top quarks taking into account the deformation in mass shape of the signal in the presence of the continuum background [454].

The LHC has the potential to explore a broad range of SUSY parameter space through the search for non-SM-like Higgs bosons. Nevertheless, Fig. 11.16 shows a broad region with intermediate $tan\beta$ and large values of m_A that is not accessed by current searches, and in which the most promising channel is the very difficult search for $t\bar{t}$ decays with its aforementioned intricacies. In this region of parameter space it is possible that only the SM-like Higgs boson can be within the LHC's reach. If no other state of the EWSB sector than H is discovered, it may be challenging to determine only from the Higgs sector whether there is a supersymmetric extension of the SM in nature.

(iii) Searches for a CP-odd state decaying to hZ

Similarly to the search for a CP-even high mass Higgs boson decaying to a pair of Higgs bosons, the search for a CP-odd states decaying hZ was carried out at the LHC by the ATLAS and CMS collaborations in various channels: (i) the $(Z \to \ell\ell)(h \to b\bar{b})$, (ii) the $(Z \to \nu\nu)(h \to b\bar{b})$, (iii) the $(Z \to \ell\ell)(h \to \tau\tau)$, (iv) and the $(Z \to \ell\ell)(h \to \tau\tau)$, final states. The searches where the A boson decays to a pair of b quarks have been performed both in the regime where both b-jets are resolved and in the boosted regime where the two b-jets are merged in a single larger radius jet. These searches have been

used to constrain the parameter space of 2HDMs. In the MSSM these searches place limits on small values of $tan\beta$ for masses of A comprised between 220 GeV and 360 GeV as illustrated in Fig. 11.16.

(iv) Searches low mass states

Searches for pseudoscalar Higgs bosons at intermediate to low masses, below the Z mass (in the 25 GeV to 80 GeV mass range) have been performed by the CMS collaboration both in the $\tau^+\tau^-$ [497] and the $\mu^+\mu^-$ [498] decay channels. A light pseudoscalar in this mass range is excluded by current direct constraints in the MSSM but not in general 2HDMs [499]. These searches are done in the decay channels where the pseudoscalar Higgs boson decays to a pair of taus or muons and is produced in association with a pair of b-quarks.

Searches for low mass Higgs bosons were also performed in the diphoton channel by both the ATLAS and CMS collaborations [500, 501] and Run 1. The CMS collaboration has updated the results of this search with the full 2016 dataset [502]. A modest excess has been observed by the CMS collaboration at a mass of 95.3 GeV and a local significance of 2.8σ (the corresponding global significance is 1.3σ). An slight excess was also seen by CMS in the 8 TeV data at a slightly higher mass of 97.6 GeV with a local significance of 2.0σ (1.47σ global). No significant excess has been observed in this region with the ATLAS experiment and the Run 1 data only.

(v) Searches for charged Higgs bosons $H^\pm$

At e^+e^- colliders charged Higgs bosons can be pair produced in the s-channel via γ or Z boson exchange. This process is dominant in the LEP centre-of-mass energies range *i.e.* up to 209 GeV. At higher centre-of-mass energies, other processes can play an important role such as the production in top quark decays via $t \to b + H^+$ if $m_{H^\pm} < m_t - m_b$ or via the one-loop process $e^+e^- \to W^\pm H^\mp$ [503, 504], which allows the production of a charged Higgs boson with $m_{H^\pm} > \sqrt{s}/2$, even when H^+H^- production is kinematically forbidden. Other single charged Higgs production mechanisms include $t\bar{b}H^-/\,\bar{t}bH^+$ production [104], $\tau^+\nu H^-/\,\tau^-\bar{\nu}H^+$ production [505], and a variety of processes in which $H^\pm$ is produced in association with a one or two other gauge and/or Higgs bosons [506].

At hadron colliders, charged Higgs bosons can be produced in several different modes. If $m_{H^\pm} < m_t - m_b$, the charged Higgs boson can be produced in decays of the top quark via the decay $t \to bH^\pm$. Relevant QCD and SUSY-QCD corrections to BR($t \to H^\pm b$) have been computed [507–510]. For values of $m_{H^\pm}$ near m_t, width effects are important. In addition, the full $2 \to 3$ processes $pp/p\bar{p} \to H^+\bar{t}b + X$ and $pp/p\bar{p} \to H^-t\bar{b} + X$ must be considered. If $m_{H^\pm} > m_t - m_b$, then charged Higgs boson production occurs mainly through radiation from a third generation quark. Charged Higgs bosons may also be produced singly in association with a top quark via the $2 \to 3$ partonic processes $gg,\, q\bar{q} \to t\bar{b}H^-$. For charged Higgs boson production cross section predictions for the Tevatron and the LHC, see Refs. [11, 42, 41]. Charged Higgs bosons can also be produced via associated production with $W^\pm$ bosons through $b\overline{b}$ annihilation and gg-fusion [511] and in pairs via $q\overline{q}$ annihilation [512].

(a) Exclusion limits from LEP

Charged Higgs bosons have been searched for at LEP, where the combined data of the four experiments, ALEPH, DELPHI, L3, and OPAL, were sensitive to masses of up to about 90 GeV [490] in two decay channels, the $\tau\nu$ and $c\bar{s}$. The exclusion limit independent of the admixture of the two above mentioned branching fractions was 78.6 GeV.

(b) Exclusion limits from Tevatron

Compared to the mass domain covered by LEP searches, the Tevatron covered a complementary range of charged Higgs masses. The CDF and D0 collaborations have also searched for charged Higgs bosons in top quark decays with subsequent decays to $\tau\nu$ or to $c\bar{s}$ [513–515]. For the $H^+ \to c\bar{s}$ channel, the limits on BR($t \to H^+ b$) from CDF and D0 are $\approx 20\%$ in the mass range $90\,\text{GeV} < m_{H^+} < 160\,\text{GeV}$ and assuming a branching fraction of 100% in this specific final state. $H^+ \to \tau^+\nu_\tau$ channel, D0's limits on BR($t \to H^+ b$) are also $\approx 20\%$ in the same mass range and assuming a branching fraction of 100% in this final state. These limits are valid in general 2HDMs, and they have also been interpreted in terms of the MSSM [513–515].

(c) Exclusion limits from LHC

Similarly to the Tevatron, at the LHC light charged Higgs bosons can be searched for in the decays of top quarks. The main initial production mode for light charged Higgs bosons ($m_{H^\pm} < m_t - m_b$) is top pair production. The subsequent decay modes of the charged Higgs boson for these searches are $\tau\nu$ and $c\bar{s}$. More recently ATLAS and CMS have also searched for higher mass charged Higgs bosons ($m_{H^\pm} > m_t + m_b$) in $H^+ \to t\bar{b}$. The main production modes are the associated production of a charged Higgs boson in association with a top and a bottom quark or in association with a top quark only.

The decay $H^+ \to \tau^+\nu_\tau$ is searched typically in three final state topologies: (i) lepton+jets: with $t\bar{t} \to \bar{b}WH^+ \to b\bar{b}(q\bar{q}')(\tau_{\text{lep}}\nu)$, i.e., the W boson decays hadronically and the tau decays into an electron or a muon, with two neutrinos; (ii) τ +lepton: with $t\bar{t} \to \bar{b}WH^+ \to b\bar{b}(l\nu)(\tau_{\text{had}}\nu)$ i.e., the W boson decays leptonically (with $\ell = e,\ \mu$) and the tau decays hadronically; (iii) τ+jets: $t\bar{t} \to \bar{b}WH^+ \to b\bar{b}(q\bar{q}')(\tau_{\text{had}}\nu)$, *i.e.*, both the W boson and the τ decay hadronically.

The CMS collaboration has also searched for the charged Higgs boson in the decay products of top quark pairs: $t\bar{t} \to H^\pm W^\mp b\bar{b}$ and $t\bar{t} \to H^+H^- b\bar{b}$ as well. Three types of final states with large missing transverse energy and jets originating from b-quark hadronization have been analyzed: the fully-hadronic channel with a hadronically decaying tau in association with jets, the dilepton channel with a hadronically decaying tau in association with an electron or muon and the dilepton channel with an electron-muon pair. Combining the results of these three analyses and assuming BR($H^\pm \to \tau\nu$)=1, the upper limits on BR($t \to H^+ b$) are less than 2% to 3% depending on the charged Higgs boson mass in the interval $80\,\text{GeV} < m_{H^+} < 160\,\text{GeV}$.

Both the ATLAS and CMS collaborations have also searched for high mass charged Higgs bosons decaying to a top and bottom quarks. The main production mode for this search is the associated production with one top quark (5-flavor scheme) or a top quark and and bottom quark (4-flavor scheme) in the final state. The s-channel production

mode where the charged Higgs boson is produced alone in the final state at tree level is also considered. This search is particularly intricate and it is sensitive to the modeling of the top pair production background produced in association with additional partons and in particular b-quarks. No excess was found and the results are expressed in terms of exclusion limits of cross section times branching fractions.

ATLAS and CMS have also searched for charged Higgs bosons in top quark decays assuming $\mathrm{BR}(H^+ \to c\bar{s}) = 100\%$ [463, 464], and sets limits of $\approx 20\%$ on $\mathrm{BR}(t \to H^+ b)$ in the $90\,\mathrm{GeV} < m_{H^+} < 160\,\mathrm{GeV}$ mass range.

In two Higgs doublet models the decay of the charged Higgs boson to a W- and a Z-boson is allowed only at loop level and is therefore suppressed. However the $H^\pm \to W^\pm Z$ decay channel is allowed in Higgs triplet models. The ATLAS collaboration [467] has searched for such decays, requiring that the charged Higgs boson is produced through the fusion of vector bosons. No excess with respect to the SM backgrounds has been observed in this channel, and the results are interpreted in the Georgi–Machacek model [376–379] discussed in Section VII.5.2.

At the LHC various other channels still remain to be explored, in particular searches involving additional neutral scalars in particular in WH, WA where A is the pseudo scalar MSSM Higgs boson, and Wa where a is the light CP-odd scalars of the NMSSM.

(vi) Searches for a light CP-odd Higgs boson a

A light pseudoscalar boson a is present in any two Higgs doublet mode enhanced with an additional singlet field. A prominent example is the NMSSM. The theoretical motivations for singlet extensions of the MSSM are discussed in Section VII.2. In the NMSSM, the searches now focus on the low mass pseudo-scalar boson a region for several reasons: (i) in the NMSSM, the light pseudo-scalar a boson can, as a pseudo-Goldstone boson, be a natural candidate for an axion; (ii) scenarios where $m_a > 2m_b$ and a CP-even state h decaying to a pair of a ($m_h > 2m_a$) are excluded by direct searches at LEP in the four b channel [490, 520, 476]; (iii) in the pre-discovery era, LEP limits on a CP-even Higgs boson resulted in fine tuning MSSM constraints [521] which could be evaded through non standard decays of the Higgs to aa; (iv) an NMSSM CP-odd a boson with a mass in the range 9.2–12 GeV can also account for the difference observed between the measured anomalous muon magnetic moment and its prediction [522]. A scenario that has drawn particular attention was motivated by a small excess of events 2.3σ in the SM Higgs search at LEP at Higgs boson mass of around 98 GeV. Speculative interpretations of this excess as a signal of a Higgs boson with reduced couplings to b-quarks were given [521]. Complete reviews of the NMSSM phenomenology can be found in Refs. [523, 476].

The potential benchmark scenarios have changed in the light of the Higgs boson discovery. The discovered state could be the lightest or the next-to-lightest of the three CP-even states of the NMSSM. Light pseudoscalar scenarios are still very interesting in particular for the potential axion candidate. There are three main types of direct searches for the light a boson: (i) for masses below the Υ resonance, the search is for radiative decays $\Upsilon \to a\gamma$ at B-factories; (ii) the inclusive search for in high energy pp collisions at the LHC; (iii) the search for decays of a CP-even Higgs h boson to a pair of a bosons.

Radiative decays $\Upsilon \to a\gamma$, have been searched for in various colliders, the most recent

results are searches for radiative decays of the $\Upsilon(1s)$ to $a\gamma$ with a subsequent decay of the a boson to a pair of taus at CLEO [524] and the radiative decays of the $\Upsilon(1s, 2s, 3s)$ to $a\gamma$ with subsequent decays to a pair of muons or taus by the BaBar collaboration [478, 479].

Direct inclusive searches for the light pseudo scalar a boson were performed in the $a \to \mu\mu$ channel at the Tevatron by the D0 experiment [525] and by the ATLAS [470] and CMS [526] collaborations at the LHC.

Finally searches for the decays of the Higgs boson to a pair of a bosons where performed with subsequent decays to four photons, in the four muons final state, in the two muons and two taus final state, and in the four taus final state.

No significant excess in the searches for a light CP-odd a boson were found and limits on the production times branching fractions of the a boson have been set.

References for these searches are summarized in Table 11.17.

(vii) Searches for doubly charged Higgs bosons $H^{\pm\pm}$

As discussed in Section VII.5, the generation of small neutrino masses via the standard EWSB mechanism described in Section II requires unnaturally small Yukawa couplings, provided that neutrinos are Dirac-type fermions. A Majorana mass term with a see-saw mechanism for neutrinos, would allow for naturally small masses and yield a framework for the appealing scenario of leptogenesis. However within the SM Majorana mass terms correspond to (non-renomalizable) dimension-5 operators. Such effective interactions can be generated via renormalizable interactions with an electroweak triplet of complex scalar fields (corresponding to a type-II see-saw mechanism). Other models such as the Zee–Babu model, with the introduction of two $\mathrm{SU}(2)_L$ singlets, also generate Majorana mass terms. The signature of such models would be the presence of doubly charged Higgs bosons $H^{\pm\pm}$.

The main production mechanisms of $H^{\pm\pm}$ bosons at hadron colliders are the pair production in the s-channel through the exchange of a Z boson or a photon and the associated production with a charged Higgs boson through the exchange of a W boson. Various searches for doubly charged Higgs bosons have been performed by ATLAS and CMS at Run 1 [528, 529] and Run 2 [480–482].

VII.7.1. Searches for non-standard production processes of the Higgs boson

The discovery of the Higgs boson has also allowed for searches of BSM (beyond the SM) processes involving standard decays of the Higgs boson. One example directly pertaining to the search for additional states of the EWSB sector is the search for Higgs bosons in the cascade decay of a heavy CP-even Higgs boson decaying to charged Higgs boson and a W boson, and the charged Higgs boson subsequently decaying to H and another W boson. This search has been performed by the ATLAS collaboration in $b\overline{b}$ decays of the H particle [530].

VII.7.2. Outlook of searches for additional states

The LHC program of searches for additional states covers a large variety of decay and production channels. Since the last review on the *Status of Higgs boson physics* [281]

many new channels have been explored at the LHC, *e.g.* the searches for additional states decaying into hh or Zh. The search for charged Higgs bosons has been extended to include the WZ and the very difficult $t\bar{b}$ decay channel. There are however more channels to cover, *e.g.* the search for charged Higgs bosons in the HW and AW channels.

VIII. Summary and outlook

Summary– The discovery of the Higgs boson is an important milestone in the history of particle physics as well as an extraordinary achievement of the LHC machine and the ATLAS and CMS experiments. Five years after its discovery, substantial progress in the field of Higgs boson physics has been accomplished and a significant number of measurements probing its nature have been made. They are revealing an increasingly precise profile of the Higgs boson.

Since the last edition of this review [233], the LHC has delivered in Run 2 a dataset corresponding to an integrated luminosity of more than $40\,\text{fb}^{-1}$ of 13 TeV pp collisions. After data quality requirements, this leaves about $36\,\text{fb}^{-1}$ of data collected by fully operational ATLAS and CMS detectors. Due to the substantial increase in production rates at the higher center-of-mass energy, many of Run 1 results have been updated. Milestone measurements have been performed: (i) a clear observation of the Higgs boson decay to taus has been made by the CMS experiment; (ii) unambiguous evidence for the Higgs boson decay to a pair of b quarks was provided by both the ATLAS and CMS experiments; (iii) the ATLAS and CMS experiments have also provided evidence for the production of the Higgs boson through the $t\bar{t}H$ mechanism, thus yielding direct evidence for the Yukawa coupling of the Higgs boson to top quarks, with a strength compatible with that of the Standard Model. These and all other experimental measurements are consistent with the EWSB mechanism of the Standard Model.

New theoretical calculations and developments in Monte Carlo simulation pertaining to Higgs physics are still occurring at a rapid pace. For example, the theoretical prediction for the dominant gluon fusion production mode now includes the latest N3LO result, which is twice as precise as previous N2LO calculations. With these improvements in the state-of-the-art in theory predictions and the increase in luminosity and center-of-mass energy, Higgs physics has definitively entered a precision era.

Since the discovery of the Higgs boson, new ideas have emerged to probe its rare decays and production modes, as well as indirectly measure the Higgs boson width through the study of its off-shell couplings, or via on-shell interference effects. The Higgs boson has now become part of the standard toolkit in searches for new physics.

Many extensions of the SM at higher energies call for an enlargement of the EWSB sector. Hence, direct searches for additional scalar states can provide valuable insights on the dynamics of the EWSB mechanism. The ATLAS and CMS experiments have searched for additional Higgs bosons in the Run 2 data, and imposed constraints in broad ranges of mass and couplings for various extended Higgs scenarios.

The landscape of Higgs physics has been extended extraordinarily since the discovery. In addition, Run 2 is still ongoing and after its completion the amount of data collected

is expected to increase three-fold. The current dataset is approximately one percent of the total dataset foreseen for the High Luminosity phase of the LHC project. This perspective brings new challenges to increase further the reach in precision and it also widens the possibilities of unveiling the nature of the electroweak symmetry breaking.

Outlook– The unitarization of the vector boson scattering (VBS) amplitudes, dominated at high energies by their longitudinal polarizations, has been the basis of the *no lose* theorem at the LHC, and was a determining consideration in the building of the accelerator and the detectors. It motivated the existence of a Higgs boson or the observability of manifestations of strong dynamics at TeV scale. Now that a Higgs boson has been found and its couplings to gauge bosons are consistent with the SM predictions, perturbative unitarity is preserved to a large amount with the sole exchange of the Higgs boson, and without the need for any additional states. VBS is, however, still an important channel to investigate further in order to better understand the nature of the Higgs sector and the possible completion of the SM at the TeV scale. In association with the double Higgs boson production channel by vector boson fusion, VBS could, for instance, confirm that the Higgs boson is part of a weak doublet and also establish whether it is an elementary object or a composite state that could emerge as a pseudo-Nambu–Goldstone boson from a new underlying broken symmetry.

The Higgs boson couplings are not dictated by any local gauge symmetry. Thus, in addition to a new particle, the LHC has also discovered a new force, different in nature from the other fundamental interactions since it is non-universal and distinguishes between the three families of quarks and leptons. The existence of the Higgs boson embodies the problem of an unnatural cancellation among the quantum corrections to its mass if new physics is present at scale significantly higher than the EW scale. The non-observation of additional states which could stabilize the Higgs boson mass is a challenge for natural scenarios like supersymmetry or models with a new strong interaction in which the Higgs boson is not a fundamental particle. This increasingly pressing paradox starts questioning the principle of naturalness.

The search for the Higgs boson has occupied the particle physics community for the last 50 years. Its discovery has shaped and sharpened the physics programs of the LHC and of prospective future accelerators. The experimental data together with the progress in theory mark the beginning of a new era of precision Higgs boson measurements.

Acknowledgements

We would like to thank many of our colleagues for proofreading this review, for useful criticism and their input in general: W. Altmannshofer, G. Branco, J. Campbell, F. Cerutti, C. Csáki, R. Contino, J. Conway, N. Craig, A. David, J.B. De Vivie, J.R. Espinosa, A. Falkowski, W. Fischer, S. Forte, M. Grazzini, H. Haber, S. Heinemeyer, J. Hubisz, A. Korytov, B. Jäger, H. Ji, T. Junk, P. Langacker, J. Lykken, F. Maltoni, B. Mansoulié R. Mishra, M. Mühlleitner, B. Murray, M. Neubert, G. Perez, G. Petrucciani, A. Pomarol, E. Pontón, D. Rebuzzi, E. Salvioni, N. Shah, G. Shaughnessy, M. Spira, O. Stål, A. Strumia, K. Tackmann, R. Tanaka, J. Terning, A. Vartak, C. Wagner, and A. Weiler. We are also most grateful to the ATLAS, CDF, CMS and D0 collaborations for their help with this review.

M.C. is supported by Fermilab, that is operated by Fermi Research Alliance, LLC under Contract No. DE–AC02–07CH11359 with the United States Department of Energy. C.G. is supported by the European Commission through the Marie Curie Career Integration Grant 631962, by the Helmholtz Association and by the Collaborative Research Center SFB676 of the Deutsche Forschungsgemeinschaft (DFG), Particles, Strings and the Early Universe. M.K. is supported by the ANR HiggsNet grant. V.S. is supported by the grant DE–SC0009919 of the United States Department of Energy.

References

1. G. Aad *et al.* [ATLAS Collab.], Phys. Lett. **B716**, 1 (2012).
2. S. Chatrchyan *et al.* [CMS Collab.], Phys. Lett. **B716**, 30 (2012).
3. S.L. Glashow, Nucl. Phys. **20**, 579 (1961);
   S. Weinberg, Phys. Rev. Lett. **19**, 1264 (1967);
   A. Salam, *Elementary Particle Theory*, eds.: Svartholm, Almquist and Wiksells, Stockholm, 1968;
   S. Glashow, J. Iliopoulos, and L. Maiani, Phys. Rev. **D2**, 1285 (1970).
4. F. Englert and R. Brout, Phys. Rev. Lett. **13**, 321 (1964);
   P.W. Higgs, Phys. Rev. Lett. **13**, 508 (1964) and Phys. Rev. **145**, 1156 (1966);
   G.S. Guralnik, C.R. Hagen, and T.W. Kibble, Phys. Rev. Lett. **13**, 585 (1964).
5. J.M. Cornwall, D.N. Levin, and G. Tiktopoulos, Phys. Rev. Lett. **30**, 1286 (1973) and Phys. Rev. **D10**, 1145 (1974);
   C.H. Llewellyn Smith, Phys. Lett. **B46**, 233 (1973).
6. B.W. Lee, C. Quigg, and H.B. Thacker, Phys. Rev. **D16**, 1519 (1977).
7. K. Wilson, Phys. Rev. D 3,1818(1971);
   G. 't Hooft, in *Proc. of 1979 Cargèse Institute on Recent Developments in Gauge Theories,* p. 135 Press, New York 1980;
   For a recent review, see G.F. Giudice, PoS EPS **-HEP2013**, 163 (2013).
8. J. Parsons, and A. Pomarol, *Extra Dimenions*, in this volume.
9. J. Wess and B. Zumino, Nucl. Phys. **B70**, 39 (1974) and Phys. Lett. **49B**, 52 (1974);
   H.P. Nilles, Phys. Rev. **C110**, 1 (1984);
   S.P. Martin, `arXiv:hep-ph/9709356` (1997);
   P. Fayet, Phys. Lett. **B69**, 489 (1977), Phys. Lett. **B84**, 421 (1979), Phys. Lett. **B86**, 272 (1979) and Nucl. Phys. **B101**, 81 (2001).
10. E. Witten, Nucl. Phys. **B188**, 513 (1981);
    R.K. Kaul, Phys. Lett. **B109**, 19 (1982) and Pramana **19**, 183 (1982);
    L. Susskind, Phys. Rev. **104**, 181 (1984).
11. H.E. Haber and G.L. Kane, Phys. Rev. **C117**, 75 (1985).
12. J. F. Gunion *et al.*, *The Higgs Hunter's Guide*, Addison-Wesley (1990).
13. S. Weinberg, Phys. Rev. **D13**, 974 (1979) and Phys. Rev. **D19**, 1277 (1979);
    L. Susskind, Phys. Rev. **D20**, 2619 (1979);
    for a review, see C.T. Hill and E.H. Simmons, Phys. Reports **381**, 235 (2003) [E: **390**, 553 (2004)].
14. D. B. Kaplan and H. Georgi, Phys. Lett. **B136**, 183 (1984).
15. G. Panico and A. Wulzer, Lect. Notes Phys. **913**, 1 (2016).
16. C. Csaki, C. Grojean and J. Terning, Rev. Mod. Phys. **88**, 045001 (2016).
17. C. Csaki *et al.*, Phys. Rev. **D62**, 045015 (2000);
    for other references, see the 2014 edition of this review.
18. W. D. Goldberger, B. Grinstein, and W. Skiba, Phys. Rev. Lett. **100**, 111802 (2008);
    J. Fan *et al.*, Phys. Rev. **D79**, 035017 (2009);

B. Bellazzini *et al.*, Eur. Phys. J. **C73**, 2333 (2013);
Z. Chacko and R.K. Mishra, Phys. Rev. **D87**, 115006 (2013);
Z. Chacko, R. Franceschini, and R.K. Mishra, JHEP **1304**, 015 (2013).
19. Z. Chacko, H.S. Goh and R. Harnik, Phys. Rev. Lett. **96**, 231802 (2006) and JHEP **0601**, 108 (2006).
20. N. Craig, A. Katz, M. Strassler and R. Sundrum, JHEP **1507**, 105 (2015);
N. Craig, S. Knapen and P. Longhi, Phys. Rev. Lett. **114**, 061803 (2015).
21. P.W. Graham, D. E. Kaplan and S. Rajendran, Phys. Rev. Lett. **115**, 221801 (2015);
J.R. Espinosa *et al.*, Phys. Rev. Lett. **115**, 251803 (2015).
22. T. van Ritbergen and R.G. Stuart, Phys. Rev. Lett. **82**, 488 (1999) and Nucl. Phys. **B564**, 343 (2000);
M. Steinhauser and T. Seidensticker, Phys. Lett. **B467**, 271 (1999);
D.M. Webber *et al.* [MuLan Collab.], Phys. Rev. Lett. **106**, 041803 (2011).
23. J. Ellis, M.K. Gaillard, and D.V. Nanopoulos, Nucl. Phys. **B106**, 292 (1976).
24. M.A. Shifman *et al.*, Sov. J. Nucl. Phys. **30**, 711 (1979) [Yad. Fiz. **30**, 1368 (1979)].
25. P. Sikivie *et al.*, Nucl. Phys. **B173**, 189 (1980);
H. Georgi, Ann. Rev. Nucl. and Part. Sci. **43**, 209 (1993).
26. M.J.G. Veltman, Nucl. Phys. **B123**, 89 (1977).
27. I.V. Krive and A.D. Linde, Nucl. Phys. **B117**, 265 (1976);
for other references, see the 2014 edition of this review.
28. J.R. Espinosa and M. Quiros, Phys. Lett. **B353**, 257 (1995);
G. Isidori, G. Ridolfi, and A. Strumia, Nucl. Phys. **B609**, 387 (2001).
29. V. Branchina, E. Messina and M. Sher, Phys. Rev. **D91**, 013003 (2015).
30. A. Hook *et al.*, JHEP **1501**, 061 (2015);
J. Kearney, H. Yoo and K.M. Zurek, Phys. Rev. **D91**, 123537 (2015).
31. A. Andreassen, W. Frost and M. D. Schwartz, arXiv:1707.08124 [hep-ph].;
S. Chigusa, T. Moroi and Y. Shoji, arXiv:1707.09301 [hep-ph]..
32. J. Elias-Miro *et al.*, Phys. Lett. **B709**, 222 (2012);
G. Degrassi *et al.*, JHEP **1208**, 098 (2012);
D. Buttazzo *et al.*, JHEP **1312**, 089 (2013);
J.R. Espinosa *et al.*, JHEP **1509**, 174 (2015).
33. C.D. Froggatt and H.B. Nielsen, Phys. Lett. **B368**, 96 (1996);
M. Shaposhnikov and C. Wetterich, Phys. Lett. **B683**, 196 (2010);
M. Holthausen, K.S. Lim, and M. Lindner, JHEP **1202**, 037 (2012).
34. F.L. Bezrukov and M. Shaposhnikov, Phys. Lett. **B659**, 703 (2008);
F.L. Bezrukov, A. Magnin, and M. Shaposhnikov, Phys. Lett. **B675**, 88 (2009).
35. A. Salvio, Phys. Lett. **B727**, 234 (2013).
36. B.A. Kniehl, Phys. Reports **240**, 211 (1994).
37. M. Spira, Fortsch. Phys. **46**, 203 (1998).
38. M. Carena and H.E. Haber, Prog. in Part. Nucl. Phys. **50**, 152 (2003).
39. A. Djouadi, Phys. Reports **457**, 1 (2008).
40. S. Dittmaier *et al.*, [LHC Higgs Cross Section Working Group], CERN–2011–002, `arXiv:1101.0593 [hep-ph]` (2011).

41. S. Dittmaier *et al.*, [LHC Higgs Cross Section Working Group], CERN–2012–002, arXiv:1201.3084 [hep-ph] (2012).
42. S. Heinemeyer *et al.*, [LHC Higgs Cross Section Working Group], CERN–2013–004, arXiv:1307.1347 [hep-ph] (2013).
43. D. de Florian *et al.*, [LHC Higgs Cross Section Working Group], CERN–2017–002-M, arXiv:1610.07922[hep-ph] (2016).
44. LHC Higgs Cross Section Working Group, https://twiki.cern.ch/twiki/bin/view/LHCPhysics/LHCHXSWG.
45. T. Aaltonen *et al.* [CDF and D0 Collaborations], Phys. Rev. **D88**, 052014 (2013).
46. H.M. Georgi *et al.*, Phys. Rev. Lett. **40**, 692 (1978).
47. D. Graudenz, M. Spira, and P.M. Zerwas, Phys. Rev. Lett. **70**, 1372 (1993).
48. M. Spira *et al.*, Nucl. Phys. **B453**, 17 (1995).
49. S. Dawson, Nucl. Phys. **B359**, 283 (1991);
    A. Djouadi, M. Spira, and P.M. Zerwas, Phys. Lett. **B264**, 440 (1991).
50. R.V. Harlander and W.B. Kilgore, Phys. Rev. Lett. **88**, 201801 (2002);
    C. Anastasiou and K. Melnikov, Nucl. Phys. **B646**, 220 (2002);
    V. Ravindran, J. Smith, and W.L. van Neerven, Nucl. Phys. **B665**, 325 (2003).
51. C. Anastasiou *et al.*, Phys. Rev. Lett. **114**, 212001 (2015);
    C. Anastasiou *et al.*, JHEP **1605**, 058 (2016).
52. R.V. Harlander and K.J. Ozeren, JHEP **0911**, 088 (2009);
    A. Pak, M. Rogal, and M. Steinhauser, JHEP **1002**, 025 (2010).
53. A. Djouadi and P. Gambino, Phys. Rev. Lett. **73**, 2528 (1994);
    S. Actis *et al.*, Phys. Lett. **B670**, 12 (2008);
    U. Aglietti *et al.*, Phys. Lett. **B595**, 432 (2004);
    G. Degrassi and F. Maltoni, Phys. Lett. **B600**, 255 (2004).
54. C. Anastasiou, R. Boughezal, and F. Petriello, JHEP **0904**, 003 (2009).
55. S. Catani *et al.*, JHEP **0307**, 028 (2003);
    S. Moch and A. Vogt, Phys. Lett. **B631**, 48 (2005);
    E. Laenen and L. Magnea, Phys. Lett. **B632**, 270 (2006);
    A. Idilbi *et al.*, Phys. Rev. **D73**, 077501 (2006);
    V. Ravindran, Nucl. Phys. **B752**, 173 (2006);
    V. Ahrens *et al.*, Eur. Phys. J. **C62**, 333 (2009).
56. V. Ahrens *et al.*, Phys. Lett. **B698**, 271 (2011);
    D. de Florian and M. Grazzini, Phys. Lett. **B718**, 117 (2012);
    C. Anastasiou *et al.*, JHEP **1204**, 004 (2012).
57. M. Bonvini *et al.*, JHEP **1608**, 105 (2016).
58. J.C. Collins, D.E. Soper and G.F. Sterman, Nucl. Phys. **B250**, 199 (1985).
59. D. de Florian *et al.*, JHEP **1111**, 064 (2011);
    T. Becher and M. Neubert, Eur. Phys. J. **C71**, 1665 (2011);
    J.Y. Chiu *et al.*, JHEP **1205**, 084 (2012);
    J. Wang *et al.*, Phys. Rev. **D86**, 094026 (2012);
    T. Becher, M. Neubert and D. Wilhelm, JHEP **1305**, 110 (2013).
60. S. Catani and M. Grazzini, Eur. Phys. J. **C72**, 2013 (2012) [E: **C72**, 2132 (2012)].

61. W.Y. Keung and F.J. Petriello, Phys. Rev. **D80**, 01007 (2009);
S. Buhler *et al.*, JHEP **1207**, 115 (2012).

62. R. Frederix, S. Frixione, E. Vryonidou and M. Wiesemann, JHEP **1608**, 006 (2016);;
F. Caola, S. Forte, S. Marzani, C. Muselli and G. Vita, JHEP **1608**, 50 (2016);;
N. Greiner, S. Höche, G. Luisoni, M. Schönherr and J. C. Winter JHEP **1701**, 091 (2017).

63. R.V. Harlander, T. Neumann, K.J. Ozeren and M. Wiesemann, JHEP **1208**, 139 (2012);
T. Neumann and M. Wiesemann, JHEP **1411**, 150 (2014).

64. R.V. Harlander, S. Liebler, and H. Mantler, Comp. Phys. Comm. **184**, 1605 (2013).

65. D. de Florian, M. Grazzini, and Z. Kunszt, Phys. Rev. Lett. **82**, 5209 (1999);
C.J. Glosser and C. R. Schmidt, JHEP **0212**, 016 (2002);
V. Ravindran, J. Smith and W. L. Van Neerven, Nucl. Phys. **B634**, 247 (2002);
X. Liu and F. Petriello, Phys. Rev. **D87**, 014018 (2013).

66. J.M. Campbell, R.K. Ellis, and G. Zanderighi, JHEP **0610**, 028 (2006);
J.M. Campbell, R.K. Ellis, and C. Williams, Phys. Rev. **D81**, 074023 (2010).

67. R. Boughezal *et al.*, JHEP **1306**, 072 (2013);
R. Boughezal *et al.*, Phys. Rev. Lett. **115**, 082003 (2015).

68. C.F. Berger *et al.*, JHEP **1104**, 092 (2011);
A. Banfi, G.P. Salam, and G. Zanderighi, JHEP **1206**, 159 (2012);
T. Becher and M. Neubert, JHEP **1207**, 108 (2012);
A. Banfi *et al.*, Phys. Rev. Lett. **109**, 202001 (2012);
F.J. Tackmann, J.R. Walsh, and S. Zuberi, Phys. Rev. **D86**, 053011 (2012);
T. Becher, M. Neubert, and L. Rothen, JHEP **1310**, 125 (2013).

69. A. Banfi *et al.*, JHEP **1604**, 049 (2016).

70. I. Moult and I. W. Stewart, JHEP **1409**, 129 (2014).

71. M. Duhrssen *et al.*, Phys. Rev. **D70**, 113009 (2004).

72. T. Han, G. Valencia, and S. Willenbrock, Phys. Rev. Lett. **69**, 3274 (1992);
T. Figy, C. Oleari, and D. Zeppenfeld, Phys. Rev. **D68**, 073005 (2003);
T. Figy and D. Zeppenfeld, Phys. Lett. **B591**, 297 (2004);
E.L. Berger and J. Campbell, Phys. Rev. **D70**, 073011 (2004);
M. Ciccolini, A. Denner, and S. Dittmaier, Phys. Rev. Lett. **99**, 161803 (2007);
M. Ciccolini, A. Denner, and S. Dittmaier, Phys. Rev. **D77**, 103002 (2008);
A. Denner, S. Dittmaier, and A. Muck, `HAWK`,
`http://omnibus.uni-freiburg.de/~sd565/programs/hawk/hawk.html`;
K. Arnold *et al.*, `VBFNLO`, Comp. Phys. Comm. **180**, 1661 (2009);
M. Spira, `VV2H`, `http://people.web.psi.ch/spira/vv2h`;
N. Adam *et al.*, `arXiv:0803.1154 [hep-ph]` (2008);
T. Figy, S. Palmer, and G. Weiglein, JHEP **1202**, 105 (2012).

73. P. Nason and C. Oleari, JHEP **1002**, 037 (2010);
S. Frixione, P. Torrielli, and M. Zaro, Phys. Lett. **B726**, 273 (2013);
F. Maltoni, K. Mawatari, and M. Zaro, Eur. Phys. J. **C74**, 2710 (2014).

74. P. Bolzoni *et al.*, Phys. Rev. Lett. **105**, 011801 (2010);
P. Bolzoni *et al.*, Phys. Rev. **D85**, 035002 (2012).
75. M. Cacciari *et al.*, Phys. Rev. Lett. **115**, 082002 (2015).
76. S.L. Glashow, D.V. Nanopoulos, and A. Yildiz, Phys. Rev. **D18**, 1724 (1978);
T. Han and S. Willenbrock, Phys. Lett. **B273**, 167 (1991);
T. Han, G. Valencia, and S. Willenbrock, Phys. Rev. Lett. **69**, 3274 (1992);
H. Baer, B. Bailey, and J.F. Owens, Phys. Rev. **D47**, 2730 (1993);
J. Ohnemus and W.J. Stirling, Phys. Rev. **D47**, 2722 (1993).
77. A. Stange, W. Marciano, and S. Willenbrock, Phys. Rev. **D49**, 1354 (1994).
78. A. Stange, W. Marciano, and S. Willenbrock, Phys. Rev. **D50**, 4491 (1994).
79. M.L. Ciccolini, S. Dittmaier, and M. Kramer, Phys. Rev. **D68**, 073003 (2003);
A. Denner, S Dittmaier, and S. Kalweit, JHEP **1203**, 075 (2012).
80. R. Hamberg, W.L. van Neerven, and T. Matsuura, Nucl. Phys. **B359**, 343 (1991).
81. O. Brein, A. Djouadi, and R. Harlander, Phys. Lett. **B579**, 149 (2004);
L. Altenkamp *et al.*, JHEP **1302**, 078 (2013).
82. O. Brein *et al.*, Eur. Phys. J. **C72**, 1868 (2012).
83. O. Brein, R.V. Harlander, and T.J. Zirke, Comp. Phys. Comm. **184**, 998 (2013).
84. A. Denner *et al.*, JHEP **1203**, 075 (2012).
85. G. Ferrera, M. Grazzini, and F. Tramontano, Phys. Rev. Lett. **107**, 152003 (2011).
86. G. Ferrera, M. Grazzini and F. Tramontano, Phys. Lett. **B740**, 51 (2015).
87. J.M. Campbell, R.K. Ellis and C. Williams, JHEP **1606**, 179 (2016).
88. W. Astill *et al.*, JHEP **1606**, 154 (2016).
89. R. Raitio and W.W. Wada, Phys. Rev. **D19**, 941 (1979);
J.N. Ng and P. Zakarauskas, Nucl. Phys. **B247**, 339 (1984);
J.F. Gunion, Phys. Lett. **B261**, 510 (1991);
W.J. Marciano and F.E. Paige, Phys. Rev. Lett. **66**, 2433 (1991).
90. W. Beenakker *et al.*, Phys. Rev. Lett. **87**, 201805 (2001);
L. Reina and S. Dawson, Phys. Rev. Lett. **87**, 201804 (2001);
S. Dawson *et al.*, Phys. Rev. **D67**, 071503 (2003);
W. Beenakker *et al.*, Nucl. Phys. **B653**, 151 (2003).
91. R. Frederix *et al.*, Phys. Lett. **B701**, 427 (2011);
M. Garzelli *et al.*, Europhys. Lett. **96**, 11001 (2011).
92. F. Demartin *et al.*, Eur. Phys. J. **C75**, 267 (2015).
93. K.A. Assamagan *et al.*, [Higgs Working Group, "Physics at TeV Colliders" workshop, Les Houches, 2003], `arXiv:hep-ph/0406152` (2004).
94. R.V. Harlander and W.B. Kilgore, Phys. Rev. **D68**, 013001 (2003);
J. M. Campbell *et al.*, Phys. Rev. **D67**, 095002 (2003);
S. Dawson *et al.*, Phys. Rev. Lett. **94**, 031802 (2005);
S. Dittmaier, M. Kramer, and M. Spira, Phys. Rev. **D70**, 074010 (2004);
S. Dawson *et al.*, Phys. Rev. **D69**, 074027 (2004).
95. W.J. Stirling and D.J. Summers, Phys. Lett. **B283**, 411 (1992);
F. Maltoni *et al.*, Phys. Rev. **D64**, 094023 (2001).
96. S. Dawson, S. Dittmaier and M. Spira, Phys. Rev. **D58**, 115012 (1998).
97. D. de Florian and J. Mazzitelli, Phys. Rev. Lett. **111**, 201801 (2013).

98. S. Borowka *et al.*, Phys. Rev. Lett. **117**, 012001 (2016).
99. B.L. Ioffe and V.A. Khoze, Sov. J. Nucl. Phys. **9**, 50 (1978).
100. D.R.T. Jones and S. Petcov, Phys. Lett. **B84**, 440 (1979);
R.N. Cahn and S. Dawson, Phys. Lett. **B136**, 196 (1984);
G.L. Kane, W.W. Repko, and W.B. Rolnick, Phys. Lett. **B148**, 367 (1984);
G. Altarelli, B. Mele, and F. Pitolli, Nucl. Phys. **B287**, 205 (1987);
W. Kilian, M. Kramer, and P.M. Zerwas, Phys. Lett. **B373**, 135 (1996).
101. B.A. Kniehl, Z. Phys. **C55**, 605 (1992).
102. J. Fleischer and F. Jegerlehner, Nucl. Phys. **B216**, 469 (1983);
A. Denner *et al.*, Z. Phys. **C56**, 261 (1992).
103. B.A. Kniehl, Int. J. Mod. Phys. **A17**, 1457 (2002).
104. K.J. Gaemers and G.J. Gounaris, Phys. Lett. **B77**, 379 (1978);
A. Djouadi, J. Kalinowski, and P. M. Zerwas, Z. Phys. **C54**, 255 (1992);
B.A. Kniehl, F. Madricardo, and M. Steinhauser, Phys. Rev. **D66**, 054016 (2002).
105. S. Dittmaier *et al.*, Phys. Lett. **B441**, 383 (1998);
S. Dittmaier *et al.*, Phys. Lett. **B478**, 247 (2000);
S. Dawson and L. Reina, Phys. Rev. **D59**, 054012 (1999).
106. S. Dawson *et al.*, [Higgs Working Group, "Snowmass on the Mississippi" workshop] `arXiv:1310.8361 [hep-ex]` (2013).
107. D.M. Asner *et al.*, [ILC Higgs white paper, "Snowmass on the Mississippi" workshop] `arXiv:1310.0763 [hep-ph]` (2013).
108. A. Denner *et al.*, Eur. Phys. J. **C71**, 1753 (2011).
109. A. Djouadi, J. Kalinowski, and M. Spira, Comp. Phys. Comm. **108**, 56 (1998);
A. Djouadi *et al.*, `arXiv:1003.1643 [hep-ph]` (2010).
110. S. Gorishnii *et al.*, Mod. Phys. Lett. **A5**, 2703 (1990);
S. Gorishnii *et al.*, Phys. Rev. **D43**, 1633 (1991);
A.L. Kataev and V.T. Kim, Mod. Phys. Lett. **A9**, 1309 (1994);
L.R. Surguladze, Phys. Lett. **B341**, 60 (1994);
S. Larin, T. van Ritbergen, and J. Vermaseren, Phys. Lett. **B362**, 134 (1995);
K. Chetyrkin and A. Kwiatkowski, Nucl. Phys. **B461**, 3 (1996);
K. Chetyrkin, Phys. Lett. **B390**, 309 (1997);
P.A. Baikov, K.G. Chetyrkin, and J.H. Kuhn, Phys. Rev. Lett. **96**, 012003 (2006).
111. J. Fleischer and F. Jegerlehner, Phys. Rev. **D23**, 2001 (1981);
D. Bardin, B. Vilensky, and P. Khristova, Sov. J. Nucl. Phys. **53**, 152 (1991);
A. Dabelstein and W. Hollik, Z. Phys. **C53**, 507 (1992);
B.A. Kniehl, Nucl. Phys. **B376**, 3 (1992);
A. Djouadi *et al.*, *Proceedings* e^+e^- *collisions at 500 GeV* (1991).
112. T. Inami, T. Kubota, and Y. Okada, Z. Phys. **C18**, 69 (1983);
K.G. Chetyrkin, B.A. Kniehl, and M. Steinhauser, Phys. Rev. Lett. **79**, 353 (1997);
P.A. Baikov and K.G. Chetyrkin, Phys. Rev. Lett. **97**, 061803 (2006).
113. H.Q. Zheng and D.D. Wu, Phys. Rev. **D42**, 3760 (1990);
A. Djouadi *et al.*, Phys. Lett. **B257**, 187 (1991);
S. Dawson and R. Kauffman, Phys. Rev. **D47**, 1264 (1993);
A. Djouadi, M. Spira, and P. Zerwas, Phys. Lett. **B311**, 255 (1993);

K. Melnikov and O.I. Yakovlev, Phys. Lett. **B312**, 179 (1993);
M. Inoue *et al.*, Mod. Phys. Lett. **A9**, 1189 (1994).
114. P. Maierhofer and P. Marquard, Phys. Lett. **B721**, 131 (2013).
115. U. Uglietti *et al.*, Phys. Lett. **B595**, 432 (2004);
G. Degrassi and F. Maltoni, Phys. Lett. **B600**, 255 (2004);
S. Actis *et al.*, Phys. Lett. **B670**, 12 (2008);
U. Aglietti *et al.*, Phys. Lett. **B600**, 57 (2004);
G. Degrassi and F. Maltoni, Nucl. Phys. **B724**, 183 (2005);
U. Aglietti *et al.*, [Tevatron for LHC report: Higgs] `arXiv:hep-ph/0612172` (2006).
116. A. Abbasabadi *et al.*, Phys. Rev. **D55**, 5647 (1997);
A. Abbasabadi and W.W. Repko, Phys. Rev. **D71**, 017304 (2005);
A. Abbasabadi and W.W. Repko, JHEP **0608**, 048 (2006);
D.A. Dicus and W.W. Repko, Phys. Rev. **D87**, 077301 (2013);
L.B. Chen, C.F. Qiao, and R.L. Zhu, Phys. Lett. **B726**, 306 (2013);
Y. Sun, H.R. Chang, and D.N. Gao, JHEP **1305**, 061 (2013);
G. Passarino, Phys. Lett. **B727**, 424 (2013).
117. M. Spira, A. Djouadi, and P.M. Zerwas, Phys. Lett. **B276**, 350 (1992).
118. A. Bredenstein *et al.*, Phys. Rev. **D74**, 013004 (2006);
A. Bredenstein *et al.*, JHEP **0702**, 080 (2007);
A. Bredenstein *et al.*, `Prophecy4f`: A Monte Carlo generator for a proper description of the Higgs decay into 4 fermions,
`http://omnibus.uni-freiburg.de/~sd565/programs/prophecy4f/prophecy4f.html`.
119. A. Ghinculov, Phys. Lett. **B337**, 137 (1994) [E: **B346**, 426 (1995)];
L. Durand, B.A. Kniehl, and K. Riesselmann, Phys. Rev. **D51**, 5007 (1995);
L. Durand, K. Riesselmann, and B.A. Kniehl, Phys. Rev. Lett. **72**, 2534 (1994) [E: **74**, 1699 (1995)].
120. E. Braaten and J.P. Leveille, Phys. Rev. **D22**, 715 (1980);
L. Durand, K. Riesselmann, and B.A. Kniehl, Phys. Rev. Lett. **72**, 2534 (1994);
E. Gross, G. Wolf, and B.A. Kniehl, Z. Phys. **C63**, 417 (1994) [E: *ibid.*, **C66**, 32 (1995)];
A. Ghinculov, Phys. Lett. **B337**, 137 (1994) and Nucl. Phys. **B455**, 21 (1995);
A. Djouadi, M. Spira, and P.M. Zerwas, Z. Phys. **C70**, 427 (1996);
A. Frink *et al.*, Phys. Rev. **D54**, 4548 (1996);
K.G. Chetyrkin and M. Steinhauser, Phys. Lett. **B408**, 320 (1997);
R. Harlander and M. Steinhauser, Phys. Rev. **D56**, 3980 (1997);
A.L. Kataev, Sov. Phys. JETP Lett. **66**, 327 (1997);
S. Actis *et al.*, Nucl. Phys. **B811**, 182 (2009).
121. J. Erler and A. Freitas, *Electroweak Model and Constraints on New Physics*, in this volume.
122. R. Barate *et al.* [LEP Working Group for Higgs boson searches and ALEPH, DELPHI, L3, and OPAL Collaborations], Phys. Lett. **B565**, 61 (2003).
123. CDF and D0 Collaborations, Phys. Rev. **D88**, 052014 (2013).
124. ATLAS Collab., ATLAS-CONF-2017-045 (2017).
125. CMS Collab., CMS-PAS-HIG-16-041 (2017).

126. G. Aad *et al.* [ATLAS Collab.], Phys. Rev. **D90**, 112015 (2014).
127. S. Chatrchyan *et al.* [CMS Collab.], Eur. Phys. J. **C74**, 3076 (2014).
128. CMS Collab., CMS-PAS-HIG-16-040 (2016).
129. G. Aad *et al.* [ATLAS Collab.], Phys. Rev. **D91**, 012006 (2015).
130. S. Chatrchyan *et al.* [CMS Collab.], Phys. Rev. **D89**, 092007 (2014).
131. S. Chatrchyan *et al.* [CMS Collab.], JHEP **12**, 034 (2012).
132. ATLAS Collab., ATLAS-CONF-2017-043 (2017).
133. G. Aad *et al.* [Atlas and CMS Collaborations], Phys. Rev. Lett. **114**, 191803 (2015).
134. ATLAS Collab., ATLAS-CONF-2017-046 (2017).
135. ATLAS Collab., ATL-PHYS-PUB-2016-009 (2016).
136. G. Aad *et al.* [ATLAS Collab.], Phys. Rev. **D92**, 012006 (2015).
137. S. Chatrchyan *et al.* [CMS Collab.], JHEP **01**, 096 (2014).
138. G. Aad *et al.* [ATLAS Collab.], JHEP **08**, 137 (2015).
139. ATLAS Collab., ATLAS-CONF-2016-112 (2016).
140. CMS Collab., CMS-PAS-HIG-16-021 (2016).
141. S. Chatrchyan *et al.* [CMS Collab.], JHEP **05**, 104 (2014).
142. G. Aad *et al.* [ATLAS Collab.], JHEP **04**, 117 (2015).
143. ATLAS and CMS Collaborations, ATLAS-CONF-2015-044 and CMS-PAS-HIG-15-002 (2015).
144. CMS Collab., CERN-EP-2017-181 (2017).
145. T. Aaltonen *et al.* [CDF and D0 Collaborations], Phys. Rev. Lett. **109**, 071804 (2012).
146. J.M. Butterworth *et al.*, Phys. Rev. Lett. **100**, 242001 (2008).
147. S. Chatrchyan *et al.* [CMS Collab.], Phys. Rev. **D89**, 012003 (2014).
148. G. Aad *et al.* [ATLAS Collab.], JHEP **01**, 069 (2015).
149. ATLAS Collab., CERN-EP-2017-175 (2017).
150. CMS Collab., CERN-EP-2017-233 (2017).
151. LHCb Collab., LHCb-CONF-2016-006.
152. G. Aad *et al.* [ATLAS Collab.], JHEP **11**, 112 (2016).
153. S. Chatrchyan *et al.* [CMS Collab.], Phys. Rev. **D92**, 032008 (2015).
154. CMS Collab., CMS-PAS-HIG-16-003 (2016).
155. E. Gabrielli *et al.*, Nucl. Phys. **B781**, 64 (2007).
156. ATLAS Collab., ATLAS-CONF-2017-063 (2017).
157. CMS Collab., CERN-EP-2017-207 (2017).
158. M. Cacciari *et al.*JHEP **04**, 063 (2008).
159. ATLAS Collab., ATLAS-CONF-2015-060 (2015).
160. CMS Collab., CMS-PAS-HIG-15-005 (2016).
161. ATLAS Collab., ATLAS-CONF-2015-059 (2015).
162. CMS Collab., CMS-PAS-HIG-15-004 (2016).
163. ATLAS Collab., ATLAS-CONF-2015-069 (2015).
164. CMS Collab., CMS-PAS-HIG-15-003 (2016).
165. CMS Collab., CMS-PAS-HIG-16-003 (2016).
166. S. Chatrchyan *et al.* [CMS Collab.], JHEP **09**, 087 (2014).
167. G. Aad *et al.* [ATLAS Collab.], Phys. Lett. **B740**, 222 (2015).

168. G. Aad *et al.* [ATLAS Collab.], Phys. Lett. **B749**, 519 (2015).
169. ATLAS Collab., ATLAS-CONF-2017-076 (2017).
170. ATLAS Collab., ATLAS-CONF-2017-077 (2017).
171. CMS Collab., CMS-PAS-HIG-17-004 (2017).
172. CMS Collab., CMS-PAS-HIG-17-003 (2017).
173. CMS Collab., CMS-PAS-HIG-16-038 (2016).
174. CMS Collab., CMS-PAS-HIG-17-005 (2017).
175. CMS Collab., CMS-PAS-HIG-16-019 (2016).
176. ATLAS Collab., Phys. Lett. **B740**, 222 (2015).
177. ATLAS Collab., JHEP **129**, 010 (2017).
178. G. Aad *et al.* [ATLAS Collab.], JHEP **12**, 061 (2015).
179. CMS Collab., JHEP **02**, 079 (2017).
180. CMS Collab., CMS-PAS-TOP-2017-003 (2017).
181. G. Aad *et al.* [ATLAS Collab.], Phys. Rev. Lett. **114**, 081802 (2015).
182. G. Aad *et al.* [ATLAS Collab.], Phys. Rev. **D92**, 092004 (2015).
183. G. Aad *et al.* [ATLAS Collab.], Eur. Phys. J. **C75**, 412 (2015).
184. S. Chatrchyan *et al.* [CMS Collab.], Phys. Rev. **D90**, 112013 (2014).
185. S. Chatrchyan *et al.* [CMS Collab.], Phys. Lett. **B755**, 220 (2016).
186. S. Chatrchyan *et al.* [CMS Collab.], Phys. Lett. **B749**, 560 (2015).
187. ATLAS Collab., ATLAS-CONF-2016-004 (2016).
188. CMS Collab., CMS-PAS-HIG-2017-008 (2016).
189. ATLAS Collab., ATLAS-CONF-2016-049 (2016).
190. CMS Collab., CMS-PAS-HIG-16-026.
191. V. Khachatryan *et al.* [CMS Collab.], Phys. Lett. **B755**, 217 (2016).
192. CMS Collab., CERN-EP-2017-168.
193. ATLAS Collab., ATLAS-CONF-2016-071 (2016).
194. ATLAS Collab., ATL-PHYS-PUB-2017-001.
195. CMS Collab., CMS-PAS-FTR-15-002 (2015).
196. ATLAS Collab., ATL-PHYS-PUB-2014-019 (2014).
197. S. Chatrchyan *et al.* CMS Collab.], Phys. Lett. **B726**, 587 (2013).
198. G. Aad *et al.* [ATLAS Collab.], Phys. Lett. **B753**, 341 (2016).
199. ATLAS Collab., CERN-EP-2017-095 (2017).
200. G. Aad *et al.* [ATLAS Collab.], Phys. Lett. **B738**, 68 (2014).
201. S. Chatrchyan *et al.* [CMS Collab.], Phys. Lett. **B744**, 184 (2015).
202. G. Aad *et al.* [ATLAS Collab.], Phys. Rev. Lett. **119**, 051802 (2017).
203. S. Chatrchyan *et al.* [CMS Collab.], Phys. Lett. **B749**, 137 (2015).
204. G. Aad *et al.* [ATLAS Collab.], JHEP **1511**, 211 (2015).
205. G. Aad *et al.* [ATLAS Collab.], CERN-EP-2016-055(2016).
206. CMS Collab., CMS-PAS-HIG-17-001 (2017).
207. S. Chatrchyan *et al.* [CMS Collab.], Phys. Lett. **B763C**, 472 (2016).
208. R. Harnik *et al.*, JHEP **03**, 026 (2013).
209. C. Delaunay *et al.*, Phys. Rev. **D89**, 033014 (2014).
210. G. T. Bodwin *et al.*, Phys. Rev. **D88**, 053003 (2013).
211. G. Aad *et al.* [ATLAS Collab.], Phys. Rev. Lett. **114**, 121801 (2015).

212. ATLAS Collab., CERN-EP-2016-130 (2016).
213. A. Djouadi *et al.*, Eur. Phys. J. **C73**, 2455 (2013).
214. G. Aad *et al.* [ATLAS Collab.], Eur. Phys. J. **C75**, 337 (2015).
215. G. Aad *et al.* [ATLAS Collab.], Phys. Rev. Lett. **112**, 201802 (2014).
216. G. Aad *et al.* [ATLAS Collab.], JHEP **01**, 172 (2016).
217. G. Aad *et al.* [ATLAS Collab.], JHEP **11**, 206 (2015).
218. S. Chatrchyan *et al.* [CMS Collab.], Eur. Phys. J. **C74**, 2980 (2014).
219. S. Chatrchyan *et al.* [CMS Collab.], CMS-PAS-HIG-15-012 (2015).
220. S. Chatrchyan *et al.* [CMS Collab.], CMS-PAS-HIG-16-009 (2016).
221. S. Chatrchyan *et al.* [CMS Collab.], CMS-PAS-HIG-16-008 (2016).
222. S. Chatrchyan *et al.* [CMS Collab.], JHEP **02**, 135 (2017).
223. A. Djouadi *et al.*, Eur. Phys. J. **C73**, 2455 (2013).
224. M.J. Strassler and K.M. Zurek, Phys. Lett. **B651**, 374 (2007).
225. M.J. Strassler and K.M. Zurek, Phys. Lett. **B661**, 263 (2008).
226. T. Han *et al.*, JHEP **0807**, 008 (2008).
227. A. Falkowski *et al.*, JHEP **1005**, 077 (2010) and Phys. Rev. Lett. **105**, 241801 (2010).
228. G. Aad *et al.* [ATLAS Collab.], New J. Phys. **15**, 043009 (2013).
229. G. Aad *et al.* [ATLAS Collab.], Phys. Lett. **B721**, 32 (2013).
230. G. Aad *et al.* [ATLAS Collab.], Phys. Rev. Lett. **108**, 251801 (2012).
231. D. Tucker-Smith and N. Weiner, Phys. Rev. **D64**, 043502 (2001).
232. S. Chatrchyan *et al.* [CMS Collab.], Phys. Lett. **B726**, 564 (2013).
233. M. Carena, C. Grojean, M. Kado, and V. Sharma, *Status of Higgs boson physics*, in Review of Particle Physics, Chin. Phys. **C40** 100001 (2016).
234. G. Aad *et al.* [ATLAS Collab.], Eur. Phys. J. **C76**, 6 (2016).
235. S. Chatrchyan *et al.* [CMS Collab.], Eur. Phys. J. **C75**, 212 (2015).
236. L.D. Landau, Dokl. Akad. Nauk Ser. Fiz. **60**, 207 (1948);
C.N. Yang, Phys. Rev. **D77**, 242 (1950).
237. G. Aad *et al.* [ATLAS Collab.], Eur. Phys. J. **C75**, 476 (2015).
238. V. Khachatryan *et al.* [CMS Collab.], Phys. Rev. **D92**, 012004 (2015).
239. ATLAS Collab., Phys. Lett. **B726**, 120 (2013).
240. P. Artoisenet *et al.*, JHEP **1311**, 043 (2013);
A. Alloul, B. Fuks, and V. Sanz, JHEP **1404**, 110 (2014);
A. Falkowski *et al.*, Eur. Phys. J. **C75**, 583 (2015).
241. J. Ellis *et al.*, JHEP **1211**, 134 (2012).
242. D0 Collab., Note 6387-CONF (2013).
243. D0 Collab., Note 6406-CONF (2013).
244. A. De Rujula *et al.*, Phys. Rev. **D82**, 013003 (2010).
245. CMS Collab., CERN-EP-2017-143 (2017).
246. ATLAS Collab., Eur. Phys. J. **C75**, 335 (2015).
247. V. Khachatryan *et al.* [CMS Collab.], Phys. Rev. **D92**, 072010 (2015).
248. V. Khachatryan *et al.* [CMS Collab.], CERN-EP-2016-054 (2016).
249. G. Aad *et al.* [ATLAS Collab.], Phys. Rev. **D90**, 052004 (2014).

250. L. Dixon and S. Siu, Phys. Rev. Lett. **90**, 252001 (2003);
S. P. Martin, Phys. Rev. **D86**, 073016 (2012);
L. Dixon and Y. Li, Phys. Rev. Lett. **111**, 111802 (2013).
251. ATLAS Collab., ATL-PHYS-PUB-2013-014 (2013).
252. J. Campbell, M. Carena, R. Harnik, and Z. Liu. arXiv:1704.08259 [hep-ph], Phys. Rev. Lett. to appear.
253. ATLAS Collab., ATL-PHYS-PUB-2014-016 (2014).
254. N. Kauer and G. Passarino, JHEP **08**, 116 (2012);
F. Caola and K. Melnikov, Phys. Rev. **D88**, 054024 (2013);
J.M. Campbell, R.K. Ellis, and C. Williams, JHEP **04**, 060 (2014);
J.M. Campbell, R.K. Ellis, and C. Williams, Phys. Rev. **D89**, 053011 (2014);
C. Englert and M. Spannowsky, Phys. Rev. **D90**, 053003 (2014).
255. ATLAS Collab., ATL-PHYS-PUB-2015-024 (2015).
256. A. David *et al.* [LHC Higgs Cross Section Working Group], `arXiv:1209.0040 [hep-ph]` (2012).
257. M. Gonzalez-Alonso *et al.*, Eur. Phys. J. **C75**, 128 (2015);
A. Greljo *et al.*, Eur. Phys. J. **C76**, 158 (2016).
258. G. Buchalla, O. Cata and C. Krause, Nucl. Phys. **B880**, 552 (2014);
I. Brivio *et al.*, JHEP **1403**, 014 (2014).
259. W. Buchmuller and D. Wyler, Nucl. Phys. **B268**, 621 (1986).
260. C.J. C. Burges and H.J. Schnitzer, Nucl. Phys. **B288**, 464 (1983);
C.N. Leung, S.T. Love and S. Rao, Z. Phys. **C31**, 433 (1986).
261. B. Grzadkowski *et al.*, JHEP **1010**, 085 (2010).
262. L. Lehman and A. Martin, JHEP **1602**, 081 (2016);
B. Henning *et al.*, JHEP **1708**, 016 (2017).
263. R. Alonso *et al.*, JHEP **1404**, 159 (2014).
264. G.F. Giudice *et al.*, JHEP **0706**, 045 (2007).
265. R. Contino *et al.*, JHEP **1307**, 035 (2013).
266. J. Elias-Miro *et al.*, JHEP **1311**, 066 (2013);
R.S. Gupta, A. Pomarol and F. Riva, Phys. Rev. **D91**, 035001 (2015);
E. Masso, JHEP **1410**, 128 (2014).
267. A. Falkowski and F. Riva, JHEP **1502**, 039 (2015).
268. A. Falkowski *et al.*, Phys. Rev. Lett. **116**, 011801 (2016).
269. C. Degrande *et al.*, JHEP **1207**, 036 (2012);
J.F. Kamenik, M. Papucci, and A. Weiler, Phys. Rev. **D85**, 071501 (2012).
270. B.A. Kniehl and M. Spira, Z. Phys. **C69**, 77 (1995).
271. G. Isidori, A.V. Manohar, and M. Trott, Phys. Lett. **B728**, 131 (2014);
G. Isidori and M. Trott, JHEP **1402**, 082 (2014).
272. A. Pomarol and F. Riva, JHEP **1401**, 151 (2014).
273. R. Godbole *et al.*, Phys. Lett. **B730**, 275 (2014).
274. M. Reece, New J. Phys. **15**, 043003 (2013).
275. S. Biswas, E. Gabrielli, and B. Mele, JHEP **1301**, 088 (2013);
S. Biswas *et al.*, JHEP **07**, 073 (2013).
276. M. Farina *et al.*, JHEP **1305**, 022 (2013).

277. ATLAS Collab., JHEP **11**, 206 (2015).
278. ATLAS Collab., ATLAS-CONF-2013-072 (2013).
279. ATLAS Collab., Phys. Lett. **B753**, 69 (2016).
280. L.E. Ibanez and G.G. Ross, Phys. Lett. **B110**, 215 (1982);
L.E. Ibanez, Phys. Lett. **B118**, 73 (1982);
J. Ellis, D.V. Nanopoulos, and K. Tamvakis, Phys. Lett. **B121**, 123 (1983);
L. Alvarez-Gaume, J. Polchinski, and M.B. Wise, Nucl. Phys. **B221**, 495 (1983).
281. See the list of references in the corresponding section of the 2014 edition of this review.
282. ATLAS Collab., `twiki.cern.ch/twiki/bin/view/AtlasPublic/Publications`;
CMS Collab., `cms-results.web.cern.ch/cms-results/public-results/publications/SUS/STOP.html`.
283. See the list of references in the corresponding section of the 2016 edition of this review.
284. J. Mrazek *et al.*, Nucl. Phys. **B853**, 1 (2011).
285. D.B. Kaplan, Nucl. Phys. **B365**, 259 (1991).
286. G. Panico *et al.*, JHEP **1303**, 051 (2013).
287. H.E. Haber, *Supersymmetry*, in this volume.
288. A. Djouadi, Phys. Reports **459**, 1 (2008).
289. S. Heinemeyer *et al.*, Phys. Reports **425**, 265 (2006).
290. P. Draper, G. Lee and C.E.M. Wagner, Phys. Rev. **D89**, 055023 (2014).
291. J.F. Gunion and H.E. Haber, Phys. Rev. **D67**, 075019 (2003).
292. H.E. Haber and Y. Nir, Nucl. Phys. **B335**, 363 (1990);
A. Dabelstein, Nucl. Phys. **B456**, 25 (1995);
S. Heinemeyer, W. Hollik, and G. Weiglein, Eur. Phys. J. **C16**, 139 (2000);
A. Dobado, M. J. Herrero, and S. Penaranda, Eur. Phys. J. **C17**, 487 (2000).
293. T.D. Lee, Phys. Rev. **D8**, 1226 (1973);
P. Fayet, Nucl. Phys. **B78**, 14 (1974);
R.D. Peccei and H.R. Quinn, Phys. Rev. Lett. **38**, 1440 (1977);
P. Fayet and S. Ferrara, Phys. Reports **32**, 249 (1977);
L.J. Hall and M.B. Wise, Nucl. Phys. **B187**, 397 (1981);
V.D. Barger, J.L. Hewett, and R.J.N. Phillips, Phys. Rev. **D41**, 3421 (1990).
294. M. Carena *et al.*, JHEP **1203**, 014 (2012);
M. Carena *et al.*, JHEP **1207**, 175 (2012).
295. M. Carena, S. Mrenna, and C.E.M. Wagner, Phys. Rev. **D60**, 075010 (1999) and Phys. Rev. **D62**, 055008 (2000).
296. A. Dabelstein, Nucl. Phys. **B456**, 25 (1995);
F. Borzumati *et al.*, Nucl. Phys. **B555**, 53 (1999);
H. Eberl *et al.*, Phys. Rev. **D62**, 055006 (2000).
297. J.A. Coarasa, R.A. Jimenez, and J. Sola, Phys. Lett. **B389**, 312 (1996);
R.A. Jimenez and J. Sola, Phys. Lett. **B389**, 53 (1996);
A. Bartl *et al.*, Phys. Lett. **B378**, 167 (1996).
298. S. Heinemeyer, W. Hollik, and G. Weiglein, Eur. Phys. J. **C16**, 139 (2000).
299. H. E. Haber *et al.*, Phys. Rev. **D63**, 055004 (2001).

300. L. Hall, R. Rattazzi, and U. Sarid, Phys. Rev. **D50**, 7048 (1994); R. Hempfling, Phys. Rev. **D49**, 6168 (1994).
301. M.S. Carena *et al.*, Nucl. Phys. **B426**, 269 (1994).
302. J. Guasch, P. Hafliger, and M. Spira, Phys. Rev. **D68**, 115001 (2003); D. Noth and M. Spira, Phys. Rev. Lett. **101**, 181801 (2008) and JHEP **1106**, 084 (2011); L. Mihaila and C. Reisser, JHEP **1008**, 021 (2010).
303. M.S. Carena *et al.*, Phys. Lett. **B499**, 141 (2001).
304. A. Djouadi, J. Kalinowski, and P.M. Zerwas, Z. Phys. **C57**, 569 (1993); H. Baer *et al.*, Phys. Rev. **D47**, 1062 (1993); A. Djouadi *et al.*, Phys. Lett. **B376**, 220 (1996); A. Djouadi *et al.*, Z. Phys. **C74**, 93 (1997); S. Heinemeyer and W. Hollik, Nucl. Phys. **B474**, 32 (1996).
305. J.F. Gunion, Phys. Rev. Lett. **72**, 199 (1994); D. Choudhury and D.P. Roy, Phys. Lett. **B322**, 368 (1994); O.J. Eboli and D. Zeppenfeld, Phys. Lett. **B495**, 147 (2000); B.P. Kersevan, M. Malawski, and E. Richter-Was, Eur. Phys. J. **C29**, 541 (2003).
306. E.L. Berger *et al.*, Phys. Rev. **D66**, 095001 (2002).
307. A. Brignole *et al.*, Nucl. Phys. **B643**, 79 (2002); R. Dermisek and I. Low, Phys. Rev. **D77**, 035012 (2008).
308. A. Djouadi, Phys. Lett. **B435**, 101 (1998).
309. M.R. Buckley and D. Hooper, Phys. Rev. **D86**, 075008 (2012); for other references, see the 2014 edition of this review.
310. J.J. Cao *et al.*, JHEP **1203**, 086 (2012); R. Benbrik *et al.*, Eur. Phys. J. **C72**, 2171 (2012); Z. Kang, J. Li, and T. Li, JHEP **1211**, 024 (2012); J.F. Gunion, Y. Jiang, and S. Kraml, Phys. Lett. **B710**, 454 (2012); U. Ellwanger, JHEP **1203**, 044 (2012).
311. T. Kitahara, JHEP **1211**, 021 (2012); M. Carena *et al.*, JHEP **1302**, 114 (2013).
312. B. Batell, S. Jung, and C.E.M. Wagner, JHEP **1312**, 075 (2013).
313. C. Balazs, H.-J. He, and C.P. Yuan, Phys. Rev. **D60**, 114001 (1999).
314. G. Lee, and C.E.M. Wagner Phys. Rev. **D92**, 075032 (2015).
315. D. Dicus *et al.*, Phys. Rev. **D59**, 094016 (1999).
316. M. Carena *et al.*, Eur. Phys. J. **C45**, 797 (2006).
317. E. Boos *et al.*, Phys. Rev. **D66**, 055004 (2002); E. Boos, A. Djouadi, and A. Nikitenko, Phys. Lett. **B578**, 384 (2004); E. Boos *et al.*, Phys. Lett. **B622**, 311 (2005); M. Carena *et al.*, JHEP **1207**, 091 (2012).
318. A.A. Barrientos Bendezu and B.A. Kniehl, Phys. Rev. **D64**, 035006 (2001).
319. R.M. Barnett, H.E. Haber, and D.E. Soper, Nucl. Phys. **B306**, 697 (1988); for other references, see the 2014 edition of this review.

320. A. Djouadi, J. Ellis and J. Quevillon, JHEP **07**, 105 (2016) arXiv:1605.00542 [hep-ph](2016);
M Carena and Zhen Liu, JHEP **11**, 159 (2016).
321. M. Carena *et al.*, Eur. Phys. J. **C26**, 601 (2003);
M. Carena *et al.*, Eur. Phys. J. **C73**, 2552 (2013).
322. L. Maiani, A. D. Polosa and V. Riquer, New J. Phys. **14**, 073029 (2012) and Phys. Lett. **B718**, 465 (2012);
A. Djouadi and J. Quevillon, JHEP **1310**, 028 (2013);
A. Djouadi *et al.*, Eur. Phys. J. **C73**, 2650 (2013).
323. M. Carena *et al.*, Phys. Rev. **D91**, 035003 (2015).
324. M. Carena *et al.*, JHEP **1404**, 015 (2014).
325. K. Blum, R.T. D'Agnolo, and J. Fan, JHEP **1301**, 057 (2013);
A. Azatov *et al.*, Phys. Rev. **D86**, 075033 (2012);
J.R. Espinosa *et al.*, JHEP **1212**, 077 (2012);
R.S. Gupta, M. Montull, and F. Riva, JHEP **1304**, 132 (2013);
R.T. D'Agnolo, PhD thesis, Scuola Normale Superiore, Pisa, 2013.
326. A. Djouadi *et al.*, JHEP **1506**, 168 (2015).
327. G. D'Ambrosio *et al.*, Nucl. Phys. **B645**, 155 (2002);
R.S. Chivukula and H. Georgi, Phys. Lett. **B188**, 99 (1987);
L.J. Hall and L. Randall, Phys. Rev. Lett. **65**, 2939 (1990);
A.J. Buras *et al.*, Phys. Lett. **B500**, 161 (2001).
328. L.J. Hall, J. Lykken, and S. Weinberg, Phys. Rev. **D27**, 2359 (1983);
J.E. Kim and H.P. Nilles, Phys. Lett. **B138**, 150 (1984);
G.F. Giudice and A. Masiero, Phys. Lett. **B206**, 480 (1988);
E.J. Chun, J.E. Kim, and H.P. Nilles, Nucl. Phys. **B370**, 105 (1992);
I. Antoniadis *et al.*, Nucl. Phys. **B432**, 187 (1994).
329. P. Fayet, Phys. Lett. **B90**, 104 (1975).
330. C. Panagiotakopoulos and K. Tamvakis, Phys. Lett. **B469**, 145 (1999);
A. Dedes *et al.*, Phys. Rev. **D63**, 055009 (2001);
A. Menon, D. Morrissey, and C.E.M. Wagner, Phys. Rev. **D70**, 035005 (2004).
331. M. Cvetic *et al.*, Phys. Rev. **D56**, 2861 (1997) [E: **D58**, 119905 (1998)];
P. Langacker and J. Wang, Phys. Rev. **D58**, 115010 (1998) and references therein.
332. J. Erler, P. Langacker, and T.J. Li, Phys. Rev. **D66**, 015002 (2002);
T. Han, P. Langacker and B. McElrath, Phys. Rev. **D70**, 115006 (2004);
V. Barger *et al.*, Phys. Rev. **D73**, 115010 (2006).
333. V. Barger *et al.*, Phys. Rev. **D73**, 115010 (2006);
V. Barger, P. Langacker, and G. Shaughnessy, Phys. Rev. **D75**, 055013 (2007).
334. E. Accomando, *et al.*, hep-ph/0608079 (2006).
335. B.A. Dobrescu, G.L. Landsberg, and K.T. Matchev, Phys. Rev. **D63**, 075003 (2001).
336. R. Dermisek and J. F. Gunion, Phys. Rev. Lett. **95**, 041801 (2005).
337. O.J.P. Eboli and D. Zeppenfeld, Phys. Lett. **B495**, 147 (2000);
H. Davoudiasl, T. Han, and H.E. Logan, Phys. Rev. **D71**, 115007 (2005).

338. L. Wang and X.F. Han, Phys. Rev. **D87**, 015015 (2013);
K. Schmidt-Hoberg and F. Staub JHEP **1210**, 195 (2012);
H. An, T. Liu, and L.T. Wang, Phys. Rev. **D86**, 075030 (2012);
D.A. Vasquez *et al.*, Phys. Rev. **D86**, 035023 (2012);
S.F. King, M. Muhlleitner, and R. Nevzorov, Nucl. Phys. **B860**, 207 (2012).
339. N.D. Christensen, T. Han, Z. Liu and S. Su, JHEP **1308**, 019 (2013);
T. Han, Z. Liu and S. Su, JHEP **1408**, 093 (2014);
S.F. King *et al.*, Phys. Rev. **D90**, 095014 (2014);
N.E. Bomark *et al.*, JHEP **1502**, 044 (2015);
P. Athron *et al.*, JHEP **1501**, 153 (2015);
N.E. Bomark, S. Moretti and L. Roszkowski, J. Phys. **G43**, 105003 (2016);
T. Li and S. Su, JHEP **1511**, 068 (2015);
G. Belanger *et al.*, JHEP **1509**, 151 (2015);
J. Baglio *et al.*, JHEP **1510**, 024 (2015);
M. Guchait and J. Kumar, Int. J. Mod. Phys. **A31**, 1650069 (2016);
D. Barducci *et al.*, JHEP **1601**, 050 (2016);
M. Carena *et al.*, Phys. Rev. **D93**, 035013 (2016);
P. Bandyopadhyay, K. Huitu and S. Niyogi, JHEP **1607**, 015 (2016);
U. Ellwanger and M. Rodriguez-Vazquez, JHEP **1602**, 096 (2016);
R. Costa *et al.*, JHEP **1606**, 034 (2016);
E. Conte *et al.*, JHEP **1605**, 100 (2016).
340. LHC Higgs Cross Section Working Group, Beyond the Standard Model Higgs – NMSSM
`twiki.cern.ch/twiki/bin/view/LHCPhysics/LHCHXSWGNMSSM`.
341. M. Carena *et al.*, Phys. Rev. **D93**, 035013 (2016).
342. Courtesy of Marcin Barziak based on the public code NMSSMTools,
`www.th.u-psud.fr/NMHDECAY/nmssmtools.html`.
343. P. Batra *et al.*, JHEP **0402**, 043 (2004).
344. P. Batra *et al.*, JHEP **0406**, 032 (2004);
A. Maloney, A. Pierce, and J.G. Wacker, JHEP **0606**, 034 (2006);
Y. Zhang *et al.*, Phys. Rev. **D78**, 011302 (2008);
C.W. Chiang *et al.*, Phys. Rev. **D81**, 015006 (2010);
A.D. Medina, N.R. Shah, and C.E.M. Wagner, Phys. Rev. **D80**, 015001 (2009);
M. Endo *et al.*, Phys. Rev. **D85**, 095006 (2012);
C. Cheung and H.L. Roberts, JHEP **1312**, 018 (2013).
345. R. Huo *et al.*, Phys. Rev. **D87**, 055011 (2013).
346. S. Dimopoulos and S. Thomas, Nucl. Phys. **B465**, 23 (1996);
S. Thomas, Int. J. Mod. Phys. **A13**, 2307 (1998).
347. A. Pilaftsis and C.E.M. Wagner, Nucl. Phys. **B553**, 3 (1999).
348. S.Y. Choi, M. Drees, and J.S. Lee, Phys. Lett. **B481**, 57 (2000);
M. Carena *et al.*, Nucl. Phys. **B625**, 345 (2002).
349. M.S. Carena *et al.*, Nucl. Phys. **B586**, 92 (2000).
350. A. Pilaftsis, Phys. Rev. **D58**, 096010 (1998) and Phys. Lett. **B435**, 88 (1998);
K.S. Babu *et al.*, Phys. Rev. **D59**, 016004 (1999).

351. G.L. Kane and L.T. Wang, Phys. Lett. **B488**, 383 (2000);
S.Y. Choi, M. Drees, and J.S. Lee, Phys. Lett. **B481**, 57 (2000);
S.Y. Choi and J.S. Lee, Phys. Rev. **D61**, 015003 (2000);
S.Y. Choi, K. Hagiwara, and J.S. Lee, Phys. Rev. **D64**, 032004 (2001) and Phys. Lett. **B529**, 212 (2002);
T. Ibrahim and P. Nath, Phys. Rev. **D63**, 035009 (2001);
T. Ibrahim, Phys. Rev. **D64**, 035009 (2001);
S. Heinemeyer, Eur. Phys. J. **C22**, 521 (2001);
S.W. Ham *et al.*, Phys. Rev. **D68**, 055003 (2003).
352. M. Frank *et al.*, JHEP **0702**, 047 (2007);
S. Heinemeyer *et al.*, Phys. Lett. **B652**, 300 (2007);
T. Hahn *et al.*, `arXiv:0710.4891` (2007).
353. D.A. Demir, Phys. Rev. **D60**, 055006 (1999);
S.Y. Choi, M. Drees, and J.S. Lee, Phys. Lett. **B481**, 57 (2000);
K. E. Williams, H. Rzehak, and G. Weiglein, Eur. Phys. J. **C71**, 1669 (2011).
354. E. Christova *et al.*, Nucl. Phys. **B639**, 263 (2002) [E: Nucl. Phys. **B647**, 359 (2002)].
355. M.D. Goodsell and F. Staub, `arXiv:1604.05335 [hep-ph]` (2016);
A. Chakraborty *et al.*, Phys. Rev. **D90**, 055005 (2014);
M. Carena *et al.*, JHEP **1602**, 123 (2016).
356. J.F. Gunion and H.E. Haber, Phys. Rev. **D67**, 075019 (2003);
G.C. Branco *et al.*, Phys. Reports **516**, 1 (2012).
357. S.L. Glashow and S. Weinberg, Phys. Rev. **D15**, 1958 (1977);
E.A. Paschos, Phys. Rev. **D15**, 1966 (1977);
H. Georgi, Hadronic J. **1,** 1227 (1978);
H. Haber, G. Kane, and T. Sterling, Nucl. Phys. **B161**, 493 (1979);
A.G. Akeroyd, Phys. Lett. **B368**, 89 (1996);
A.G. Akeroyd, Nucl. Phys. **B544**, 557 (1999);
A.G. Akeroyd, A. Arhrib, and E. Naimi, Eur. Phys. J. **C20**, 51 (2001).
358. N.G. Deshpande and E. Ma, Phys. Rev. **D18**, 2574 (1978);
R. Barbieri, L.J. Hall, and V. Rychkov, Phys. Rev. **D74**, 015007 (2006);
L. Lopez Honorez *et al.*, JCAP **0702**, 028 (2007);
E. Lundstrom, M. Gustafsson, and J. Edsjo, Phys. Rev. **D79**, 035013 (2009);
E. Dolle *et al.*, Phys. Rev. **D8**, 035003 (2010);
X. Miao, S. Su, and B. Thomas, Phys. Rev. **D82**, 035009 (2010);
L. Lopez-Honorez and C. Yaguna, JCAP **1101**, 002 (2011).
359. A. Arhrib, R. Benbrik, and N. Gaur, Phys. Rev. **D85**, 095021 (2012);
B. Swiezewska and M. Krawczyk, Phys. Rev. **D88**, 035019 (2013);
A. Goudelis, B. Herrmann, and O. Stal, JHEP **1309**, 106 (2013).
360. M. Bauer, M. Carena and K. Gemmler, JHEP **1511**, 016 (2015) and Phys. Rev. **D94**, 115030 (2016).
361. C. Froggatt and H. B. Nielsen Nucl. Phys. **B147**, 277 (1979).
362. K. Babu and S. Nandi, Phys. Rev. **D62**, 033002 (2000);
G. F. Giudice and O. Lebedev, Phys. Lett. **B665**, 79 (2008).

363. V. Barger, H.E. Logan, and G. Shaughnessy, Phys. Rev. **D79**, 115018 (2009).
364. D. O'Connell, M.J. Ramsey-Musolf, and M.B. Wise, Phys. Rev. **D75**, 037701 (2007);
V. Barger *et al.*, Phys. Rev. **D77**, 035005 (2008);
V. Barger *et al.*, Phys. Rev. **D79**, 015018 (2009);
T. Robens, and T. Stefaniak, Eur. Phys. J. **C75**, 104 (2015).
365. H.E. Haber, *Proceedings of the 1990 Theoretical Advanced Study Institute in Elementary Particle Physics,* edited by M. Cvetič and Paul Langacker (World Scientific, Singapore, 1991) pp. 340–475 and references therein.
366. S. Glashow and S. Weinberg, Phys. Rev. **D15**, 1958 (1977).
367. G.C. Branco, W. Grimus, and L. Lavoura, Phys. Lett. **B380**, 119 (1996);
F.J. Botella, G.C. Branco, M.N. Rebelo Phys. Lett. **B687**, 194 (2010).
368. N. Craig and S. Thomas, JHEP **1211**, 083 (2012).
369. G.C. Branco *et al.*, Phys. Reports **516**, 1 (2012).
370. C.Y. Chen, S. Dawson, and M. Sher, Phys. Rev. **D88**, 015018 (2013).
371. B. Swiezewska and M. Krawczyk, Phys. Rev. **D88**, 035019 (2013).
372. B. Coleppa, F. Kling and S. Su, JHEP **1409**, 161 (2014);
J. Cao *et al.*, JHEP **1412**, 026 (2014);
B. Coleppa, F. Kling and S. Su, JHEP **1412**, 148 (2014);
D. Curtin, R. Essig and Y.M. Zhong, JHEP **1506**, 025 (2015);
F. Kling, A. Pyarelal and S. Su, JHEP **1511**, 051 (2015);
J. Hajer *et al.*, JHEP **1511**, 124 (2015);
W. Bernreuther *et al.*, Phys. Rev. **D93**, 034032 (2016);
S. Gori *et al.*, Phys. Rev. **D93**, 075038 (2016);
F. Kling, J.M. No and S. Su, JHEP **1609**, 093 (2016);
N. Craig *et al.*, JHEP **1701**, 018 (2017).
373. N. Craig *et al.*,JHEP **1506**, 137 (2015);
J. Hajer *et al.*, Y. Y. Li, T. Liu and J. F. H. Shiu, JHEP **1511**, 124 (2015).
374. J. Schechter and J. W. F. Valle, Phys. Rev. **D22**, 2227 (1980).
375. T.P. Cheng and L.F. Li, Phys. Rev. **D22**, 2860 (1980).
376. H. Georgi and M. Machacek, Nucl. Phys. **B262**, 463 (1985).
377. M.S. Chanowitz and M. Golden, Phys. Lett. **B165**, 105 (1985).
378. J.F. Gunion, R. Vega, and J. Wudka, Phys. Rev. **D42**, 1673 (1990).
379. H.E. Logan and M.A. Roy, Phys. Rev. **D82**, 115011 (2010).
380. H.E. Haber and H.E. Logan, Phys. Rev. **D62**, 015011 (2000).
381. A.G. Akeroyd, M. Aoki, and H. Sugiyama, Phys. Rev. **D77**, 075010 (2008).
382. P. Nath *et al.*, Nucl. Phys. (Proc. Supp.) **B200**, 185 (2010).
383. J. Garayoa and T. Schwetz, JHEP **0803**, 009 (2008).
384. J.F. Gunion, R. Vega, and J. Wudka, Phys. Rev. **D43**, 2322 (1991).
385. S. Kanemura and K. Yagyu, Phys. Rev. **D85**, 115009 (2012).
386. I. Low and J. Lykken, JHEP **1010**, 053 (2010).
387. C. Englert, E. Re, and M. Spannowsky, Phys. Rev. **D87**, 095014 (2013).
388. I. Low, J. Lykken, and G. Shaughnessy, Phys. Rev. **D86**, 093012 (2012).
389. A. Falkowski, S. Rychkov, and A. Urbano, JHEP **1204**, 073 (2012).

390. B.A. Dobrescu and J.D. Lykken, JHEP **1302**, 073 (2013).
391. D. Carmi *et al.*, JHEP **1210**, 196 (2012).
392. C.W. Chiang and K. Yagyu, JHEP **1301**, 026 (2013).
393. G. Belanger *et al.*, Phys. Rev. **D88**, 075008 (2013).
394. C. Englert, E. Re, and M. Spannowsky, Phys. Rev. **D88**, 035024 (2013).
395. B. Bellazzini, C. Csaki and J. Serra, Eur. Phys. J. **C74**, 2766 (2014).
396. N. Arkani-Hamed *et al.*, JHEP **0207**, 034 (2002).
397. N. Arkani-Hamed, A.G. Cohen, and H. Georgi, Phys. Lett. **B513**, 232 (2001).
398. N. Arkani-Hamed *et al.*, JHEP **0208**, 021 (2002).
399. M. Schmaltz, JHEP **0408**, 056 (2004).
400. M. Schmaltz, D. Stolarski, and J. Thaler, JHEP **1009**, 018 (2010).
401. M. Perelstein, Prog. in Part. Nucl. Phys. **58**, 247 (2007).
402. M. Schmaltz and D. Tucker-Smith, Ann. Rev. Nucl. and Part. Sci. **55**, 229 (2005).
403. J.A. Casas, J.R. Espinosa, and I. Hidalgo, JHEP **0503**, 038 (2005).
404. H.C. Cheng and I. Low, JHEP **0309**, 051 (2003).
405. M.S. Carena *et al.*, Phys. Rev. **D75**, 091701 (2007).
406. ATLAS Collab., ATLAS-CONF-2012-147, ATLAS-CONF-2012-109 and ATLAS-CONF-2013-024 (2012);
CMS Collab., CMS-PAS-EXO-12-048 and CMS-SUS-12-028 (2012).
407. CMS Collab., CERN-EP/2016-279 (2016);
ATLAS Collab., JHEP **1708**, 052 (2017), CERN-EP-2017-094 (2017) and ATLAS-CONF-2017-104 (2017).
408. R.S. Chivukula, M. Narain, and J. Womersley, *Dynamical Electroweak Symmetry Breaking*, in this volume.
409. H. Georgi, A.E. Nelson, and A. Manohar, Phys. Lett. **B126**, 169 (1983);
A.E. Nelson and M.J. Strassler, JHEP **0009**, 030 (2000);
S. Davidson, G. Isidori, and S. Uhlig, Phys. Lett. **B663**, 73 (2008).
410. C. Csaki, A. Falkowski, and A. Weiler, JHEP **0809**, 008 (2008);
B. Keren-Zur *et al.*, Nucl. Phys. **B867**, 429 (2013).
411. K. Agashe, R. Contino, and A. Pomarol, Nucl. Phys. **B719**, 165 (2005).
412. O. Matsedonskyi, G. Panico, and A. Wulzer, JHEP **1301**, 164 (2013);
M. Redi and A. Tesi, JHEP **1210**, 166 (2012);
D. Marzocca, M. Serone, and J. Shu, JHEP **1208**, 013 (2012);
A. Pomarol and F. Riva, JHEP **1208**, 135 (2012).
413. R. Contino and G. Servant, JHEP **0806**, 026 (2008);
J. Mrazek and A. Wulzer, Phys. Rev. **D81**, 075006 (2010).
414. A. De Simone *et al.*, JHEP **1304**, 004 (2013);
A. Azatov *et al.*, Phys. Rev. **D89**, 075001 (2014).
415. A. Falkowski, Phys. Rev. **D77**, 055018 (2008);
I. Low and A. Vichi, Phys. Rev. **D84**, 045019 (2011);
A. Azatov and J. Galloway, Phys. Rev. **D85**, 055013 (2012);
C. Delaunay, C. Grojean, and G. Perez, JHEP **1309**, 090 (2013).
416. R.K. Ellis *et al.*, Nucl. Phys. **B297**, 221 (1988);
U. Baur and E.W.N. Glover, Nucl. Phys. **B339**, 38 (1990);

O. Brein and W. Hollik, Phys. Rev. **D68**, 095006 (2003);
U. Langenegger *et al.*, JHEP **0606**, 035 (2006).
417. A. Banfi, A. Martin, and V. Sanz, JHEP **1408**, 053 (2014);
A. Azatov and A. Paul, JHEP **1401**, 014 (2014);
C. Grojean *et al.*, JHEP **1405**, 022 (2014);
M. Schlaffer *et al.*, Eur. Phys. J. **C74**, 3120 (2014);
M. Buschmann *et al.*, Phys. Rev. **D90**, 013010 (2014);
M. Buschmann *et al.*, JHEP **1502**, 038 (2015);
U. Langenegger, M. Spira and I. Strebel, `arXiv:1507.01373 [hep-ph]` (2015);
M. Grazzini *et al.*, JHEP **1703**, 115 (2017).
418. A. Azatov *et al.*, J. Exp. Theor. Phys. **120**, 354 (2015).
419. A. Azatov *et al.*, Phys. Rev. **D92**, 035001 (2015).
420. R. Contino, L. Da Rold, and A. Pomarol, Phys. Rev. **D75**, 055014 (2007).
421. D. Pappadopulo, A. Thamm, and R. Torre, JHEP **1307**, 058 (2013);
M. Montull *et al.*, Phys. Rev. **D88**, 095006 (2013).
422. M. Carena, L. Da Rold, E Pontón JHEP **1406**, 159 (2014);
D. Liu, I. Low and C. E. M. Wagner Phys. Rev. **D96**, 035013 (2017).
423. I. Low, R. Rattazzi, and A. Vichi, JHEP **1004**, 126 (2010).
424. M. Ciuchini *et al.*, JHEP **1308**, 106 (2013).
425. C. Grojean, O. Matsedonskyi, and G. Panico, JHEP **1310**, 160 (2013).
426. M. Geller and O. Telem, Phys. Rev. Lett. **114**, 191801 (2015).
427. P. Batra and Z. Chacko, Phys. Rev. D 79,095012(2009);
R. Barbieri *et al.*, JHEP **1508**, 161 (2015);
M. Low, A. Tesi and L. T. Wang, Phys. Rev. **D91**, 095012 (2015).
428. ATLAS Collab., CERN-EP-2017-132 (2017).
429. CMS Collab., CMS-PAS-HIG-17-13 (2017).
430. CMS Collab., Phys. Lett. **B767**, 147 (2017).
431. ATLAS Collab., CERN-EP-2017-095 (2017).
432. CMS Collab., CMS-PAS-HIG-16-014 (2016).
433. ATLAS Collab., ATLAS-CONF-2017-058 (2017).
434. CMS Collab., CMS-PAS-HIG-16-033 (2016).
435. CMS Collab., CMS-PAS-HIG-16-023 (2016).
436. ATLAS Collab., ATLAS-CONF-2016-082 (2016).
437. CMS Collab., CMS-PAS-HIG-16-034 (2016).
438. ATLAS Collab., ATLAS-CONF-2013-067 (2013).
439. ATLAS Collab., ATLAS-CONF-2013-027 (2013).
440. S. Chatrchyan *et al.* [CMS Collab.], Eur. Phys. J. **C73**, 2469 (2013).
441. ATLAS Collab., ATLAS-CONF-2012-018 (2012).
442. CMS Collab., CMS-PAS-HIG-13-008 (2013).
443. CMS Collab., CMS-PAS-HIG-12-046 (2012).
444. ATLAS Collab., CERN-EP-2017-147 (2017).
445. ATLAS Collab., ATLAS-CONF-2016-071.
446. V. Khachatryan *et al.* [CMS Collab.], Phys. Lett. **B755**, 217 (2016).
447. ATLAS Collab., ATLAS-CONF-2017-050 (2017).

448. CMS Collab., CMS-PAS-HIG-16-037 (2016).
449. V.M. Abazov *et al.* [D0 Collab.], Phys. Rev. Lett. **104**, 151801 (2010).
450. D0 Collab., D0 Note 5974-CONF (2011).
451. R. Aaij *et al.* [LHCb Collab.], JHEP **1305**, 132 (2013).
452. ATLAS Collab., ATLAS-CONF-2012-094 (2012).
453. ATLAS Collab., ATLAS-CONF-2016-104 (2016).
454. ATLAS Collab., CERN-EP-2017-134 (2017).
455. S. Chatrchyan *et al.* [CMS Collab.], Phys. Lett. **B722**, 207 (2013).
456. CMS Collab., CMS-PAS-HIG-16-025 (2016).
457. V.M. Abazov *et al.* [D0 Collab.], Phys. Lett. **B698**, 97 (2011).
458. T. Aaltonen *et al.* [CDF Collab.], Phys. Rev. **D85**, 032005 (2012).
459. ATLAS Collab., ATLAS-CONF-2017-055 (2017).
460. ATLAS Collab., Phys. Lett. **B744**, 163 (2015).
461. ATLAS Collab., Phys. Lett. **B759**, 555 (2016).
462. CMS Collab., CMS-PAS-HIG-16-031 (2016).
463. ATLAS Collab., ATLAS-CONF-2012-010 (2012).
464. V. Khachatryan *et al.* [CMS Collab.], JHEP **1512**, 178 (2015).
465. ATLAS Collab., ATLAS-CONF-2016-089 (2016).
466. V. Khachatryan *et al.* [CMS Collab.], JHEP **1511**, 018 (2015).
467. ATLAS Collab., Phys. Rev. Lett. **114**, 231801 (2015).
468. CMS Collab., CERN-EP-2017-068 (2017).
469. CMS Collab., CMS-PAS-HIG-16-030 (2016).
470. ATLAS Collab., ATLAS-CONF-2011-020 (2011).
471. CMS Collab., CMS-PAS-HIG-15-009 (2015).
472. ATLAS Collab., Phys. Rev. **D92**, 052002 (2015).
473. ATLAS Collab., ATLAS-CONF-2012-079 (2012).
474. CMS Collab., CMS-PAS-HIG-16-055 (2016).
475. CMS Collab., CERN-EP2016-292 (2016).
476. V.M. Abazov *et al.* [D0 Collab.], Phys. Rev. Lett. **103**, 061801 (2009).
477. S. Schael *et al.* [ALEPH Collab.], JHEP **1005**, 049 (2010).
478. B. Aubert *et al.* [BaBar Collab.], Phys. Rev. Lett. **103**, 081803 (2009).
479. B. Aubert *et al.* [BaBar Collab.], Phys. Rev. Lett. **103**, 181801 (2009).
480. ATLAS Collab., ATLAS-CONF-2016-051 (2016).
481. ATLAS Collab., ATLAS-CONF-2017-053 (2017).
482. CMS Collab., CMS-PAS-HIG-16-036 (2016).
483. ATLAS Collab., Phys. Rev. **D92**, 092004 (2015).
484. CMS Collab., CMS-PAS-HIG-13-016 (2013).
485. ATLAS Collab., ATLAS-CONF-2012-013 (2012).
486. CMS Collab., CMS-PAS-HIG-12-002 (2012).
487. CMS Collab., CMS-HIG-12-013 and CERN-PH-EP-2013-011 (2013).
488. ALEPH Collab., Phys. Lett. **B526**, 191 (2002).
489. L3 Collab., Phys. Lett. **B545**, 30 (2002).
490. S. Schael *et al.* [ALEPH, DELPHI, L3 and OPAL Collaborations and LEP Working Group for Higgs Boson Searches], Eur. Phys. J. **C47**, 547 (2006).

491. M.M. Kado and C.G. Tully, Ann. Rev. Nucl. and Part. Sci. **52**, 65 (2002).
492. OPAL Collab., Eur. Phys. J. **C23**, 397 (2002).
493. DELPHI Collab., Eur. Phys. J. **C38**, 1 (2004).
494. CMS Collab., CMS-PAS-HIG-16-007 (2016).
495. ATLAS Collab., JHEP **08**, 148 (2015).
496. S. Chatrchyan *et al.* [CMS Collab.], JHEP **09**, 029 (2012).
497. V. Khachatryan *et al.* [CMS Collab.], Phys. Lett. **B758**, 296 (2016).
498. CMS Collab., CERN-EP-2017-159 (2011).
499. J. Bernon *et al.*, Phys. Rev. **D91**, 075019 (2015).
500. ATLAS Collab., Phys. Rev. Lett. **113**, 171801 (2014).
501. CMS Collab., CMS-PAS-HIG-14-037 (2014).
502. CMS Collab., CMS-PAS-HIG-17-013 (2017).
503. S.H. Zhu, `hep-ph/9901221` (1999).
504. H.E. Logan and S. Su, Phys. Rev. **D66**, 035001 (2002).
505. A. Gutierrez-Rodriguez and O.A. Sampayo, Phys. Rev. **D62**, 055004 (2000).
506. S. Kanemura, S. Moretti, and K. Odagiri, JHEP **0102**, 011 (2001).
507. J.A. Coarasa Perez *et al.*, Eur. Phys. J. **C2**, 373 (1998);
J.A. Coarasa Perez *et al.*, Phys. Lett. **B425**, 329 (1998).
508. C.S. Li and T.C. Yuan, Phys. Rev. **D42**, 3088 (1990) [E: **D47**, 2156 (1993)];
A. Czarnecki and S. Davidson, Phys. Rev. **D47**, 3063 (1993);
C.S. Li, Y.-S. Wei, and J.-M. Yang, Phys. Lett. **B285**, 137 (1992).
509. J. Guasch, R.A. Jimenez, and J. Sola, Phys. Lett. **B360**, 47 (1995).
510. M.S. Carena *et al.*, Nucl. Phys. **B577**, 88 (2000).
511. A.A. Barrientos Bendezu and B.A. Kniehl, Phys. Rev. **D59**, 015009 (1999), Phys. Rev. **D61**, 015009 (2000) and Phys. Rev. **D63**, 015009 (2001).
512. A.A. Barrientos Bendezu and B.A. Kniehl, Nucl. Phys. **B568**, 305 (2000).
513. B. Abbott *et al.* [D0 Collab.], Phys. Rev. Lett. **82**, 4975 (1999).
514. A. Abulencia *et al.* [CDF Collab.], Phys. Rev. Lett. **96**, 042003 (2006).
515. V.M. Abazov *et al.* [D0 Collab.], Phys. Lett. **B682**, 278 (2009).
516. ATLAS Collab., JHEP **1206**, 039 (2012).
517. ATLAS Collab., JHEP **03**, 088 (2015).
518. CMS Collab., CMS-PAS-HIG-11-019 (2011).
519. G. Aad *et al.* [ATLAS Collab.], JHEP **1603**, 127 (2016).
520. J. Abdallah *et al.* [DELPHI Collab.], Eur. Phys. J. **C54**, 1 (2008) [E: **C56**, 165 (2008)].
521. R. Dermisek, Mod. Phys. Lett. **A24**, 1631 (2009).
522. J.F. Gunion, JHEP **0908**, 032 (2009).
523. U. Ellwanger, Eur. Phys. J. **C71**, 1782 (2011).
524. W. Love *et al.* [CLEO Collab.], Phys. Rev. Lett. **101**, 151802 (2008).
525. V.M. Abazov *et al.* [D0 Collab.], Phys. Rev. Lett. **103**, 061801 (2009).
526. S. Chatrchyan *et al.* [CMS Collab.], Phys. Rev. Lett. **109**, 121801 (2012).
527. CMS Collab., JHEP **01**, 079 (2016).
528. G. Aad *et al.* [ATLAS Collab.], Eur. Phys. J. **C72**, 2244 (2012).
529. S. Chatrchyan *et al.* [CMS Collab.], Eur. Phys. J. **C72**, 2189 (2012).

530. G. Aad *et al.* [ATLAS Collab.], Phys. Rev. **D89**, 032002 (2014).